AD NUMBER
AD374189
CLASSIFICATION CHANGES
TO: **UNCLASSIFIED**
FROM: **CONFIDENTIAL**
LIMITATION CHANGES
TO: **Approved for public release; distribution is unlimited.**
FROM: **Distribution authorized to U.S. Gov't. agencies and their contractors; Administrative/Operational Use; JUL 1966. Other requests shall be referred to Air Force Rocket Propulsion Lab., eDWARDS afb, ca.**
AUTHORITY
AFRPL ltr 29 Sep 1973 ; AFRPL ltr 29 Sep 1973

SECURITY MARKING

The classified or limited status of this report applies to each page, unless otherwise marked.
Separate page printouts MUST be marked accordingly.

THIS DOCUMENT CONTAINS INFORMATION AFFECTING THE NATIONAL DEFENSE OF THE UNITED STATES WITHIN THE MEANING OF THE ESPIONAGE LAWS, TITLE 18, U.S.C., SECTIONS 793 AND 794. THE TRANSMISSION OR THE REVELATION OF ITS CONTENTS IN ANY MANNER TO AN UNAUTHORIZED PERSON IS PROHIBITED BY LAW.

VOLUME III

TECHNICAL REPORT NO. AFRPL-TR-66-109

(Unclassified Title)

156-INCH DIAMETER MOTOR LIQUID INJECTION TVC PROGRAM

TEST RESULTS, MOTOR 156-6

LOCKHEED PROPULSION COMPANY
REDLANDS, CALIFORNIA

JULY 1966

SPACE SYSTEMS DIVISION
AIR FORCE SYSTEMS COMMAND
UNITED STATES AIR FORCE

CONFIDENTIAL

(14) LPC [redacted] 699-F-Vol-

Copy No. _____

(18) (19)

TECHNICAL REPORT NO. AFRPL-TR-66-109-Vol-3

(Unclassified Title)

(6) 156-INCH DIAMETER MOTOR LIQUID INJECTION TVC PROGRAM,
VOLUME III. ~~FINAL REPORT~~
TEST RESULTS, MOTOR 156-6 (U) (8)

to

(9) Final rept. 1 APR 65-31 MAR 66.

SPACE SYSTEMS DIVISION
AIR FORCE SYSTEMS COMMAND
UNITED STATES AIR FORCE

(15) (11) July 1966, (12) 196p.

AF 04(695)-772

In addition to security requirements which must be met, this document is subject to special export controls and each transmittal to foreign governments or foreign nationals may be made only with prior approval of AFRPL (RPPR/STINFO), Edwards, California 93523.

LOCKHEED PROPULSION COMPANY
P. O. BOX 111
REDLANDS, CALIFORNIA

210150

FOREWORD

Contract No. AF 04(695)-772, dated 1 April 1965, was performed by Lockheed Propulsion Company (LPC), Redlands, California, in support of Air Force Systems Command (AFSC) Space Systems Division (SSD) Program 623A, Bid Packages (BP) 13 and 14. This technical report, submitted in partial fulfillment of the Contractor Data Requirements, provides a summary of results of the entire program. The program period of performance was 1 April 1965 to 31 March 1966. The LPC secondary report number is 699-F.

The program was monitored by the Air Force Rocket Propulsion Laboratory, Research and Technology Division, Edwards, California. Cognizant Air Force Project Engineers and their office symbols are as follows:

BP 13 and 14	Capt. J. J. Dell	RPMBL
BP 13	Capt. R. Stutzman	RPMBL
BP 14	Mr. W. C. Andrepont	RPMBL
BP 13 and 14, TVC	Lt. J. Schmuck	RPMBL

Cognizant personnel at LPC are as follows:

Program Manager	Mr. F. V. Genetti
Project Engineer	Mr. J. S. Coverdale

This technical report comprises three volumes: Volume I - Technical Discussion, Books 1 and 2; Volume II - Test Results, Motor 156-5; and Volume III - Test Results, Motor 156-6.

Documents from which classified material has been extracted for use in this report are listed in the individual Reference sections of each volume and book.

The form DD 1473 and distribution list required for this report are included at the end of Volume III.

This technical report has been reviewed and is approved.

Wilbur C. Andrepont
Project Engineer

TABLE OF CONTENTS

TABLE OF CONTENTS (Continued)

LIST OF ILLUSTRATIONS

LIST OF ILLUSTRATIONS (Continued)

LIST OF ILLUSTRATIONS (Continued)

LIST OF ILLUSTRATIONS (Continued)

LIST OF ILLUSTRATIONS (Continued)

LIST OF ILLUSTRATIONS (Continued)

LIST OF TABLES

SECTION I

INTRODUCTION

(U) Lockheed Propulsion Company (LPC) submits this Final Technical Report to the Space Systems Division, Air Force Systems Command, in partial fulfillment of the requirements of Contract No. AF 04(695)-772. The contract work effort, performed in a 12-month period, was conducted under the technical cognizance of the Air Force Rocket Propulsion Laboratory (AFRPL), Edwards Air Force Base, Edwards, California. The primary objectives of this program were to fire two 156-inch diameter motors, each having a flightweight, submerged, ablative nozzle and a flight-prototype, nozzle-mounted, secondary liquid injection thrust vector control (LITVC) system.

(U) The first motor, designated Motor 156-5, had a single center segment and was a 3,000,000-pound thrust class motor; it was successfully statically fired on 14 December 1965 at LPC's Potrero Test Facility. The second motor, designated Motor 156-6, was a monolithic (nonsegmented) 1,000,000-pound thrust class motor; it was successfully statically tested on 15 January 1966.

(U) This volume presents a description of the test operations and the motor performance results of the Motor 156-6 firing conducted on 15 January 1966. Description of the test article is summarized herein; detailed descriptions are contained in Volume I.

SECTION II

SUMMARY

(C) Motor 156-6 was successfully test-fired 15 January 1966 at the Potrero Test Facility. The motor closely followed pressure and thrust predictions, delivering an average thrust of 962,800 pounds over a motor burn time of 65.0 seconds; average burn time chamber pressure was 662 psi. Specific impulse delivered during burn time was 236.2 lb-sec/lb. The standard specific impulse* was 245.2 lb-sec/lb. A photograph of the firing is presented in Figure 1.

(U) The TVC performance was normal, following the programmed duty cycle throughout the firing; all TVC components functioned normally and incurred no damage during the firing.

(C) A side force of 67,000 pounds was measured at 3.25 seconds during the first cycle, resulting in a maximum measured thrust vector angle of 4.4 degrees. The maximum measured side force of 70,000 pounds occurred at 49.5 seconds during cycle No. 12.

(U) Postfire inspection of the nozzle revealed no deficiencies in material, design, or fabrication.

(U) Most surfaces exhibited smooth and even erosion. Exceptions were the two downstream carbon-phenolic throat insert rings. Erosion was uneven in these sections where grooves and gouges were noted around the circumference.

(C) Erosion of the graphite-phenolic throat section was slightly less than anticipated. The measured throat erosion was 10.2 mil/sec as compared to a design value of 11 mil/sec.

(U) Pressurization of the TVC fluid injectant system was initiated at T-18 seconds by activating the pressure regulator by-pass unit. At T-10 seconds, a manual signal activated the main pressure regulators and closed the by-pass unit. At this time, the by-pass unit had pressurized the system to 500 psi. The main regulators brought the pressure to a nominal operating range (750 psi minimum, to 825 psi maximum) and maintained this range for the 13 duty cycles.

(U) The GN_2 supply pressure decayed to a final pressure somewhat lower than expected. The initial tank pressure was 4600 psi, and final pressure was 800 psi.

---

* Standard conditions: sea level, optimum expansion, 1000 psia chamber pressure, and 15^0 half-angle.

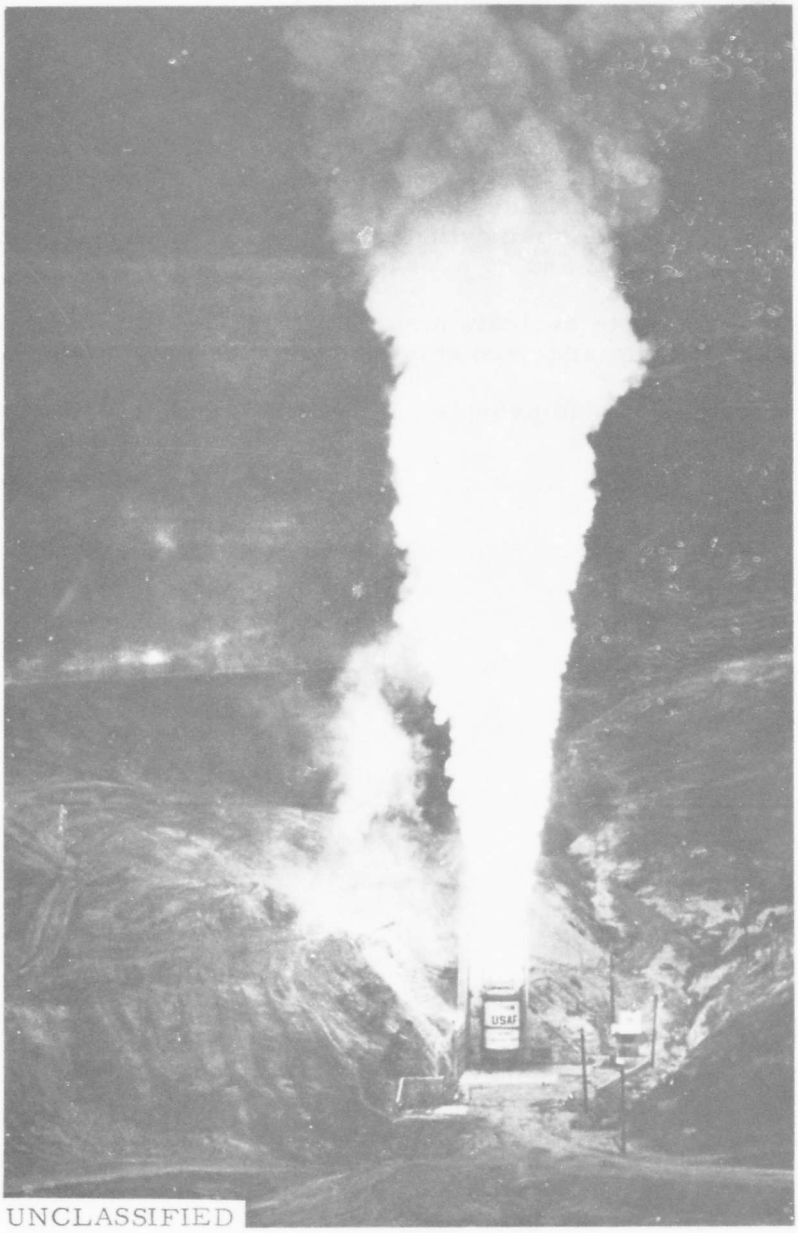

Figure 1 Motor 156-6 Immediately After Ignition

(U) Hydraulic pressure monitored near the pump outlet showed that 2965 ± 12 psig was maintained throughout the test.

(U) The motor case showed no areas of localized overheating, no indications of gas leakage, and no structural damage after the test.

(U) Inspection of the motor insulation indicated satisfactory performance of the mastic rubber (LPL-31) used in the domes. The insulation surface was charred and typically rough and uneven; however, no areas of excessive erosion were noted. The chamber cylinder showed a remaining coat or liner, indicating even grain burnout and no overheating of the motor case.

(U) All data required to evaluate motor and TVC performance were obtained. All primary data acquisition equipment functioned properly.

(U) The following sections provide detailed information on the test operations and performance results.

SECTION III

MOTOR DESCRIPTION

(U) The Motor 156-6 assembly drawing is shown in Figure 2. A summary of dimensional characteristics, a tabulation of major component weights, and a detailed motor weight breakdown are presented in Tables I, II, and III, respectively.

(U) The case for Motor 156-6 was a monolithic design and was composed of the 623A Program Bid Package 3 forward segment, the Bid Package 2 aft segment, and a new aft dome and nozzle attachment flange, welded into a single structure. A summary of case design characteristics is presented in Table IV.

(U) The case was insulated in the forward and aft domes with LPL-31, an asbestos-filled mastic insulation. Silica-filled buna-N release boots were used at the forward and aft ends of the main grain to provide stress relief at grain-case termination lines.

(U) The insulated case was lined with LPL-22, an epoxy-cured PBAN liner. The liner minimum design thickness in the uninsulated case side wall was 0.2 inch.

(U) Motor 156-6 was loaded with LPC-580C propellant, a PBAN formulation containing 18 percent aluminum and having a total solids loading of 86.9 percent.

(U) The grain configuration was a circular port with an aft-end full-diameter radial slot. The web was 49.4 inches, and the web fraction was 64 percent. The total propellant weight was 272,884 pounds.

(U) The Motor 156-6 igniter was of a pyrogen type, mounted at the forward end of the motor. The main propellant charge was 141 pounds of LPC-588 propellant, a PBAN formulation, cast and case-bonded in a steel igniter chamber. The grain configuration was a 28-point star with a ½-inch web and an average grain length of 22.5 inches.

(U) The submerged nozzle for Motor 156-6 consisted of a maraging steel support structure with ablative plastic liners on the flame-exposed surfaces. The nozzle throat diameter was 34.54 inches, the exit diameter was 98.64 inches, and the divergence half-angle was $17^{0}30'$. The over-all nozzle length was 115.1 inches, and the forward section was submerged 38.3 inches into the motor case, a submergence ratio of 46 percent. The nozzle assembly drawing is presented in Figure 3. An expanded view of the nozzle, delineating material locations and sources, is presented in Figure 4.

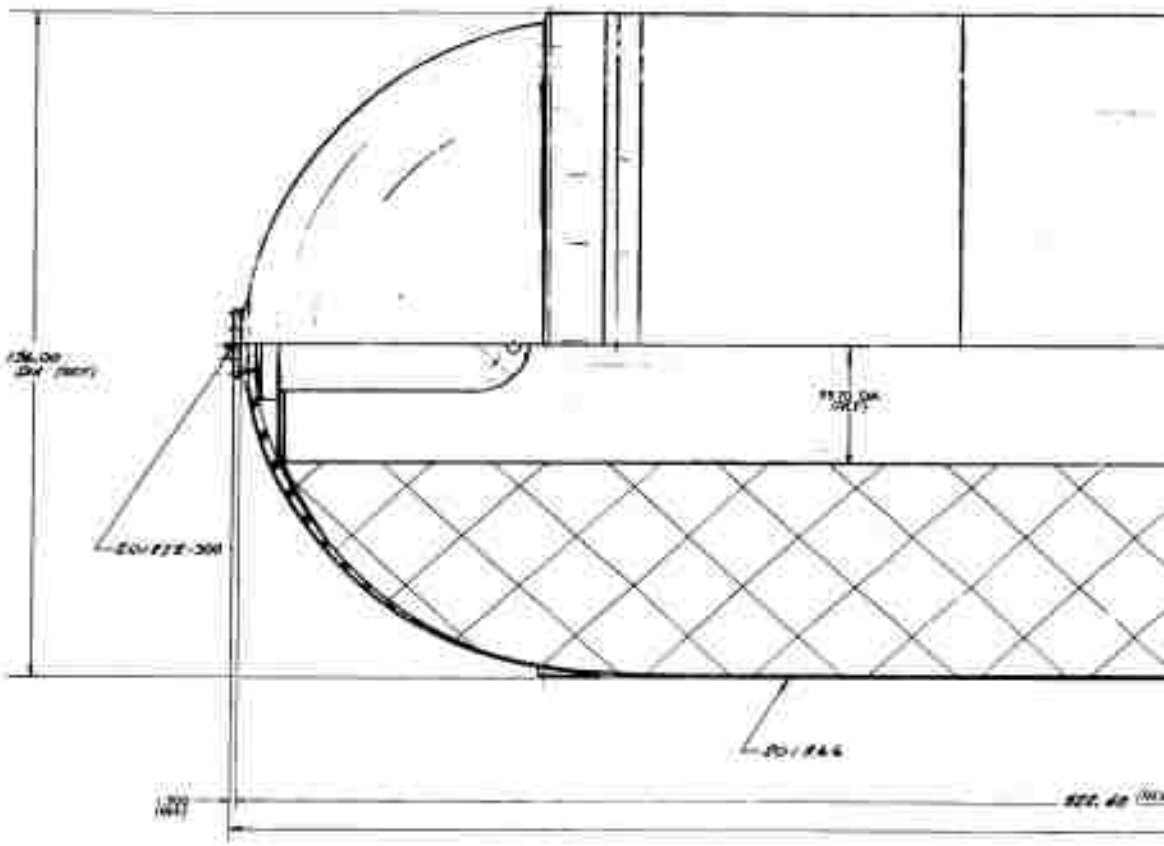

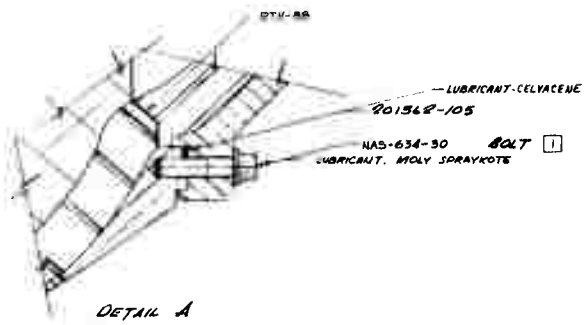

DETAIL A

UNCLASSIFIED

1

AR		A-12	ADHESIVE		LPC-139
AR	94499		LUBRICANT, MOLY SPRAYKOTE		
AR	14096		LUBRICANT, O-RING, CELMCORE		
AR		RTV-88	SEALER	RUBBER	
1		201362-105	O-RING		

201386

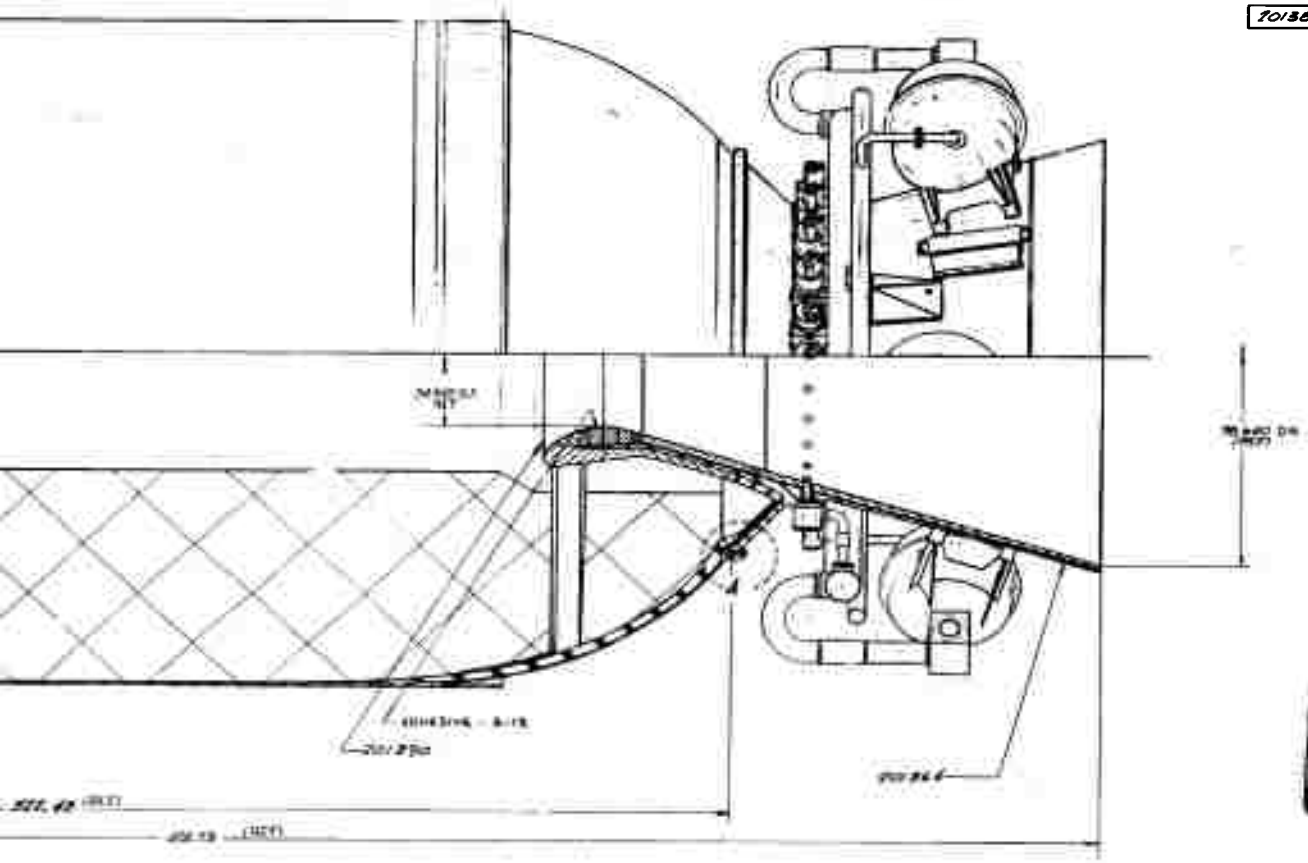

2

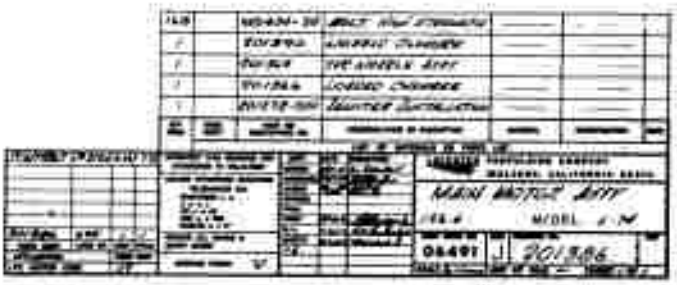

Figure 2 Motor 156-6 Assembly

TABLE I

DIMENSIONAL SUMMARY
MOTOR 156-6

Length (in.)	
Chamber	322.48
Nozzle	117.00
Motor, over-all	400.73
Diameter (in.)	
Case cylinder, inner	155.00
Case cylinder, outer	156.00
Case skirt, outer	155.96
Nozzle throat, initial	34.53
Nozzle exit, inner	98.62
Nozzle exit, outer	102.14
TVC envelope, maximum	156.00
Grain port	55.39
Ratios	
Port-to-throat, initial	2.6
Web fraction (%)	64
Nozzle submergence (%)	46

TABLE II

MAJOR COMPONENT WEIGHTS MOTOR 156-6
(in pounds)

Motor case	22,073
Insulation	5,273
Liner	1,181
Propellant	272,884
Nozzle	12,243
TVC hardware	5,416
TVC fluid	4,334
Igniter	965
Miscellaneous (attachment hardware, O-rings, etc.)	126
Total inert	47,136
Total propellant	273,025
Motor, dry weight	320,161
Motor mass fraction (dry)	0.85

TABLE III

COMPONENT WEIGHT SUMMARY, MOTOR 156-6

		Drawing No.	Weight (lb)
1.	Chamber (loaded)	201366	301,411
1.1	Chamber	201351	22,073
1.2	Insulation	201365	5,273
1.3	Liner	201365	1,181
1.4	Propellant	201366	272,884
2.	Nozzle	201352	12,243
2.1	Housing (steel)	201353	8,500
3.	LITVC hardware	--	5,416
4.	Igniter installation	201272-300	965
4.1	Headcap and pellet chamber assembly	201274	119
4.2	Loaded chamber and adapter assembly	201275-300	846
4.3	Igniter propellant	--	141
5.	Miscellaneous	--	126
5.1	Nozzle O-rings	201362-101	1
5.2	Nozzle attachment hardware	--	115
5.3	Igniter attachment hardware	--	10
6.	TVC fluid, total		4,334
6.1	Manifold and line N_2O_4*		473

* Drained off after test.

TABLE IV

MOTOR CASE DESIGN CHARACTERISTICS, MOTOR 156-6

Nominal Case Thickness	
Forward dome	0.345 / 0.300 in.
Aft dome	0.345 / 0.300 in.
Walls	0.419 / 0.474 in.
Dome Contours	**Hemispherical**
Type of Steel	**18% Nickel Maraging Steel**
Yield strength (0.2% offset) minimum	**240,000 psi**
Ultimate tensile strength, minimum	**250,000 psi**
Weld Process	**Shielded Tungsten-Arc (TIG)**
Hydrotest Pressure	**960 psig**
Design MEOP	**885 psia**
Minimum Design Yield Pressure	**1390 psia**
Maximum Design Case Temperature	**100°F**
Minimum Design Weld Efficiency	**95%**

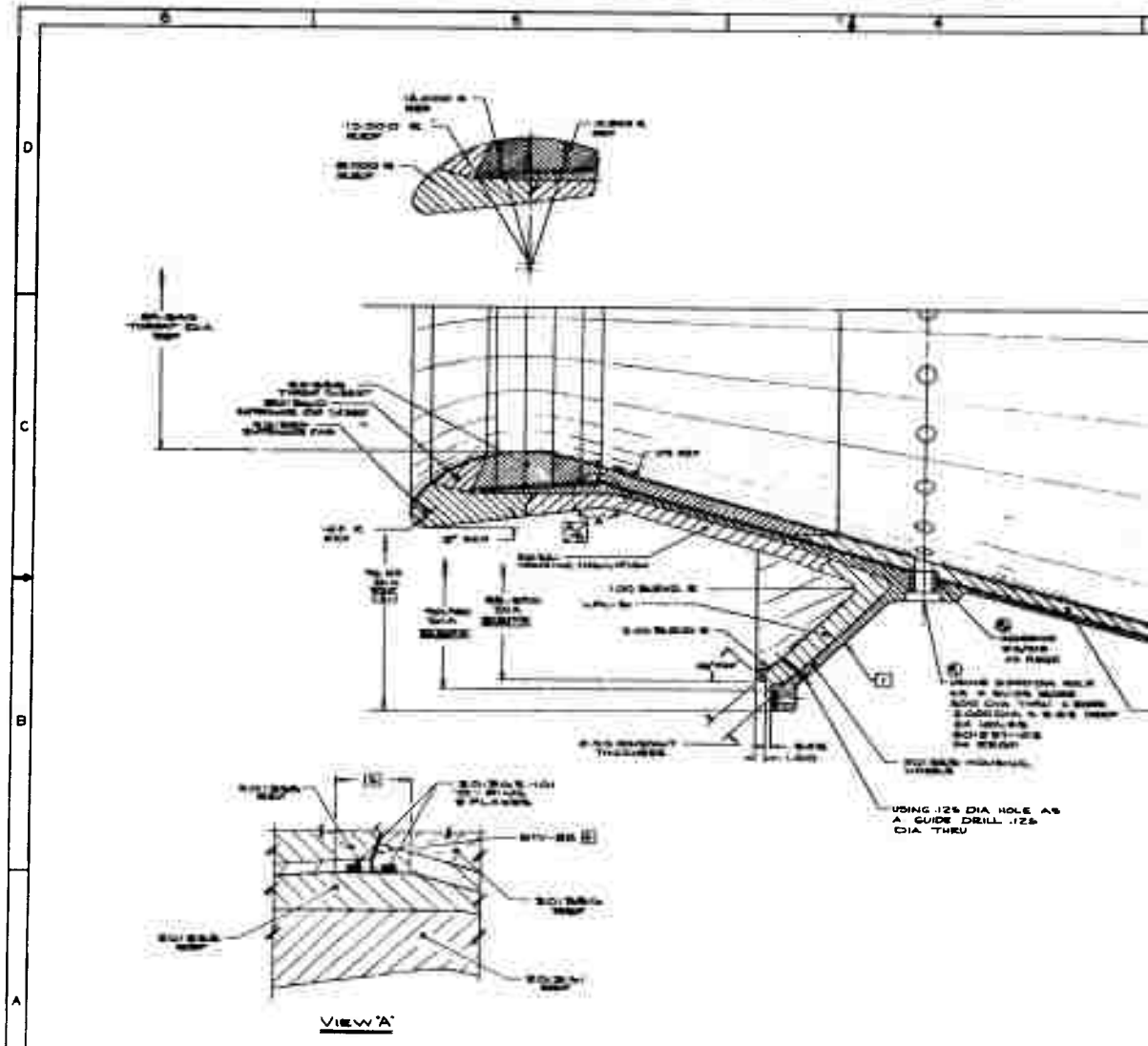

UNCLASSIFIED

5092

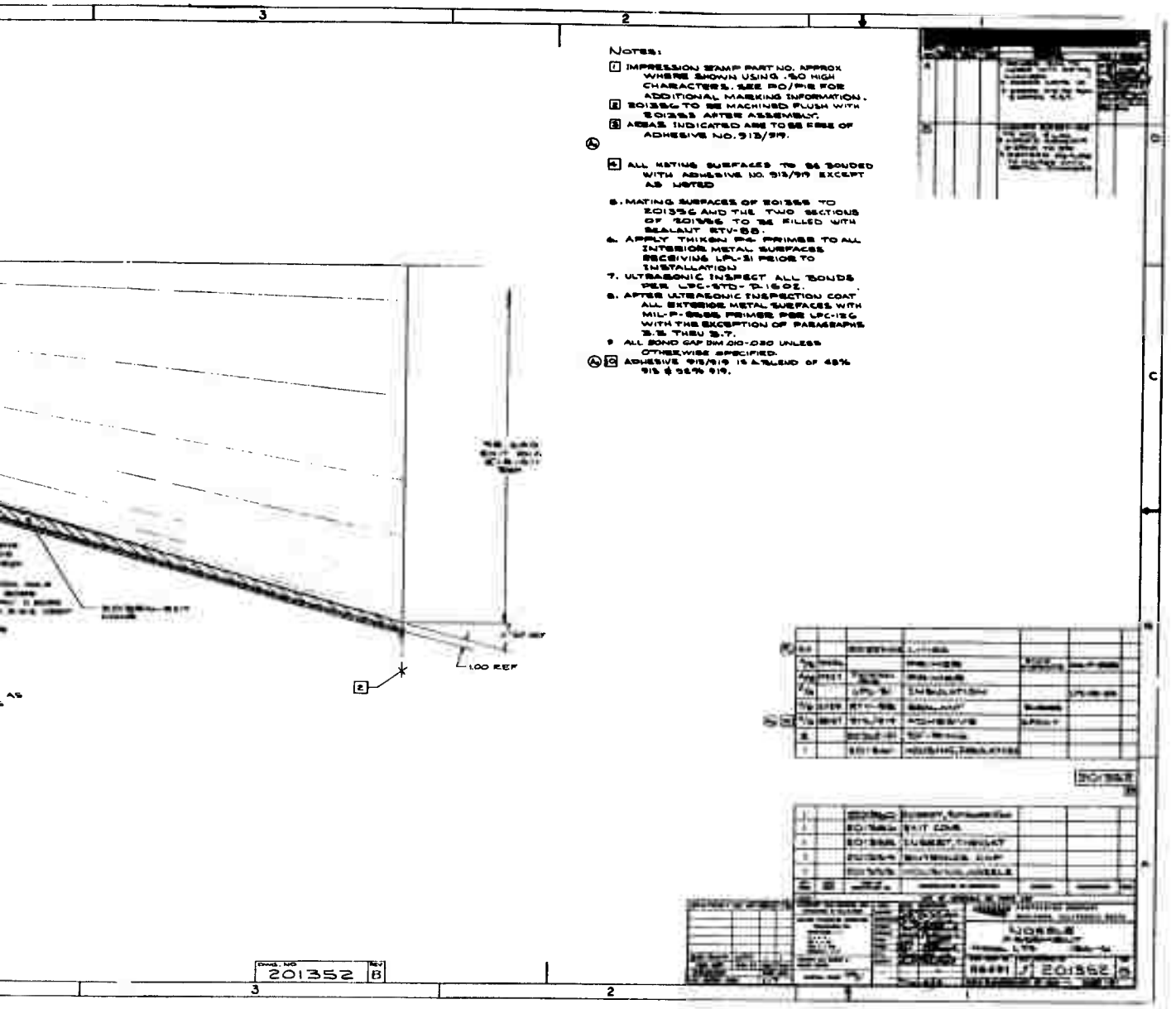

Figure 3 Nozzle Assembly, Motor 156-6

2

COMPONENTS	MATERIAL	REINFORCEMENT	RESIN
1. ENTRANCE CAP	MXC-175	HITCO CCA-1	EC 201
2. ENTRANCE CAP INSERT	MXC-175	HITCO CCA-1	EC 201
3. THROAT RING INSERTS	A. FM 5014	NATIONAL GRAPHITE CLOTH	91 LD
	B. FM 5314	HITCO GRAPHITE CLOTH	91 LD
	C. MX 4501	HITCO GRAPHITE CLOTH	EC 201
	D. MXC-175	HITCO CCA-1	EC 201
	E. MXC-175	HITCO CCA-1	EC 201
4. THROAT EXTENSION	MXC-175	HITCO CCA-1	EC 201
5. EXIT CONE	MXS-175	HITCO C-105-48	EC 201
6. HOUSING INSULATION	MXS-175	HITCO C-105-48	EC 201
7. FLANGE INSULATION	LPL-31	ASBESTOS-FILLED PBAA	
8. GLASS BACK-UP	MX-4600-1584	1584 GLASS CLOTH	EC 201
9. HOUSING	MARAGING STEEL		

66-734

Figure 4 Nozzle Components, Motor 156-6

(U) The TVC system consisted of N_2O_4 secondary injection through 24 equally spaced servoinjectors at an expansion ratio of 3.0. The fluid was pressurized by a regulated high pressure gaseous N_2 system. A motor-mounted omniaxis controller provided vectorial resolution pitch and yaw signals generated by a pre-punched tape program.

(U) All components of the TVC system were mounted to the nozzle shell within the 156-inch diameter envelope. The component arrangements and configurations are shown on the Nozzle-TVC assembly drawing (Figure 5). Tables V and VI provide TVC component design characteristics.

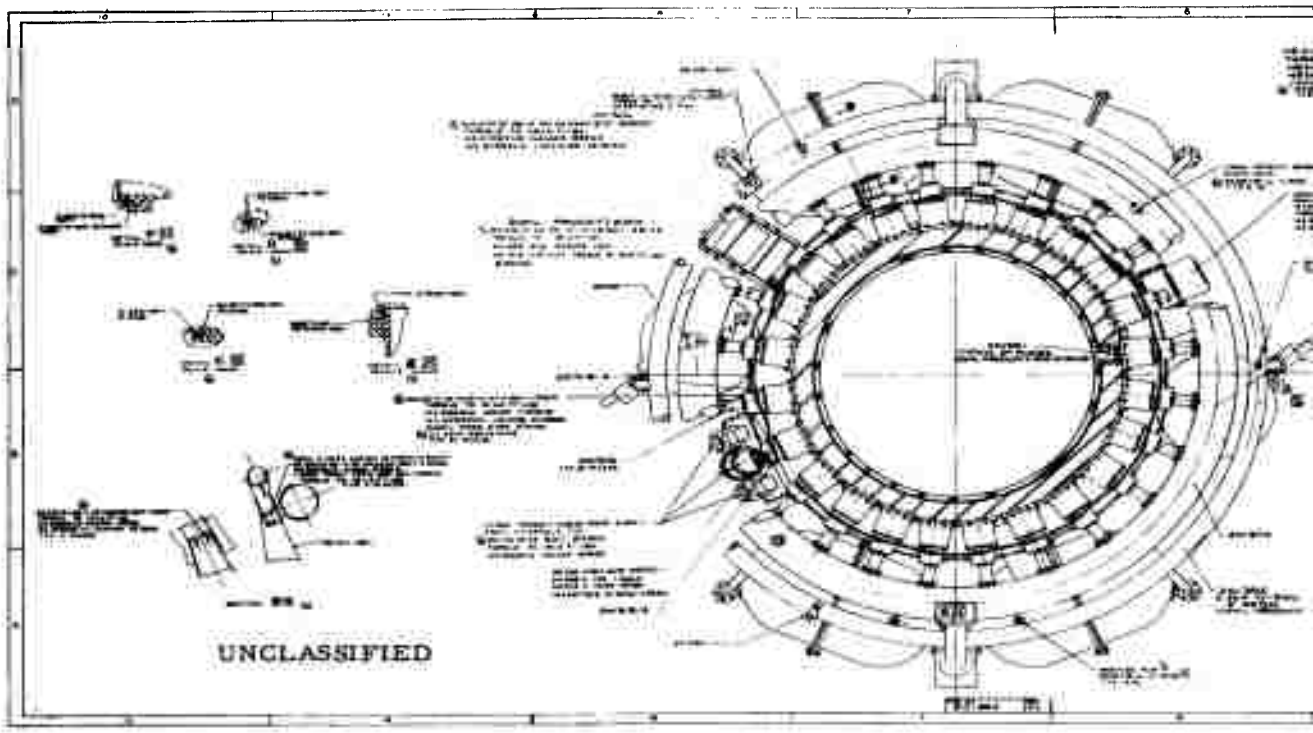
UNCLASSIFIED

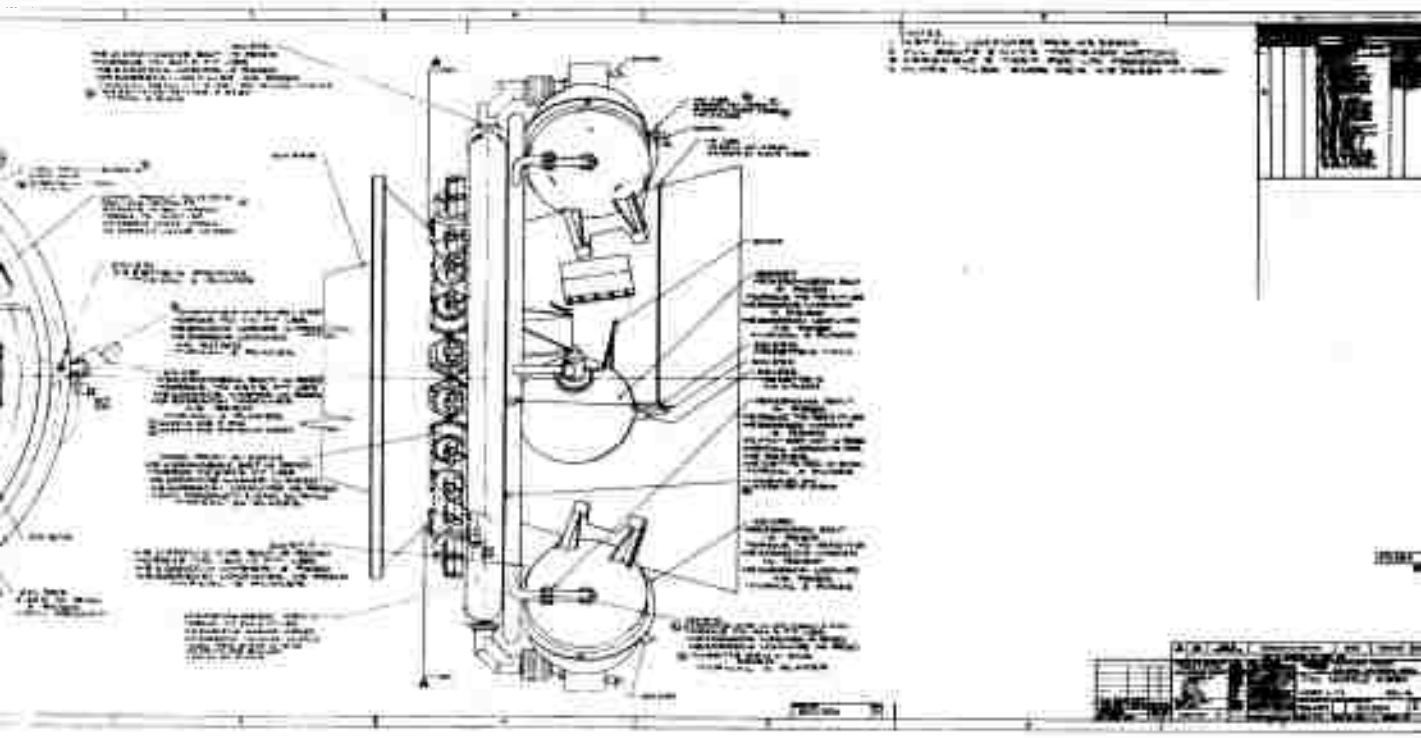

Figure 5 TVC-Nozzle Assembly, Motor 156-6

TABLE V

GN$_2$ PRESSURIZATION SUBSYSTEM
DESIGN AND DIMENSIONAL CHARACTERISTICS
MOTOR 156-6

High-Pressure Tank	
Number required	2
Maximum diameter (in.)	25.62
Over-all length (in.)	31.04
Wall thickness, minimum (in.)	0.625 Cylinder/0.375 Dome
Material	4340 Steel
Material ultimate tensile strength, minimum (psi)	190,000
Operating pressure range, nominal (psi)	5500 to 1500
Minimum design burst pressure (psi)	9000
Pressure Regulator	
Unit	
Number required	2
Type	Poppet with By-Pass
Unregulated pressure range (psig)	5900 to 1500
Ullage pressure (psi)	
1.0 ft^3 to 4.67 ft^3, ullage volume	780 ± 130
4.67 ft^3 and above, ullage volume	775 ± 35
By-pass subsystem	
Number required	1
Pre-pressurization time (sec)	1 to 6
Pre-pressurization pressure (psig)	850 ± 15
Control mode	Ullage Electrical Pressure
Manifold	
Torus diameter (in.)	122.75
Cross section diameter (in.)	3.50
Material	321 CRES
Material ultimate tensile strength, minimum (psi)	75,000
Wall thickness (in.)	0.25

TABLE VI

INJECTANT (N_2O_4) STORAGE AND TRANSFER SUBSYSTEM
DESIGN AND DIMENSIONAL CHARACTERISTICS
MOTOR 156-6

N_2O_4 Tank	
Number required	4
Maximum diameter (in.)	24.5
Over-all length (in.)	45.5
Wall thickness (in.)	0.14
Material	15-7 PH and 17-7 PH Stainless Steel
Material ultimate tensile strength, minimum (psi)	170,000
Operating pressure (psi)	775 ± 35
Hydrotest pressure (psi)	1150
Design burst pressure (psi)	1600
Bladder	
Type	Reversible-Postive Explosion
Material	
Elastomer	Chlorobutyl
Metal (N_2O_4 side)	304 Stainless Steel Foil
Thickness (in.)	
Elastomer	0.060 to 0.070
Metal	0.004 to 0.006
Expulsion efficiency, minimum (%)	95
Manifold	
Torus diameter (in.)	108.0
Cross-section diameter (in.)	7.50
Material	321 CRES
Material ultimate tensile strength, minimum (psi)	75,000
Wall thickness, minimum (in.)	0.25
Operating pressure (psi)	775
Hydrotest pressure (psi)	1150
Design burst pressure (psi)	1600

SECTION IV

MOTOR ASSEMBLY AND TEST PREPARATIONS

(U) 1. Motor Assembly

(U) On 23 December 1965, the 156-6 monolithic motor was delivered to the Potrero Proving Ground Large Solid Motor Test Bay for installation in the thrust stand, and on 27 December the motor was installed. (See Figure 6.) The motor weighed 307,140 pounds, including portions of the handling equipment, and was transferred to the thrust stand by the 200-ton Manitowoc crane, using a 100-foot boom. No difficulties were encountered during the transfer and installation of the motor on the thrust collector. Prior to this operation, the thrust stand had been carefully re-aligned and levelled; positioning of the motor therefore merely required alignment of the scribe marks located on the motor case skirt with the scribe marks located on the thrust collector adapter ring. The case was then bolted to the thrust collector ring. The aft lateral thrust ring, thrust ring adapter, and the upper lateral load cell assemblies, which consisted of two 100,000-pound columns in parallel and one 200,000-pound column at 90 degrees, were installed. Some difficulty was encountered during installation of the thrust ring adapter to the motor aft skirt because of an out-of-round condition of the skirt. However, the operation was completed successfully and only minor adjustments to the lateral load cell assemblies were necessary.

(U) After the motor was installed in the thrust stand and prior to installation of the nozzle, the slot mandrel was removed from the motor and repair work at the aft end insulation was completed. Prior to installation of the igniter, it was necessary to trim the insulation at the igniter port area to permit the necessary metal-to-metal contact between the igniter headcap and the igniter chamber.

(U) The igniter was installed in the motor without difficulty. The igniter chamber was lowered through the motor propellant grain cavity and bolted to the igniter headcap assembly which projected into the igniter port. The headcap assembly, in turn, was bolted to the motor head dome.

(U) One restraint ring was installed around the motor case and was suspended away from the case by a cable which was attached to the aft lateral thrust collector. A minimum clearance of three inches existed between the restraint ring and the motor case. Four tie-down cables, each capable of withstanding a 200,000-pound load, also were attached between the thrust collector and test bay tie-down bracket as part of the motor restraint system.

(U) After the TVC system had been partially assembled on the nozzle, the nozzle was installed on the motor (Figure 7). An out-of-round condition at the nozzle-case interface caused installation difficulties, and it was also necessary to trip some insulation from the nozzle mating surface. The O-ring was installed in the O-ring groove of the motor case, and RTV was applied to each face of the mating insulations immediately prior to installation of the nozzle.

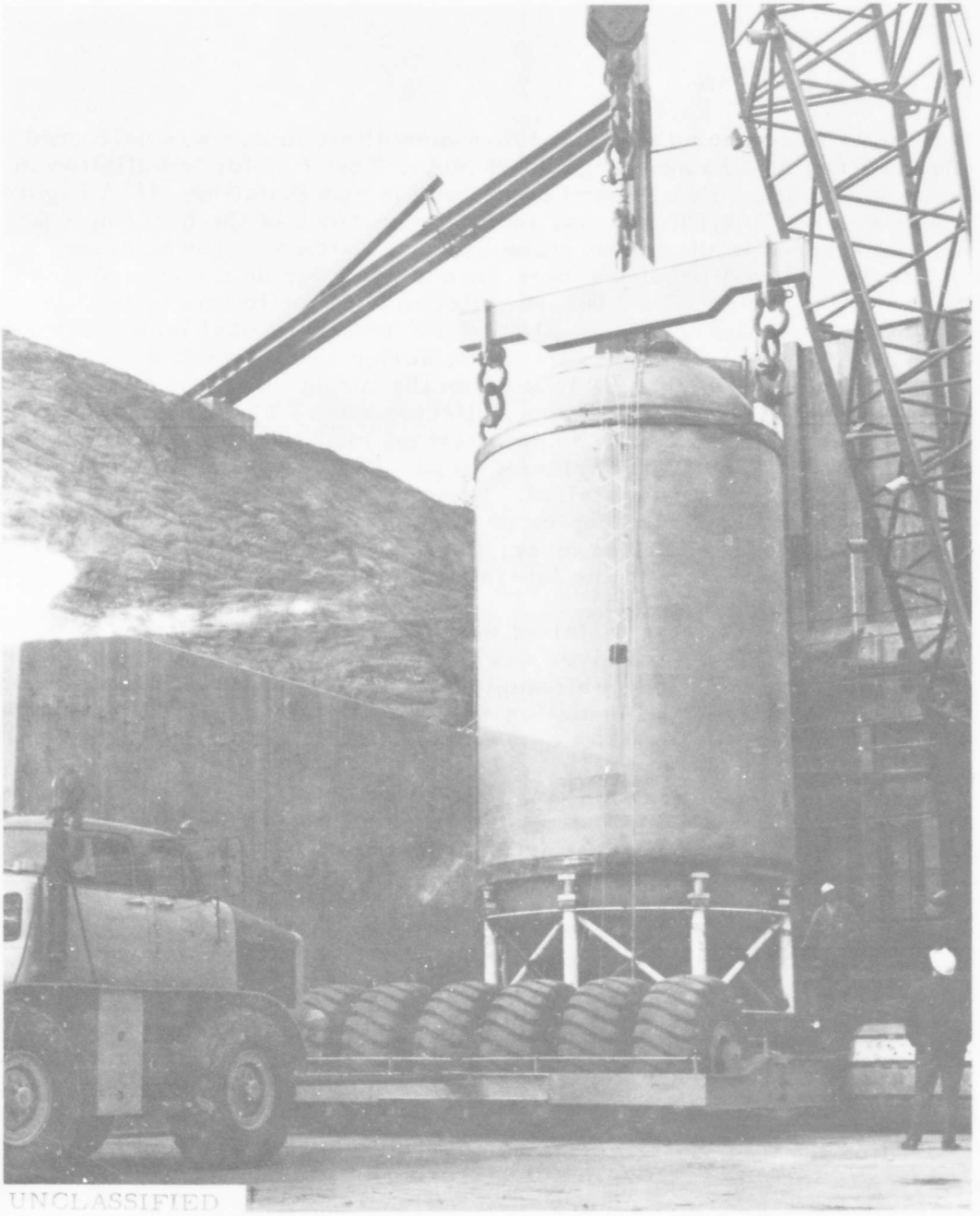

Figure 6 Motor 156-6 Installation in Thrust Stand

5757

Figure 7 Motor 156-6 Nozzle Installation

(U) A styrofoam closure had been cemented in the entrance cone of the nozzle prior to assembly in order to permit a leak test of the motor to be conducted. The motor assembly was pressurized to 20 psi and held at this pressure for 20 minutes with no evidence of leakage. The motor was then maintained at a pressure of 5 psi until the day before the test, when it was released to install the chamber pressure transducers. When the 5 psi pressure was relieved, the nozzle closure unbonded from the nozzle and was held in place by a line which had been previously installed for this purpose.

(U) Equal distribution of the motor weight on the three axial load cells and alignment of the motor was accomplished by installing shims as required between the axial shroud flexures and the thrust collector.

(U) Instrumentation calibration was conducted in accordance with standard approved procedures detailed in the test plan. A one-hour countdown hold was necessitated when the console display failed to indicate that transfer from ground power to airborne power had occurred. The sequencer abort occurred after instrumentation cameras had pulled film, and reloading was required. The motor was successfully test-fired at 11:30 a.m. on 15 January 1966.

(U) 2. TVC System Assembly and Checkout

a. Assembly. The completed nozzle assembly was transferred from the transporting fixture to the assembly stand upon its receipt at Potrero Production and Test Facility. This stand also served as a mapping tool fixture for recording the nozzle ablatives contour prior to and after motor firing. After completion of the mapping operation, the assembly of the TVC components to the nozzle housing was begun. The sequence of assembly was as follows:

(1) The 24 surge arrestor-burst disc assemblies were inserted into the injector valve mounting holes in the nozzle housing after shimming to a height of minimal interference fit.

(2) The 24 injector valve assemblies were installed to the nozzle housing. The valves were positioned by serial number, as shown in Figure 8.

(3) The hydraulic manifolds (pressure and return) were connected to the injector valve assemblies.

(4) First, the 24 fluid transfer ducts were connected to the N_2O_4 toroidal manifold; then, this subassembly was lowered, with the ducts being inserted in the injector valve housings as the manifold was being lowered.

(5) The two N_2O_4 tank and connector block subassemblies (four tanks and two blocks) were installed on the nozzle. The previously installed N_2O_4 transfer lines were connected to the blocks simultaneously.

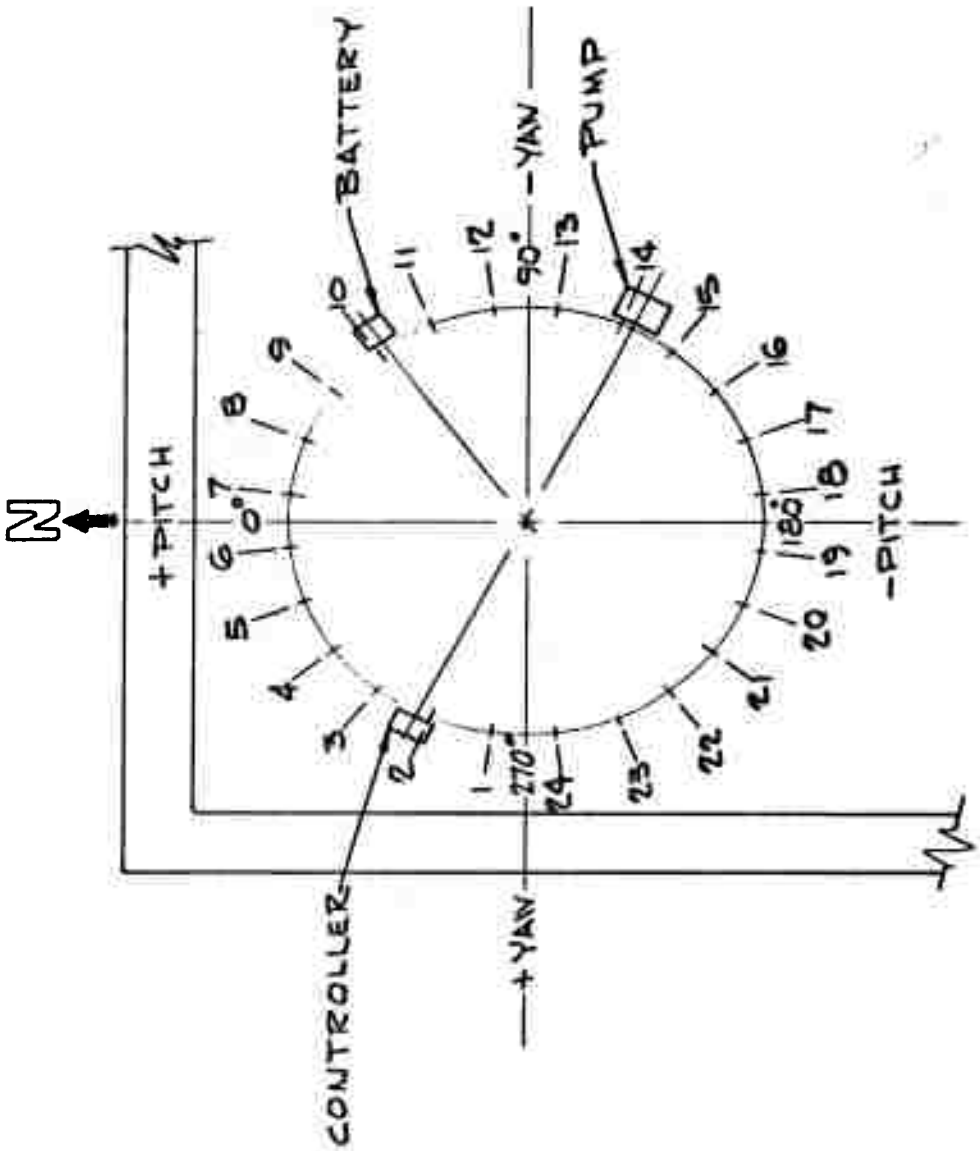

Figure 8 TVC Valve Orientation Chart, Motor 156-6

(6) The two high-pressure GN_2 tanks were mounted to the nozzle housings, the pressure regulators attached to the tanks, and the GN_2 manifold was raised to connect to the regulators and the low-pressure N_2O_4 tanks inlet ducts.

(7) The hydraulic pump was installed on the nozzle, and the hydraulic fluid system was connected. This involved plumbing the auxiliary ground system into the manifolds in parallel to the airborne pump.

(8) Next, the complete electrical system was installed. This system was composed of the omniaxis controller and associated harnesses, the battery, the pressure regulator system electrical harness, the controller power cable, and the power lines to the hydraulic pump.

(U) Upon completion of this phase of assembly, the nozzle and TVC assembly was mated to the motor in the firing bay. (Figure 9.)

(U) After the nozzle-to-motor mating operation was finished, the TVC assembly was completed. This included:

- Installing the high-pressure GN_2 fill system on the motor assembly and mating it to the ground source.
- Installing the fluid fill system (N_2O_4) and connecting it to the ground system. This system also was used for postfire draining for this test.
- Connecting the water quench system to the N_2O_4 manifold.
- Connecting the command input electrical harness to the controller.

This completed the TVC assembly, and pending final checkout results, the system was ready for filling operations. The completely assembled motor, nozzle, and TVC system are shown in Figure 10. A TVC system checkout was performed after installation on the motor.

(U) b. TVC Checkout. The TVC system assembly was modified with 4 cover plates installed on the manifold outlet ducts to permit an operational checkout of the GN_2 pressurization system without affecting the N_2O_4 side of the TVC system. A pressure monitor transducer and the 2 pressure switches were mounted to these cover plates. Three separate GN_2 system tests were conducted, and the results indicated that the system was functioning properly and was ready for the test firing.

(U) The TVC system modification was removed, and the remaining checkout operations were conducted. These included:

- Hydrotests of all components of the pressurization, fluid, and hydraulic systems.

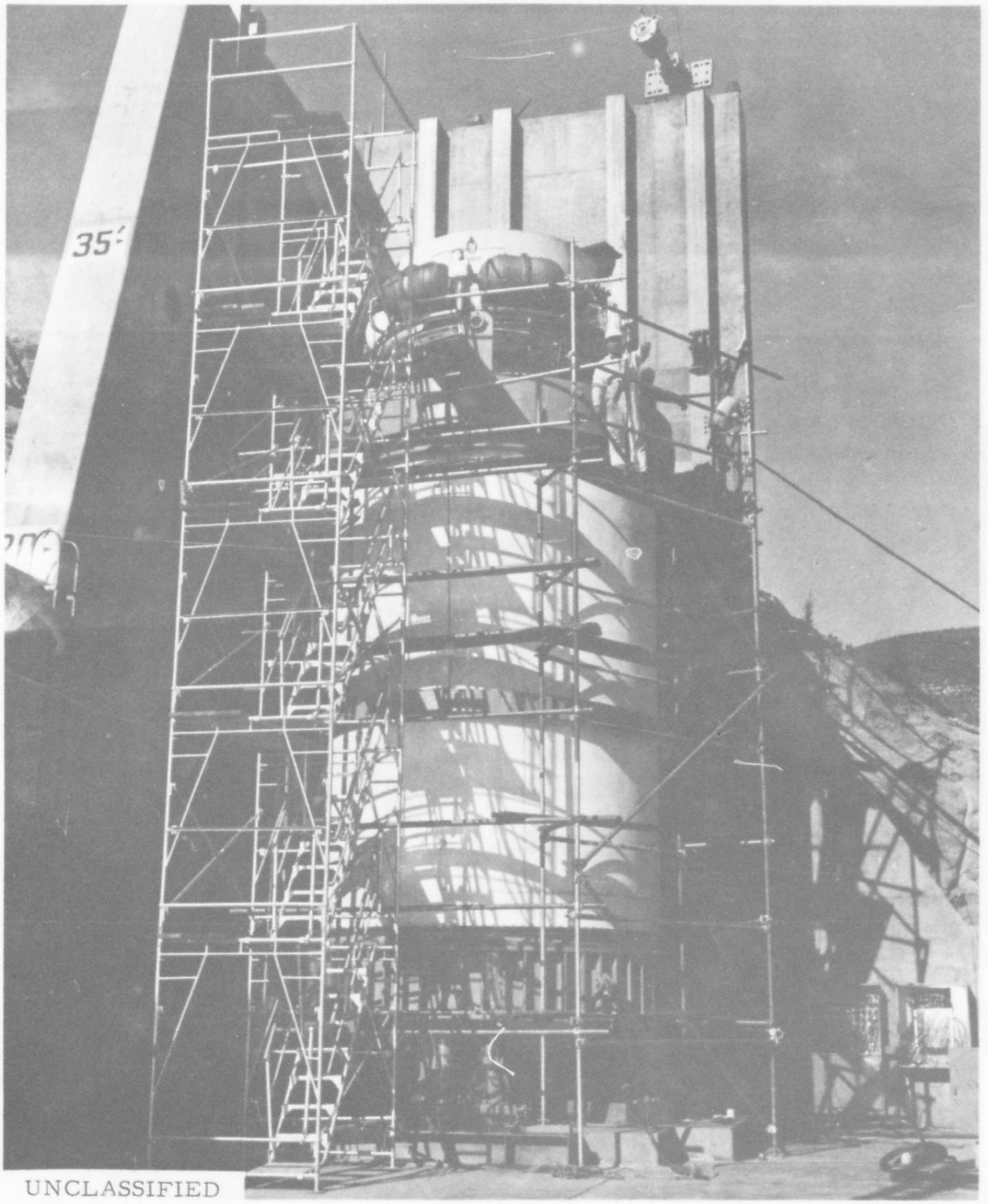

Figure 9 View of Nozzle-TVC System, Motor 156-6

Figure 10 Completely Assembled Motor 156-6 in Test Stand

- Low-pressure leak tests of each of the assembled N_2O_4 tanks after the bladders had been installed.
- Leak tests of the high pressure GN_2 system.
- Low pressure leak tests of the N_2O_4 system prior to installing the N_2O_4 tanks.
- Numerous tests of the ground hydraulic pump, and the nozzle-mounted hydraulic pump using both ground and airborne electrical power.
- Numerous operational tests of the command signal input, resolver output, and injector valves.
- Continuity checks of the various electrical harnesses.

(U) c. Instrumentation, Data Acquisition, and Data Reduction.

(U) (1) Instrumentation. Motor 156-6 was instrumented for static test firing in accordance with the instrumentation chart shown in Table VII. Primary data (i.e., axial and lateral thrust, motor chamber, N_2O_4 manifold and nozzle pressures, injector valve displacements and TVC command signals) were recorded on the Beckman 210 digital data acquisition system (DDAS). These data also were recorded redundantly on oscillographs. Quick-look and secondary data also were recorded oscillographically.

(U) The three flexured 700,000-pound axial force transducers were calibrated by the shunt electrical calibration method using a six-wire system. This involves shunting accurately known resistances across one arm of the transducer bridge and recording the output. (A physical calibration of each transducer had been conducted previously at the National Bureau of Standards.) By comparing the bridge output when shunted by the known resistor with the physical calibration output, the calibration factor for shunt-to-force was established; then, in the test bay, it was only necessary to utilize the electrical calibration, since its equivalent force value had been established. Three 200-ton hydraulic rams, located adjacent to alternate axial load cells, were used to lift the motor assembly off the cells for calibration purposes.

(U) The two lateral 50,000-pound force transducers located between the forward thrust ring and the test bay rails also were calibrated by the shunt-to-force calibration method.

(U) In addition to electrical calibrations, the two 100,000-pound lateral load cells and the 200,000-pound lateral load cell located between the aft thrust ring and the test bay rails were subjected to physical in-place calibrations. This was accomplished with a special flexured lateral calibration assembly consisting of a hydraulic press and a 200,000-pound standard calibration load cell with digital readout.

TABLE VII

INSTRUMENTATION CHART, MOTOR 156-6

MEASUREMENT				DATA ACQUISITION		
Type	Location	Identification	Calibration Range (units shown)	Type	Min Freq Resp (cps)	Miscellaneous
Force	Axial	F-1A	700,000	Digital*	200	
Force	Axial	F-1B	700,000	Oscillograph	60	
Force	Axial	F-2A	700,000	Digital	200	
Force	Axial	F-2B	700,000	Oscillograph	60	
Force	Axial	F-3A	700,000	Digital	200	
Force	Axial	F-3B	700,000	Oscillograph	60	
Force	Lateral (lower)	F-7A	50,000	Digital	200	
Force	Lateral	F-7B	50,000	Oscillograph	60	
Force	Lateral	F-8A	50,000	Digital	200	
Force	Lateral	F-8B	50,000	Oscillograph	60	
Force	Lateral (upper)	F-9A	200,000	Digital	200	
Force	Lateral	F-9B	200,000	Oscillograph	60	
Force	Lateral	F-10A	100,000	Digital	200	
Force	Lateral	F-10B	100,000	Oscillograph	60	
Force	Lateral	F-11A	100,000	Digital	200	
Force	Lateral	F-11B	100,000	Oscillograph	60	
Pressure tee to	Chamber, Fwd	PC-1	1,000	Digital	200	
Pressure	Chamber, Fwd	PC-2	1,000	Quick-look	60	Remote Control Bakr
Pressure	Chamber, Aft	PC-3	1,000	Digital	200	
Pressure tee to	Igniter	PC-4	1,500	Digital	200	
Pressure	Igniter	PC-5	1,500	Oscillograph	60	
Pressure tee to	Nozzle	PN-1A	250	Digital	200	
Pressure	Nozzle	PN-1B	250	Oscillograph	60	
Pressure tee to	Nozzle	PN-2A	250	Digital	200	
Pressure	Nozzle	PN-2B	250	Oscillograph	60	
Pressure tee to	Nozzle	PN-3A	250	Digital	200	
Pressure	Nozzle	PN-3B	250	Oscillograph	60	
Pressure tee to	Nozzle	PN-4A	250	Digital	200	
Pressure	Nozzle	PN-4B	250	Oscillograph	60	

* For force measurement data acquisition, digital system records all Bridge A of load cells, oscillograph measures all Bridge B.

TABLE VII

INSTRUMENTATION CHART, MOTOR 156-6 (Continued)

MEASUREMENT				DATA ACQUISITION		
Type	Location	Identification	Calibration Range (psi)	Type	Min Freq Resp (cps)	Miscellaneous
Pressure tee	N_2O_4 Manifold	PM-1A	1,000	Digital	200	
Pressure	N_2O_4 Manifold	PM-1B	1,000	Quick-look	60	Remote Control Bnkr
Pressure	N_2O_4 Manifold	PM-2	1,000	Digital	200	
Pressure	GN_2 Tank	PT-1	7,500	Oscillograph	60	
Pressure	GN_2 Tank	PT-2	7,500	Oscillograph	60	
Pressure tee	N_2O_4 Tank (GN_2 side)	PT-5A	1,000	Oscillograph	60	
Pressure	N_2O_4 Tank (GN_2 side)	PT-5B	1,000	Quick-look	60	Remote Control Bnkr
Pressure	N_2O_4 Tank (GN_2 side)	PT-6	1,000	Oscillograph	60	
Pressure	Hydraulic Manifold	PH-1	3,000	Quick-look	60	Remote Control Bnkr
Command Signal	Tape Programmer tee to	CS-P	----	Digital	20	Pitch
Command Signal	Tape Programmer	CS-P	----	Oscillograph	60	Pitch
Command Signal	Tape Programmer tee to	CS-Y	----	Digital	20	Yaw
Command Signal	Tape Programmer	CS-Y	----	Oscillograph	60	Yaw
Displacement	Injector Valves tee to	FB-1 through FB-24	----	(24) Digital	40	24 Channels
Displacement	Injector Valves	FB-1 through FB-24	----	(24) Oscillograph	60	24 Channels
Temperature	Motor Case	5 ea per Figure __	600°F	Digital	1	5 Channels
Temperature	Nozzle	5 ea per Figure __	600°F	Digital	1	5 Channels
Temperature tee to	N_2O_4 Manifold	TM-1, TM-2	-100 to +500°F	Digital	1	2 Channels
Temperature	GN_2 Tanks	TT-1, TT-2	-100 to +500°F	Digital	1	2 Channels
Temperature	N_2O_4 Tanks	TT-3, TT-4	-100 to +500°F	Digital	1	2 Channels
Strain	Motor Case	10 ea per Figure __	Hoop-0.01 in./in. Long. -0.002 in./in.	Oscillograph	60	10 Channels
Strain	Nozzle	10 ea per Figure __	Per Figure __	Oscillograph	60	10 Channels
Acceleration	TVC Components	3 ea per Figure 9	50G	Oscillograph	3KC	3 Channels
Acceleration	Nozzle	3 ea per Figure 13	50G	Oscillograph	3KC	3 Channels

NOTES:
Oscillograph paper speed 16 in./sec.
Retain same identification of parameters as indicated in Figures and this Chart.
Program for 70 seconds.
Note quick-look requirements for pressure readout in Remote Control Bunker. These include GO/NO-GO readouts.
Remote control of all systems at Remote Control Bunker.

(U) Pressure, temperature, strain, and vibration instrumentation locations are shown in Figures 11 and 12.

(U) The Teledyne pressure transducers used to measure chamber and nozzle pressures were calibrated electrically and physically using a certified dead-weight table.

(U) All strain gages were checked and calibrated by the electrical shunt method, using precision shunt resistors.

(U) The thermocouples were calibrated by applying known precision voltage which simulated different temperatures and recorded as calibration steps. The chromel-alumel thermocouples were calibrated through a 150°F reference junction, using a standard calibration chart.

(U) Motion picture coverage was obtained with eight cameras, one equipped with a 1200-foot reel to permit coverage of the entire test at higher frame speeds. In addition, still cameras placed at strategic locations were sequenced to take pictures during the firing.

(U) (2) Data Acquisition. Four 36-channel oscillographs and an 80-channel DDAS were utilized for this test.

(U) The Beckman 210 system consists of two commutated subsystems. One subsystem is a 40-data channel, low-level (millivolts) multiplexer section with 3 time-shared amplifiers. The other subsystem is a 15-data channel, high-level section with 10 channels, having an amplifier for each channel and 5 channels for direct voltage signal inputs (no system amplification for these channels). All the amplifiers have fixed gain positions of ±10, ±30, ±50, and ±100 millivolts, full-scale. A block diagram of the DDAS is shown in Figure 13.

(U) Commutation of switching for the 55 channels of the DDAS is at a fixed rate of 15,625 samples or data points per second. By means of a digital program patchboard, the total system sampling rate of 15,625 samples per second may be distributed in various combinations of "rates per channel" per group among the 55 commutated data channels in four groups to be identified as sequencers A, B, C, and D, but with these programming limitations: (1) the sampling assignments or "rates per channel" per sequencer group determines the "sampling rate per channel" for the remainder of channels in the respective group; (2) the summation of samples per second of the four groups cannot exceed 15,625 samples or data points; and (3) 20-to-1 is the maximum ratio between the highest "sampling rate per channel" in a group and the lowest "sampling rate per channel" of any other group that can be programmed. In other words, if 1000 samples per second is assigned to Group D, then the least sampling rate of any other sequencer group (A, B or C) cannot be less than 50 samples per second per channel.

(U) In addition to the 55 channels of commutation capability in the DDAS, a 30-channel subcommutating network patchable into any one of the low-level multiplexer channels is available which will provide 30 data channels with a

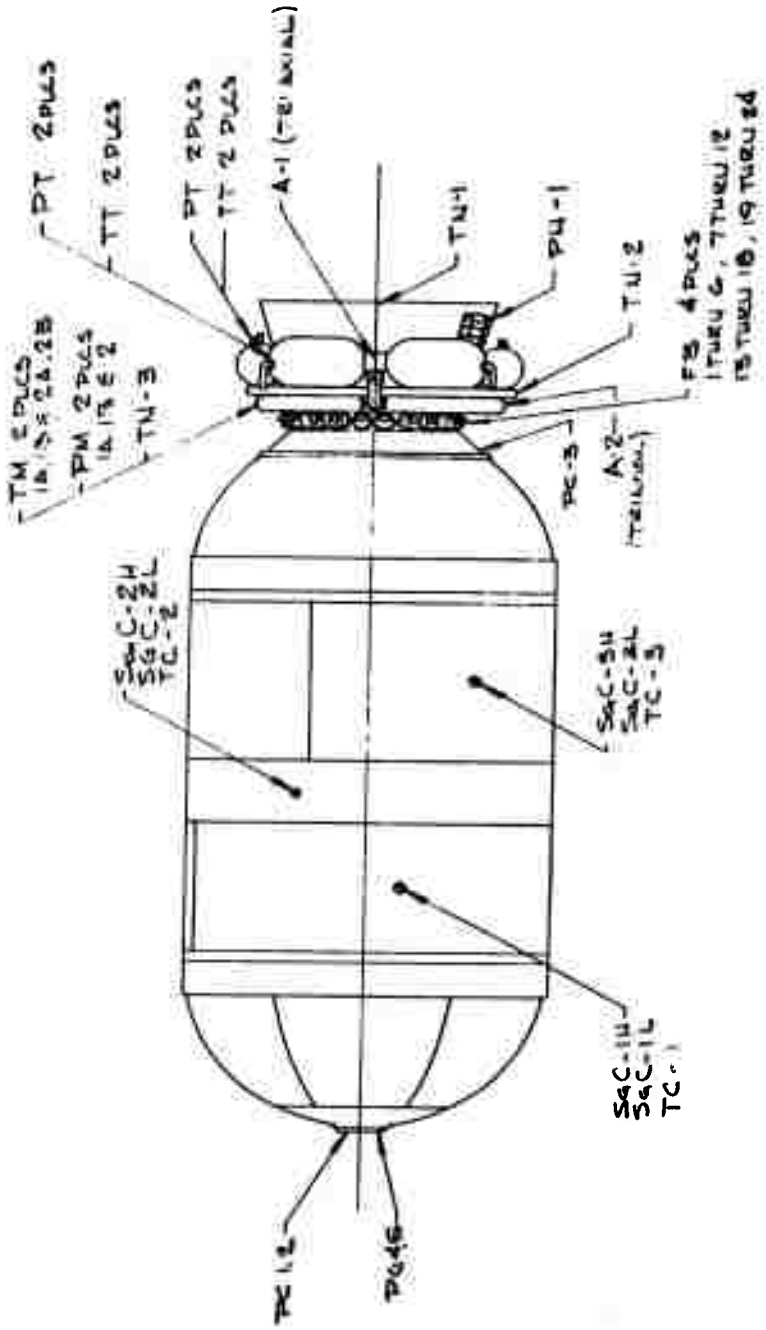

Figure 11 Motor Case Instrumentation Locations, Motor 156-6

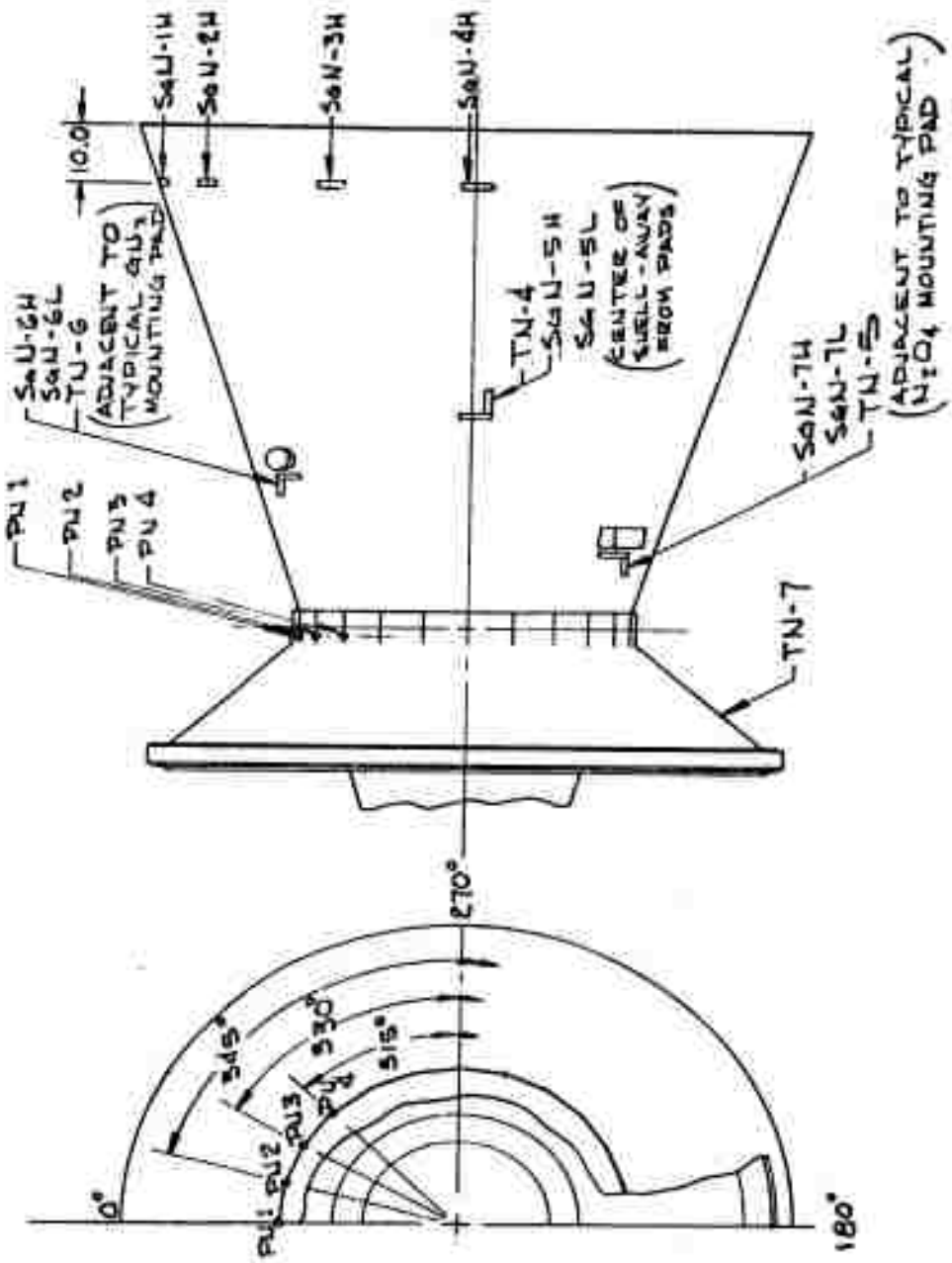

Figure 12 Nozzle Instrumentation Locations, Motor 156-6

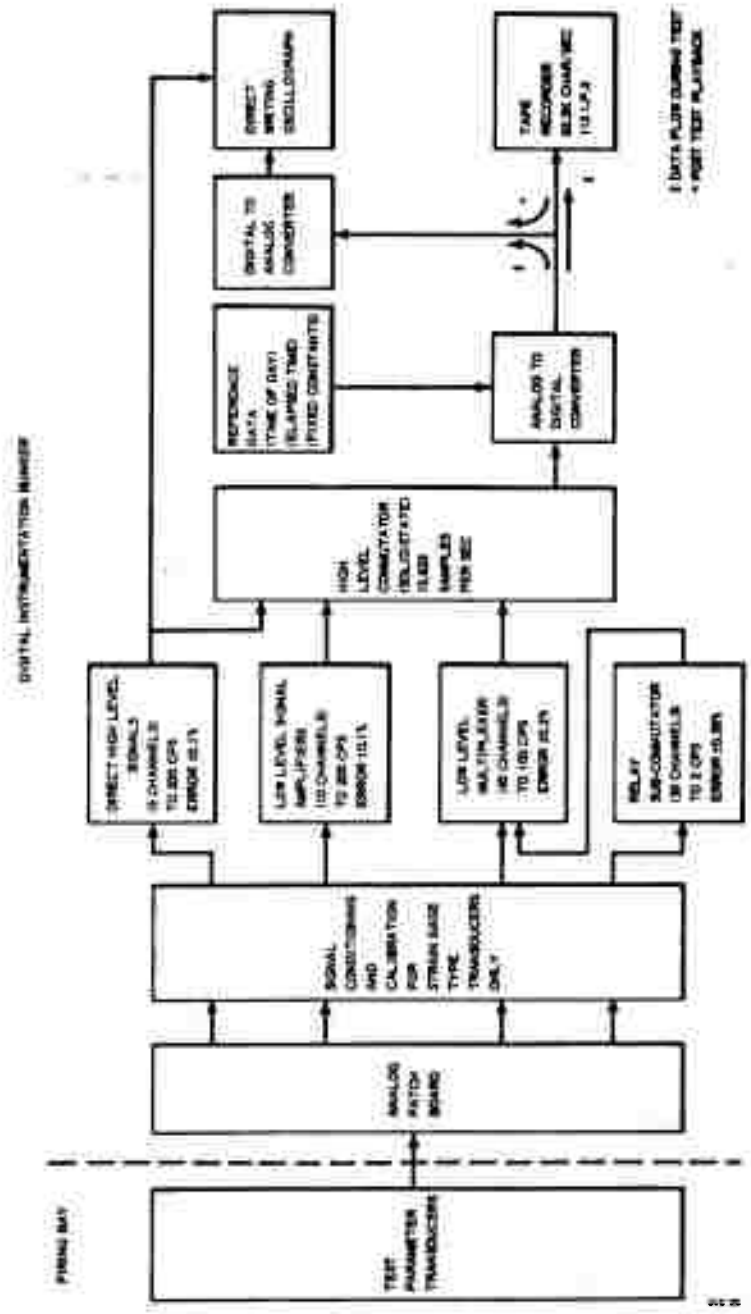

Figure 13 Block Diagram of Digital Data Acquisition System, Motor 156-6

sampling rate of 5 samples per second per channel. Also, the subcommutation sampling rate per channel can be increased (maximum 20 samples per second) by cross-strapping the 30 channels to a lesser number of total channels.

(U) To provide acceptable time correlation between digitized data parameters and motor firing time, a time data channel which provides accumulated-time information from actual motor firing time (t_o) was recorded continuously with the digitized data to a resolution of 100 microseconds.

(U) (3) Data Reduction. Test parameters recorded by the Beckman digital data acquisition system were sampled, converted to a numerical count, and recorded serially in binary-coded decimal form on magnetic tape.

(U) The tape recorded during the firing and the tape recorded during the calibration procedure were played on the computer (IBM 360) which converted the data to engineering untis by application of calibration constants. Physically-measured parameters (e.g., propellant weight, atmospheric pressure, temperature) were tabulated, keypunched, and entered in the computer, along with appropriate times and integrals to calculate motor ballistics.

(U) The data recorded on the digital system were returned to the Redlands Facility for reduction, using the IBM 360 Computer, and the required output was automatically plotted and printed.

(U) The output of the digital reduction program is itemized in Appendix I. Definitions and symbols of ballistic parameters are presented in Appendix II.

SECTION V

TEST RESULTS AND ANALYSIS

(U) Ambient temperatures, pressure, and relative humidity were 56°F, 13.7 psia, and 50 percent, respectively, at the time of motor test firing. Skies were clear, and visibility was unlimited.

(C) 1. Internal Ballistic Performance

(C) a. Motor Performance. Motor 156-6 delivered a total impulse of 64,451,000 lb-sec. An average thrust of 964,000 pounds and an average forward chamber pressure of 664 psia were measured over a burning time of 65.00 seconds. The maximum thrust and pressure were 1,025,000 pounds and 692 psia, respectively. Specific impulse delivered during burn time was 236.4 lb-sec/lb. The standard* specific impulse was 245.5 lb-sec/lb. (See Appendix I for ballistic nomenclature.)

(U) The forward chamber pressure versus time curve is shown in Figure 14. Axial thrust versus time curves for axial thrust corrected for propellant weight expended, and axial thrust corrected for TVC augmentation are presented in Figures 15 and 16, respectively.

(U) Curves of calculated propellant weight expended versus time and instantaneous throat area versus time are presented in Figures 17 and 18, respectively. (Methods of calculation are described in Appendix II.)

(C) b. Comparison of Predicted and Measured Data. A comparison of predicted and measured parameters for Motor 156-6 is presented in Table VIII. A comparison of measured data and program objectives is presented in Table IX. There was excellent agreement between predicted and measured data for all significant performance parameters.

(C) The greatest over-all performance deviations occurred between predicted and measured tail-off parameters. The magnitude of propellant expended during the tail-off phase was much less than expected. This is exemplified by measured tail-off impulse, which was 44 percent less than predicted. Another indicator was action time, which was 2.4 percent less than expected while burn time was only 0.6 percent less than expected.

(C) The performance prediction parameters of characteristic exhaust velocity (c^*) and over-all nozzle efficiency varied from their respective design values by -2.06 percent and +0.84 percent, respectively. These variations are attributed to the use of empirical data for a higher throat-to-port ratio subscale motor to select design values for Motor 156-6.

* Standard conditions: sea level, optimum expansion, 1000 psia chamber pressure, and 15-degree half angle.

PREVIOUS PAGE WAS BLANK, THEREFORE NOT FILMED.

CONFIDENTIAL

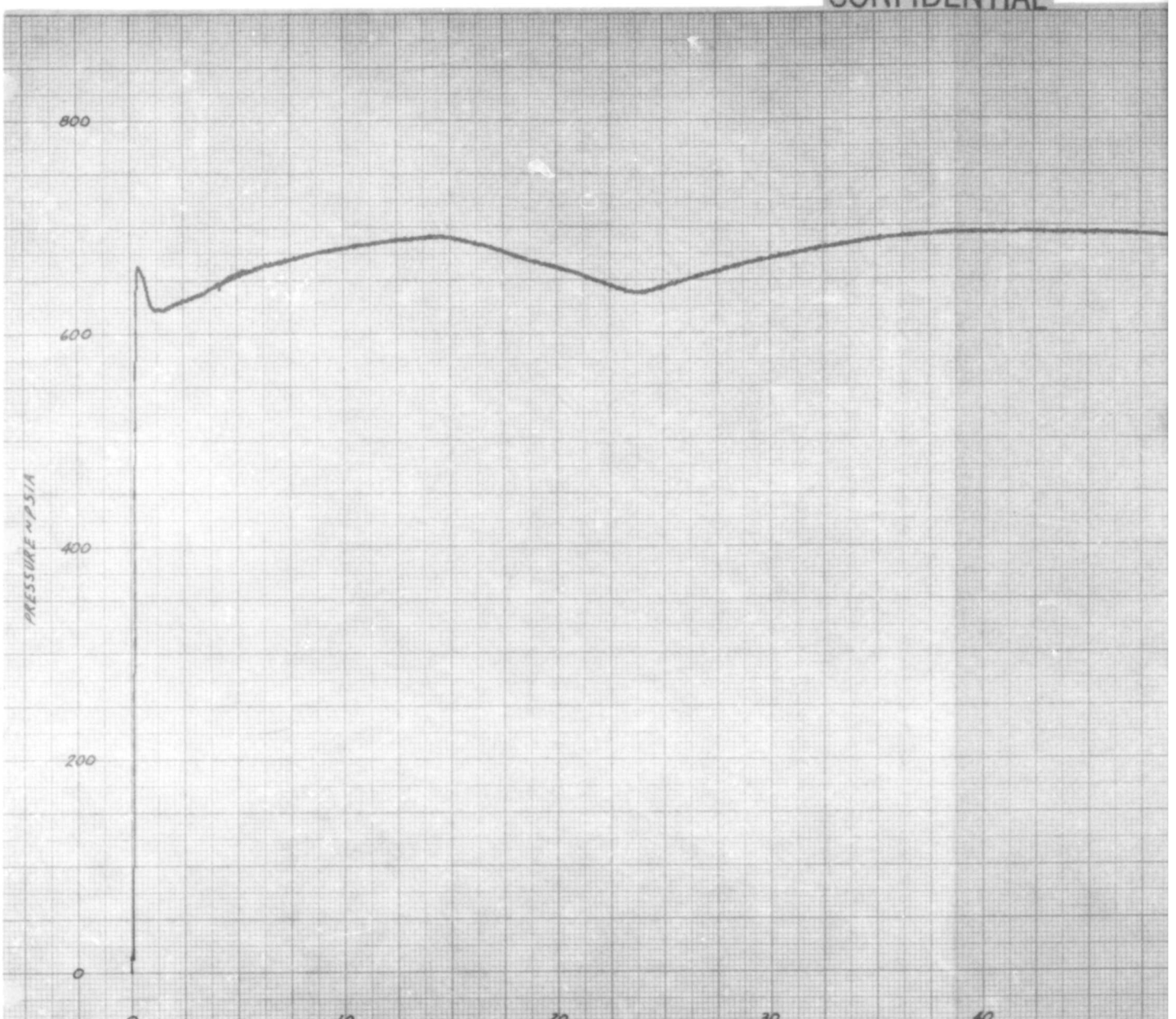

CONFIDENTIAL

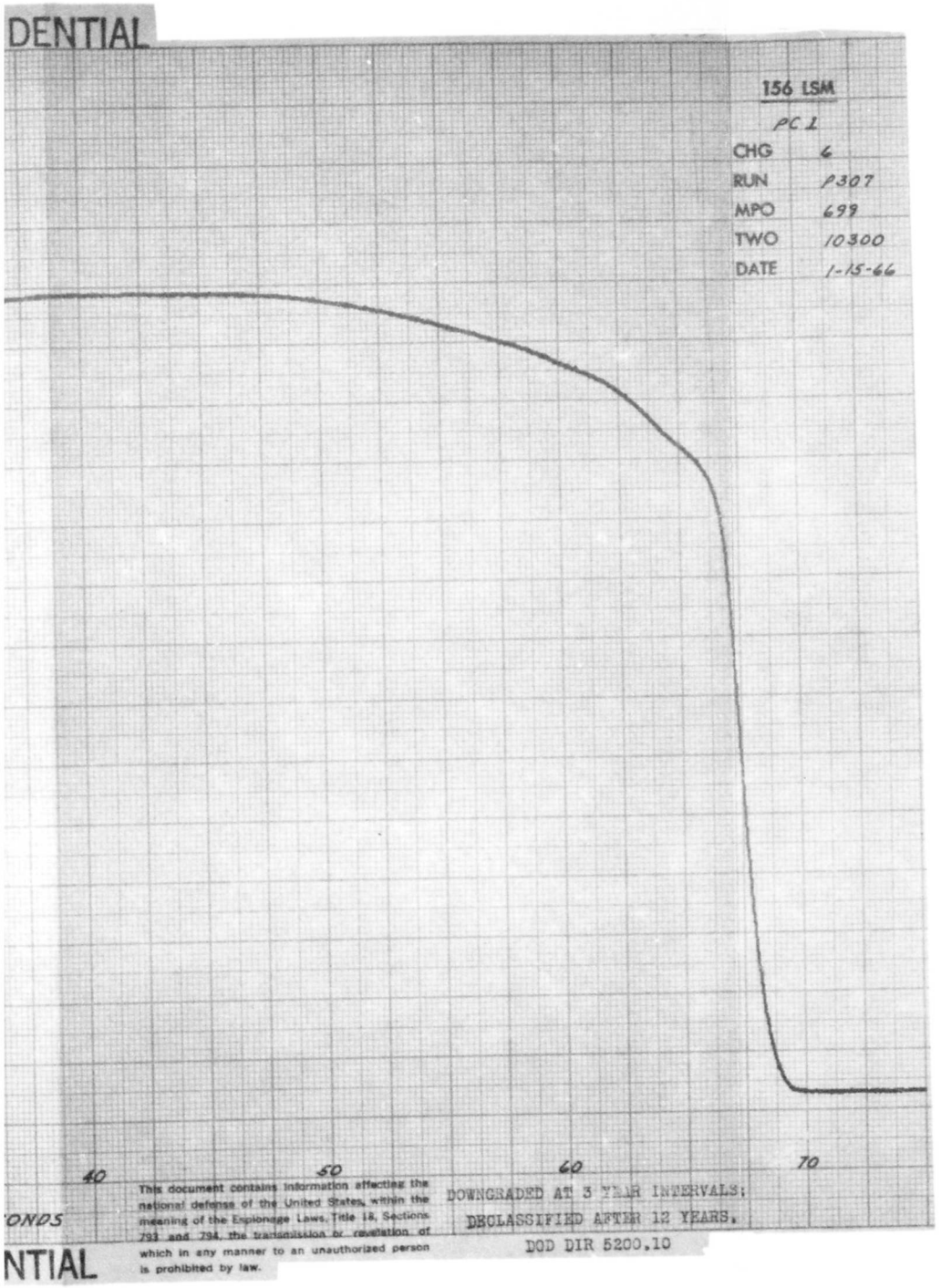

Figure 14 Forward Chamber Pressure versus Time, Motor 156-6

PREVIOUS PAGE WAS BLANK, THEREFORE NOT FILMED.

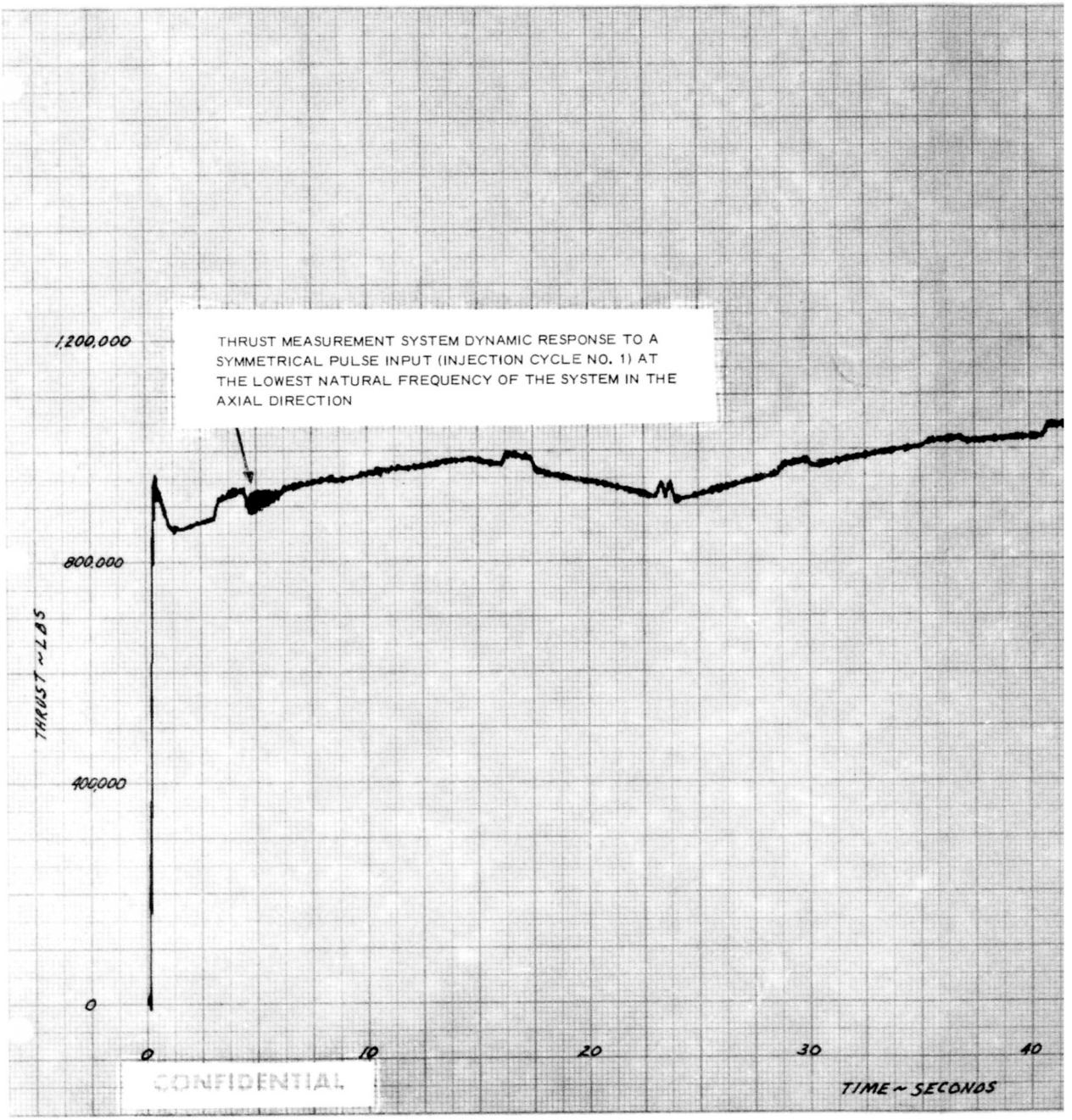

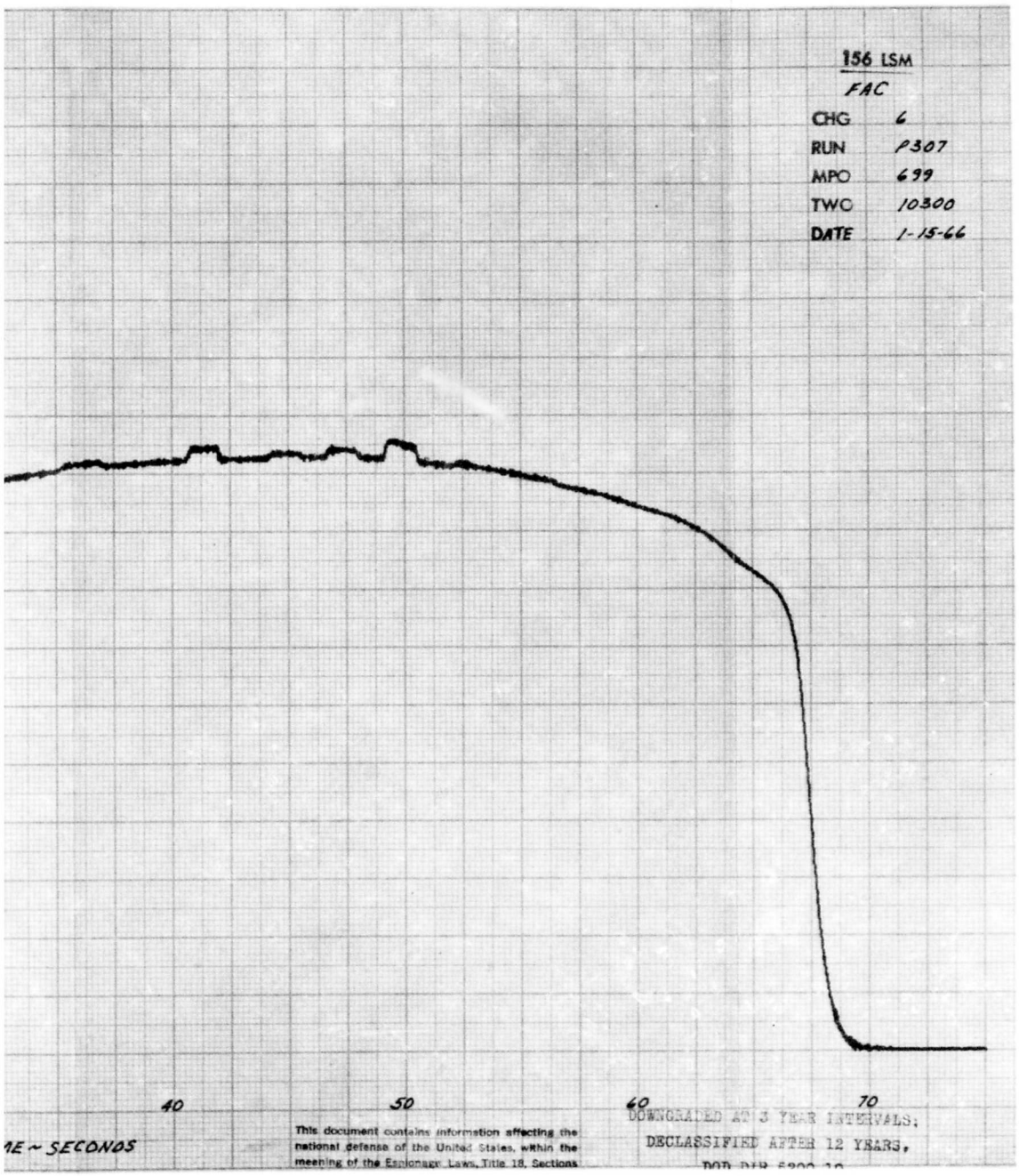

Figure 15 Axial Thrust versus Time, Corrected for Propellant Weight Expended, Motor 156-6

PREVIOUS PAGE WAS BLANK, THEREFORE NOT FILMED.

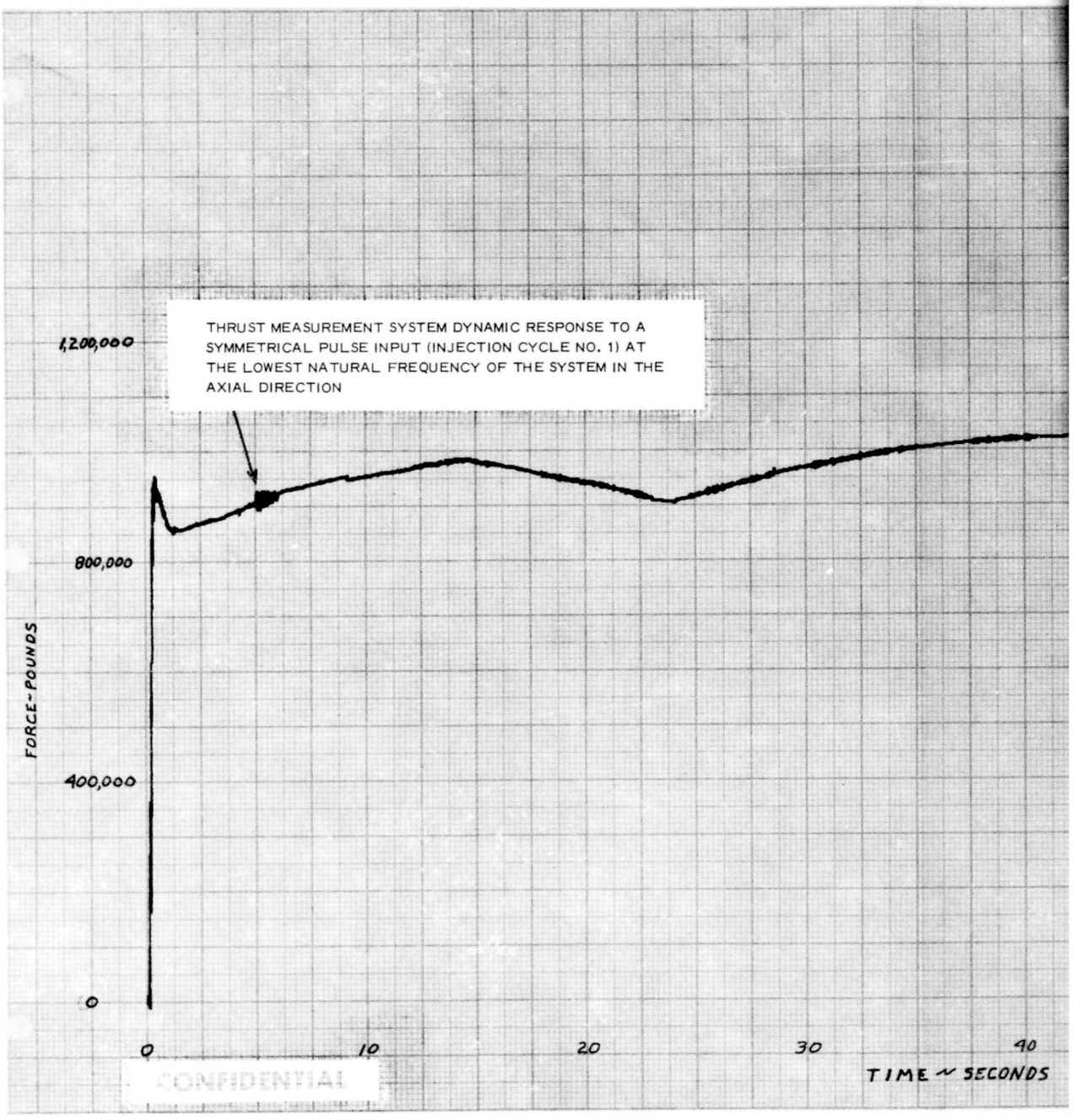

1

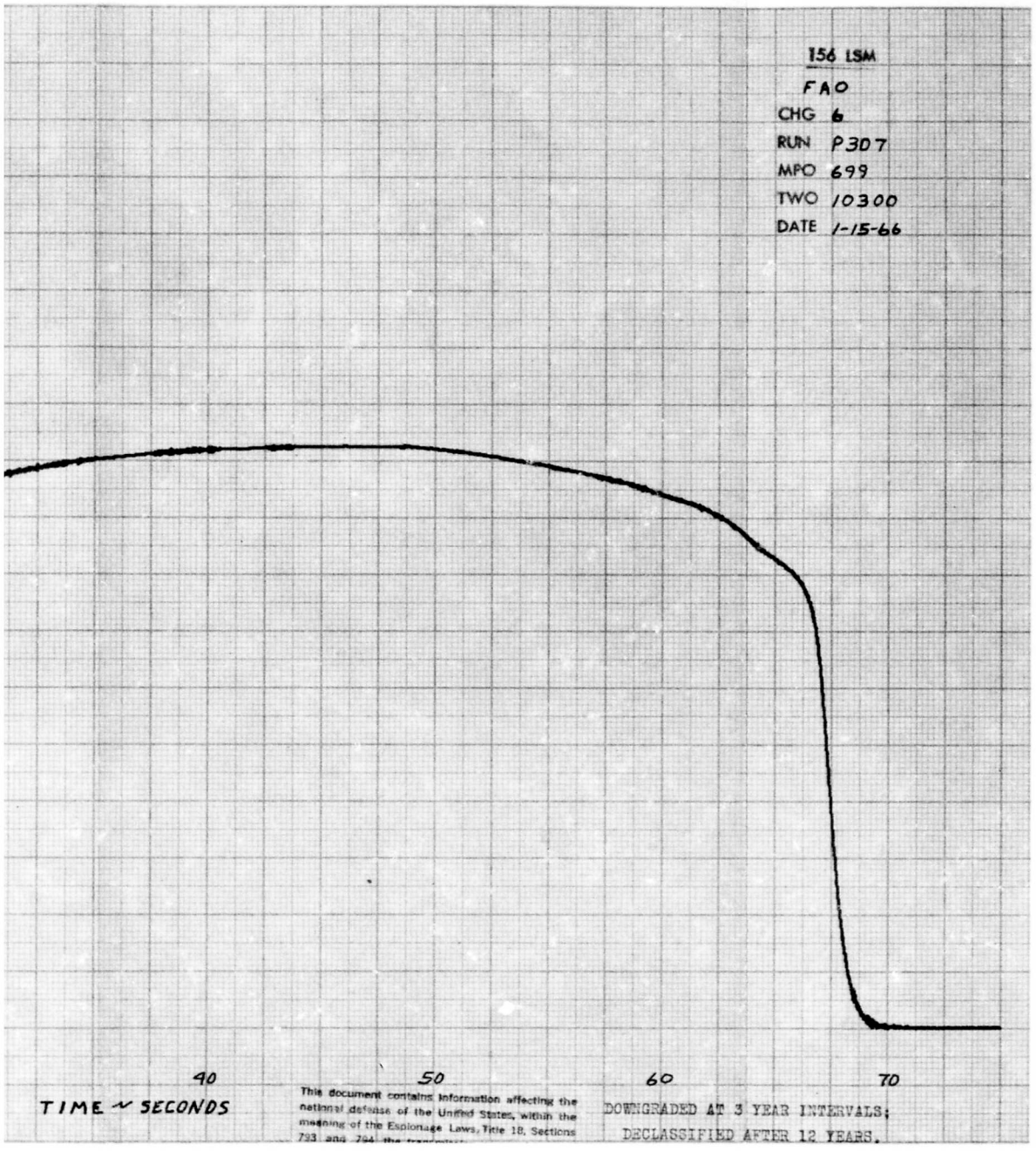

2

Figure 16 Axial Thrust versus Time, Corrected for TVC Augmentation, Motor 156-6

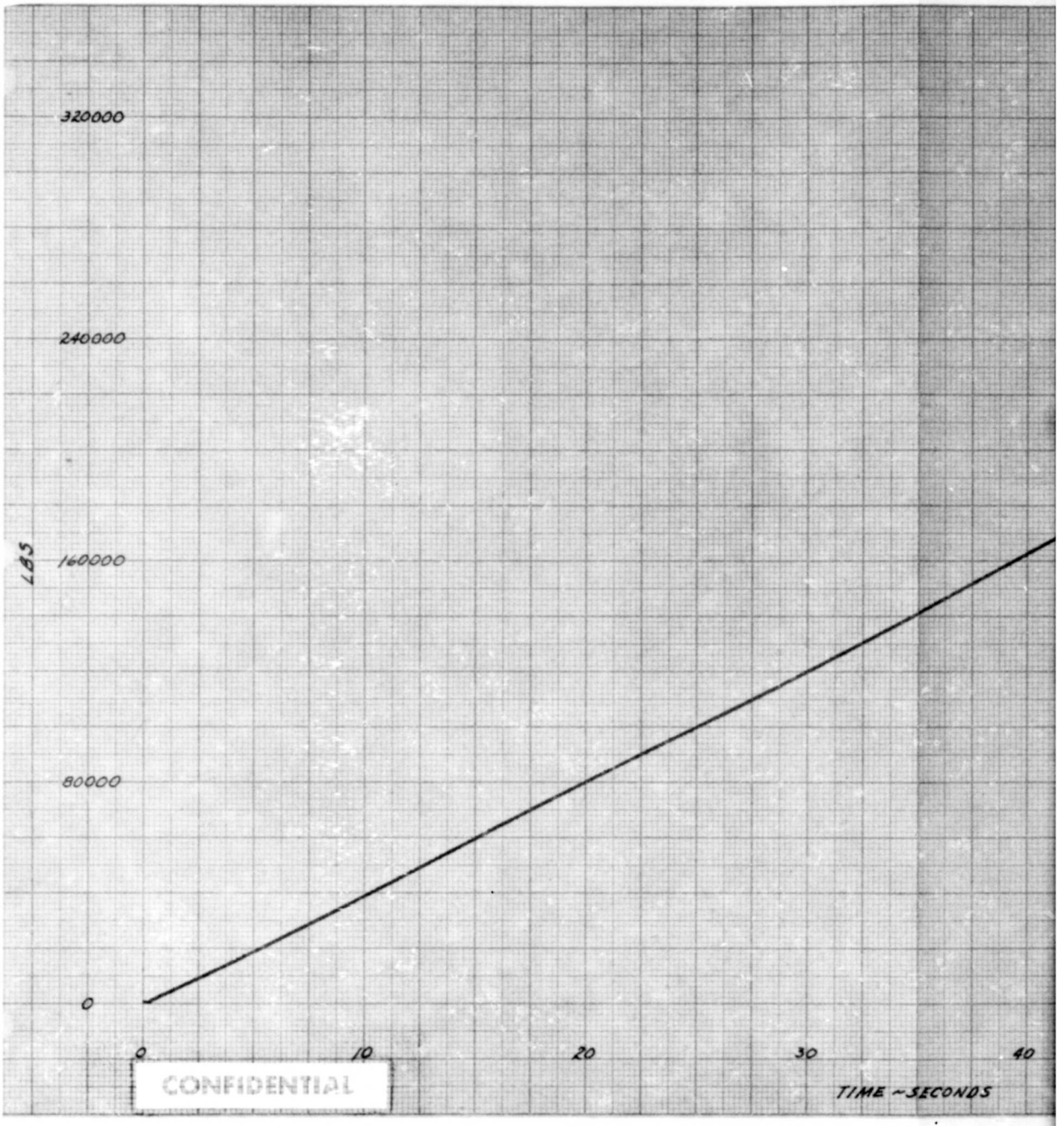

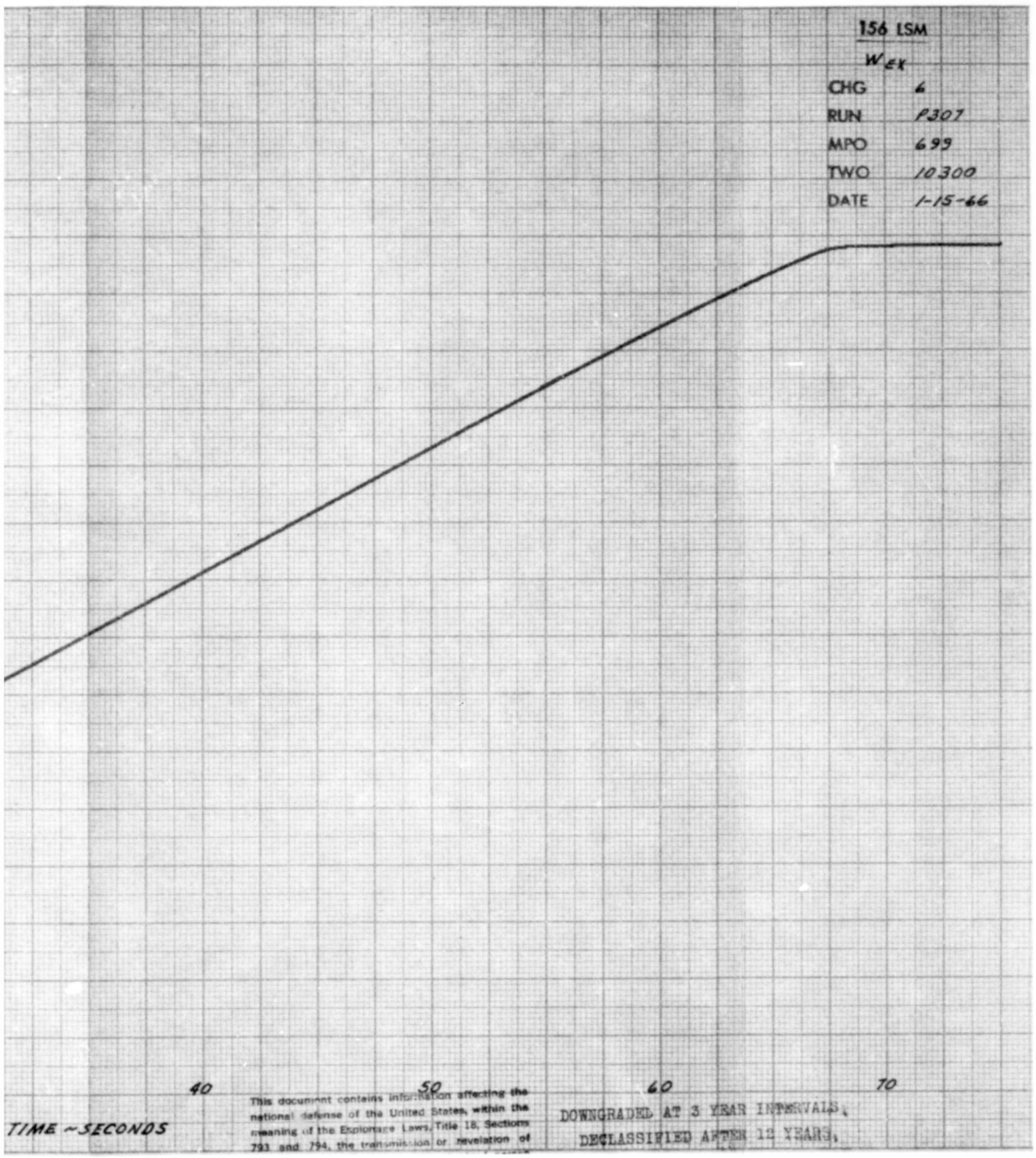

Figure 17 Propellant Weight Expended versus Time, Motor 156-6

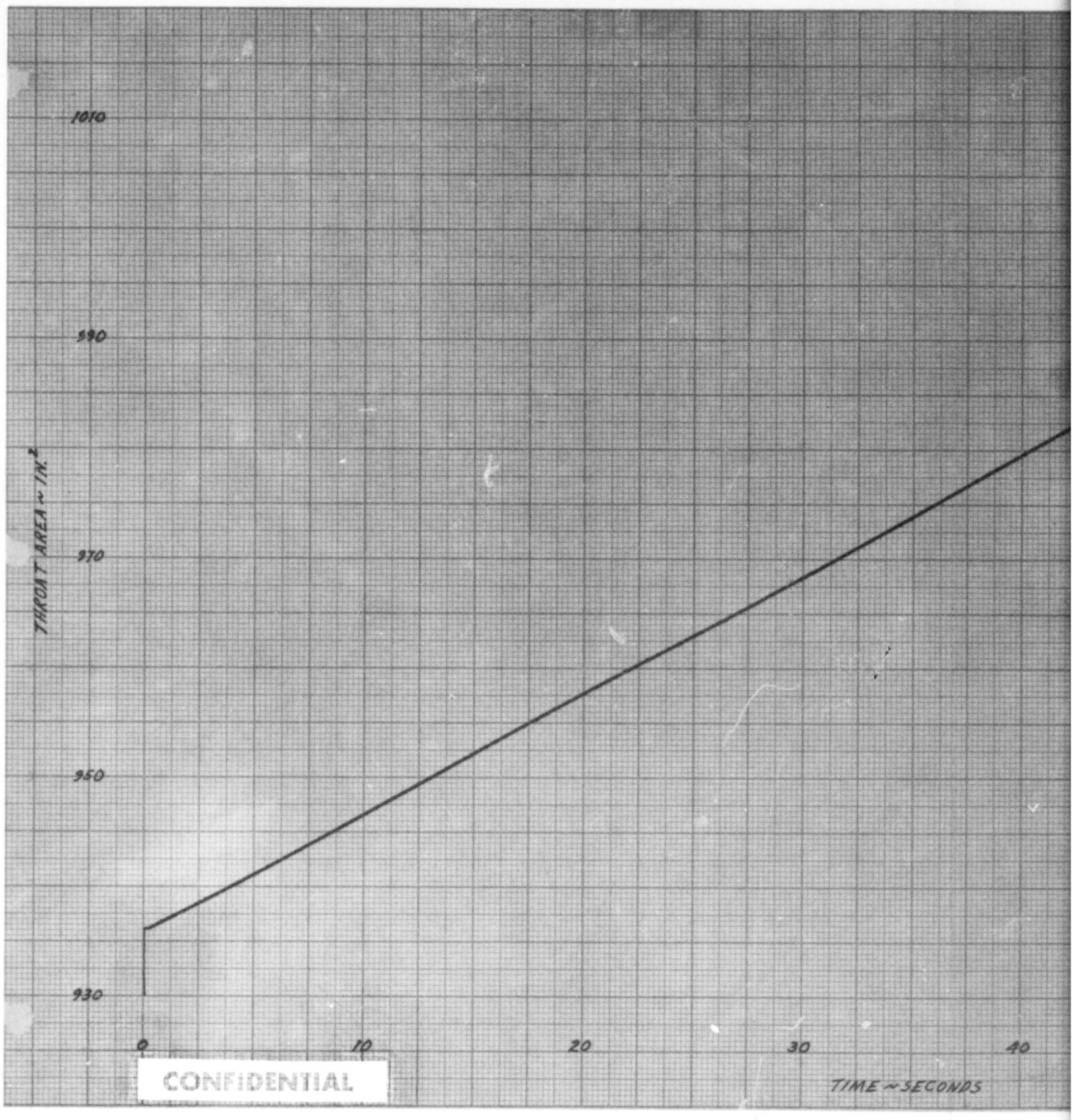

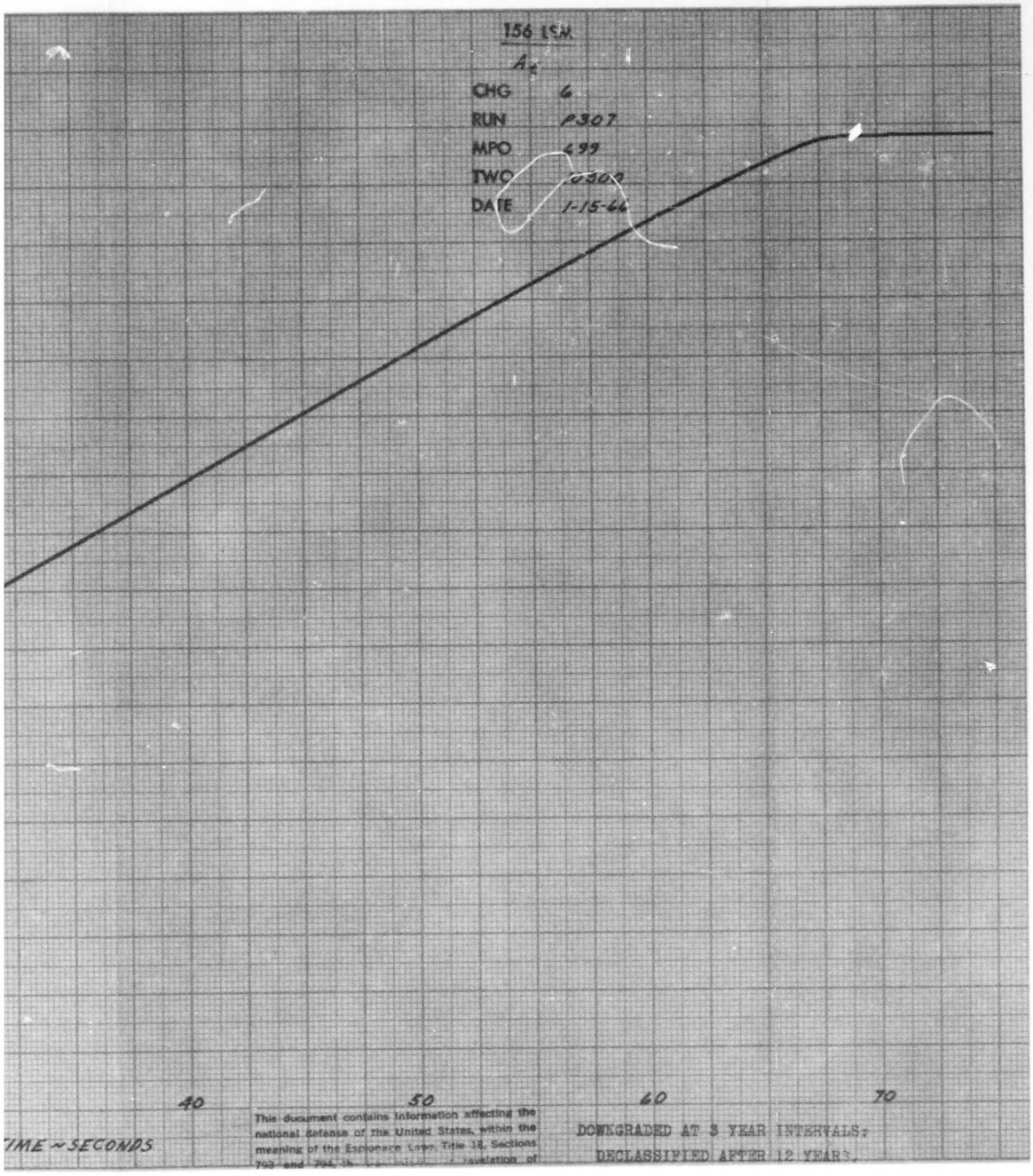

Figure 18 Throat Area versus Time, Motor 156-6

TABLE VIII

BALLISTIC PERFORMANCE AND CHARACTERISTICS, MOTOR 156-6

Performance Prediction Parameters	Predicted	Measured	Percentage of Variation $\frac{M-P}{P} \times 100$
Ratio of specific heats	1.17	--	
Propellant density (lb/in.^{3})	0.0645	0.0649	+0.62
Burn rate at 1000 psi, 70°F (in./sec)	0.816	0.837	+2.57
Burn rate slope	0.30	--	
Characteristic exhaust velocity (ft/sec)	5,200	5,093	-2.06
Motor Characteristics			
Average burning area (in.^{2})	85,050	--	
Propellant port diameter (in.)	55.39	--	
Port-to-throat ratio	2.57	--	
Propellant web (in.)	49.4	--	
Propellant weight (lb)	272,884	--	
Average throat area (in.^{2})	979.8	972.37	-0.76
Average throat diameter (in.)	35.32	35.19	-0.37
Initial throat area (in.^{2})	936.4	--	
Initial throat diameter (in.)	34.53	--	
Nozzle throat ablation rate (mil/sec)	11	9.9	-10
Initial exit area (in.^{2})	7,639	--	
Initial exit diameter (in.)	98.62	--	
Average expansion ratio	7.80	7.86	+0.77
Divergence half angle (deg)	17.5	--	
Performance			
Grain temperature (°F)	70	--	
Ambient pressure (psia)	13.7	13.7	
Burn time (sec)	65.37	65.00	-0.57
Action time (sec)	70.00	68.33	-2.39
Burn time average pressure (psia)	655	664	+1.37
Action time average pressure (psia)	639	650	+1.72
Maximum pressure (psia)	689	692	+0.44
Burn time average thrust (lb)	947,000	964,000	+1.80
Action time average thrust (lb)	925,000	943,000	+1.95
Maximum thrust (lb)	1,018,000	1,025,000	+0.69
Total impulse (lb/sec)	65,157,000	64,451,000	-1.08
Tail-off impulse (lb/sec)	3,270,000	1,820,000	-44.34
Nozzle efficiency, over-all	0.946	0.954	+0.84
Theoretical thrust coefficient	1.564	1.565	+0.06
Average burn rate during burn time (in./sec)*	0.718	0.739	+2.92
TVC Performance			
Maximum deflection angle (deg)*	5.03	4.35	-13.5
Maximum side force (lb)*	77,200	67,300	-12.8
Total side impulse (lb-sec)	684,100	646,100	-5.6
Ratio: $\frac{\text{side impulse}}{\text{axial impulse}}$ (%)	1.05	1.03	-1.9
Total injectant expelled (lb)	2,855	2,890	+1.2
Maximum injectant flow rate (lb/sec)*	382	351	-8.1

* Duty Cycle No. 1

TABLE IX

COMPARISON OF MEASURED DATA AND PROGRAM PERFORMANCE OBJECTIVES, MOTOR 156-6

	Objective	Measured
Burning time average thrust, 70°F and sea level (lb)	1,000,000 (nominal)	956,000
Action time, 70°F (sec)	70 (maximum)	68.33
Total impulse, 70°F and sea level (lb-sec)	65,000,000 (minimum)	63,920,000
Tail-off impulse, 70°F and sea level, 8% of total impulse, maximum (lb-sec)	5,200,000 (maximum)	1,785,000

(C) c. Pressure Curve Profile Comparison. To obtain a profile comparison, the predicted pressure versus time curve was normalized to account for differences between the measured and predicted average pressures and burning times. The comparison of the normalized predicted curve and the measured curve is shown in Figure 19.

(C) The predicted and measured curves deviated significantly in three areas. The first area is between t = 5 and t = 20 seconds during burning of the small aft-end grain, when measured pressure was higher than predicted. The maximum deviation was 20 psi (3 percent) and occurred at t = 14 seconds. The second area is defined by the burnout of the small aft grain. The measured burn-out time was t = 24 seconds; the predicted value was at t = 25 seconds. This deviation in time offset the two curves so that predicted pressure was lower than measured pressure from t = 25 to t = 38 seconds. The maximum deviation occurred initially and had a value of 13 psi (2.1 percent). Comparing burn-out pressure levels only, the deviation was 6 psi (1 percent). The largest deviation occurred in the third area, from t = 40 seconds to web burnout. The measured pressure started falling below the predicted level at t = 40 seconds and reached a maximum value at web burnout of 68 psia, a deviation of 11.5 percent.

(C) The effect of a radial temperature gradient was investigated to attempt a reconcilement of the measured and predicted curve profiles. The estimated radial temperature-gradient for Motor 156-6 at the time of firing is shown in Figure 20. This gradient shows a grain port temperature of 92°F and a terminal, or maximum, outer-diameter temperature of 52°F. Adjusting the predicted curve by considering the effects of this gradient would result in the following:

(1) The initial predicted level (from t = 1 to t = 3 seconds) would increase by 2.4 percent, or an average of about 15 psi. However, the predicted and measured curves already agree for this duration.

(2) For the maximum deviation during burning of the small aft grain (t = 14 seconds), the temperature effect (T = 14°F) would account for 2.3 percent (15 psi) of the indicated 20-psi difference.

(3) The average grain temperature to the time of small aft-grain burnout (t = 24 seconds) was estimated to be 88°F. This temperature would result in a time difference of 2 percent (0.5 second) between predicted and measured duration.

(4) The maximum temperature effect occurred at web burnout, when a temperature differential of 24°F was noted. This would account for only 3.7 percent (21 psi) of the indicated 68-psi difference.

(U) With the exception of item (1), the estimated radial temperature gradient would tend to explain the differences between the predicted and measured pressure curves. On a quantitative basis, items (2) and (3) are accounted for within experimental accuracy. Item (4) is only partially explained; however, its trend is in the proper direction.

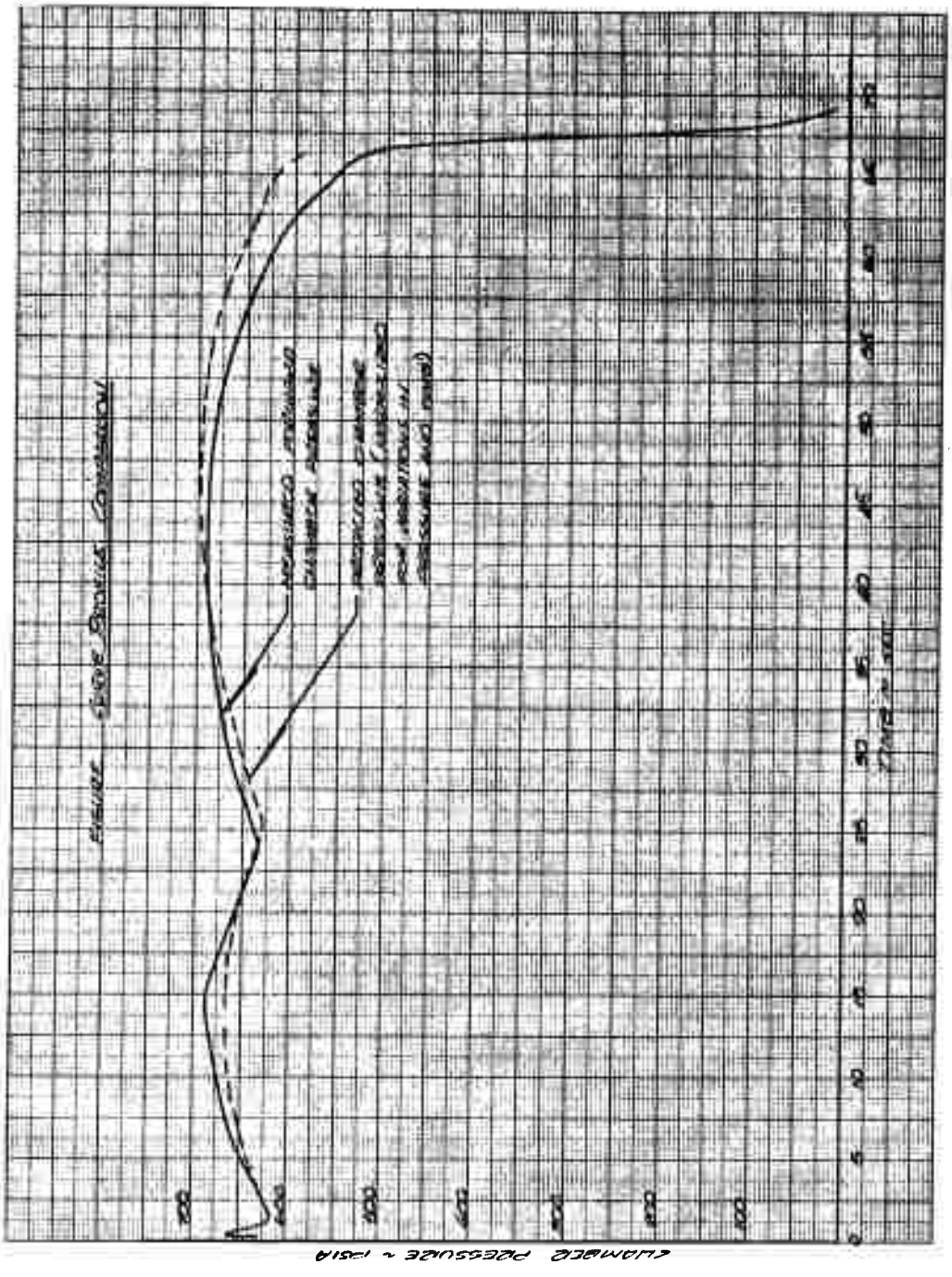

Figure 19 Measured and Predicted Chamber Pressure, Curve Profile Comparison, Motor 156-6

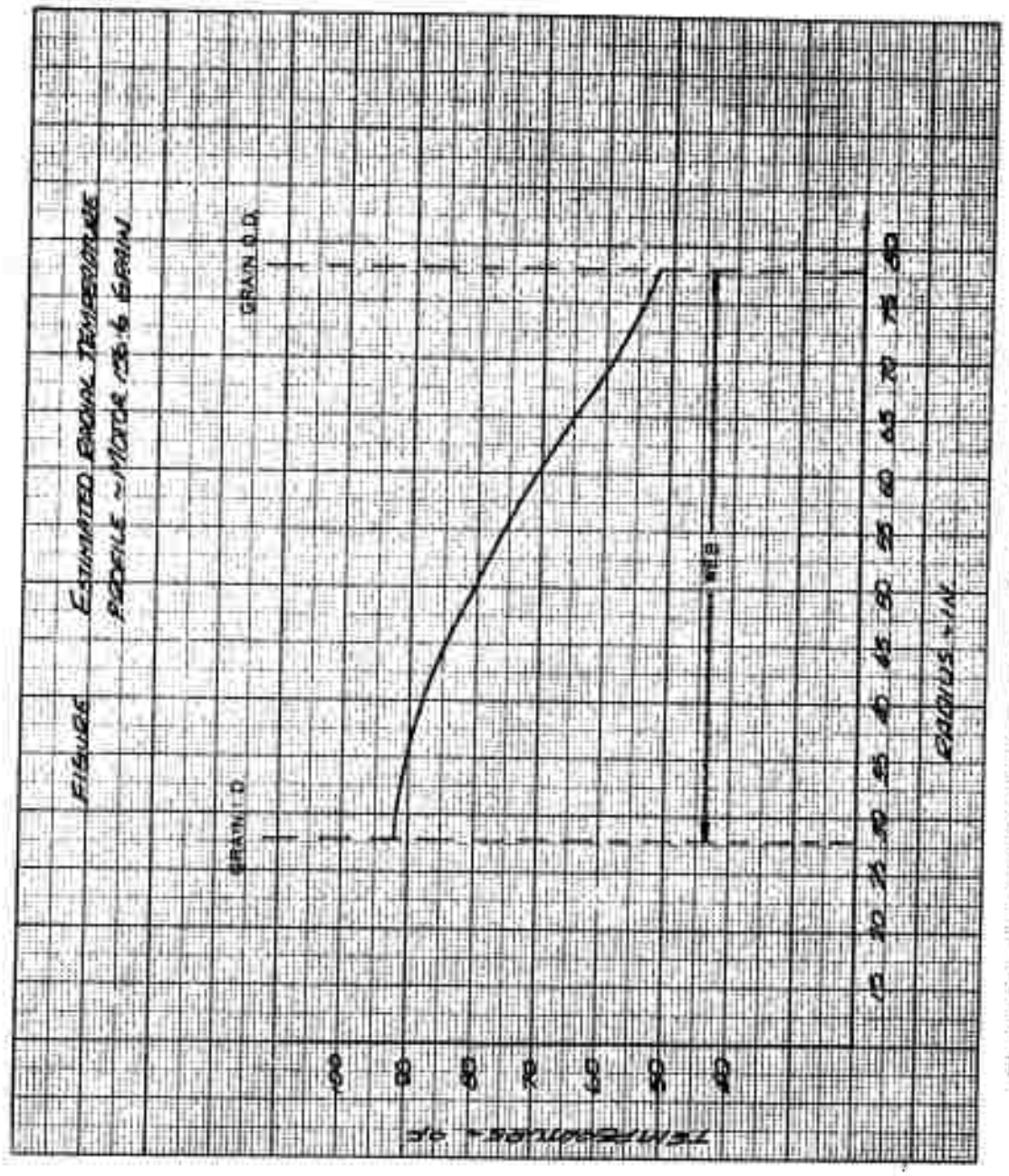

Figure 20 Estimated Radial Temperature Profile, Motor 156-6 Propellant Grain

(U) Additional factors were considered which could contribute to the measured and predicted curve profile deviations. These factors, including inaccuracies in calculating burning surfaces and the effects of transient phenomena, are discussed below.

(U) As seen from subsection III 1.c, the as-built grain geometry varies somewhat from a symmetrical configuration. In fact, the port is slightly conical in shape instead of cylindrical. For this particular type of variation, the effect would be to increase initial burning area and to decrease final burning area due to nonuniform web burnout. It appears probable that a rigorous determination of burning surfaces from the as-built grain geometry would provide a closer reconcilement of predicted and measured curves.

(U) The second factor is offered as a possible qualitative explanation of the initial portion of the firing (t = 1 to t = 5 seconds) in which indications point to a lower-than-expected measured pressure with regard to temperature effects and burning-surface inaccuracies. It is probable that the transition between the ignition phase and equilibrium burning could last longer than predicted.

(C) d. Aft-To-Forward End Pressure Relation. A pressure tap was located in the nozzle flange to monitor chamber pressure in the cavity formed by the motor case and the submerged portion of the nozzle. The pressure recorded at this location is shown in Figure 21.

(U) For the initial 6 seconds of the firing, the aft cavity pressure tap was plugged, and no data were recorded. The missing data were extrapolated from hoop strain measurements taken from a gage located on the cylindrical portion of the motor chamber near its aft end. These data were used in the comparisons discussed below.

(U) The ratio of aft-end pressure-to-forward-end pressure versus time is plotted in Figure 22. This same ratio is plotted against throat-to-port ratio (J) in Figure 23, where J was determined from the estimated throat area profile and port area calculated from measured chamber pressure and burning rate relationships.

(U) The one-dimensional flow relationships developed by Price for mass addition were compared with the measured pressure ratio in Figure 23. These relationships include the ratio of stagnation pressure to forward-end pressure (P_s/P_o) and static pressure to forward-end pressure (P/P_o). This comparison shows agreement within 1 percent between theoretical ratio of stagnation-to-forward-end pressure (P_s/P_o), and the measured aft-to-forward-end pressure ratio.

CONFIDENTIAL

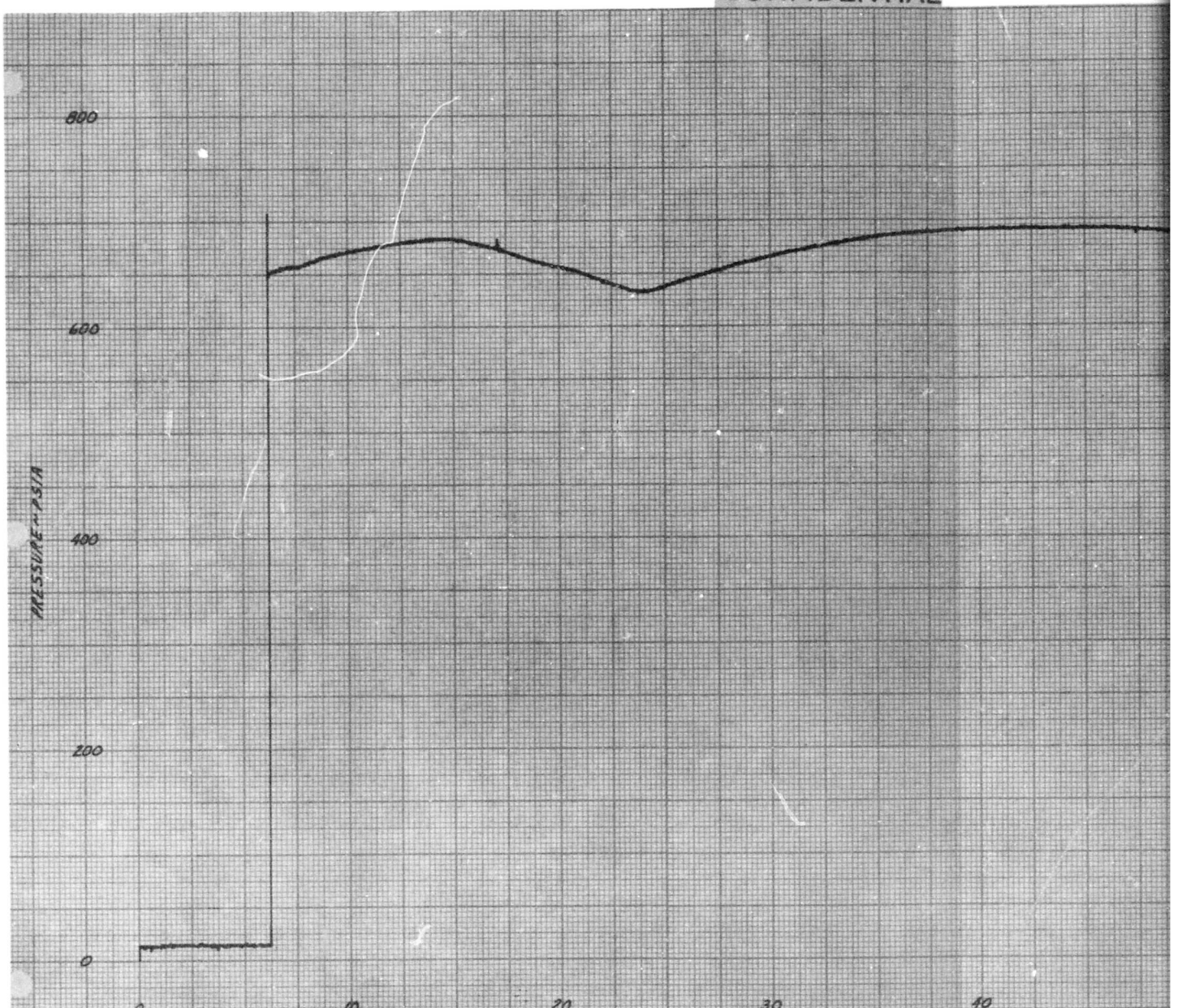

CONFIDENTIAL

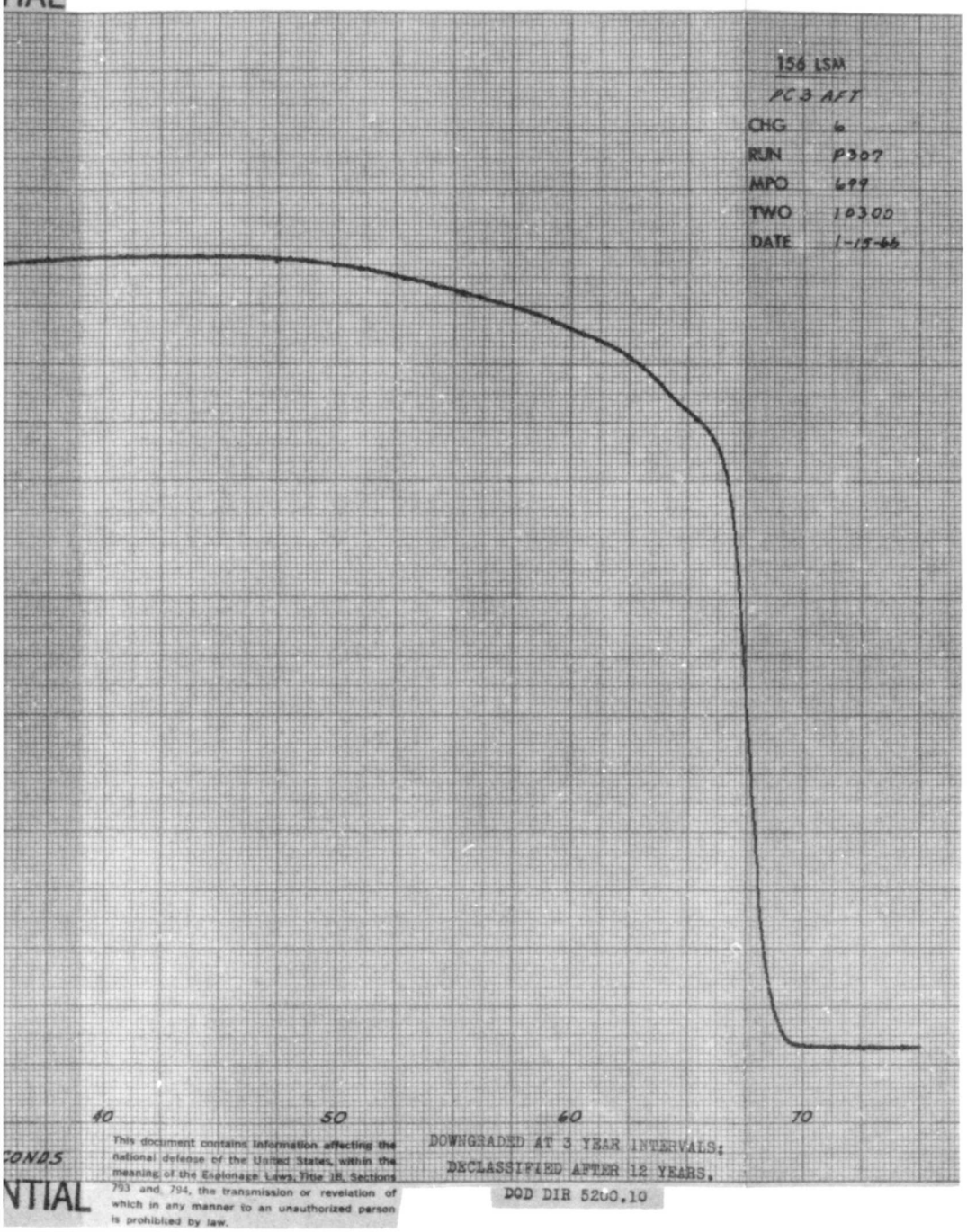

Figure 21 Aft Chamber Pressure versus Time, Motor 156-6

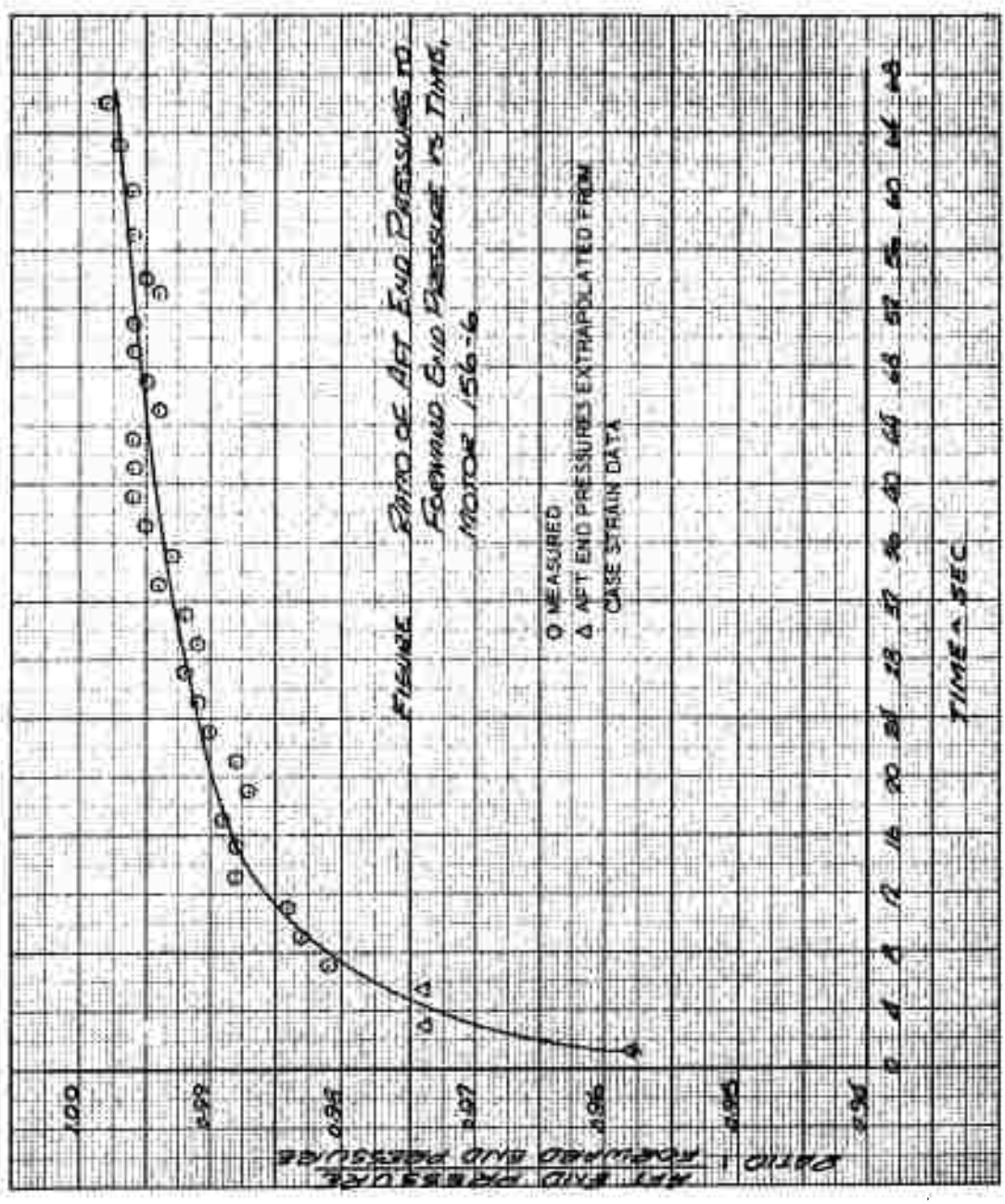

Figure 22 Ratio of Aft End Pressure to Forward End Pressure versus Time, Motor 156-6

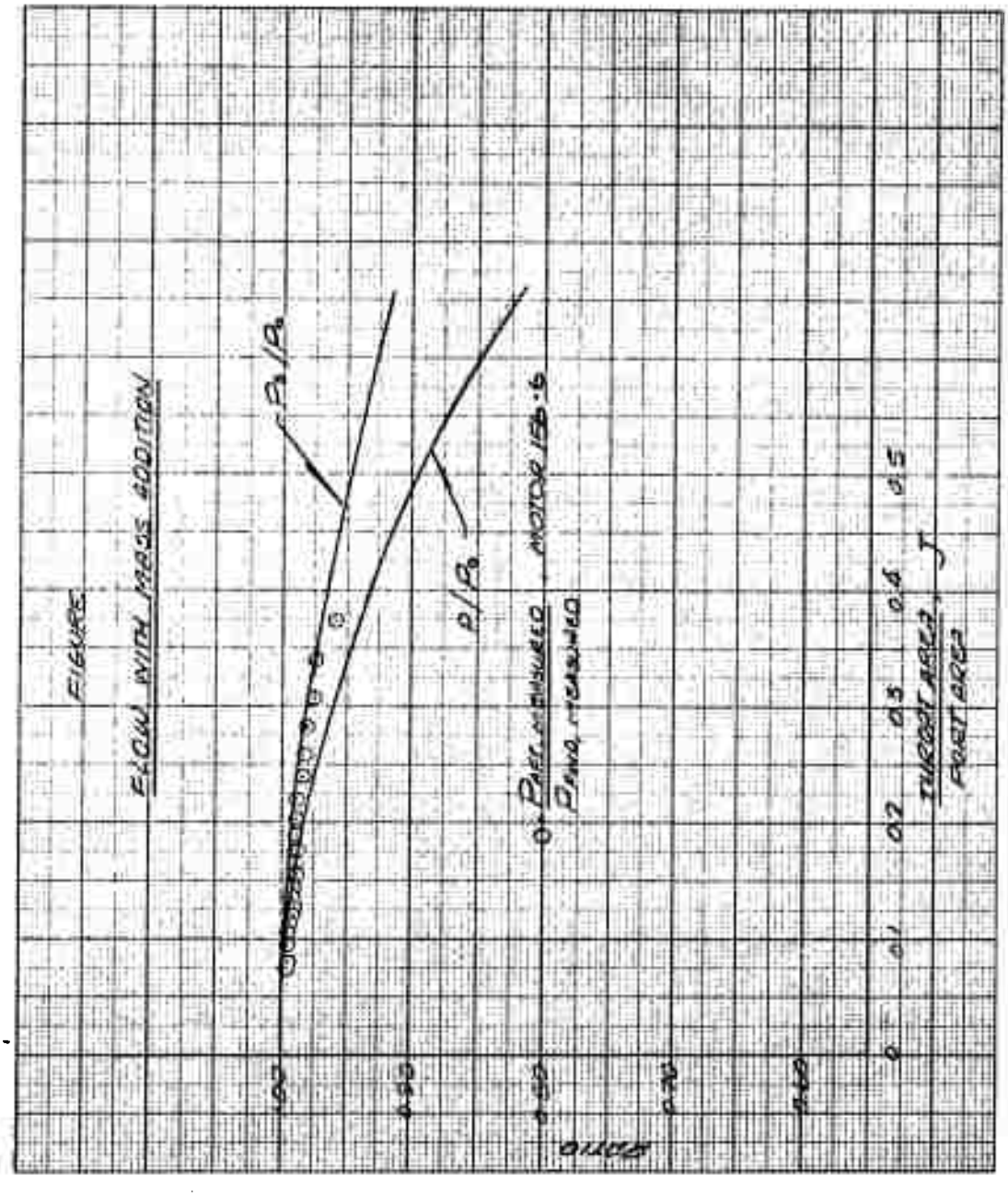

Figure 23 Flow with Mass Addition

(U) e. Nozzle Discharge Coefficient. Instantaneous nozzle discharge coefficients for Motor 156-6 were calculated from test data according to the following relation:

$$C_d = \frac{F_{ao}}{P_c A_t C_f \lambda}$$

where, at any time:

F_{ao} is the axial thrust corrected for TVC augmentation (lb)

P_c is the measured forward or aft chamber pressure (psia)

A_t is the throat area (in.^{2})

$C_f = C_{f_{vac}} - \frac{\epsilon P_a}{P_c}$, where P_a = 13.7 psia at the Potrero Production and Test Facility, and ϵ is the nozzle expansion ratio

$\lambda = \frac{1 + \cos\alpha}{2} = 0.9769$ where the nozzle half angle, $\alpha = 17.5^0$

(U) The nozzle discharge coefficients were computed based on measured head-end and aft-end pressures. These data are shown in Figure 24.

(U) Discharge coefficients based on aft-end pressure exceeded unity during the initial 7 seconds of the firing. This indicates that stagnation conditions were not being measured in the aft cavity for this period. For the same interval, discharge coefficients based on head-end pressure reflected mass addition effects in that the initial discharge coefficients were low and increased with time, or as velocity and pressure drop decreased in the port.

(U) Instantaneous discharge coefficients were obtained from aft stagnation pressures calculated from forward-end pressures using the ratios derived by Price. These data, as compared to forward-end discharge coefficients, are shown in Figure 25 plotted against time. The data show that the theoretical pressure ratios yielded discharge coefficients which were initially higher than unity and which then converged with the coefficients determined from forward-end pressure as the firing progressed. At t = 25 seconds, the two values were essentially the same. The variation in discharge coefficients during the early stages of the firing indicates that the theory tends to predict higher pressure drops than actually are achieved for the higher values of J.

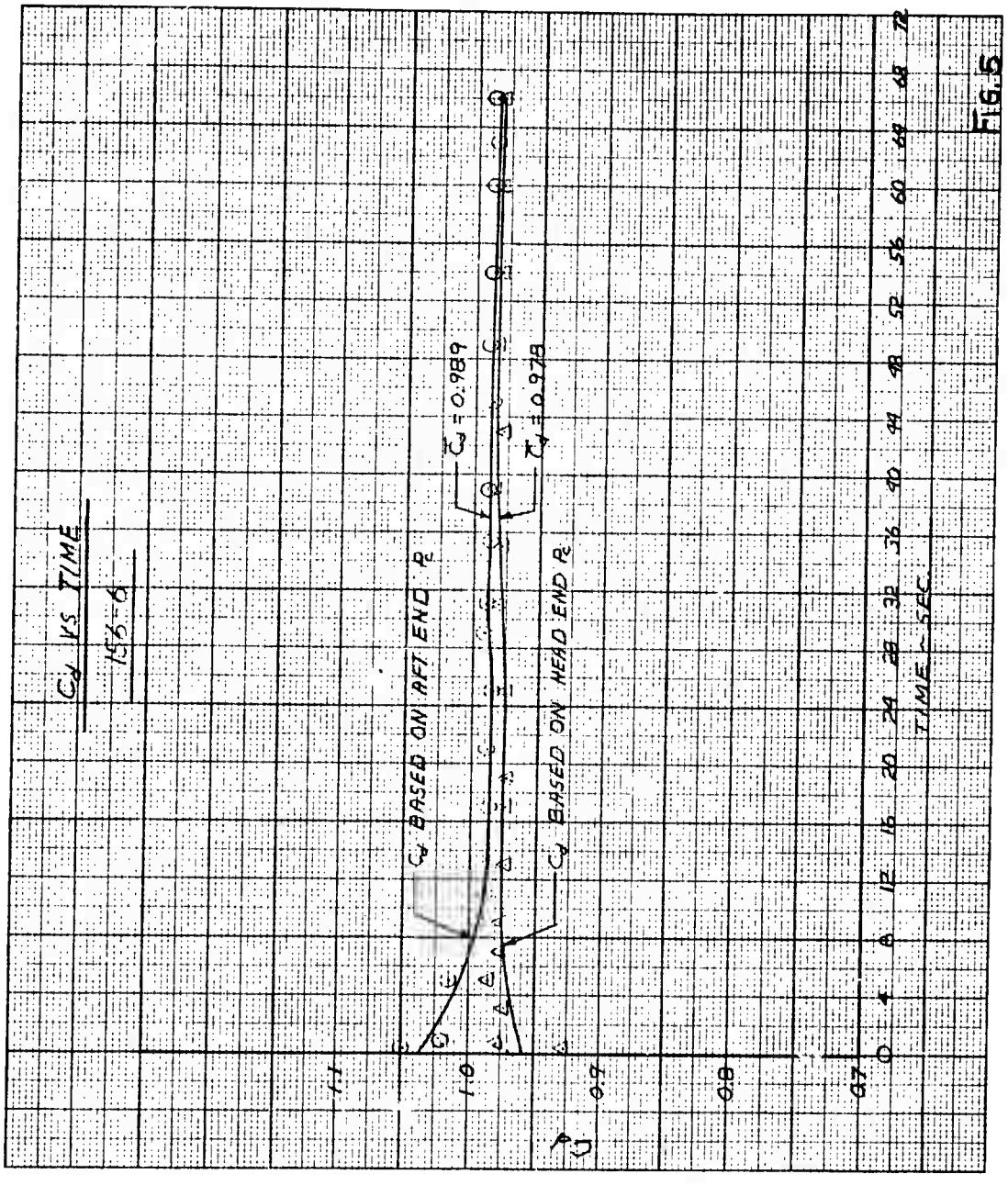

Figure 24 Discharge Coefficients versus Time, Motor 156-6

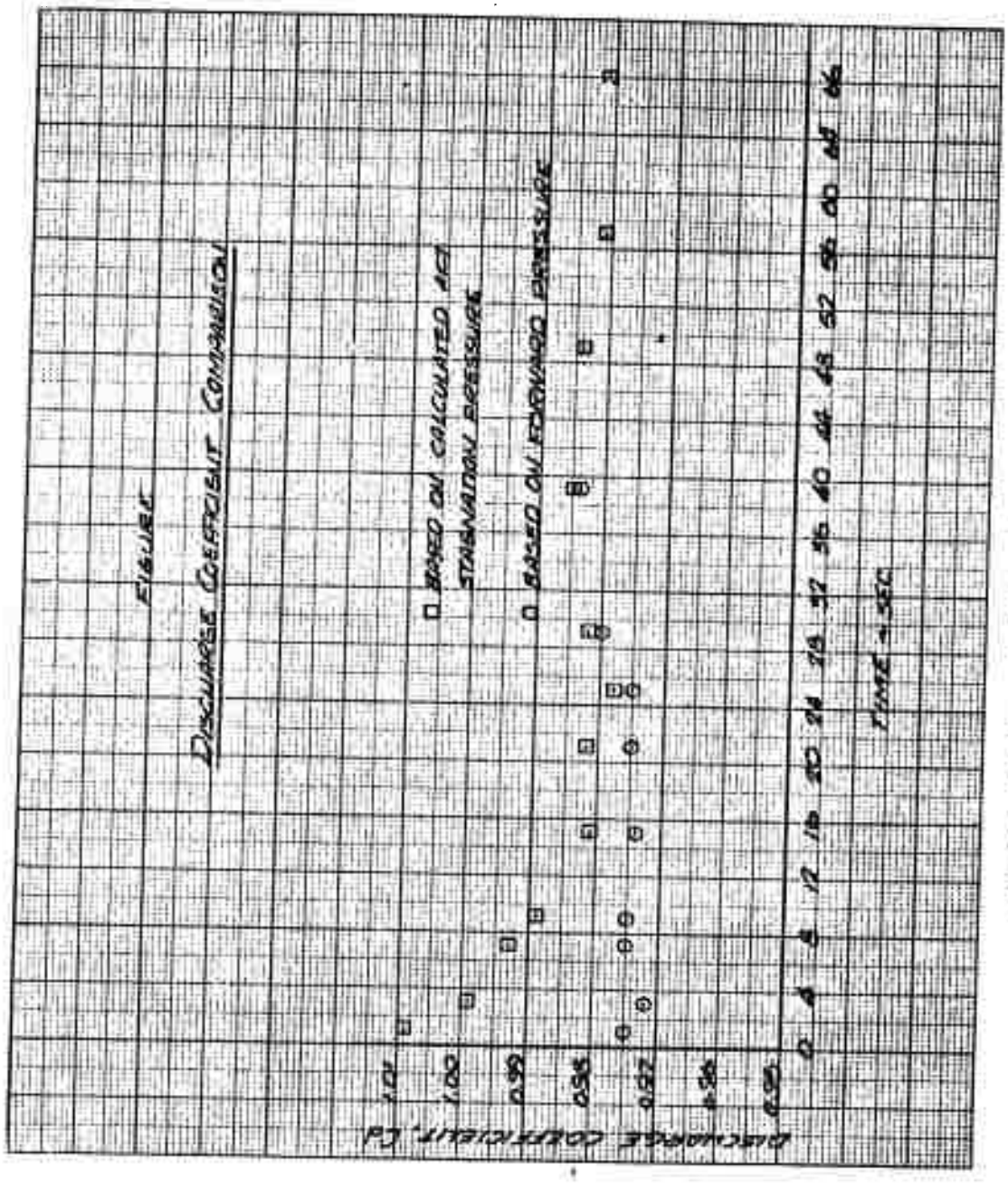

Figure 25 Discharge Coefficient Comparison, Motor 156-6

(C) f. Motor Ignition. Ignition of Motor 156-6 was generally as expected. The time required to reach 75 percent of maximum chamber-pressure was 0.248 second and the maximum chamber-pressure reached during the ignition phase was 657 psia. These values compare favorably with their predicted counterparts, 0.228 second and 670 psia, respectively.

(U) The measured ignition transient curve, which is the chamber pressure plotted against expanded time, is presented in Figure 26.

(C) 2. TVC System Performance

(C) a. Performance. The side forces measured by the individual side force cells are presented in Figures 49 through 53 in Appendix III. These forces were summed for the pitch and yaw planes to obtain the total side force in each plane (Figures 54 and 55 of Appendix III). There were no irregularities in the side force traces. There was considerable overshoot and ringing of the thrust stand (about 12-percent overshoot) as was expected for the fast response times required for the TVC system (equivalent to $1\frac{1}{4}$ cps).

(C) The pitch and yaw side force traces indicate that a thrust misalignment of about 3000 pounds was present during the firing. This misalignment represents 0.3 percent of the axial thrust, or a deflection angle of about 0.17 degrees. To obtain a more accurate representation of the side forces generated during periods of liquid injection, side forces were adjusted to remove the thrust misalignment effect.

(U) The corrected pitch and yaw side forces are shown in Figures 27 and 28, respectively, in the form of the ratio of side force to nominal axial thrust F_s/F_{ao}. (See subsection V 1.a.) This ratio will hereafter be referred to as the side force ratio.

(U) Because of the omniaxial capability of the TVC system, a more meaningful force parameter is the resultant side force, F_{sr}, which is the vectoral sum of the pitch and yaw side force components. Therefore, the pitch and yaw side force ratios were summed to obtain the resultant side force ratio shown in Figure 29. The resultant side force (Figure 30) and thrust deflection angle, $\delta = \tan^{-1} F_{sr}/F_{ao}$, (Figure 31) were then computed.

(C) The maximum thrust deflection angle measured during this test was $\delta = 4.35$ degrees (neglecting thrust overshoot) during the first injection period (cycle). The thrust deflection angles obtained during all major cycles (i. e., on the order of 3 degrees or more) on the average, approximated the expected deflections. About half of the decrease was attributable to low flow rates and the remainder to lower than expected side specific impulse. During several of the lower thrust deflection cycles, the expected performance values were exceeded; these results were attributed generally to higher than expected flow rates. In some instances, however, the side specific impulse appears to be greater than expected.

CONFIDENTIAL

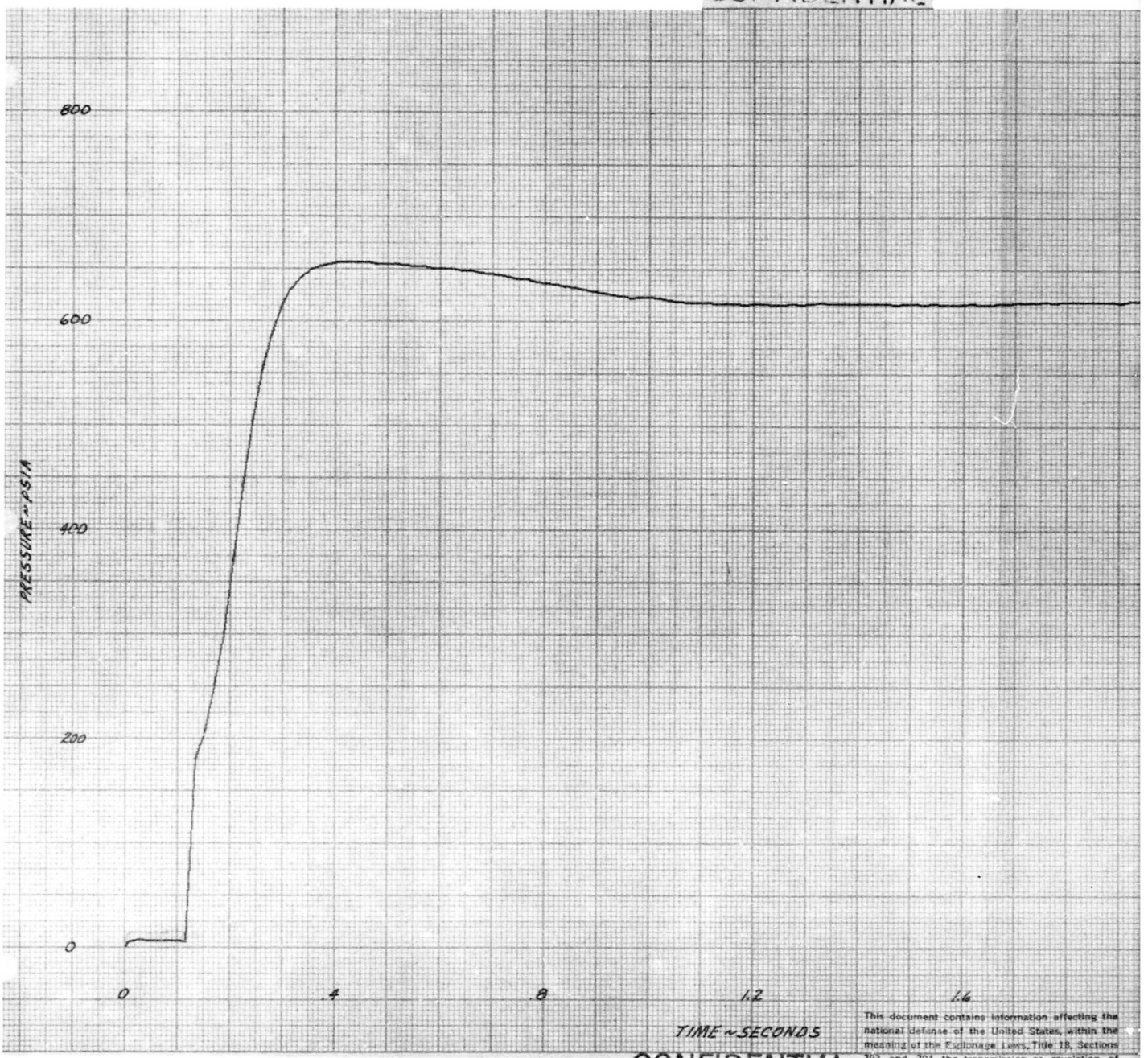

CONFIDENTIAL

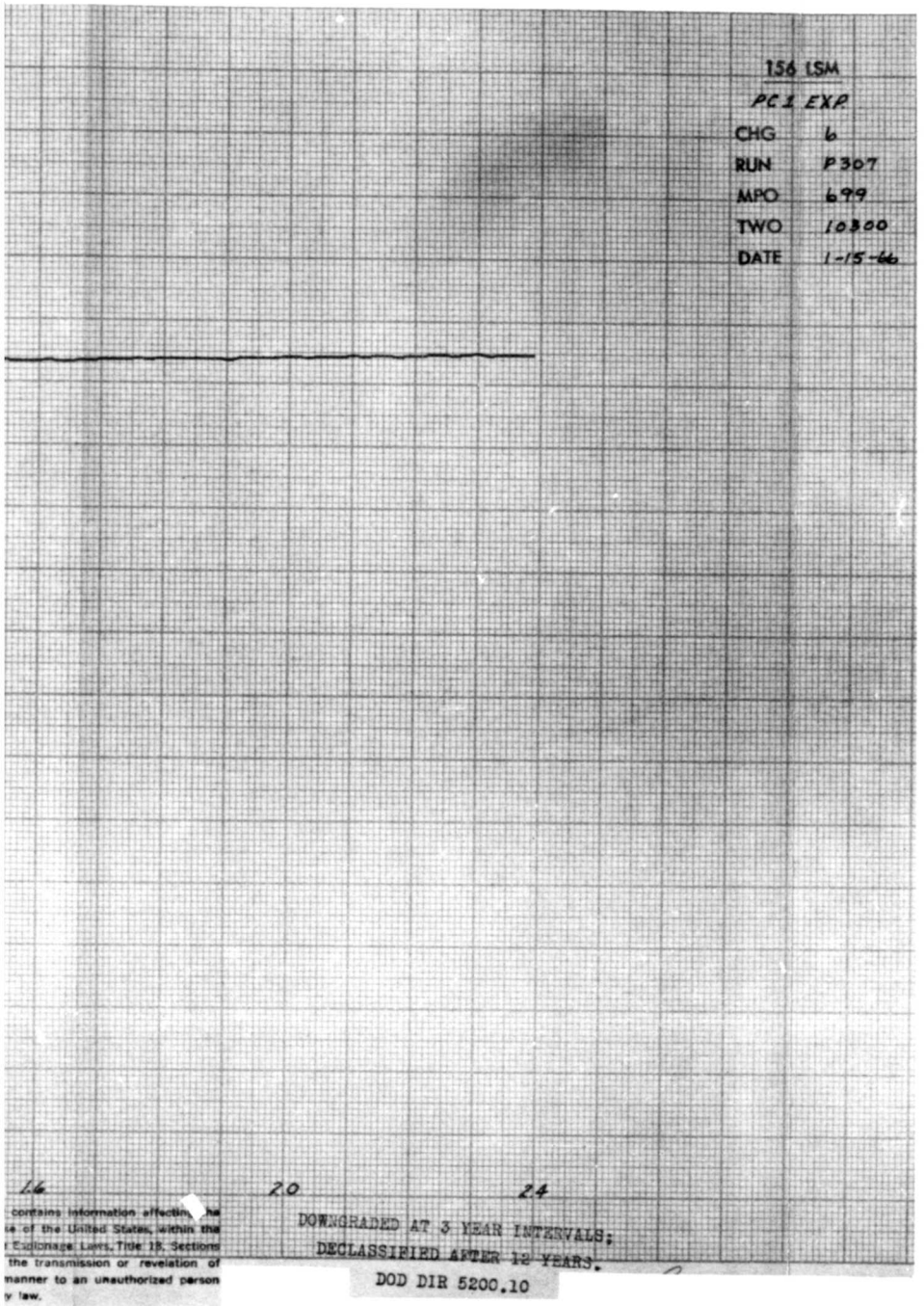

Figure 26 Expanded Forward Chamber Pressure versus Time, Motor 156-6

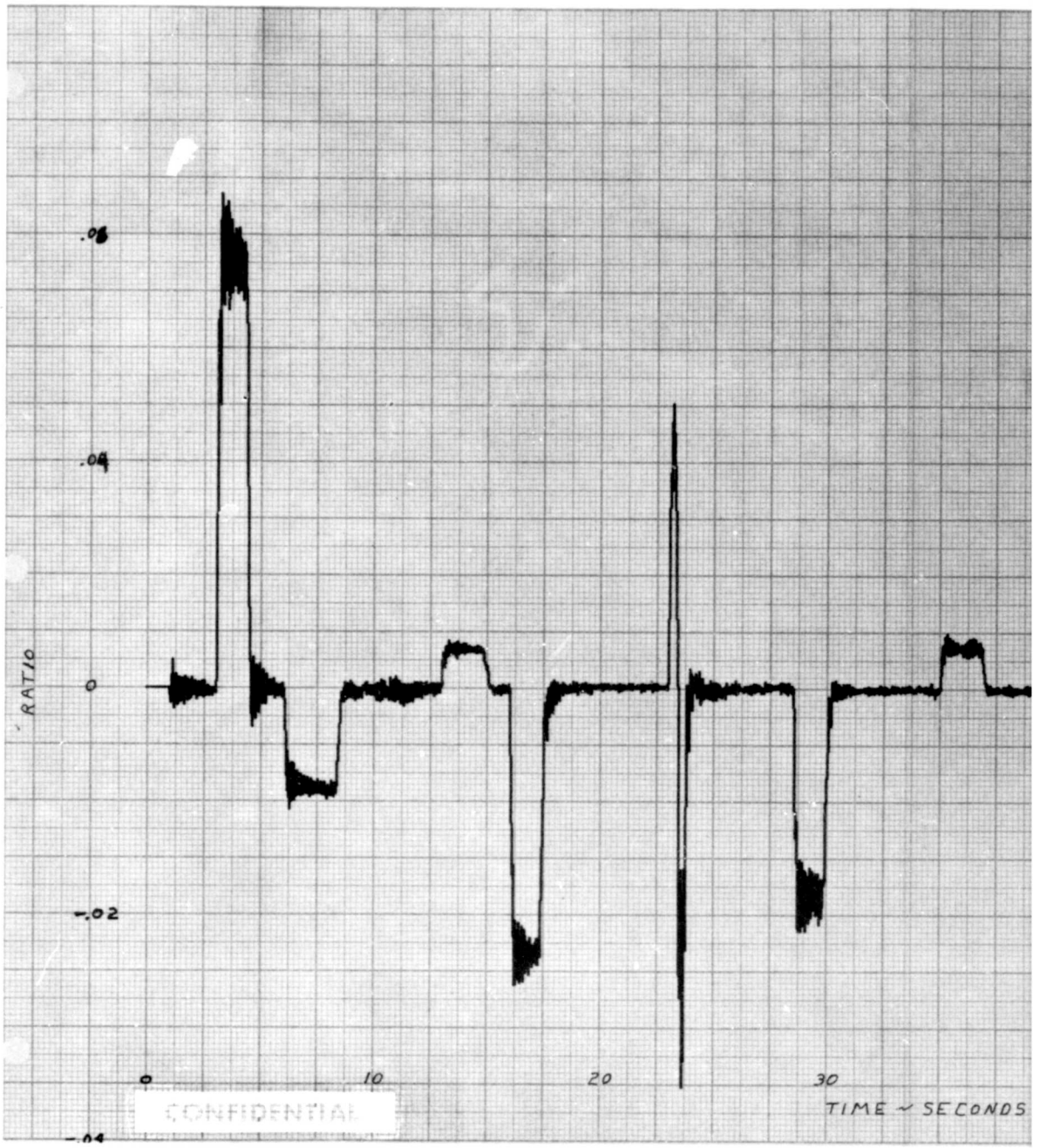

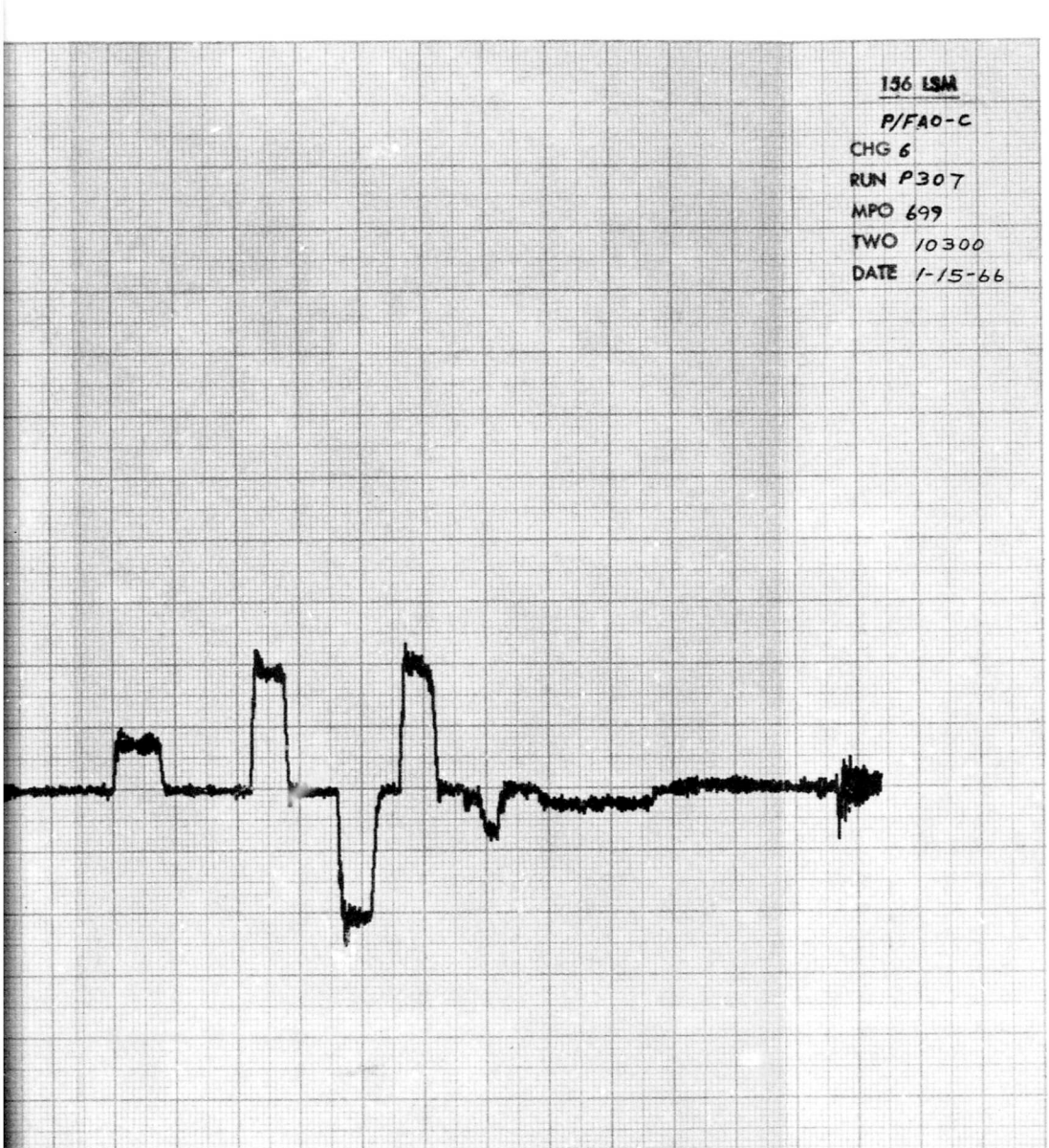

Figure 27 Corrected Side Force Ratio (Pitch Plane) versus Time, Motor 156-6

CONFIDENTIAL

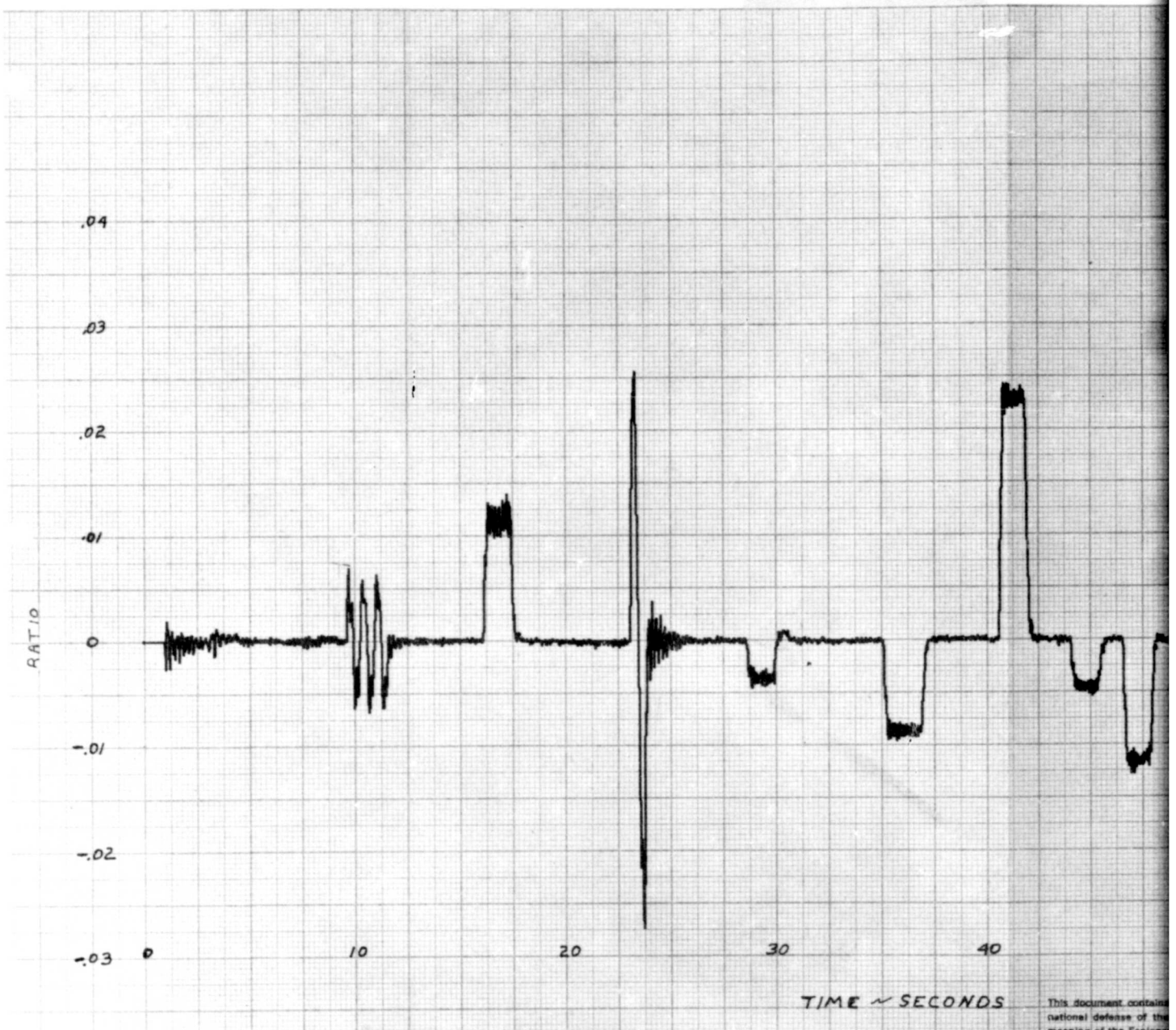

CONFIDENTIAL

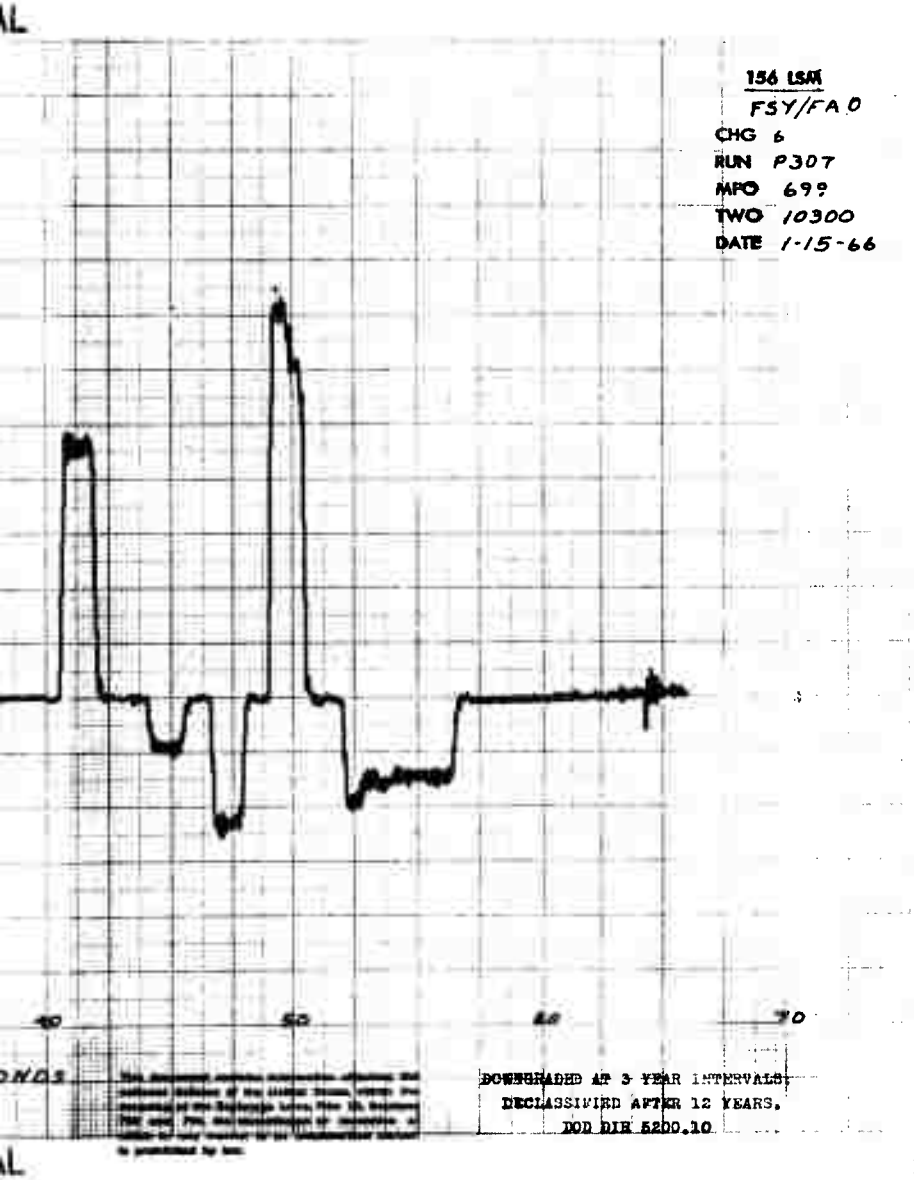

Figure 28 Corrected Side Force Ratio (Yaw Plane) versus Time, Motor 156-6

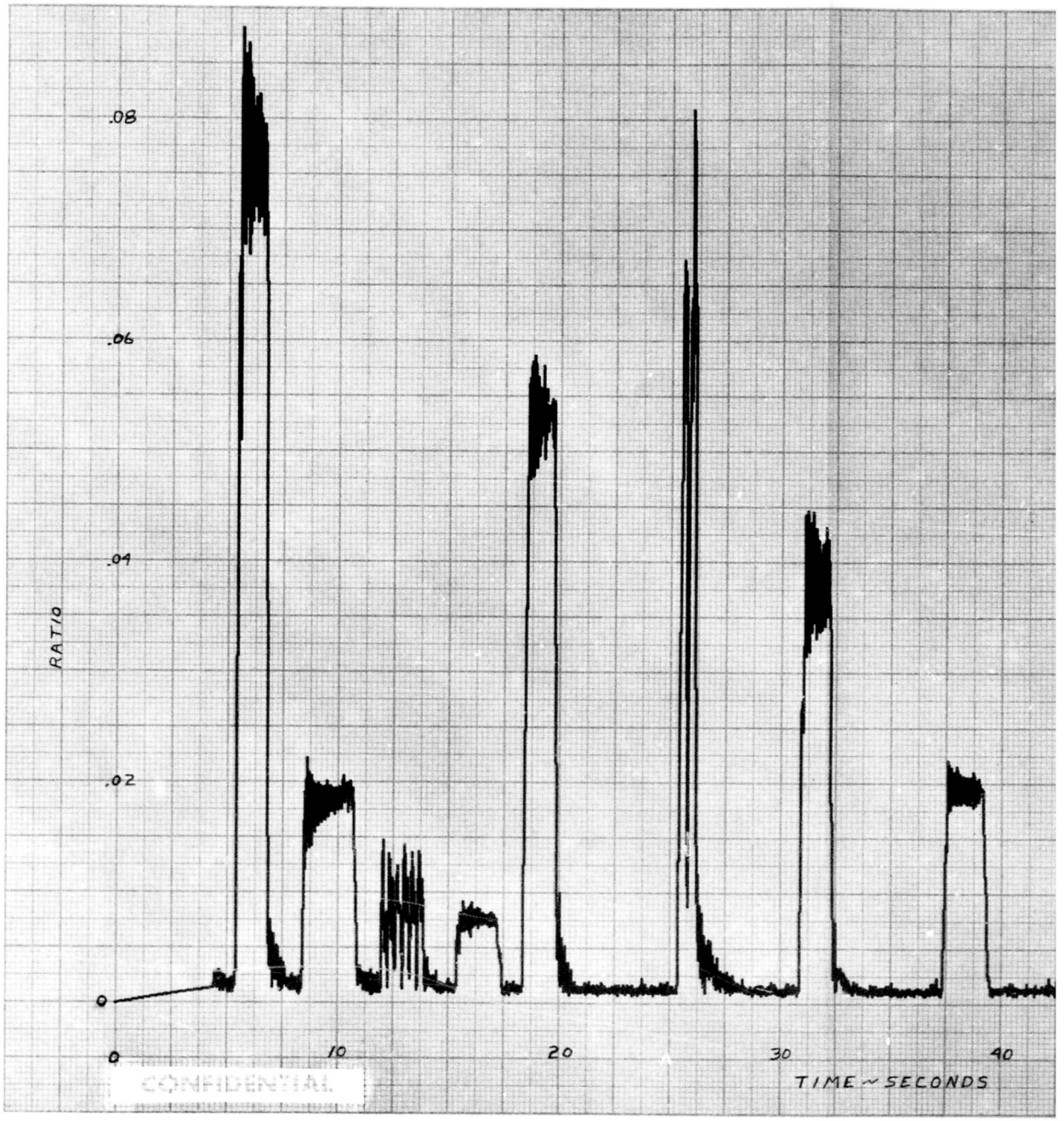

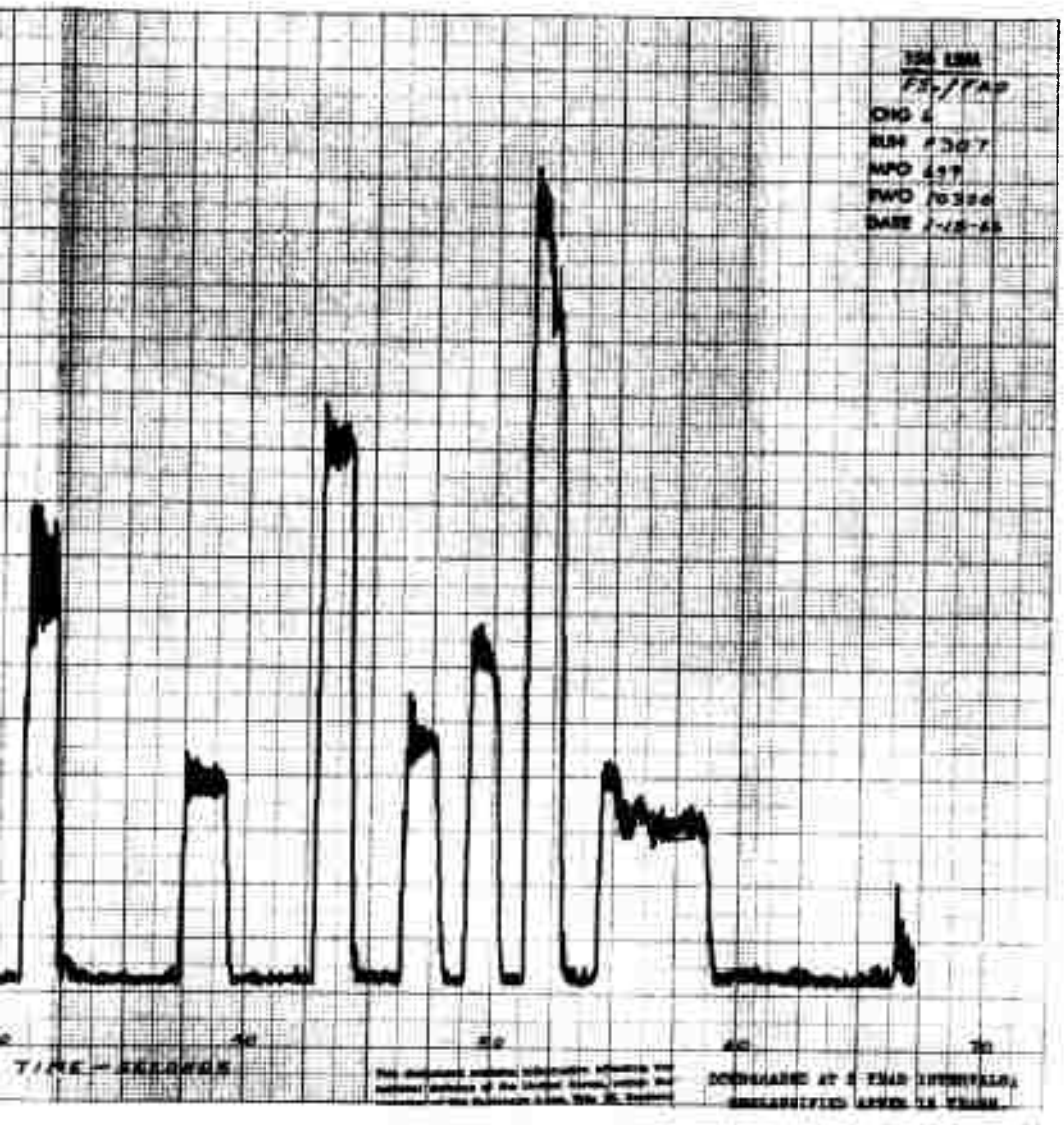

Figure 29 Resultant Side Force Ratio versus Time, Motor 156-6

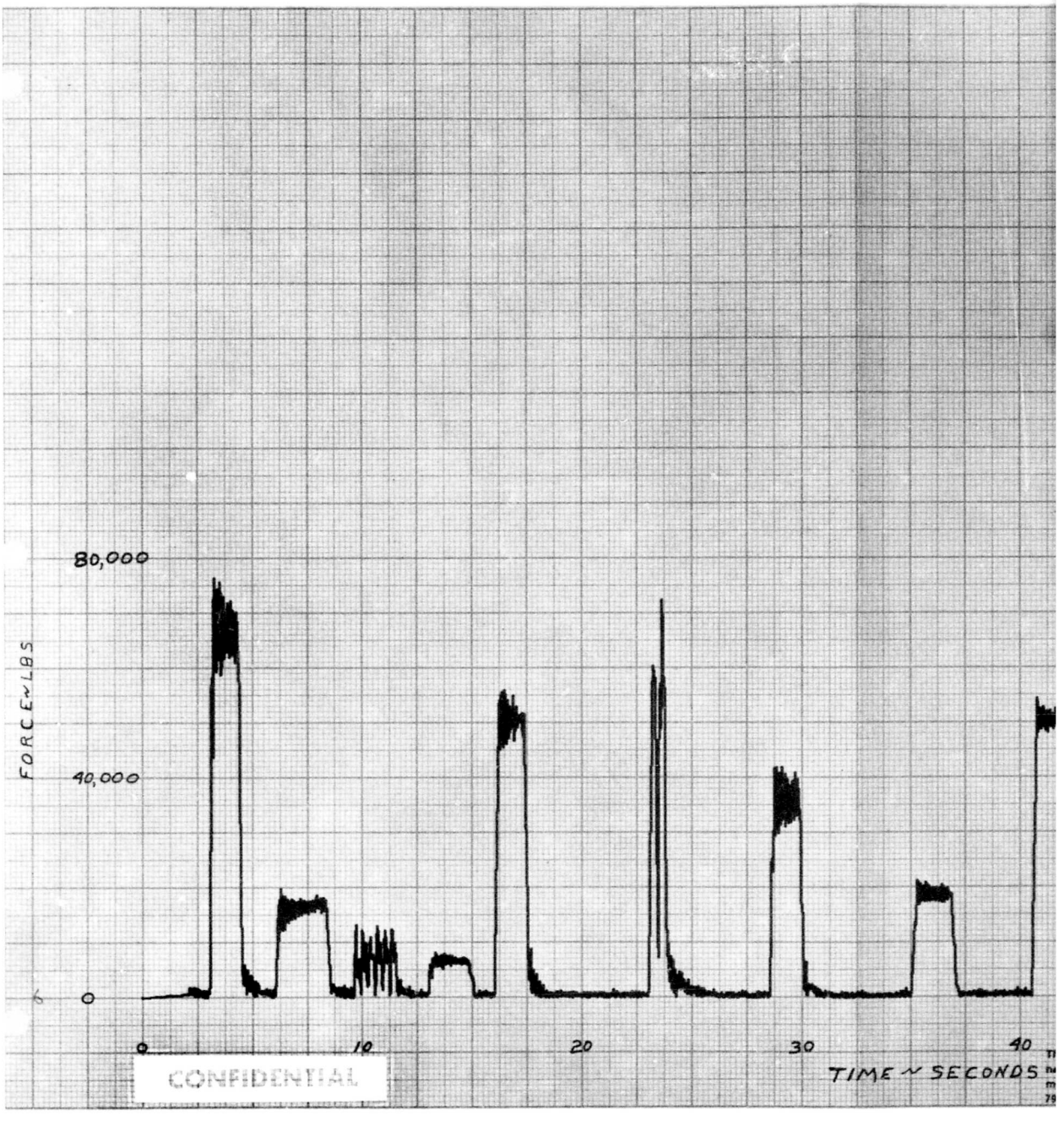

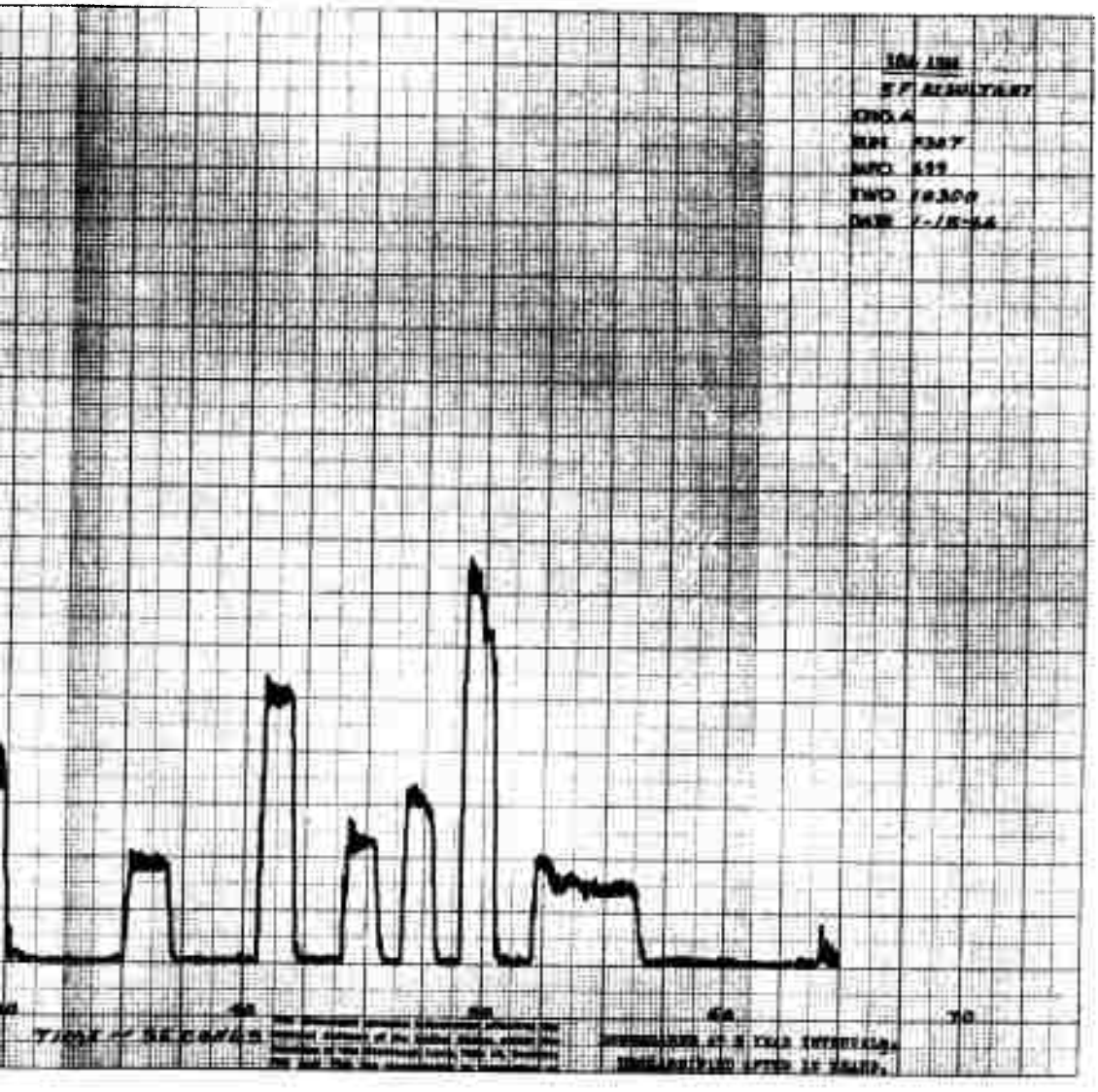

Figure 30 Resultant Side Force versus Time, Motor 156-6

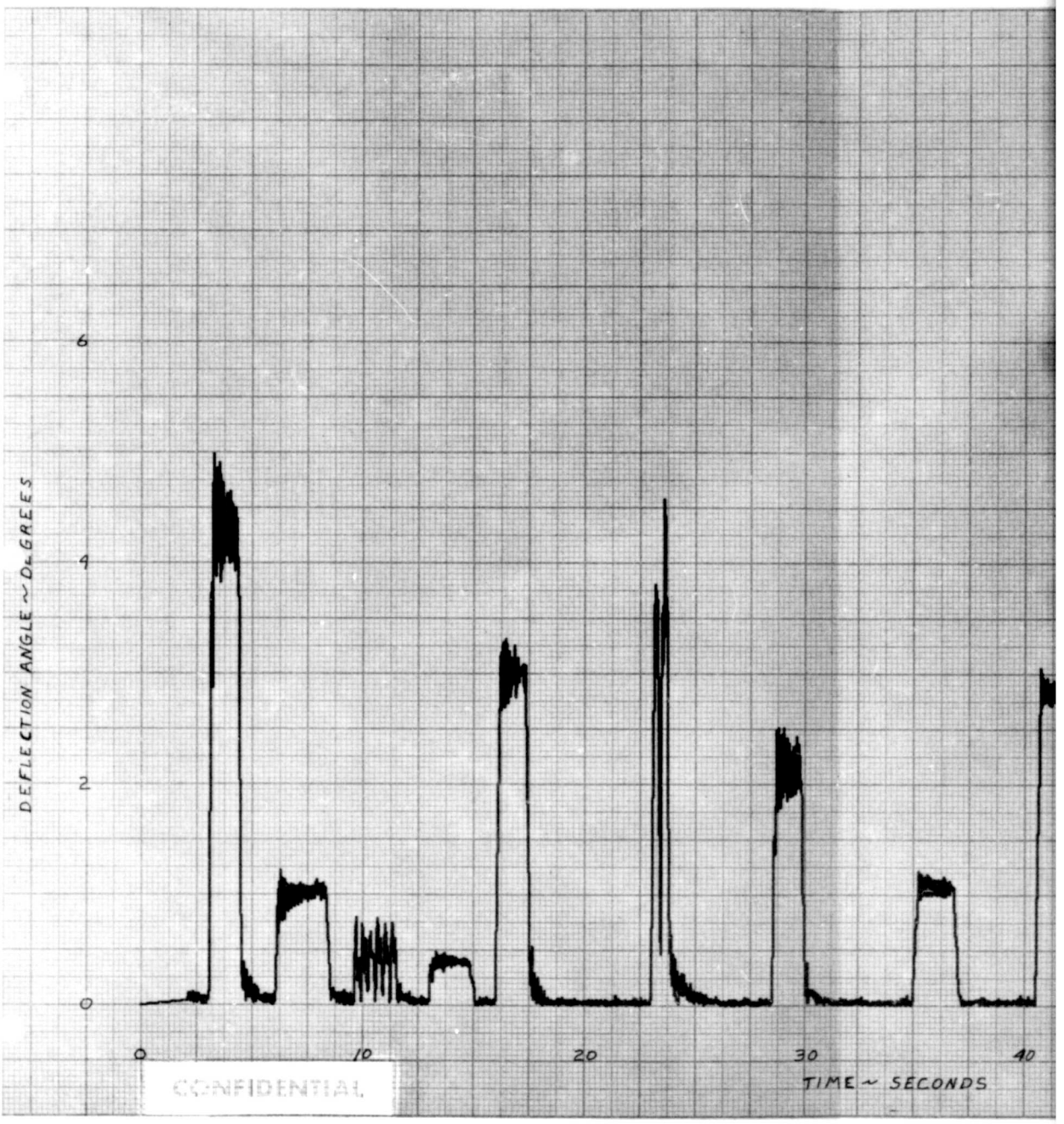

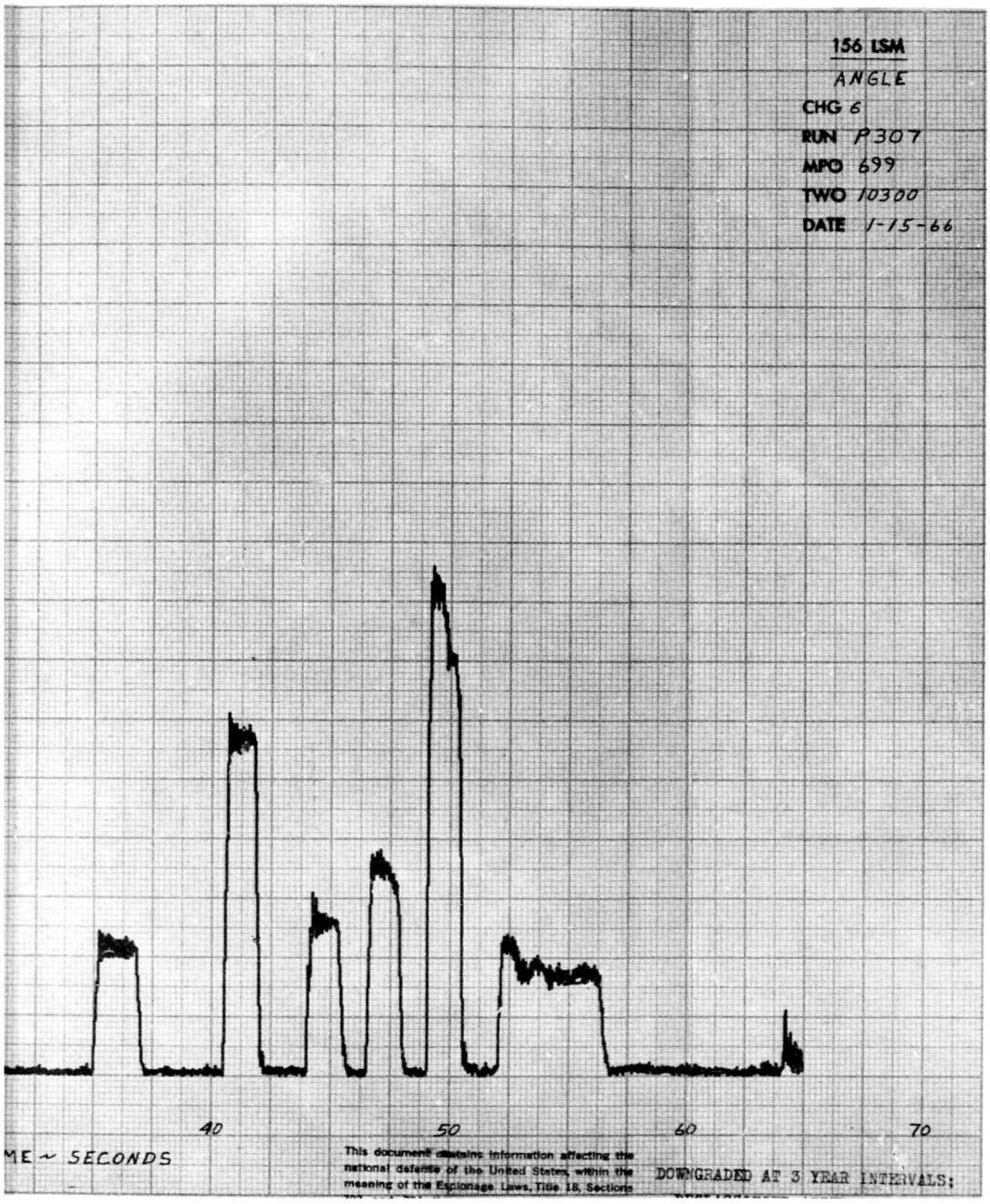

Figure 31 Thrust Deflection Angle versus Time, Motor 156-6

(C) During cycle 6(b), the thrust deflection angle reached a maximum of $\delta = 4.57$ degrees. Part of this deflection is probably the result of thrust overshoot. However, it can be noted that two additional valves had opened partially on this cycle, thereby contributing to the amplifications of the side force. Therefore, this cycle was disregarded in subsequent analyses.

(U) Thrust overshoot is defined as the ratio of measured thrust resulting from the dynamic response of the thrust measurement system to the equilibrium or average thrust. The thrust overshoot is a function of the shape or the driving force, i.e., ramp, sinusoidal, etc., the rise time (or the time from zero to equilibrium conditions for the driving force), and the natural period of the thrust measurement system. Ringing is the oscillatory condition characteristic of a dynamically responding spring-mass system. The ringing duration is a function of the system damping coefficient.

(U) Since flow meters were not installed on the TVC system, the flow rates were not directly measured; they were determined from the injector valve pintle positions using the vendor-supplied calibration curve. This calibration curve, representative of the 24 injector valves, correlates the flow rate of an individual valve (at the reference pressure and density levels indicated) to the pintle position (as measured by the feedback potentiometer voltage in percent of the full open position), as shown in Figure 32.

(C) Using the pintle position data from the test firing (subsection V 2.b), the flow rates for each valve were established at the reference conditions (injectant density, $\rho_i = 90.8$ lb/ft^3 and pressure differential across the injector valve, $\Delta P = 670$ psi) and summed to obtain the reference injectant flow rate, $\dot{w}_{sr}$, for the bank of values used during each cycle. The injectant density is a function of the injectant temperature. The injectant temperature was roughly constant at 90°F, for which the density of N_2O_4 is 88.3 lb/ft^3, and the density was assumed to be constant for data reduction purposes.

(U) The pressure differential across the injector valves was established from the injectant (manifold) pressure, P_M (subsection V 2.c), the pressure losses through the manifold and valve inlet lines, P_L, and the pressure in the nozzle, P_N (subsection V 2.d).

(C) Having established ρ_i and ΔP for the test conditions, the injectant flow rate was computed from

$$\dot{w}_s = \dot{w}_{sr} \sqrt{\frac{\Delta P}{670} \frac{\rho_i}{90.8}}$$

(C) The flow rates were computed only at selected times during each cycle. The side specific impulse, as defined by

$$I_{sps} = F_{sr}/\dot{w}_s$$

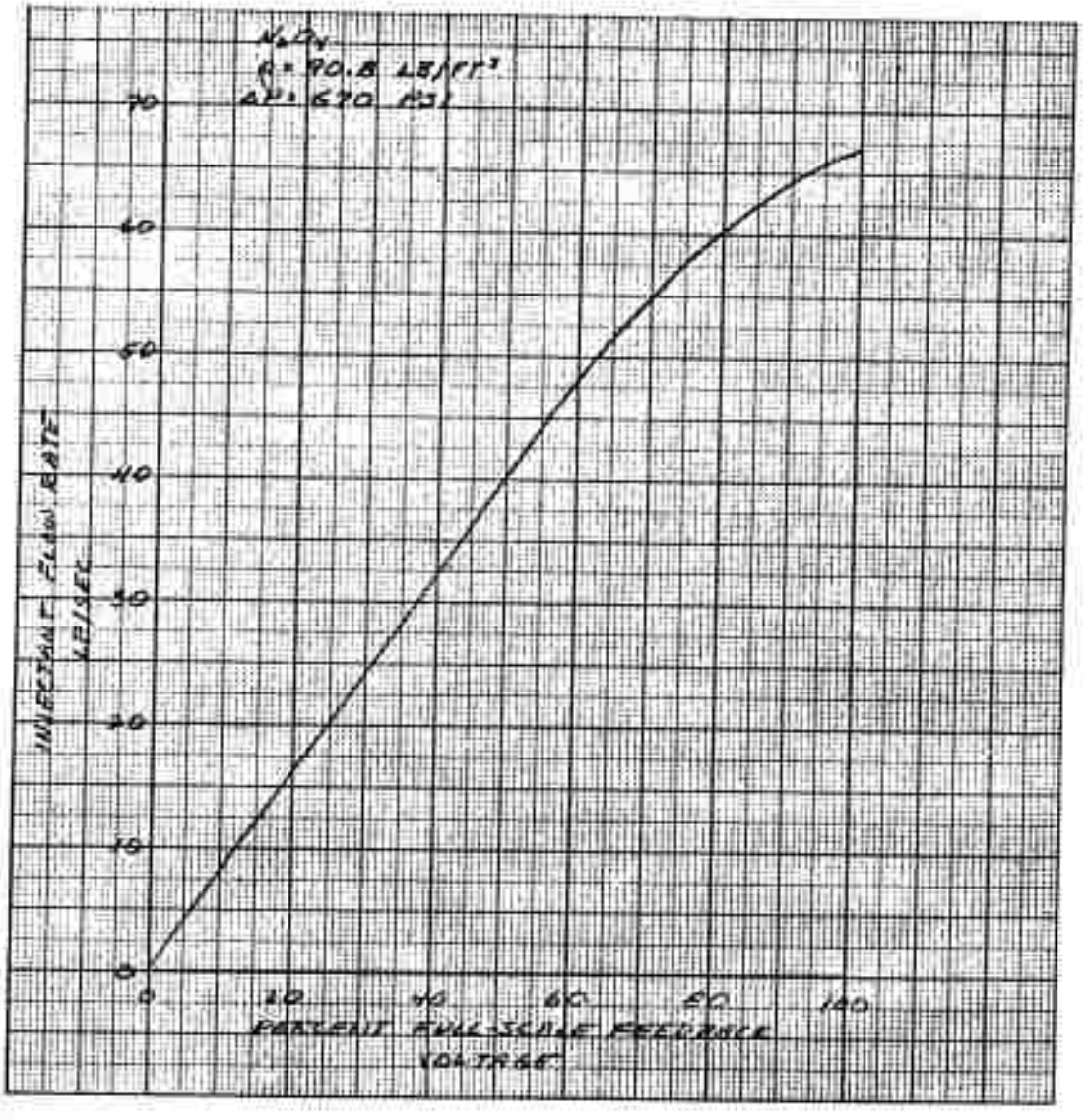

Figure 32 Injectant Flow Rate per Valve, Motor 156-6

was computed at times corresponding to the flow rate calculations. The results are plotted against the thrust deflection angle and compared to the expected I_{sps} level in Figure 33. The data exhibit considerable scatter at the lower deflection angles, probably as a result of the inaccuracy of the flow rate calculations, which, in turn, results from inconsistencies in the injector valve feedback positions. At the high deflection angles, the measured performance was about 10 percent below the expected level; at the low deflection angles, it appears to be about 15 percent lower than anticipated. This performance level is comparable to that of Motor 156-5.

(U) A performance summary of the TVC system during each cycle is presented in Table X. The side impulse, $I_s = \int F_{sr} dt$, was 646,150 lbf-sec, or 1.03 percent of the total axial impulse. The total amount of injectant expelled during the test was 2890 pounds.

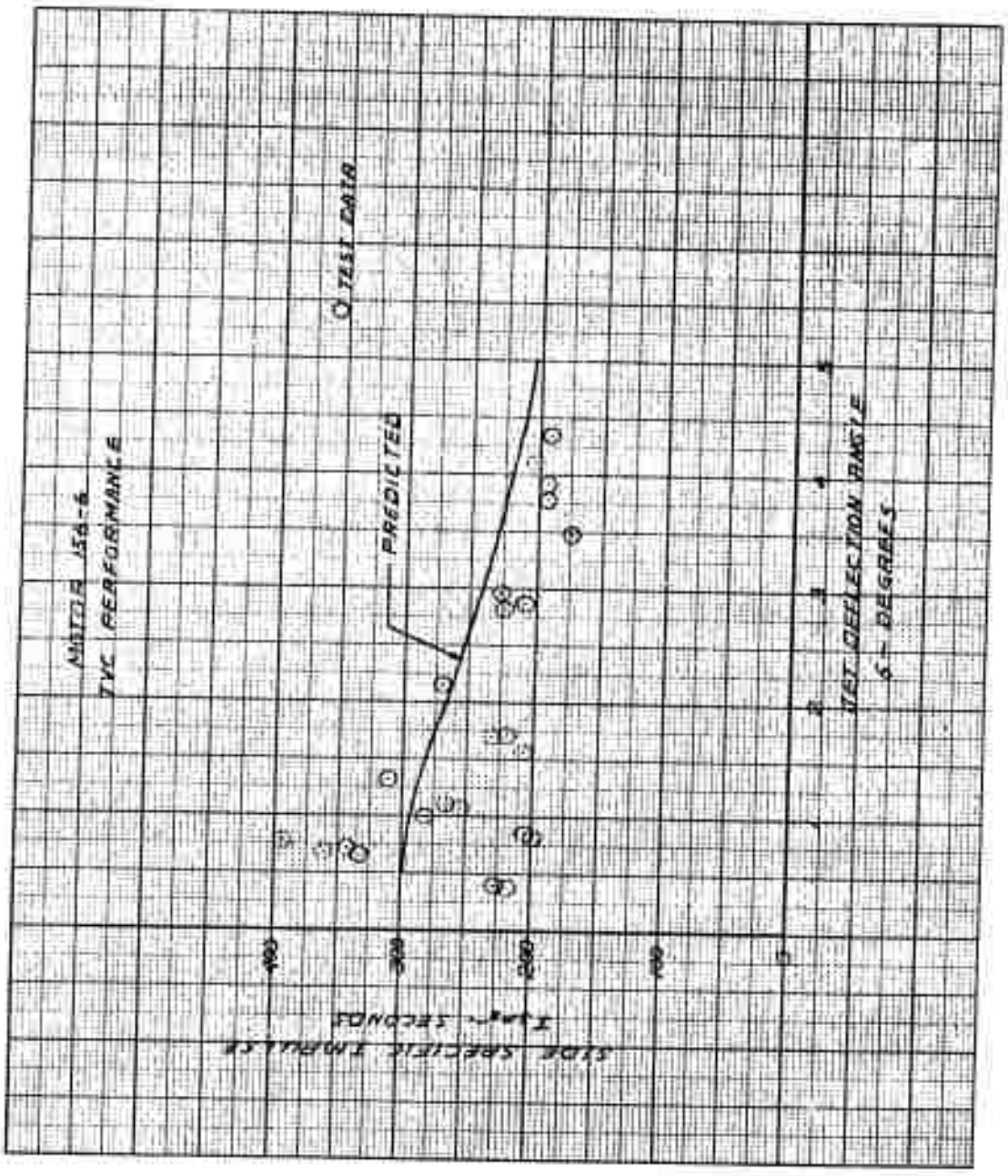

FIGURE 33 TVC Performance, Motor 156-6

Table X

TVC PERFORMANCE SUMMARY, MOTOR 156-6

Cycle	Injectant Flow Rate (lbm/sec)	Resultant Side Force (lbf x 10^{-3})	Thrust Deflection (deg)	Side Specific Impulse (sec)	Injectant Expelled (lbm)	Side Impulse (lbf-sec x 10^{-3})
1	351	67.3	4.35	192	462	88.5
2	58	16.3	1.00	281	139	39.0
3(a)	33	13.0	0.78	394	6	2.1
3(b)	35	12.0	0.72	343	6	2.2
3(c)	33	11.0	0.65	333	7	2.4
3(d)	36	13.0	0.78	361	7	2.4
3(e)	33	12.0	0.72	364	7	2.4
3(f)	35	12.0	0.72	343	7	2.5
4	30	6.8	0.40	227	57	12.8
5	223	50.4	2.97	226	307	69.5
6(a)	309	60.0	3.78	194	87	16.8
6(b)	304*	72.5**	4.57**	239***	81*	19.2
7	134	36.2	2.15	270	182	49.2
8	74	18.8	1.07	254	137	34.8
9	225	50.3	2.82	224	301	67.2
10	76	23.6	1.32	311	103	32.1
11	132	30.5	1.70	231	178	41.1
12	360	70.0	3.92	194	475	92.4
13	72	14.7	0.85	204	341	69.5

66-734

* Does not include flow from additional valves which were open
** Includes thrust overshoot
*** Includes thrust overshoot but not additional valve flow.

(U) b. Duty Cycle. The duty cycle for the 156-6 TVC system, as agreed upon by the Air Force and LPC, is shown in Figure 34; this figure illustrates the magnitude and direction of the required thrust deflections.

(U) The measured pitch and yaw input voltage command signals to the omniaxis controller are shown in Figures 35 and 36. These command signals were vectorially summed by the omniaxis controller to provide the signals to open the 24 injector valves. The individual valve pintle positions were monitored by means of internal feedback potentiometers. The feedback data for all 24 valves are shown in Figures 56 through 79 of Appendix III.

(U) In summary, the injection subsystem functioned sufficiently well to meet the objectives of the duty cycle. However, refinements and improvements are needed in the omniaxis controller and/or valve circuitry to obtain better accuracy and reproducibility.

(U) The dead-band at which the injector valves were to open appeared to meet the LPC design specifications. However, there were deviations from the design requirements as shown in Table XI . This table shows the reference flow rates for which the system was to be designed and the calculated reference flow rates obtained from a spot check of the prefire checkout of the TVC system and during the static firing. The injection system behaved erratically in that the valves did not open to the proper positions, and they did not open to a consistent position during the two operations of the system.

(U) There were several notable operational irregularities of the injection subsystem. In cycle 6(b), only valves 13 through 18 were to have operated; however, valves 19 through 24 also indicated partial opening as this cycle was initiated. This abnormality resulted either from erratic signals generated by the omniaxis controller or from an inexact synchronization of the pitch and yaw command signals. During cycle 9, valves 4 and 5 opened initially as required but then closed to an intermediate position for the remainder of the cycle. Valves 7 and 8 also operated in this mode during cycle 11. Since the command signal input to the controller exhibited no such irregularity, this abnormality was generated within the controller or valves, or it resulted from a malfunction of the feedback potentiometer.

(C) c. System Pressurization. The TVC pressurization subsystem was activated 18 seconds before the firing. The pressure regulator bypass unit raised the ullage pressure to 500 psia within 8 seconds. The main regulator unit was manually activated at this time, raising the ullage pressure to the 850 psia design level within an additional 0.3 second. The ullage pressure then decayed slowly due to heat dissipation to 770 psi at 0.25 second after motor ignition. The main pressure regulators then opened to maintain the ullage pressure between 740 and 825 psia during the first cycle. After the first cycle, the ullage volume had increased sufficiently to enable the regulators to maintain the ullage pressure between 760 and 810 psia. The ullage pressure, as measured on the GN_2 side of the N_2O_4 tank bladder, is shown in Figure 37.

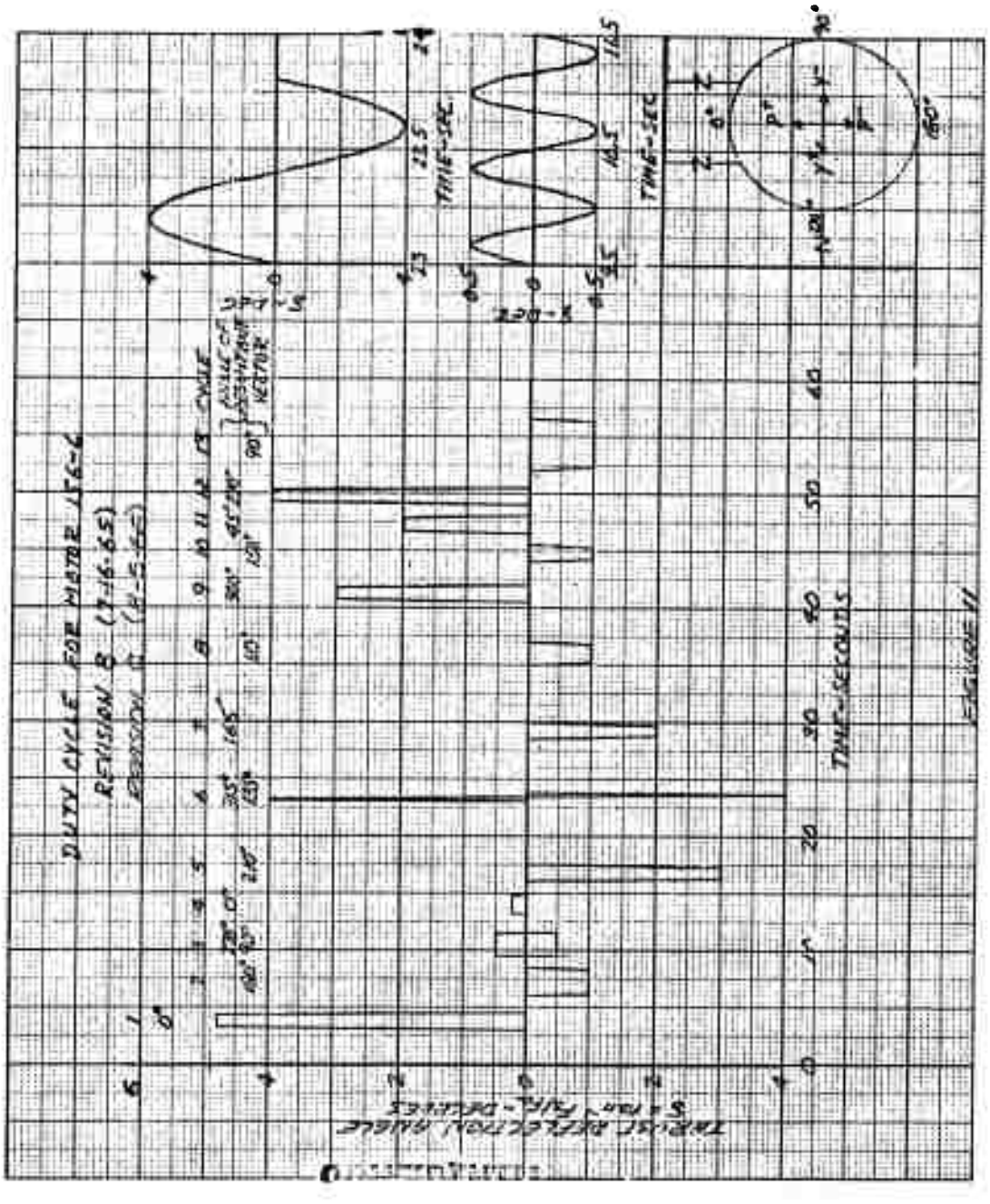

Figure 34 Duty Cycle, Motor 156-6, Revision C

PREVIOUS PAGE WAS BLANK, THEREFORE NOT FILMED.

CONFIDENTIAL

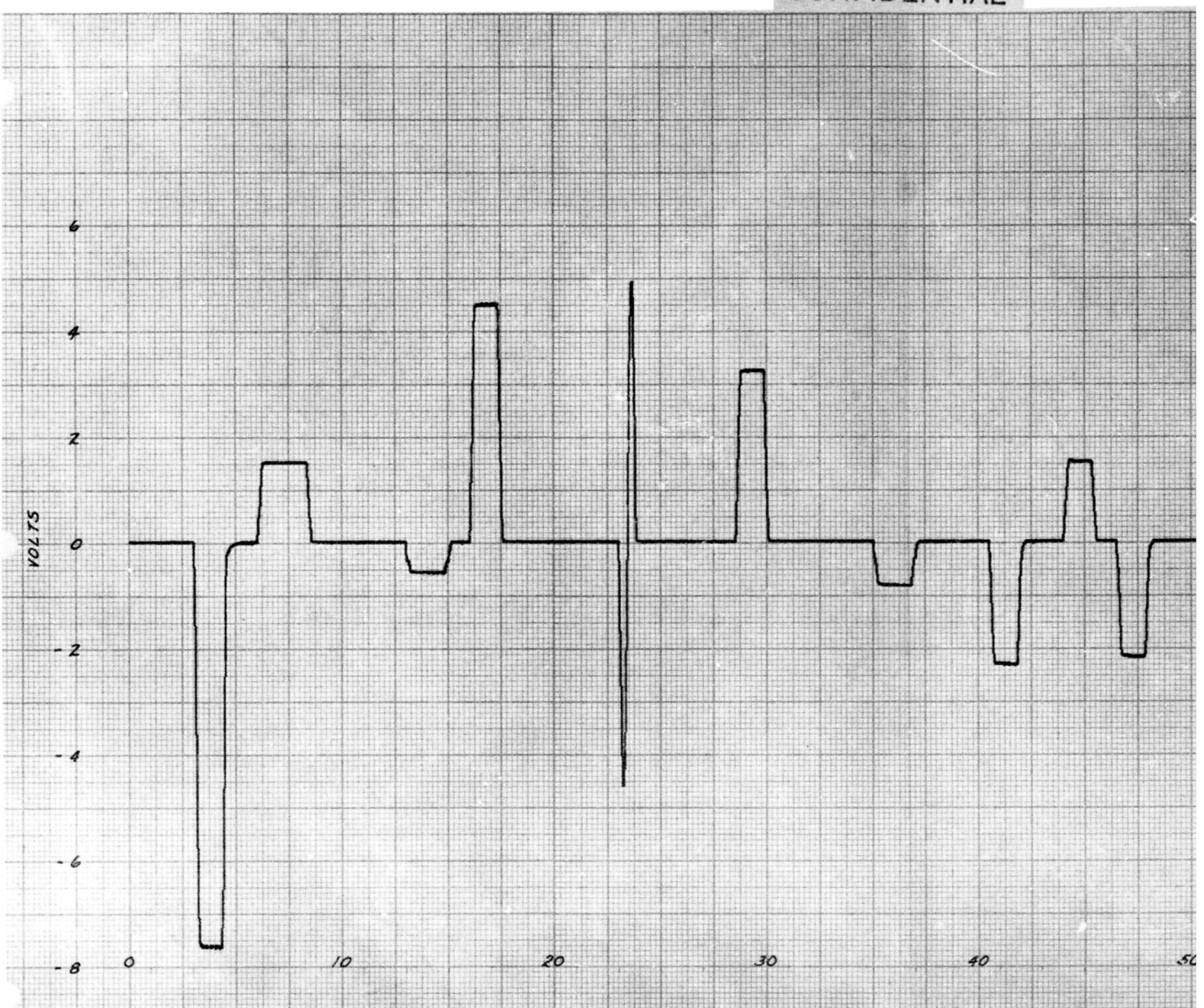

CONFIDENTIAL

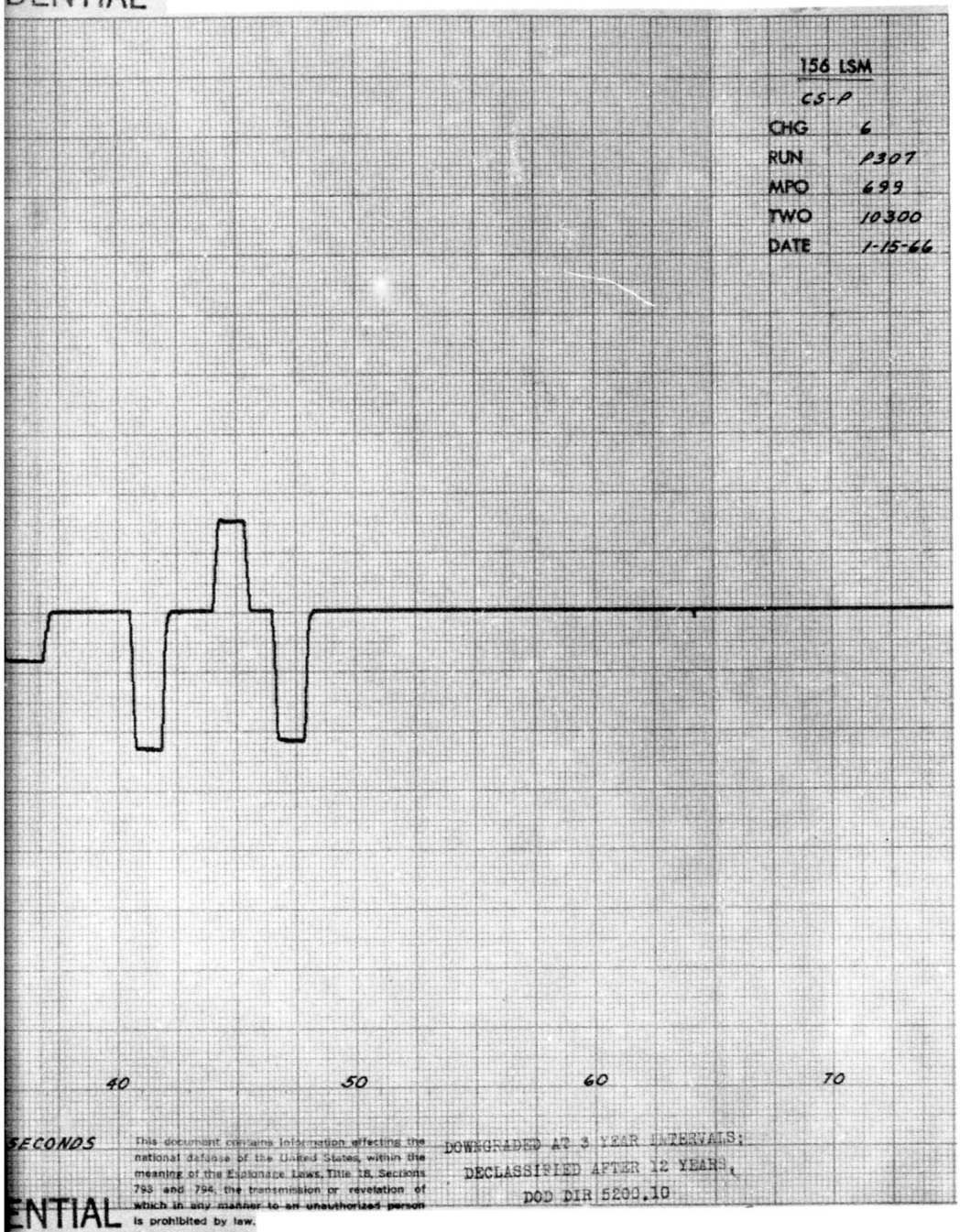

2

Figure 35 Command Input Signal Pitch Coordinates, Motor 156-6

PREVIOUS PAGE WAS BLANK, THEREFORE NOT FILMED.

CONFIDENTIAL

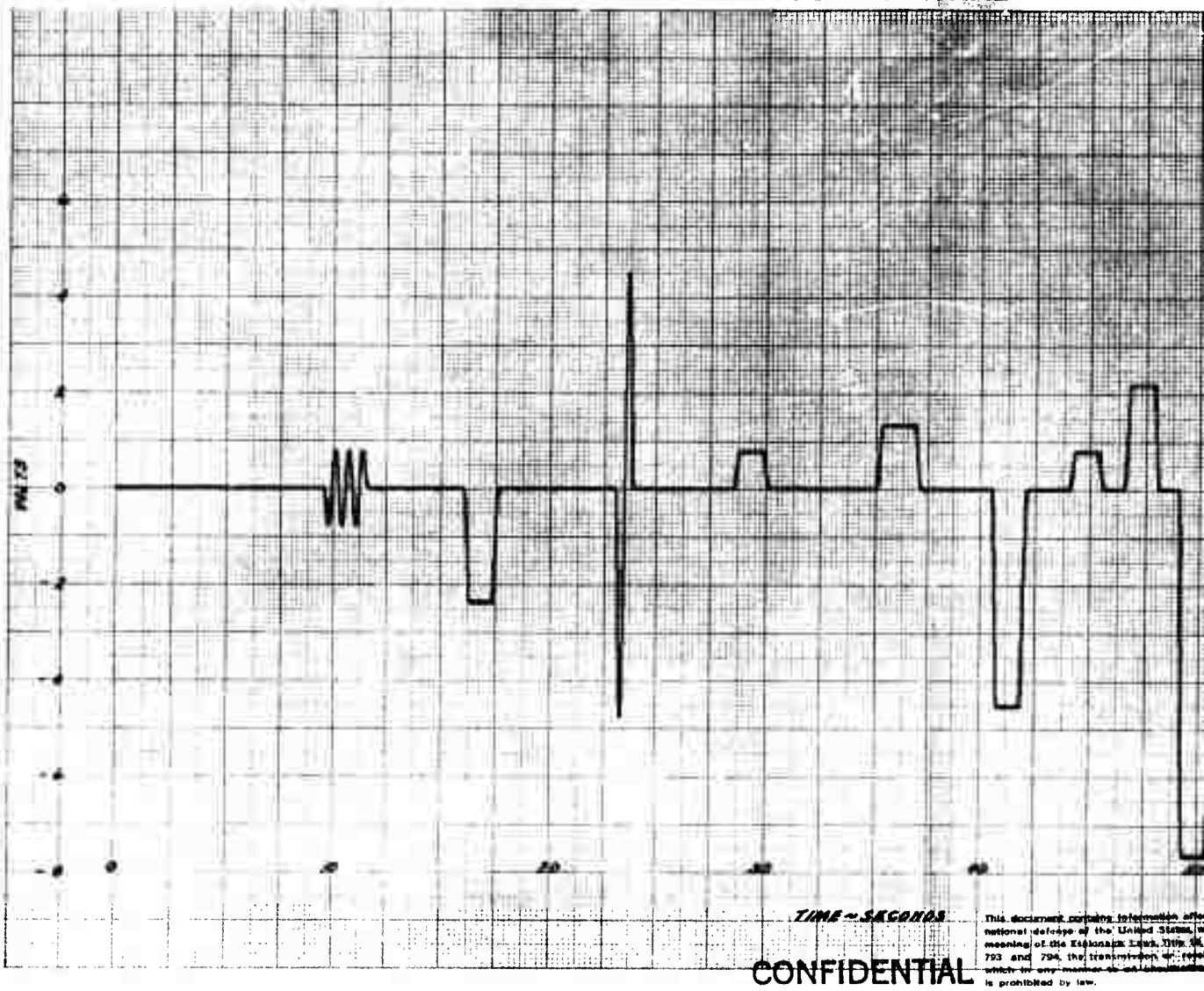

CONFIDENTIAL

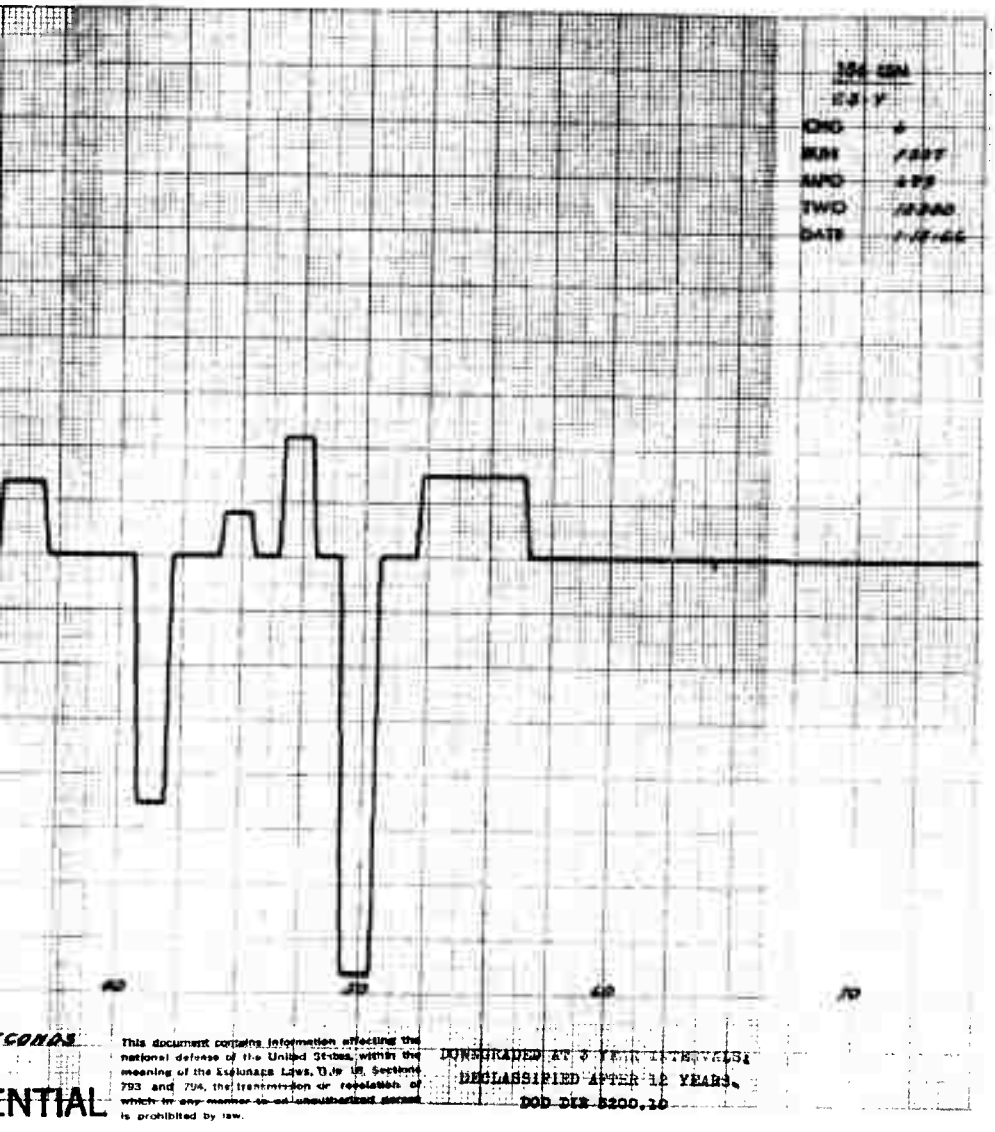

Figure 36 Command Input Signal, Yaw Coordinates, Motor 156-6

Table XI

INJECTOR VALVE OPERATION, MOTOR 156-6

Cycle	Reference Injectant Flow Rate (lb/sec)		
	Design	Prefire Checkout	Firing
1	387	382	372
2	57	58	58
3(a)	30	26	33
4	15	17	30
5	234	236	229
11	146	123	135
12	387	393	389

66-734

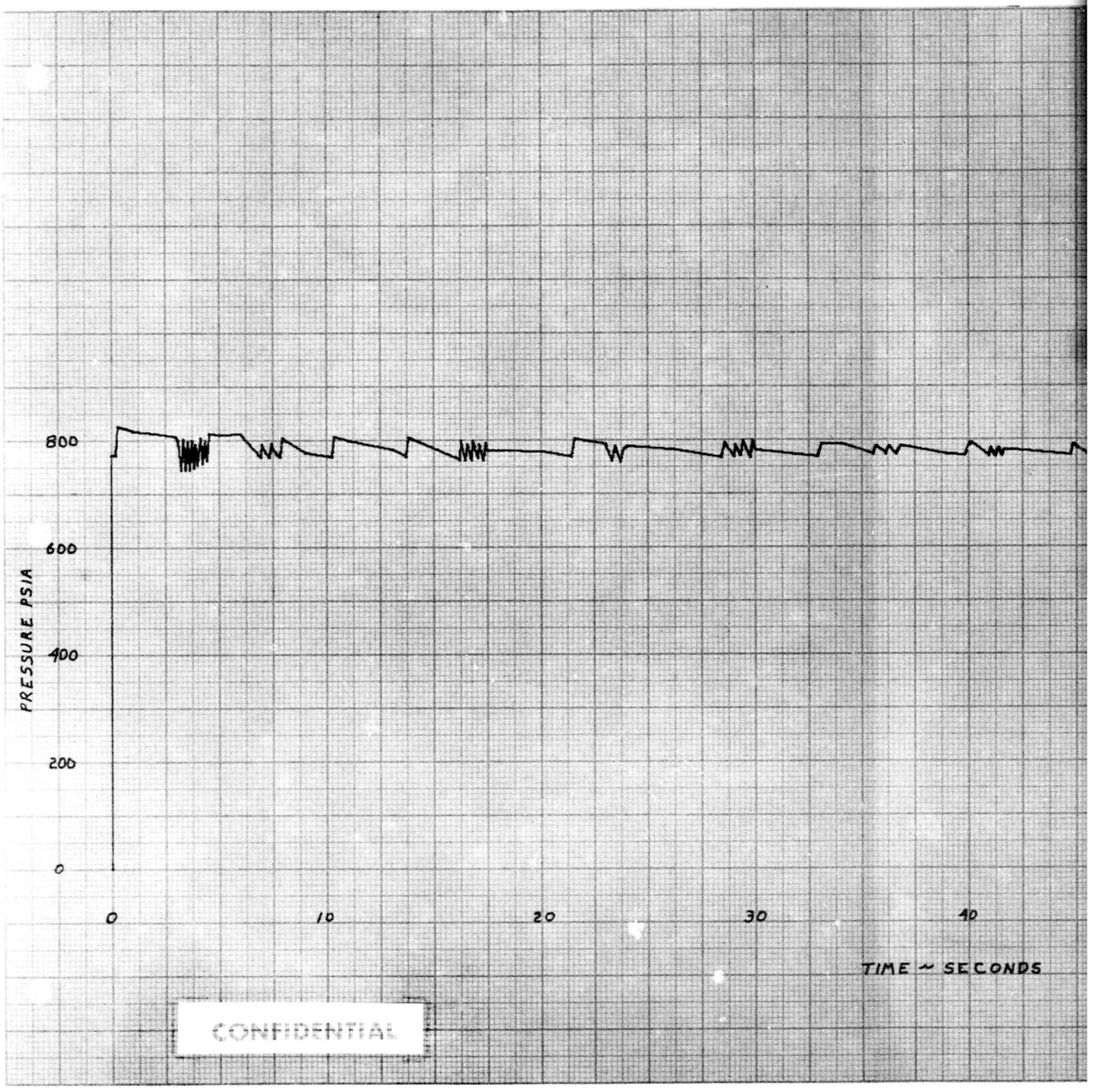

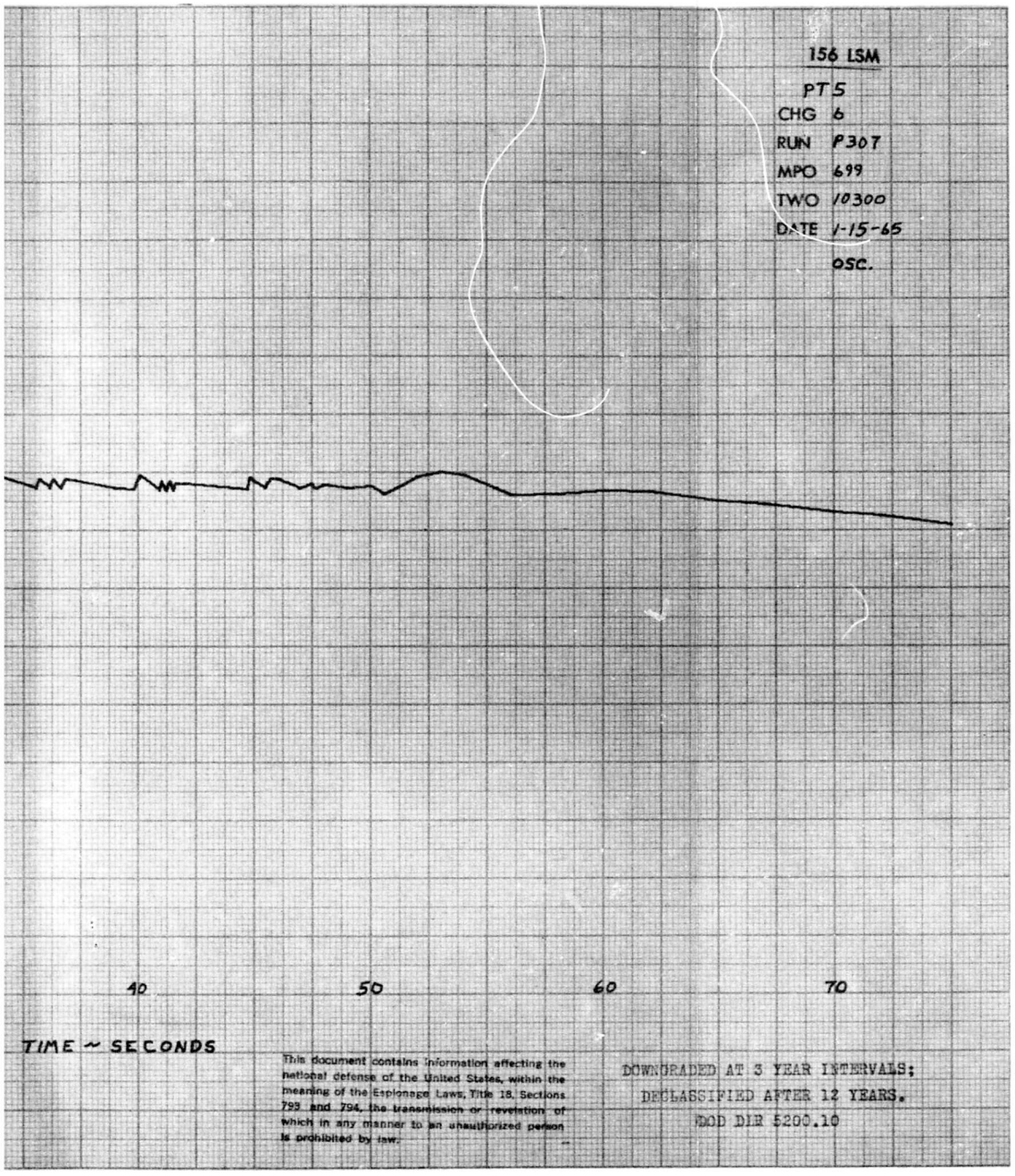

Figure 37 Ullage Pressure (GN_2 Side of N_2O_4 Tank Bladder) versus Time, Motor 156-6

(U) The injectant pressure, measured in the N_2O_4 manifold, is presented in Figure 38. The injectant pressure was slightly less than the ullage pressure during injection periods because of line losses and also exhibited greater oscillations than the ullage pressure because of the damping effect of the N_2O_4 bladder. A severe pressure oscillation, indicative of water-hammer, occurred at 25.5 seconds. The cause of this abnormality is not apparent, since none of the TVC system components were in operation at this time and there was no indication of any external disturbance.

(C) The GN_2 supply tanks were pressurized to 5500 psi prior to the test. During the bypass operation of prepressurizing the injectant systems, the supply pressure decreased to 4600 psi. The supply pressure during the firing duration is presented in Figure 39. The pressure decayed during each injectant cycle, but rose slightly during periods of no TVC activity because of heat transferred to the GN_2 from the tank walls. During the final two cycles, the supply pressure was below the nominal 1500 psi required to maintain sonic flow through the pressure regulators. During these two cycles, the injectant pressure (Figure 38) and the side force (Figure 16) decreased over the duration of the cycle. The decrease was more noticable during the 12th cycle, which required a high flow rate through the regulators.

(U) d. Nozzle Pressures. Four pressure taps were installed on the Motor 156-6 nozzle exit cone, midway between the injection ports, to establish the back pressure governing the injectant flow rates. The location of the pressure taps are shown in Figure 12. The recorded data (Figures 71 through 83 of Appendix III) indicate that the pressure taps may have plugged at several times during the test.

(U) Using the data points which appeared valid, the ratio of the nozzle pressure to chamber pressure during periods of injection was plotted against the circumferential location of the pressure taps, as shown in Figure 40. These data then were crossplotted to establish the effective pressure rise in the nozzle as a function of thrust deflection angle (Figure 41). This curve was used to compute injectant flow rates.

(C) e. Thrust Augmentation. Since the high pressure forces generated during periods of secondary injection act normal to the nozzle wall, a force component acts in the axial direction to provide increased thrust while injecting. The difference between the thrust level which would be obtained without injection and that obtained with injection is termed thrust augmentation, ΔF_a.

(U) The thrust augmentation recorded during the Motor 156-6 firing is shown in Figure 42. The data obtained during cycles 2 through 4 were garbled by low amplitude high frequency oscillations. Therefore, these data were disregarded in correlating the results. Also, the calculation of ΔF_a involved a small difference of two large numbers and, therefore, was not considered to be accurate for small thrust deflections.

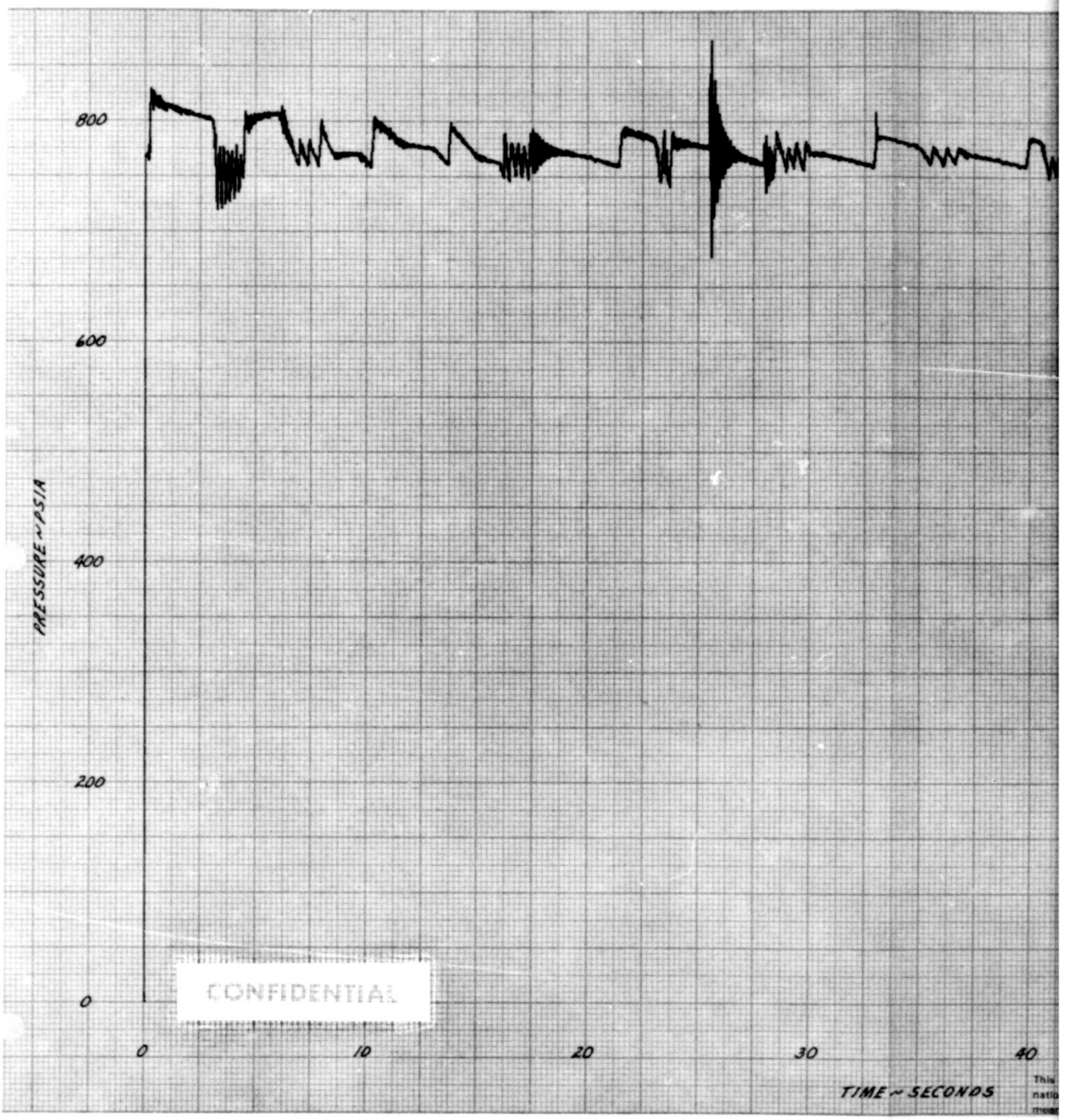

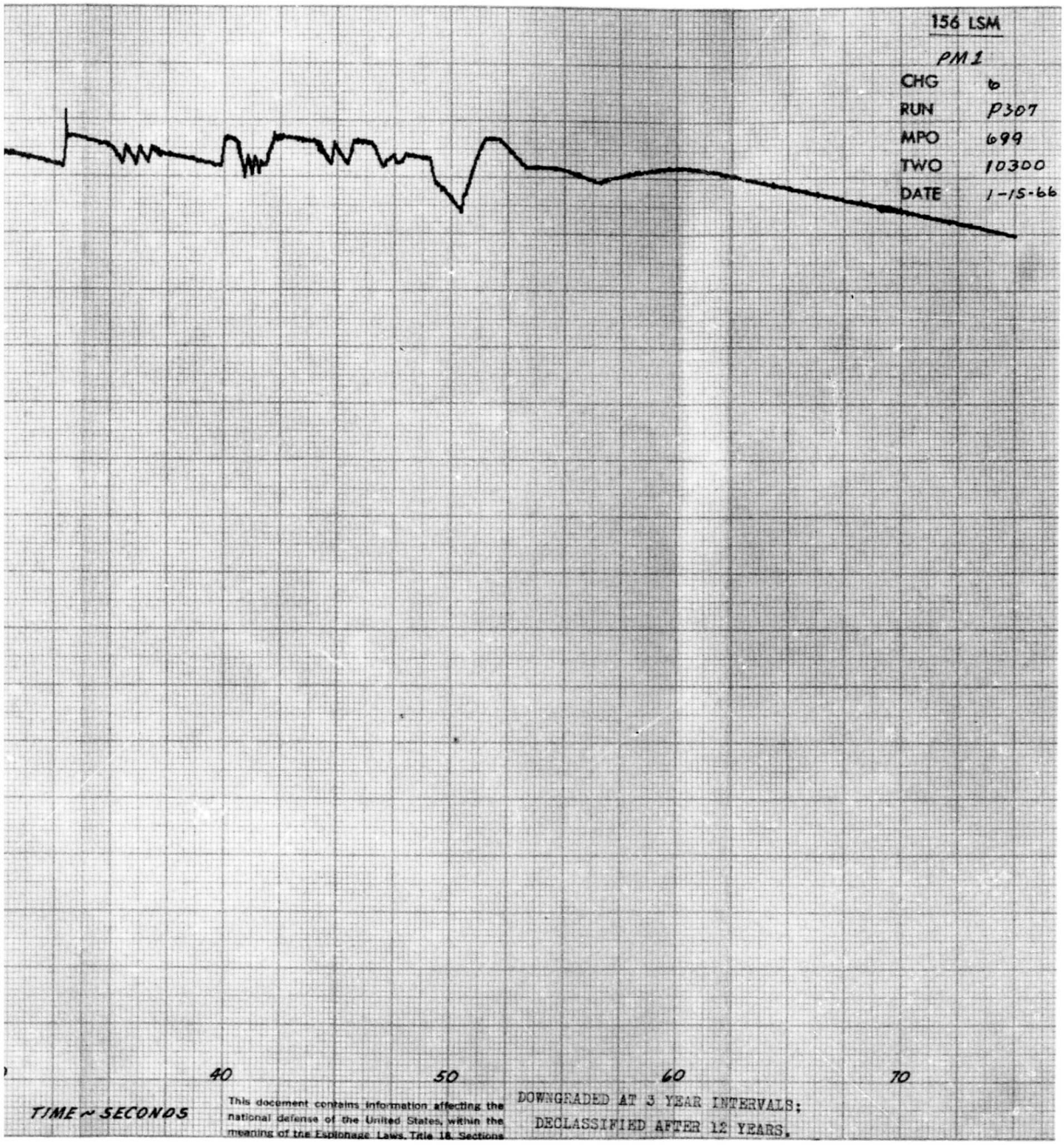

Figure 38 Injectant Pressure (N_2O_4 Manifold) versus Time, Motor 156-6

CONFIDENTIAL

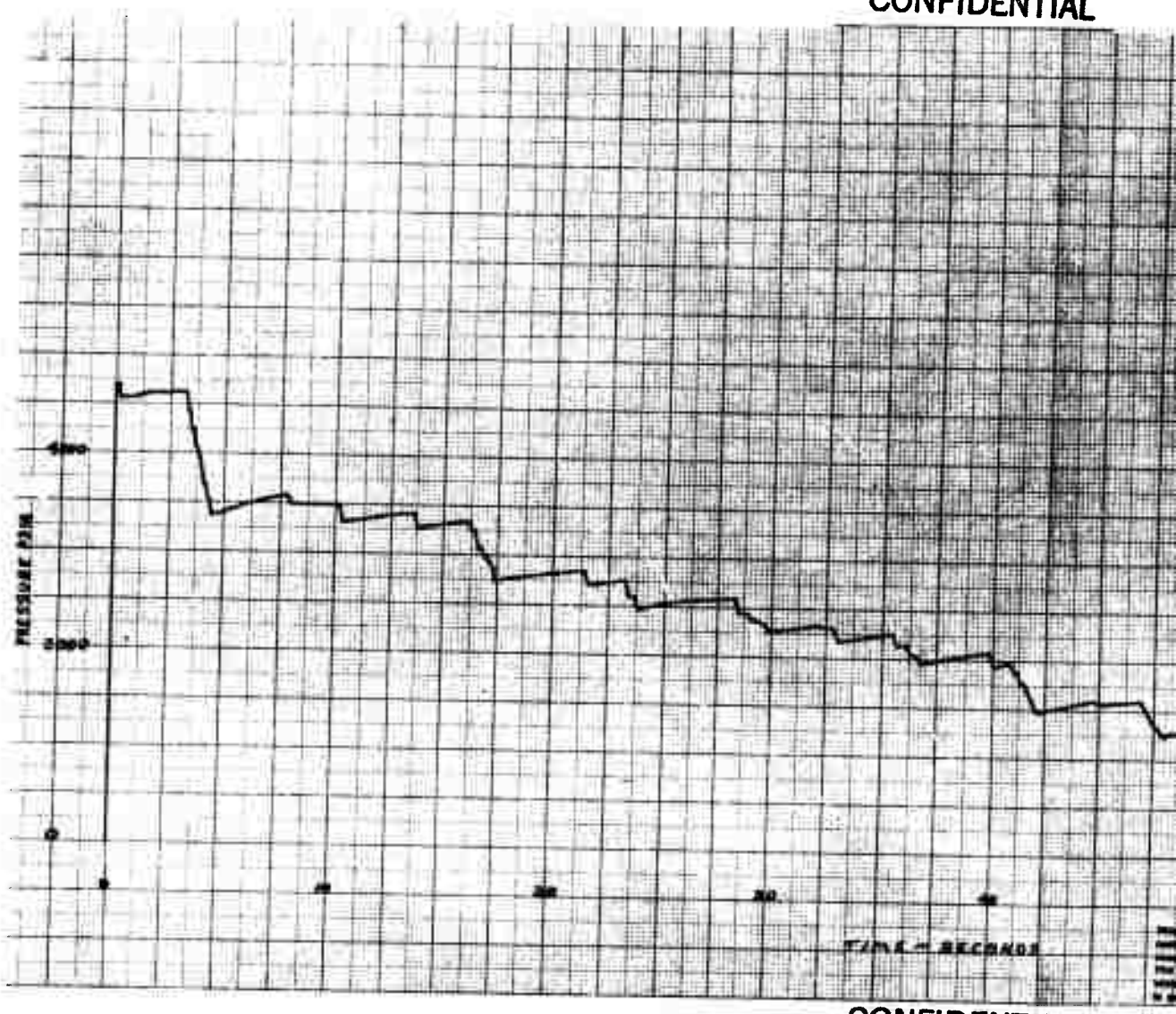

CONFIDENTIAL

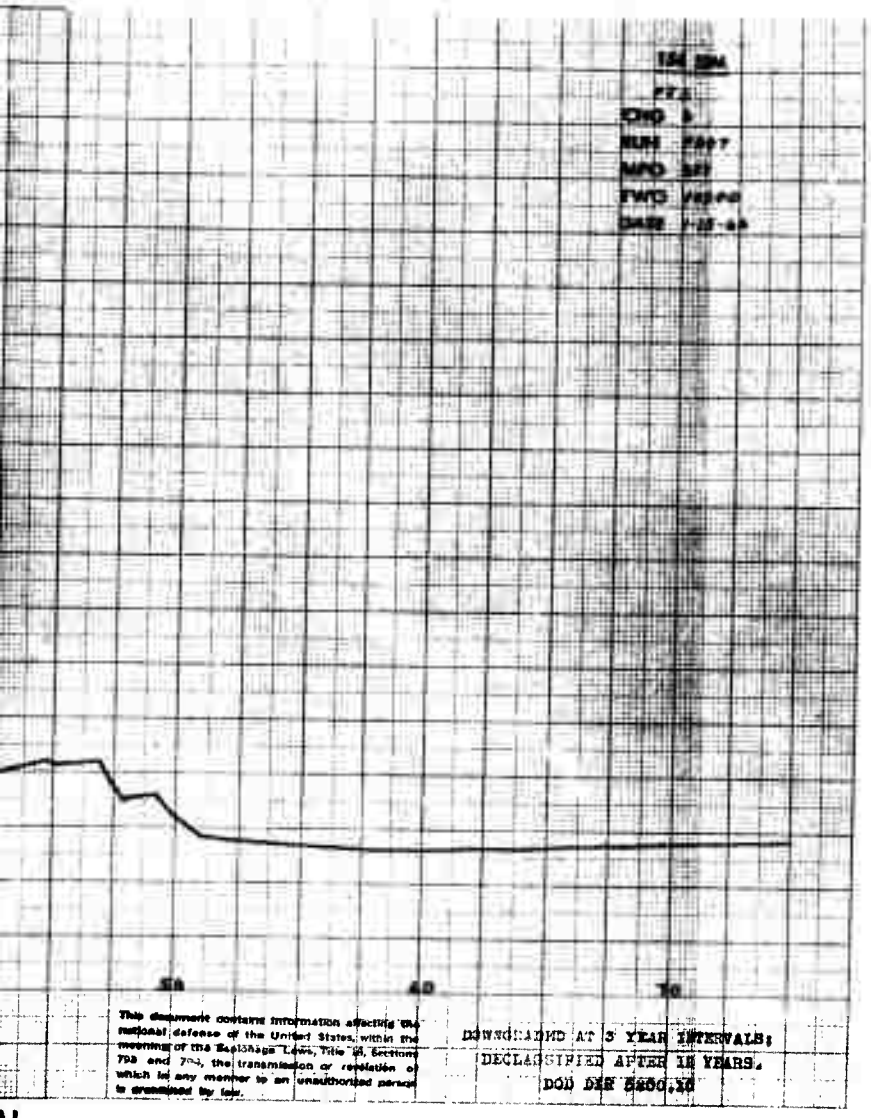

Figure 39 Supply Pressure versus Time, Motor 156-6

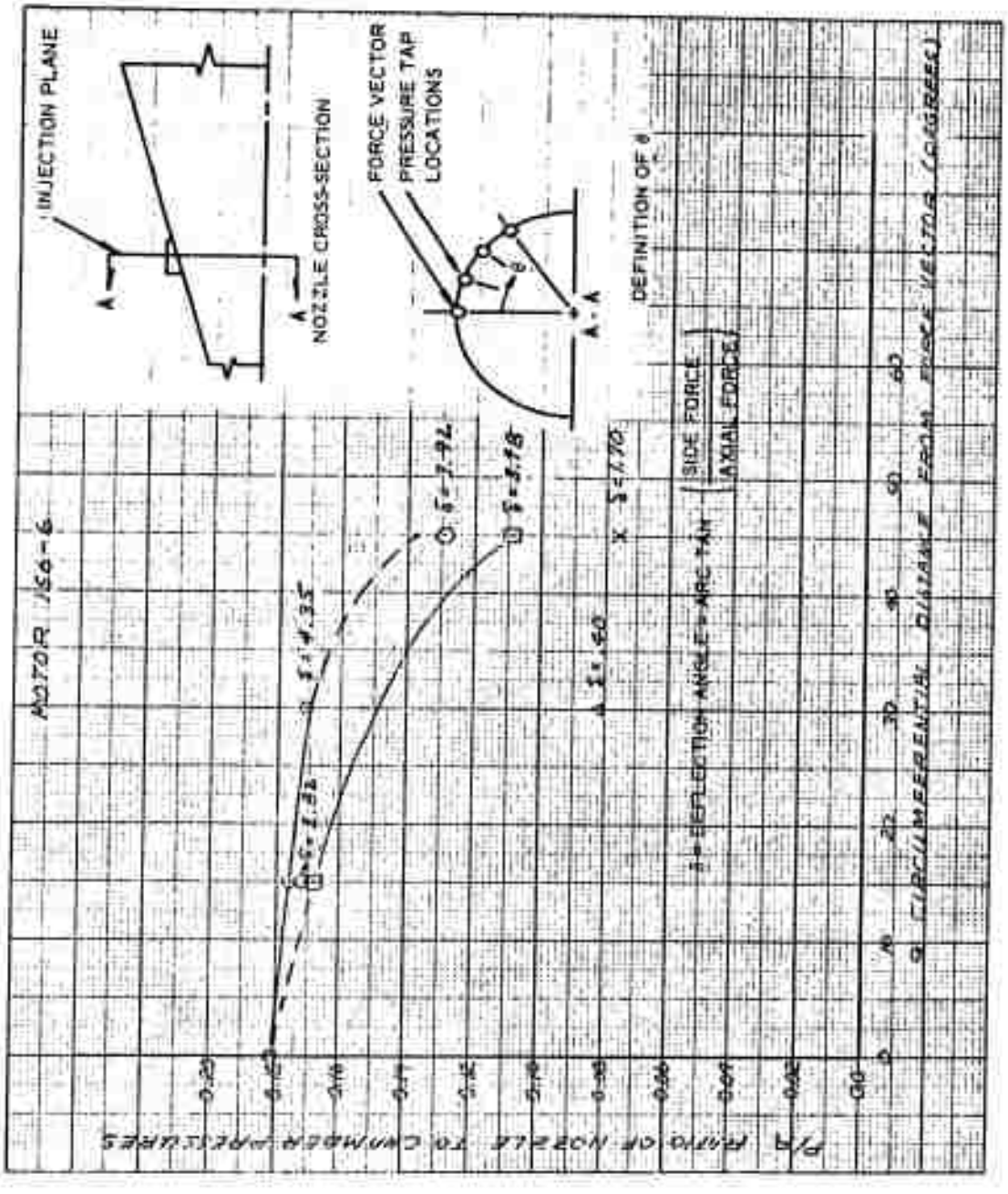

Figure 40 Ratio of Nozzle to Chamber Pressures versus Pressure Tap Location, Motor 156-6

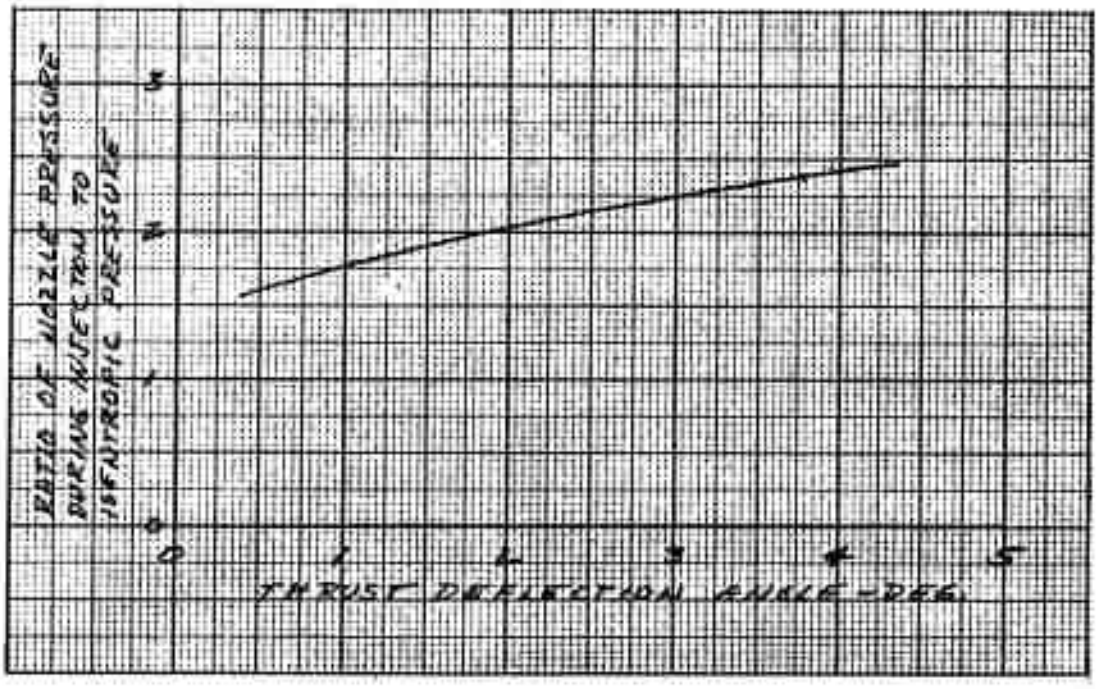

Figure 41 Nozzle Pressure Rise in Plane of Injection, Motor 156-6

CONFIDENTIAL

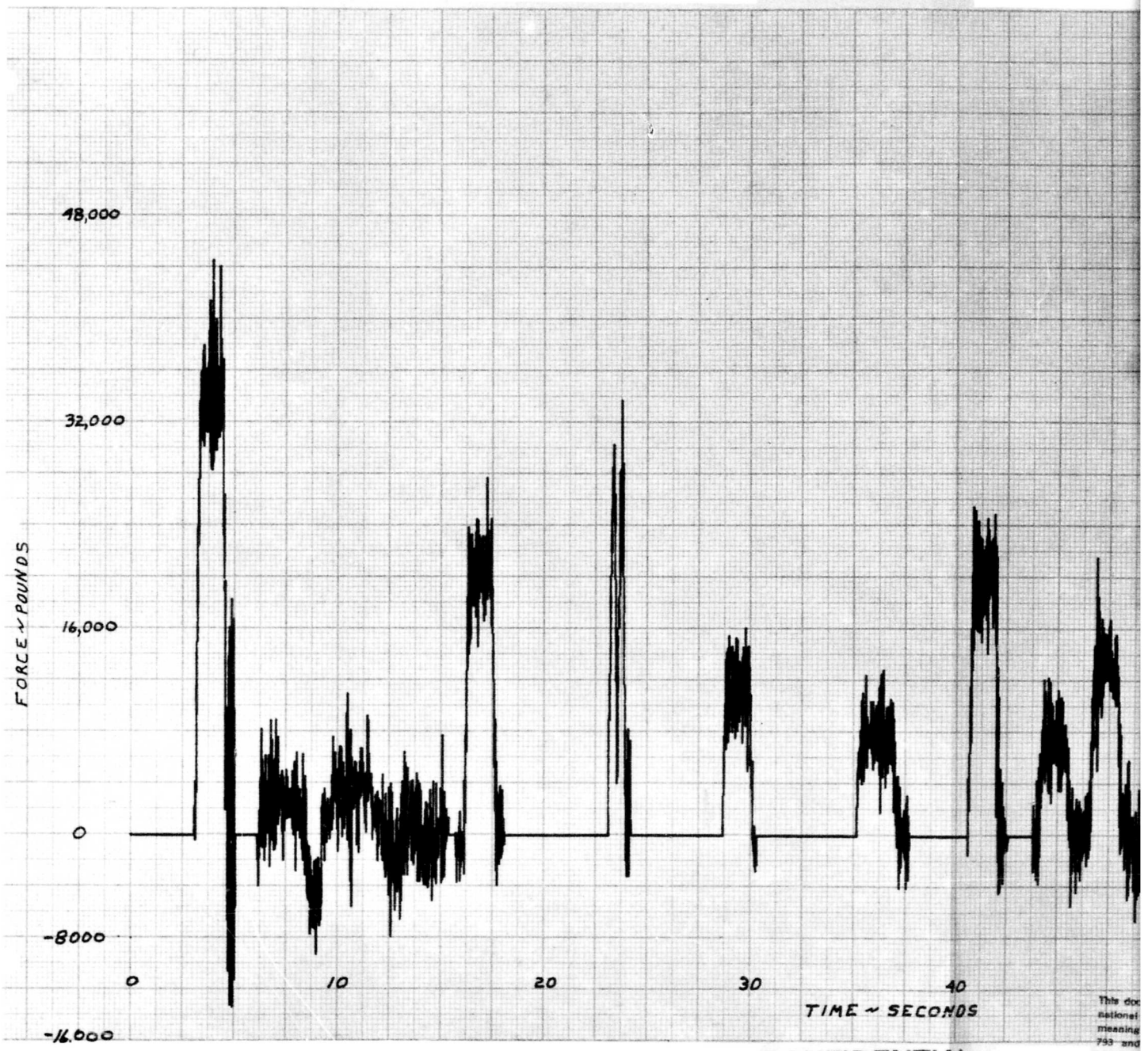

CONFIDENTIAL

NTIAL

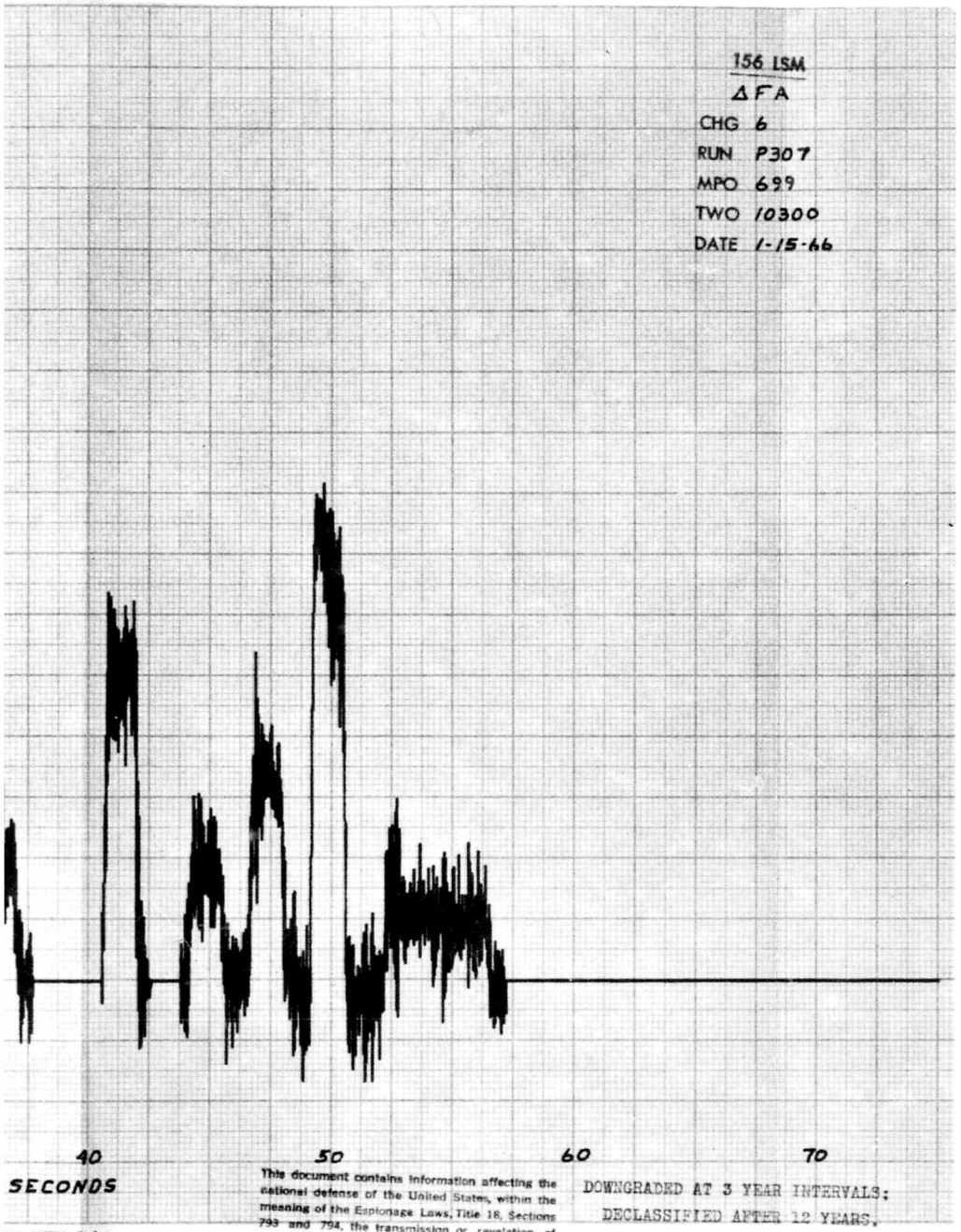

ENTIAL

2

Figure 42 Thrust Augmentation, Motor 156-6

(C) The data obtained for cycles 1 and 5 through 13 are plotted against the side thrust ratio in Figure 43. This plot indicates that the thrust augmentation increases with increasing side force and is about 46 percent of the side thrust level at a thrust deflection angle of 4 degrees.

(C) 3. Motor Postfire Inspection and Analysis

(C) a. Nozzle.

(C) (1) Postfire performance summary. The performance of the Motor 156-6 nozzle materials was satisfactory. The nozzle entrance cap insert fell into the motor during cooldown, and the two aft carbon-phenolic throat inserts experienced erosion rates approximately twice as great as the design prediction. Greater-than-design-predicted erosion also was experienced in the areas of liquid injection. Less-than-predicted-erosion was experienced by the nozzle entrance cap.

(U) The erosion profile of the ablative plastic materials is depicted in Figure 44. The measured erosion data referenced by longitudinal lengths and area ratios are presented in Table XII. Char data are presented in Table XIII. These data compare favorably with the predicted values shown in Figures 37 and 38 of Volume I, Book 1 and in Table VIII of Volume I, Book 1. The measured values are within 3 percent of the predicted values.

(U) The V-61 mastic rubber insulation at the nozzle flange showed only a slight indication of material loss. The surface was evenly charred with no indication of significant flow in this area.

(C) The silica-phenolic housing insulation showed minor erosion amounting to an average of 1.6 mils/sec, significantly lower than that experienced on Motor 156-5. The outside diameter of the carbon-phenolic nozzle entrance cap exhibited negligible erosion and random separation of the cloth plies. The separations followed the ply orientation which was in the direction of the helical layup with the plies parallel to the nozzle centerline. Erosion on the forward edge of the nozzle entrance cap was fairly even with only slight variations in depth. Maximum erosion in this area was 0.92 inch. The entrance cap insert had separated from the nozzle assembly after the firing and dropped to the forward end of the chamber. The parts of the insert were retrieved, reassembled, and measured. The insert had random erosion grooves that followed the ply orientation. Maximum erosion depth in the grooves was approximately 1.0 inch.

(U) Throat rings a, b, and c showed good erosion resistance. A maximum of 13.53 mils per second was measured at the throat (ring c). The forward edge of the "a" ring showed the effects of exposure on the leading edge caused by the gouged area of the entrance cap insert. (Figure 45.) These areas smoothed out approximately midway across the length of the part. Rings "b" and "c" were evenly eroded and smooth. Rings "d" and "e" had a continuous series of pock marks around the circumference. These marks or gouges formed a pattern in the direction of the ply orientation of the helical layup.

(C) The exit cone liner was a composite, parallel tape-wrapped structure of carbon and silica-phenolic with a glass-phenolic overwrap. Erosion of the

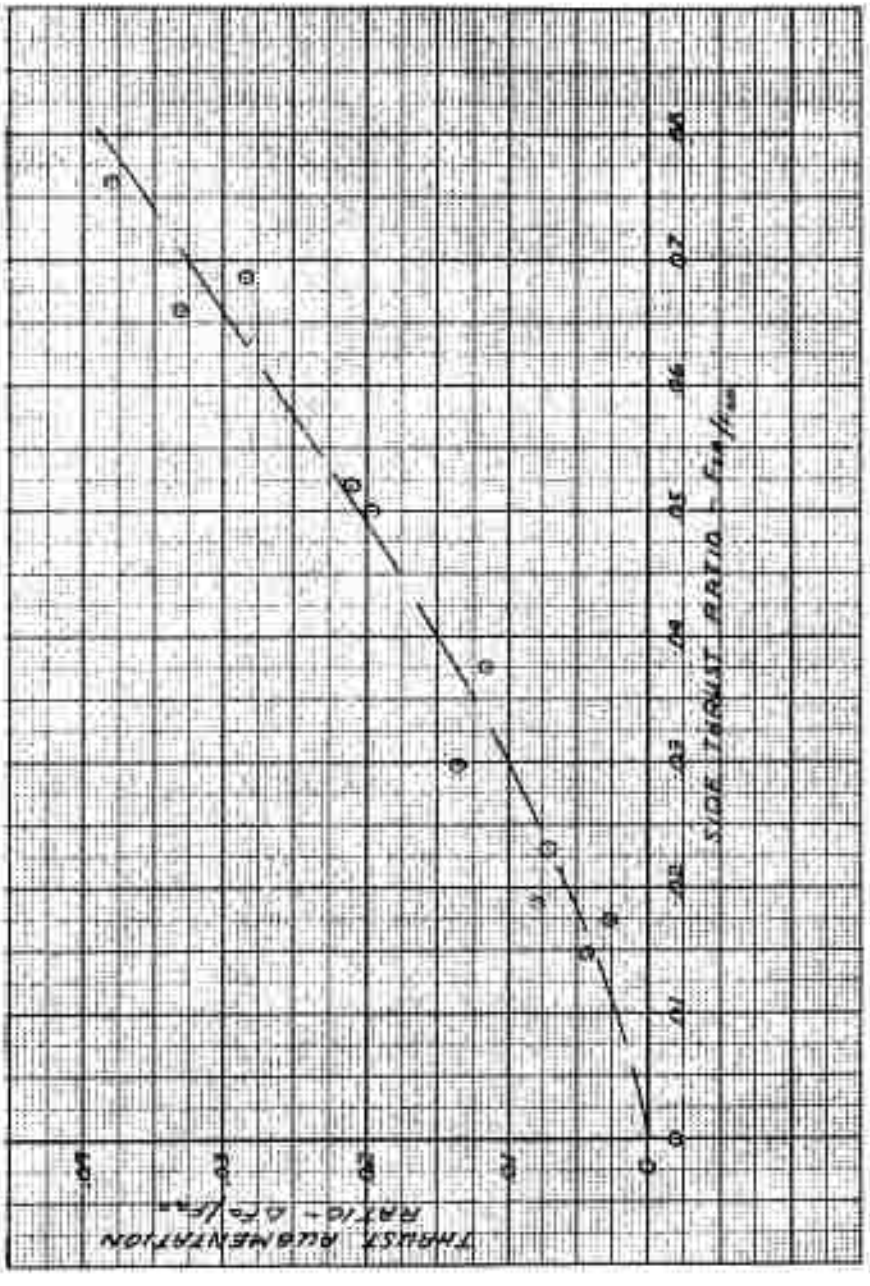

Figure 43 Thrust Augmentation versus Side Thrust Ratio, Motor 156-6

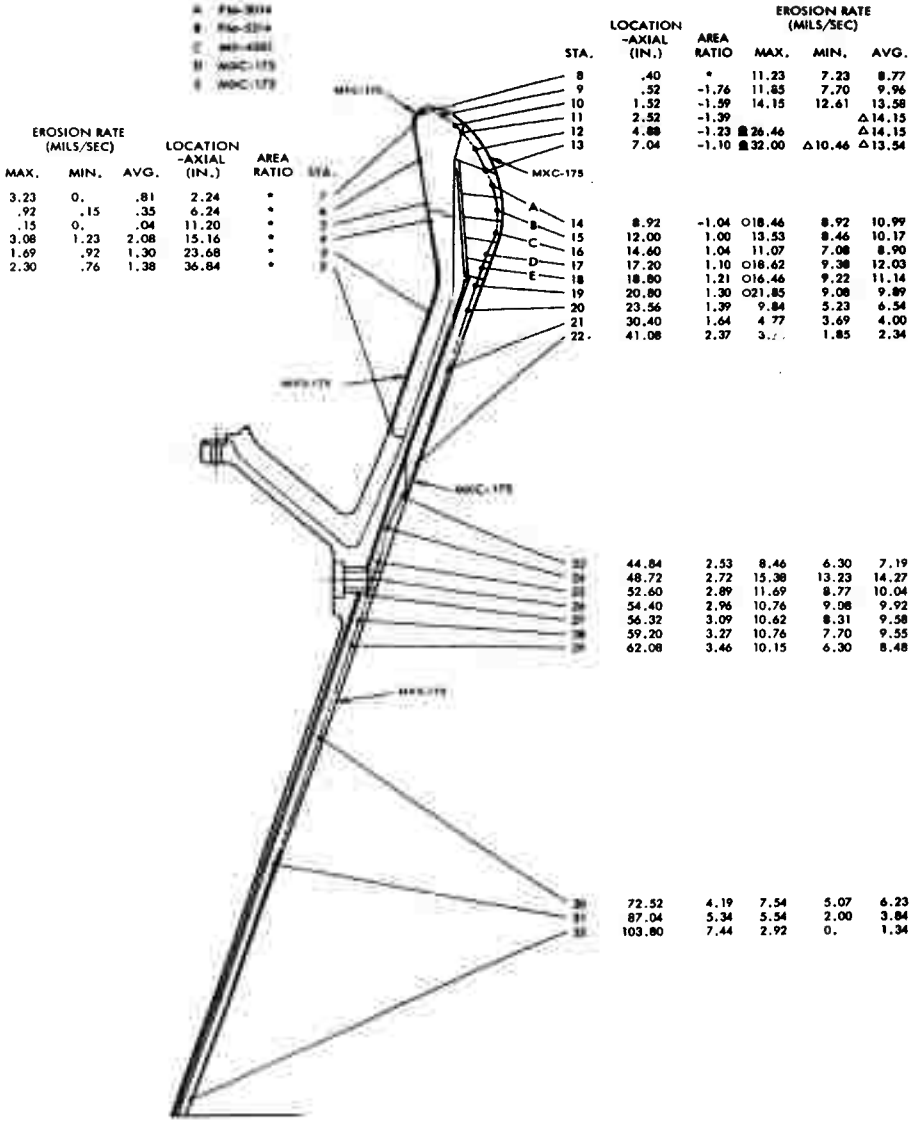

STA.	LOCATION -AXIAL (IN.)	AREA RATIO	EROSION RATE (MILS/SEC) MAX.	MIN.	AVG.
8	.40	*	11.23	7.23	8.77
9	.52	-1.76	11.85	7.70	9.96
10	1.52	-1.59	14.15	12.61	13.58
11	2.52	-1.39			Δ14.15
12	4.88	-1.23	■26.46		Δ14.15
13	7.04	-1.10	■32.00	Δ10.46	Δ13.54
14	8.92	-1.04	O18.46	8.92	10.99
15	12.00	1.00	13.53	8.46	10.17
16	14.60	1.04	11.07	7.08	8.90
17	17.20	1.10	O18.62	9.38	12.03
18	18.80	1.21	O16.46	9.22	11.14
19	20.80	1.30	O21.85	9.08	9.89
20	23.56	1.39	9.84	5.23	6.54
21	30.40	1.64	4.77	3.69	4.00
22	41.08	2.37	3.[illegible]	1.85	2.34
[illegible]	44.84	2.53	8.46	6.30	7.19
[illegible]	48.72	2.72	15.38	13.23	14.27
[illegible]	52.60	2.89	11.69	8.77	10.04
[illegible]	54.40	2.96	10.76	9.08	9.92
[illegible]	56.32	3.09	10.62	8.31	9.58
[illegible]	59.20	3.27	10.76	7.70	9.55
[illegible]	62.08	3.46	10.15	6.30	8.48
[illegible]	72.52	4.19	7.54	5.07	6.23
[illegible]	87.04	5.34	5.54	2.00	3.84
[illegible]	103.80	7.44	2.92	0.	1.34

STA.	EROSION RATE (MILS/SEC) MAX.	MIN.	AVG.	LOCATION -AXIAL (IN.)	AREA RATIO
[illegible]	3.23	0.	.81	2.24	*
[illegible]	.92	.15	.35	6.24	*
[illegible]	.15	0.	.04	11.20	*
[illegible]	3.08	1.23	2.08	15.16	*
[illegible]	1.69	.92	1.30	23.68	*
[illegible]	2.30	.76	1.38	36.84	*

Figure 44 Nozzle Ablatives Erosion Profile, Motor 156-6

* OUTSIDE DIAMETER LOCATIONS
Δ TAKEN FROM PART SEPARATE FROM NOZZLE ASSY
O GOUGE

TABLE XII

MEASURED NOZZLE EROSION FROM MAPPING TEMPLATE DATA, MOTOR 156-6

Material	Station No.	Area Ratio	Total Eroded Thickness (inches) 0°	30°	45°	60°	90°	120°	135°	150°	180°	210°	225°	240°	270°	300°	315°	330°
MXS-175	2	--	0.10				0.15				0.05				0.06			
MXS-175	3	--	0.08				0.11				0.06				0.09			
MXS-175	4	--	0.12				0.20				0.08				0.14			
MXC-175	5	--	-0.12				0.00				-0.03				0.01			
MXC-175	6	--	0.02				0.06				-0.07				0.01			
MXC-175	7	--	-0.01		0.21		-0.03		0.06		0.00		-0.08		0.15		-0.03	
MXC-175	8	--	0.53		0.49		0.55		0.70		0.47		0.49		0.73		0.60	
MXC-175	9	-1.76	0.50		0.58		0.65		0.77		0.58		0.62		0.77		0.71	
MXC-175	10	-1.59	0.92				0.87				0.82				0.92			
MXC-175	11	-1.39	Stations 11, 12, and 13 are located on the entrance cap insert which became disengaged from the nozzle and fell into the motor chamber after the firing. Therefore, no mapping template data are available for these stations.															
MXC-175	12	-1.23																
MXC-175	13	-1.10																
MX-4500	14	-1.04	0.77	0.61		0.68	0.67	0.83		0.81	0.79	0.58		0.68	1.20*	0.78		0.66
MX-4501	15	1.00	0.58	0.55		0.69	0.56	0.69		0.78	0.71	0.58		0.57	0.88	0.73		0.61
MX-4501	16	1.04	0.46	0.52		0.53	0.50	0.59		0.61	0.67	0.58		0.56	0.72	0.65		0.55
MXC-175	17	1.10	0.76		1.21*		0.85		0.61		1.19*		0.73		0.95		0.79	
MXC-175	18	1.21	0.60		0.79		0.64		0.94		0.63		0.69		1.07*		0.78	
MXC-175	19	1.30	0.59				0.74				0.60				1.42*			
MXC-175	20	1.39	0.34				0.34				0.38				0.64			
MXC-175	21	1.64	0.25				0.24				0.24				0.31			
MXC-175	22	2.37	0.14				0.12				0.14				0.21			
MXS-175	23	2.53	0.41				0.42				0.49				0.55			
MXS-175	24	2.72	0.86				0.95				0.90				1.00			
MXS-175	25	2.89	0.62	0.64		0.65	0.63	0.57		0.62	0.63	0.67		0.63	0.76	0.70		0.71
MXS-175	26	2.96	0.59	0.61		0.64	0.62	0.68		0.65	0.64	0.63		0.63	0.70	0.67		0.68
MXS-175	27	3.09	0.60	0.60		0.54	0.61	0.62		0.64	0.65	0.62		0.61	0.69	0.63		0.67
MXS-175	28	3.27	0.60		0.50		0.59		0.68		0.68		0.61		0.70		0.61	
MXS-175	29	3.46	0.57		0.41		0.49		0.55		0.58		0.57		0.66		0.58	
MXS-175	30	4.19	0.35				0.33				0.45				0.49			
MXS-175	31	5.34	0.25				0.13				0.26				0.36			
MXS-175	32	7.44	0.04				-0.09				0.03				0.19			

* Gouge

** Based on 65.0 seconds burn time

NOTE: 150-pounds of additional V-61 applied in Station No. 1 following the prefire mapping.

TABLE XIII

CHAR AND TOTAL HEAT PENETRATION SUMMARY, MOTOR 156-6 NOZZLE

Sample Number	Area Ratio	Char Depth (in.)†	Total Heat Penetration (in.)††	Remarks
1-090	*	0.188	0.344	
2-090	*	0.171	0.312	
3-090	*	(Indeterminate)	(Indeterminate)	Sample was delaminated
4-090	**	(Indeterminate)	(Indeterminate)	Charred over entire surface
5-090	1.335	0.375	0.531	Measured normal to upper surface
6-090	1.124	1.155	(Indeterminate)	Local delamination occurred
7-090	1.000	0.593	1.062	Minor delamination occurred
8-090	1.145	0.703	0.343	
9-090	1.185	0.421	1.062	Upper layer delamination in char area and separation from virgin material
10-090	1.390	≈0.437	≈0.843	Upper layer delamination in char area and separation from virgin material
11-090	2.053	0.468	0.781	Minor lower layer delamination
12-090	2.215	(Indeterminate)	(Indeterminate)	Sample delamination at char-decomposition interface
12-270	2.215	0.484	0.578	Measurements were made normal to the upper surface of the sample on as near a level plane as possible
13-090	2.361	(Indeterminate)	(Indeterminate)	Sample delaminated
13-270	2.361	0.531	0.593	Upper layer delamination Virgin material delamination
14-090	2.423	(Indeterminate)	0.593	Char region delamination
14-270	2.423	0.265	0.562	Delamination in decomposition region Virgin material delamination
15-090	2.476	0.281	0.500	Virgin material delamination
15-270	2.476	0.312	0.546	Virgin material delamination
16-090	3.006	0.484	0.562	Char region delamination
16-270	3.006	0.453	0.562	Minor delamination of virgin material
17-090	3.801	0.390	0.531	
18-090	4.717	0.390	0.562	Minor delamination in decomposition region

* Nozzle backside

** Nosecap tip

† Char Depth - Depth where the phenolic resin has completely pyrolyzed, i.e., the material density reaches char density.

†† Total Heat Penetration - Depth where the phenolic resin begins to pyrolyze.

Note: In some instances, compensation for delamination was made by compressing the layers before measurements were made. Resin decomposition regions are estimated, based on hardness characteristics near the virgin material.

Figure 45 Postfire View of Throat Section

carbon-phenolic throat extension showed the effects of the severe condition of the "d" and "e" throat rings. Material loss at the aft end of the carbon was slight. The typical heavy erosion downstream of the carbon-to-silica interface was as expected. The maximum depth of erosion in this area was 1.00 inch. At the injector ports, increased surface regression occurred as predicted. Figure 46 is a typical view of the exit liner in the area of the injector ports. The remaining length of the exit cone was in excellent condition with negligible erosion at the exit.

(U) The nozzle steel housing showed no evidence of damage or heat effects.

(C) (2) Nozzle ablatives performance analysis. A discussion of individual insulator component performance follows.

(U) The nozzle housing insulation extended along the external radius of the submerged portion of the nozzle from the aft closure area to a point approximately opposite the nozzle throat. The Motor 156-6 nozzle housing was bias tape-wrapped, silica-phenolic material. Measured erosion rates for the Motor 156-6 housing insulation ranged from 1.23 to 3.08 mils/sec. Erosion was nearly uniform along the length of the part.

(U) The nozzle entrance cap extended forward of the nozzle-housing-insulator and formed the re-entry section of the nozzle. The entrance cap insert defined the throat approach contour and formed the entrance cap and throat sections. The entrance cap and entrance cap insert were constructed from MXC 175, a carbon-phenolic tape material.

(C) No appreciable erosion was evident at the entrance cap-nozzle housing interface. Erosion increased along the backside of the entrance cap, reaching a value of 11.23 mils/sec at the nozzle nose. Erosion rates increased uniformly to 14.15 mils/sec at the entrance cap-entrance cap insert interface.

(U) Loss of the entrance cap insert precluded obtaining postfire erosion measurements in the normal manner. No charring of the entrance cap or throat section bondline interfaces was noted (Figure 47), indicating that the insert was lost during motor cooldown. Reconstruction and examination of recovered pieces showed localized gouging with uniform erosion over the remaining ungouged areas. Measurements taken from the reconstructed nozzle entrance cap are compared with design dimensions in Figure 48. The insert was delaminated in planes parallel to the orientation of the tape plies. It appears that the material delaminated in several areas. The smaller pieces could not be held by the entrance cap retention angle, and loss of the entire insert resulted after motor depressurization.

(C) The Motor 156-6 nozzle section consisted of 5 individual segments, 3 of graphite-phenolic and 2 of carbon-phenolic, extending from a subsonic area ratio of approximately 1.06 to a supersonic area ratio of 1.22. The graphite-phenolic segments formed the subsonic and sonic section of the throat insert; the carbon-phenolic material was used in the supersonic region. Erosion of

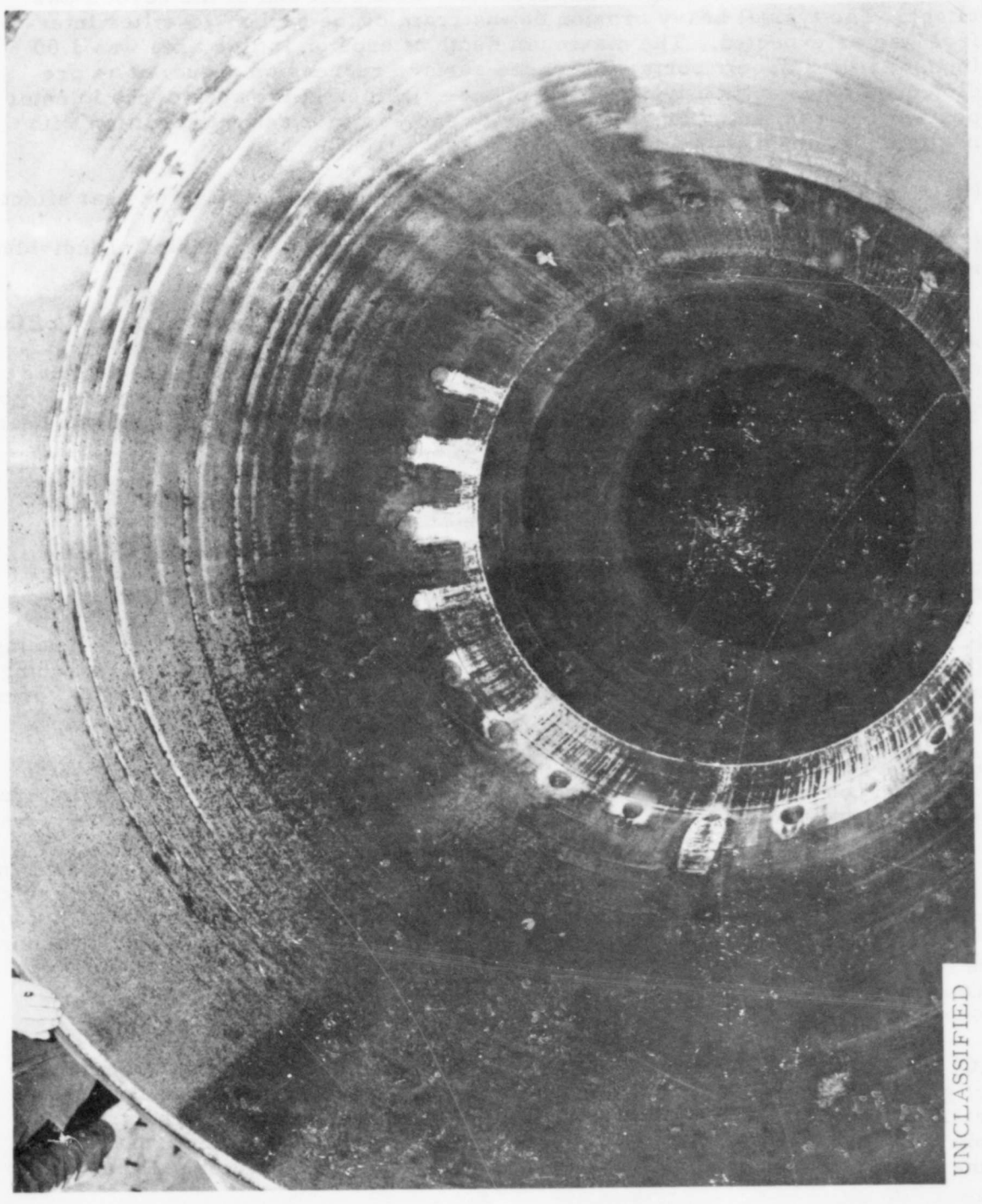

Figure 46 Exit Liner in Injector Port Area, Typical View, Motor 156-6

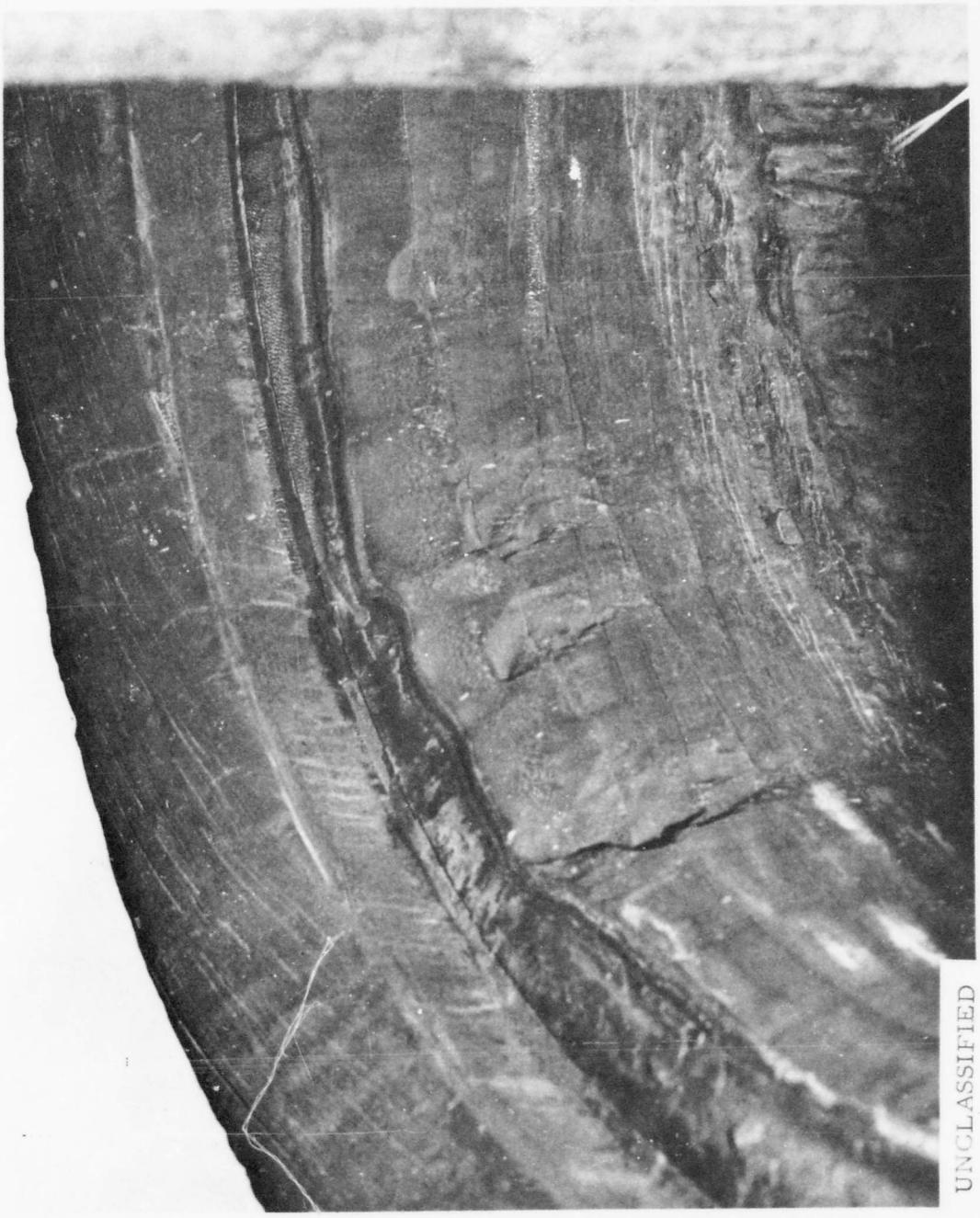

Figure 47 Postfire View of Entrance Cap and Throat Section

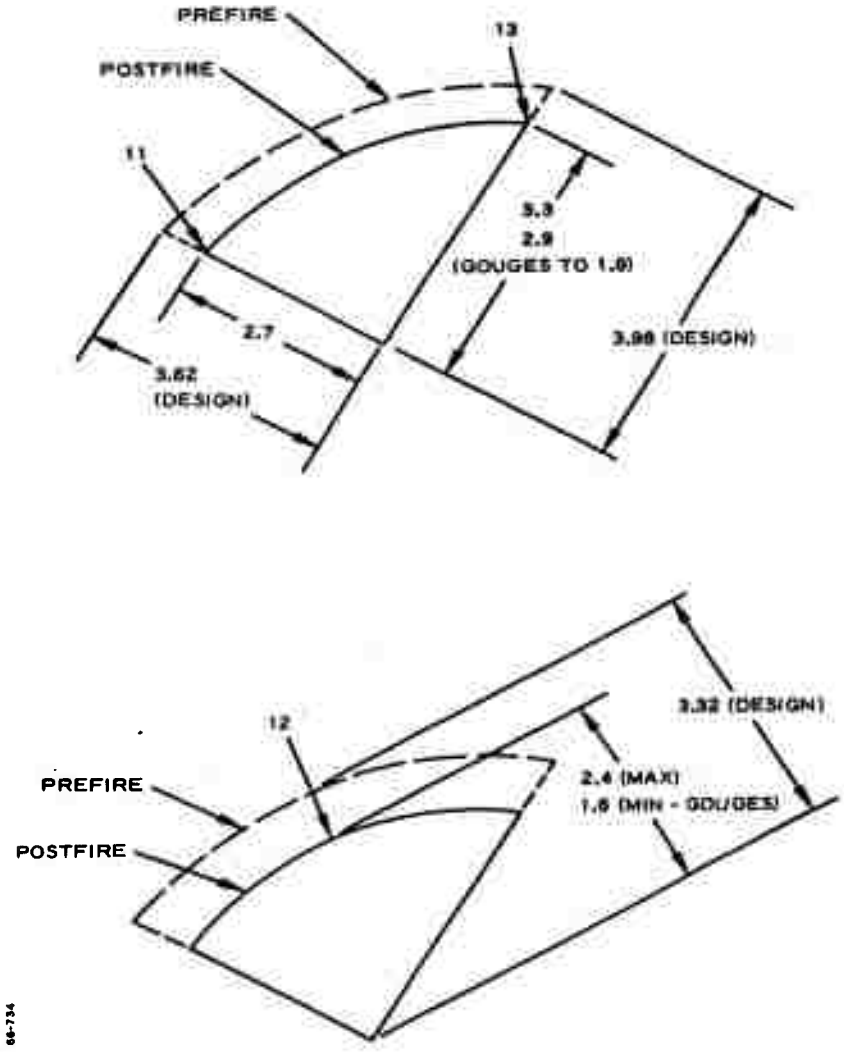

Figure 48 Comparison of Reconstructed Entrance Cap Insert and Design, Motor 156-6

the graphite-phenolic segments agreed closely with predicted values. Erosion increased from 12.77 mils/sec at a subsonic area ratio of 1.04 to 13.53 mils/sec at the throat. Erosion at the supersonic segment location (1.04) was 11.07 mils/sec. Erosion was uniform, and maximum-minimum values varied by approximately 4 mils/sec.

(C) Erosion of the carbon phenolic (MXC-175) segments was consistently greater than for the graphite-phenolic material. Severe circumferential gouging also was evident with a maximum gouge depth of 1.21 inches measured from the initial prefire surface. The average erosion rate for the ungouged areas was 12.03 mils/sec at an area ratio of 1.1 and 11.14 mils/sec at an area ratio of 1.21. These data indicate that the carbon-phenolic segments were deficient in material, ply orientation, or method of manufacture.

(U) The throat extension component extended aft from the throat section to an area ratio of 2.46 for Motor 156-6. The material was carbon-phenolic tape, MXC-175.

(C) Average erosion rates for the Motor 156-6 throat extension material ranged from 9.89 mils/sec at an area ratio of 1.3 to 2.34 mils/sec at an area ratio of 2.37. Erosion at the throat segment-nozzle extension interface reflected the gouging experienced by the carbon-phenolic throat insert segments.

(U) The exit cone liner extended from the throat extension to the nozzle exit plane and included the area of TVC liquid injection. The exit cone liner material was silica-phenolic tape, MXS-175.

(C) The maximum area of erosion for the Motor 156-6 exit cone liner was approximately 5 inches aft of the throat extension-exit cone liner interface. A maximum rate of 15.38 mils/sec was recorded. The interface material change would have little effect at this location; the measured erosion rates reflect the increased erosive and heating environment caused by the fluid injection shock system. Erosion decreased uniformly along the exit cone except in the immediate area of the TVC ports. The average erosion rate at the nozzle exit plane was 1.34 mils/sec. Localized erosion in the area aft of the TVC ports was less than that experienced upstream of the ports.

(C) (3) Acceleration environment. Six accelerometers were used to measure acceleration in three directions at two locations on the nozzle TVC assembly. One triad of accelerometers was mounted on the nozzle shell adjacent to the mounting pads for the GN_2 tank. The accelerometers at this location were oriented orthogonally in the direction normal to the shell surface, in the meridional direction, and in the circumferential direction. The other triad of accelerometers was mounted on the N_2O_4 manifold and oriented in the axial, transverse, and circumferential directions of the motor.

(U) The acceleration measurements were recorded on an oscillograph which precluded a detailed harmonic analysis of the results. Significant acceleration was recorded only during periods of TVC injection. The oscillograph records clearly indicate that a severe vibration environment existed only at these times.

(U) During TVC injection, the accelerations consisted of high frequency oscillations which appeared as hash on the oscillograph superimposed on a low frequency oscillation (less than 5 cps). This low frequency oscillation was well-defined for measurements normal to the nozzle shell adjacent to the GN_2 tank. For other locations and directions, it was difficult to define and measure the relatively small amplitude of the low frequency disturbances in the presence of large amplitude hash.

(U) The maximum amplitudes of the low and high frequency oscillations are listed below.

MAXIMUM ACCELERATION AMPLITUDES (g's)

Location	Direction	Low Frequency	High Frequency
Nozzle shell adjacent to GN_2 tank	Meridional	5	± 43
	Circumferential	2	± 28
	Normal	48	± 32
N_2O_4 Manifold	Axial	5	± 32
	Circumferential	4	± 42
	Transverse	2	± 37

(U) The high values of the low frequency acceleration normal to the nozzle were somewhat higher than previous measurements of acceleration on 120-inch diameter motor nozzles with liquid injection TVC (1, 2, 3). The peak amplitudes of the high frequency oscillations also were higher than expected, based on 120-inch diameter motor firings; the severity of the oscillations compared to the equivalent static design loads of 53 g's transverse and circumferential and 32 g's axial for nozzle-mounted TVC equipment cannot be assessed without a detailed harmonic analysis of the data which could not be undertaken because of the data format.

(U) b. Motor Case. The motor case showed no areas of excessive heating or gas leakage and no structural damage. Disassembly of the nozzle and the igniter and visual inspection of the O-rings and RTV joint-sealer indicated that there was no gas penetration into these areas. Thermocouples located on the motor chamber showed essentially no change in temperature during the firing duration.

(U) Temperature and strain data obtained from gages located on the cylindrical and dome sections of the motor chamber are included in Appendix III.

(C) c. Motor Case Insulation. Visual inspection of the insulation used in the motor chamber domes indicated satisfactory performance of the LPL-31 mastic rubber. The insulation surfaces were typically rough and uneven; however, no areas of excessive erosion were visible. The chamber cylinder showed a remaining coat of liner, indicating even grain burnout and no overheating of the motor case.

(U) Prefire and postfire thickness measurements were taken at the aft flange at eight circumferential stations, 45 degrees apart. The measurement scheme and the data are presented in Table XIV. Data obtained from other measurements were invalid. Data obtained from other measurements taken in the forward and aft domes are considered invalid because the prefire and postfire locations were not indexed properly.

(C) The average heat penetration rate was 4.90 mils/sec. The maximum rate at one location was 13.08 mils/sec. The maximum rate used for design purposes was 14.8 mils/sec. Thus, the as-built mastic insulation configuration exhibited an additional safety factor of 13 percent over the minimum expected margin.

(U) d. TVC System

(U) (1) Summary. Visual inspection of the TVC system during dismantling operations showed that no damage was sustained as a result of the static test firing of the motor.

(U) (2) Pressurization Subsystem. Visual inspection showed that all components were in excellent condition after the firing.

(U) (3) Injectant Subsystem. Examination of N_2O_4 tanks and ducting revealed no significant indications of N O leakage. Inspection of bladder assemblies was not accomplished, however, because scheduling commitments would not allow disassembly of the N_2O_4 tanks.

(U) (4) Injector Valve Subassembly. Inspection of the valve-nozzle mating surface showed no indication of N_2O_4 or exhaust gas leakage. Examination of the valve pilot housing and pintles showed only minor material erosion.

(U) (5) Hydraulic Power Subsystem. Postfire inspection of the hydraulic power subsystem showed the components to be in excellent condition.

(U) (6) Electrical Power Subsystem. Inspection of all components of this system showed that no damage was incurred from the motor firing.

Table XIV

INSULATION MEASUREMENTS, MOTOR 156-6

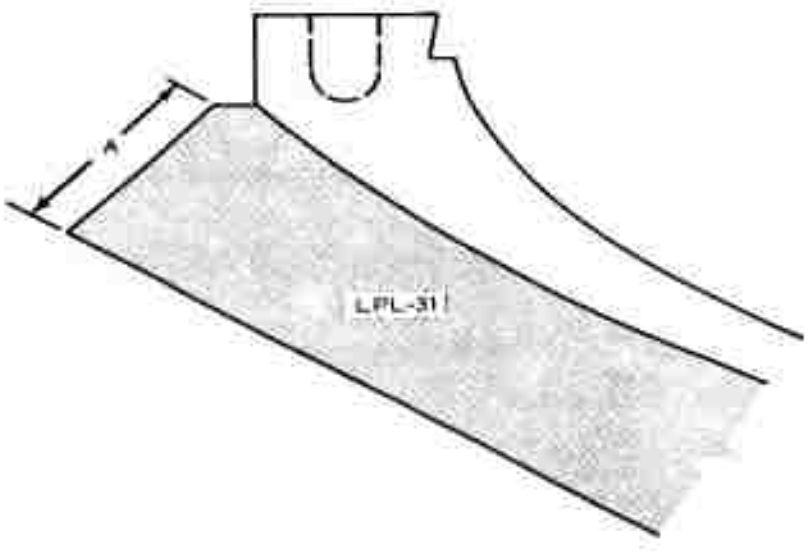

Dimension A

STATION	PREFIRE, (IN.)	POSTFIRE, (IN.)	HEAT PENETRATION, (IN.)
0°	2.00	1.80	0.20
45°	1.80	1.50	0.30
90°	1.85	1.00	0.85
135°	1.80	1.55	0.25
180°	1.70	1.50	0.20
225°	1.70	1.60	0.10
270°	1.90	1.60	0.30
315°	1.95	1.60	0.35
AVERAGE RATE* (MIL/SEC)			4.90
MAXIMUM RATE (MIL/SEC)			13.08
MINIMUM RATE (MIL/SEC)			1.54

66-734

*BASED ON t = 65.00 SECONDS.

REFERENCES

1. United Technology Center, Sunnyvale, Test Evaluation Report (Ground Test) XSR-47-UT-1-3, ER-UTC 64-98, 22 April 1964.

2. United Technology Center, Sunnyvale, Test Evaluation Report (Ground Test) XSR-47-UT-1, ER-UTC 64-265, 21 December 1964.

3. United Technology Center, Sunnyvale, Test Evaluation Report (Ground Test) XSR-47-UT-1 (UA 1205-10), ER-UTC 65-55, 1 April 1965.

APPENDIX I

Motors 156-5 and 156-6

Items	Comments
	See pages B-1 through B-3 for information on number of curves, scales and other comments.
1. Forward chamber pressure (P_{c_1} - psia) vs. time (sec.)	
2. Aft chamber pressure (P_{c_2}-psia) vs time (sec.)	
3. a) Expanded forward chamber pressure (psia) vs time (sec.)	
b). Expanded igniter pressure (psia) vs time (sec.)	
4. Measured axial force (lbs) (uncorrected for weight) vs time (sec.)	Summation of 6 load cells on 156-5 and 3 load cells on 156-6.
5. Measured axial thrust (F_a lbs) (corrected for weight) vs. time (sec.)	See pages A-1 and A-2 for weight correction method.

6. Nominal axial thrust (Fa_0-lbs) vs. time (sec.)

Nominal thrust is found during fluid injection periods from

a) $$Fa_o = Fa_1 + \frac{Fa_2 - Fa_1}{Pc_2 - Pc_1} (Pc - Pc_1)$$

when $$\frac{Pc_2 - Pc_1}{Pc_1} > \pm 0.01 \quad \underline{\text{and}} \quad \frac{Fa_2 - Fa_1}{Pc_2 - Pc_1} > 0$$

b) $$Fa_o = Fa_1 + \frac{Fa_2 - Fa_1}{t_2 - t_1} (t - t_1)$$

when $$\frac{Pc_2 - Pc_1}{Pc_1} < \pm 0.01 \quad \underline{\text{or}} \quad \frac{Fa_2 - Fa_1}{Pc_2 - Pc_1} < 0$$

Where t_1 = time at beginning of cycle as shown on page A-3

t_2 = time at end of cycle as shown on page A-3.

Fa_{t_1} and Pc_1 = thrust (item 5) and pressure (item 1) at time t_1

Fa_{t_2} and Pc_2 = thrust (item 5) and pressure (item 1) at time t_2.

During periods of time not specified in page A-3, nominal thrust equals measured thrust (item 5).

Item 5 minus item 6.

7. Thrust augmentation (ΔFa-lbs) vs time (sec.)

Plot cells F-9, F-10 and F-11 on one graph and cells F-7 and F-8 on the other graph.

8. Side thrust (from each cell) (lb) vs time (sec.)

9. Side thrust (Fs-lbs) (sum of appropriate cells) vs. time (sec.).

Sum cells F-8 + F-10 + F-11 and plot for pitch plane. Sum cells F-7 + F-9 and plot for yaw plane.

10. Side thrust ratio (Fs/Fa_o) vs. time (sec.)

Divide item 9 by item 6 for both pitch and yaw planes.

11. Thrust misalignment ($\frac{\Delta Fs}{Fa_o}$) vs. time (sec.)

Average side thrust ratio (item 10) during time periods shown on page A-4 for both pitch and yaw planes.

12. Side thrust ratio (Fs/Fa_o) (corrected for thrust misalignment) vs. time (sec.)	Average the valves of thrust misalignment (item 11) immediately prior to and following the cycle which is being corrected as shown on page A-5, and add this value to item 10 for both pitch and yaw planes.
13. Resultant side thrust ratio (Fs_r/Fa_o) vs. time (sec.)	Vectorially sum side thrust ratios (item 12) in pitch and yaw planes. $\frac{Fs_R}{Fa_o} = \left[\left(\frac{Fs_p}{Fa_o}\right)^2 + \left(\frac{Fs_Y}{Fa_o}\right)^2\right]^{\frac{1}{2}}$
14. Resultant thrust deflection angle (δ - degrees) vs. time (sec.)	$\delta = \tan^{-1}\left(\frac{Fs_R}{Fa_o}\right) = \tan^{-1}\left[\text{Item 13}\right]$
15. Direction of resultant side thrust angle (θ - degrees) vs. time (sec.)	$\theta = \tan^{-1}(-Fs_y/Fs_p) = \tan^{-1}[-\text{item } 12_Y/\text{item } 12_P]$ or $= \sin^{-1}(Fs_p/Fs_r) = \sin^{-1}[-\text{item } 12_P/\text{item } 13]$ or $= \cos^{-1}(-Fs_y/Fs_r) = \cos^{-1}[-\text{item } 12_Y/\text{item } 13]$ Angle is measured from the positive pitch plane, with the first quadrant between positive pitch and negative yaw. Angle will range numerically between 0° and 360°.
16. Resultant side thrust (Fs_r - lbs) vs. time (sec.)	Multiply item 13 by item 6.
17. Command signal (C-volts) vs. time (sec.)	Separate curves for pitch and yaw.
18. Resultant command signal (C_R-volts) vs time (sec.)	Resultant of pitch and yaw input $C_R = \left[C_P^2 + C_Y^2\right]^{\frac{1}{2}}$
19. Resultant side thrust (Fs_R - lbs) vs. resultant command signal (C_R - volts)	Plot item 16 vs. item 18 (hystersis plots for each cycle)
20. Valve pintle position (S-volts) (feed back) vs. time (sec.)	
21. Manifold pressure (P_M-psia) vs. time (sec.)	P_{M1} = pressure at 315° location P_{M2} = pressure at 135° location

22. Effective manifold pressure (P_{Me} - psia) vs time (sec.)

Compute angle ϕ : $\phi = \theta + 45°$ $0° \leq \theta \leq 315°$
$\phi = \theta - 315°$ $315° < \theta \leq 360°$

where θ is item 15. Then compute effective manifold pressure from

$$P_{Me} = \frac{180-\phi}{180} P_{M1} + \frac{\phi}{180} P_{M2} \qquad \phi < 180°$$

$$\frac{\phi-180}{180} P_{M1} + \frac{360-\phi}{180} P_{M2} \qquad \phi > 180°$$

23. Nozzle pressure (P_N - psia) vs time (sec.)

24. Nozzle pressure ratio at injection ports (P_{Ni}/P_C) vs. resultant side thrust ratio (Fs_R/Fa_o)

Average nozzle pressures (item 23) as indicated on page A-6. Then non-dimensionalize these pressures by dividing by the average chamber pressure during the time interval under consideration. These pressure ratios (P_{Ni}/P_C) will be manually plotted against the resultant side thrust ratio (item 13), and a curve fared through the data. The equation to this curve will be fed back into the digital program. (NOTE: Check with Analysis before starting this calculation.)

25. Average nozzle pressure at injection ports (P_{Ni} - psia) vs time (sec.)

At time, t, select (P_{Ni}/P_C)(item 24 using Fs_R/Fa_o item 13) and multiply (P_{Ni}/P_C) by chamber pressure (item 1) to get average nozzle pressure at injection ports (P_{Ni}).

26. Pressure differential across injection valves (ΔP - psi) vs time.

Subtract item 25 and a constant (to be supplied) from item 22. $\Delta P = P_{Me} - P_{Ni} - K$

27. Manifold temperature (T_M - °F) vs time (sec.)

28. Injectant flow rate ($\dot{W}_s$ - lb/sec) vs time (sec.)

Feed equation for vendor supplied calibration curve of $\dot{W}_C$ vs voltage into digital program. This curve will be adjusted to a given fluid density and pressure differential. Enter curve using valve pintle position (item 20) and read out flow rate, $\dot{W}_C$(lb/sec). Compute average of the two manifold temperatures (item 27) and obtain injectant density from equation.

$$\rho_c = 95.75 - 0.0825\ \bar{T}_M \ (lb/ft^3)$$

Then compute injectant flow rate from

$$\dot{W}_S = \dot{W}_C \left[\frac{\rho_c \Delta P}{\rho_C \Delta P_C} \right]^{\frac{1}{2}} (lb/sec)$$

where ΔP = item 26

ΔP_c = constant (to be determined later)

ρ_c = constant (to be determined later)

29. Side specific impulse (Isp_s - sec) vs. time (sec.)

Multiply item 13 by item 6 and divide by item 28

30. Total side impulse (I_s - lb-sec) vs. time (sec.)

$$\int_2^{t_f} \left(\frac{Fsr}{Fao}\right) Fa_o \, dt = \int_2^{t_f} (\text{item 13}) \times (\text{item 6}) \, dt$$

where t_f = 52 sec (156-5)

t_f = 60 sec (156-6)

31. Nitrogen tank temperature (T_{GH} - °F) vs. time (sec.)

32. Ullage tank temperature (Tu - °F) vs. time (sec.)

33. Nozzle temperature (°F) vs. time (sec.)

34. Case temperatures (°F) vs. time (sec.)

35. Normal ballistic data

Print out only. Follow equations on Page A-7 for specified ballistic calculations. All other calculations will employ standard methods. In computations involving axial thrust, use item 6.

Procedure to be used to correct axial thrust for weight loss:

I. Add the weight exhausted to the measured axial thrust at each time.

II. The weight exhausted will be based on the following assumptions:

(a) C* remains constant during the test

(b) The nozzle throat erosion is proportional to the ratio of the pressure integral at any time to the total pressure integral.

III. The following equations are to be used:

(a) $$A_t = A_{t_i} + (A_{t_f} - A_{t_i}) \frac{\int_o^t Po_1 dt}{\int_o^{t_{total}} Po_1 dt}$$

(b) $$\bar{A}_t = \frac{\int_o^{t_{total}} A_t \, dt}{t_{total}}$$

(c) $$C^* = \frac{g \cdot \bar{A}_t \int_o^{t_{total}} Po_1 dt}{W_{exhausted}}$$

($W_{exhausted}$ (total pre-fire motor, nozzle & TVC weight minus total post-fire motor, nozzle & TVC weight)

NOTE: Water added during quench must be subtracted from post-fire weight

(d) $$W_{exhausted\ at\ anytime} = \frac{g \int_o^t A_t P_{o_1} dt}{C^*}$$

A_t = Throat area at any time.

A_{t_i} = Initial throat area.

A_{t_f} = Final throat area.

$\int_o^t P_{c_1} dt$ = Pressure Integral to any time.

$\int_o^{t_{total}} P_{c_1} dt$ = Total pressure integral.

$\bar{A}_t$ = Average throat area over total burn time.

C* = Characteristic exhaust velocity.

Periods during which axial thrust will be corrected to nominal axial thrust (Item 6).

Cycle (Period)	Motor 156-5		Motor 156-6	
	t_1(sec)	t_2(sec)	t_1(sec)	t_2(sec)
1	2.5	5.5	2.5	5.0
2	5.5	9.5	5.5	9.0
3	9.5	12.0	9.0	12.0
4	15.0	17.5	12.5	15.5
5	20.0	23.5	15.5	18.0
6	30.0	32.5	22.5	24.5
7	35.5	38.5	28.0	30.5
8	38.5	41.5	34.5	37.5
9	41.5	44.5	40.0	42.5
10	45.0	50.0	43.5	46.0
11			46.0	48.5
12			46.5	51.0
13			51.5	57.0

When selecting the exact point (time) at which the values of thrust and pressure are taken, use a point where both thrust and pressure are not abnormally high or low.

Periods during which side thrust ratio (item 10) is to be averaged. To be used in computing item 11.

	Motor 156-5		Motor 156-6	
Period	**t (initial)**	**t (final)**	**t (initial)**	**t (final)**
1	2.0	2.9	2.0	2.9
2	5.2	5.9	4.8	5.9
3	9.2	9.9	8.7	9.4
4	11.7	12.7	11.7	12.9
5	14.5	15.4	15.2	15.9
6	17.5	18.5	17.7	19.0
7	19.5	20.4	22.0	22.9
8	23.2	24.5	24.2	25.5
9	29.5	30.4	27.5	28.4
10	32.2	33.5	30.2	31.5
11	35.0	35.9	34.0	34.9
12	38.2	38.9	37.2	38.5
13	41.2	41.9	39.5	40.4
14	44.2	45.4	42.2	43.9
15	49.7	51.0	45.7	46.4
16			48.2	48.9
17			50.0	51.9
18			56.7	58.0

Motors 156-5 and 156-6

Average thrust misalignment during cycles (item 12).
Refer to page A-4 for times corresponding to the periods listed below.

Cycle	Periods	
	156-5	156-6
1	1 and 2	1 and 2
2	2 " 3	2 " 3
3	3 " 4	3 " 4
4	5 " 6	4 " 5
5	7 " 8	5 " 6
6	9 " 10	7 " 8
7	11 " 12	9 " 10
8	12 " 13	11 " 12
9	13 " 14	13 " 14
10	14 " 15	14 " 15
11		15 " 16
12		16 " 17
13		17 " 18

For ballistic purposes the pre- and post-fire weight of the motor (only) is required. The nozzle throat area will be calculated as shown below:

$$A_t = A_{t_i} + (A_{t_f} - A_{t_i}) \frac{\int_o^t P_{c_1} dt}{\int_o^{t_{total}} P_{c_1} dt}$$

The average throat area will be:

$$\bar{A}_{t_{t_b}} = \frac{\int_o^{t_b} A_t \, dt}{t_b}$$

and,

$$C^* = \frac{g \, \bar{A}_{t_{t_b}} \int_o^{t_b} P_{c_1} dt}{W_p \text{ (propellant weight expended to web action time } (t_b).)}$$

where $\bar{A}_{t_{t_b}}$ = Average throat area over web action time

t_b = Web action time

$\int_o^{t_b} P_{c_1} dt$ = Pressure integral over web action time

MOTOR 156-5

Item	Number of Curves	Number of Graphs	Scale (per inch) Ordinate	Comments
1	1	1	100 psia	(Abscissa scale is 4 sec/inch and abscissa to be located 1 inch from bottom of graph, on all plots below unless otherwise noted)
2	1	1	100 psia	
3a	1	1	100 psia	Stop plot at t=2.4 sec (abscissa scale is 0.2 sec/inch)
3b	1	1	100 psia	Stop plot at t=2.4 sec (abscissa scale is 0.2 sec/inch)
4	1	1	500,000 lb	Locate abscissa 3 inches from bottom
5	1	1	500,000 lb	
6	1	1	500,000 lb	
7	1	1	20,000 lb	
8	2	1	40,000 lb	Yaw plane (Locate abscissa 2 inches from bottom)
	3	1	20,000 lb	Pitch plane (Locate abscissa 2 inches from bottom)
9	2	2	40,000 lb	Locate abscissa 2 inches from bottom
10	2	2	0.01	
11				Print out only
12	2	2	0.01	
13	1	1	0.01	
14	1	1	1.0	
15				Print out only
16	1	1	40,000 lb	
17	2	2	2 volts	Abscissa to be set at middle of graph
18	1	1	1 volt	
19	10	10	40,000 lb	Abscissa is Resultant Command Signal (item 18) Plot 1 volt/inch.
20	24	8	1 volt	Identify each curve by valve numbers
21	2	1	100 psia	
22	1	1	100 psia	
23	4	1	40 psia	Identify each curve
24				Print out only-curves manually plotted
25	1	1	40 psia	
26	1	1	100 psid	
27	2	1	20°F	
28	1	1	200 lb/sec	
29	1	1	50 sec	
30				Print out only
31	4	1	20°F	Identify each curve
32	4	1	20°F	Identify each curve
33	5	1	40°F)	Identify each curve. Abscissa scale is 10 sec/inch for 60 sec, then change scale to 2 min/inch out to 10 min.
34	5	1	40°F)	
35				Print out only

MOTOR 156-6

Item	No. of Curves	No. of Graphs	Scale (per inch) Ordinate	Comments (Abscissa scale is 4 sec/inch, and abscissa is to be located 1 inch from bottom of graph, unless otherwise noted)
1	1	1	100 psia	
2	1	1	100 psia	
3a	1	1	100 psia	Stop plot at t = 2.4 sec (abscissa scale is 0.2 sec/inch)
3b	1	1	100 psia	Stop plot at t = 2.4 sec (abscissa scale is 0.2 sec/inch)
4	1	1	200,000 lb	Locate abscissa 3 inches from bottom
5	1	1	200,000 lb	
6	1	1	200,000 lb	
7	1	1	8,000 lb	
8	2	1	20,000 lb	Yaw plane (locate abscissa 2 inches from bottom)
	3	1	10,000 lb	Pitch plane (locate abscissa 2 inches from bottom)
9	2	2	20,000 lb	Locate abscissa 2 inches from bottom
10	2	2	0.01	
11				Print out only
12	2	2	0.01	
13	1	1	0.01	
14	1	1	L.O	
15				Print out only
16	1	1	20,000 lb	
17	2	2	2 volts	Abscissa to be set at middle of graph
18	1	1	1 volt	Abscissa is Resultant Command Signal (item 18) Plot 1 volt/in.
19	13	13	20,000 lb	
20	24	8	1 volt	Identify each curve by valve number
21	2	1	100 psia	
22	1	1	100 psia	
23	4	1	40 psia	Identify each curve
24				Print out only - curves manually plotted
25	1	1	40 psia	

(continued)

MOTOR 156-6 (continued)

Item	No. of Curves	No. of Graphs	Scale (per inch) Ordinate	Comments
26	1	1	100 psid	
27	2	1	20°F	
28	1	1	50 lb/sec	
29	1	1	50 sec	
30				Print out only
31	2	1	20°F	Identify each curve
32	2	1	20°F	Identify each curve
33	5	1	40°F	Identify each curve. Abscissa scale is 10 sec/inch for
34	5	1	40°F	60 sec, then change scale to 2 min/inch.
35				Print out only

APPENDIX II

DEFINITIONS AND SYMBOLS

1. TIME (sec)

1.1 Time

General parameter representation. t

1.2 Action time t_a

$t_5 - t_2$

Action time is defined as the interval from 10% of maximum pressure during rise to 10% of maximum pressure during tail-off.

1.3 Burning time

$t_4 - t_3$

Burning time is defined as the interval from 75% of maximum pressure during rise to the point of pressure-time trace which lies on the line bisecting the angle formed by the tangents to trace prior to and immediately after the beginning of tail-off. t_b

1.4 Ignition delay time

$t_3 - t_o$ t_d

Ignition delay is defined as the time interval between the fire signal and 75% maximum chamber pressure during ignition rise.

1.5 Zero time

Console fire-switch time of activation. t_o

1.6 Ignition rise time

$t_3 - t_2$ t_r

2. PRESSURE (psia)

2.1 Pressure

A representation of the general concept of force per unit area. P

2.2 Ambient barometric pressure

The existing static force/area due to the surrounding atmosphere P_a

2.3 Burn time average pressure

The chamber internal pressure averaged for the "burn time" portion of the pressure-time curve. $\bar{P}_b$

2.5 Chamber pressure

The force/area directed outward from the inside of the motor case. P_c

2.6 Maximum ignition pressure

The peak chamber pressure due to ignition. $P_{i_{max}}$

2.7 Maximum chamber pressure excluding ignition transient. P_{max}

2.8 Nozzle exit plane pressure P_e

3. THRUST (lb_f)

3.1 Thrust; force

A representative of the general concept of thrust. F

3.2 Action time average thrust

The motor thrust averaged for the "action time" portion of the thrust-time curve. $\bar{F}_a$

3.3 Burn time average thrust

The motor thrust averaged for the "burning time" portion of the thrust-time curve. $\bar{F}_b$

3.4 Maximum ignition thrust $F_{i_{max}}$

3.5 Maximum thrust excluding ignition

Maximum thrust is defined as the maximum value of thrust produced during normal motor operation. F_{max}

4. IMPULSE (lb_f - sec)

4.1 Impulse

The force-time integral for undefined time limits or altitude. A representation of the general concept of impulse. I

4.2 Burn time impulse

The area under the "burning time" portion of the thrust-time curve. I_B

4.3 Action time impulse I_A

The area under the "action time" portion of the thrust-time curve.

4.4 Total impulse, deliverable total impulse

The total measurable area under the thrust-time curve $(t_6 - t_1)$ I_t

5. WEIGHTS (lb_m)

5.1 Weight W

5.2 Propellant weight W_p

5.3 Weight at burnout W_{b_o}

5.4 Motor gross weight

$W_m = W_p + W_i$ W_m

5.5 Inert Weight

Inert motor weight, which includes the motor case, nozzle, internal insulation, igniter, the TVC system, its power supply, and its attachment and/or base insulation (if required). W_i

6. SPECIFIC IMPULSE (lb_f - sec/lb_m)

6.1 Propellant specific impulse

General parameter representation. No conditions need be specified. No correction shall be required for liner loss where the decrease in liner weight is less than 0.25% of the weight of the propellant. I_{sp}

6.2 Theoretical propellant specific impulse

1000/vacuum; optimum area ratio expansion; equilibrium composition I^*_{sps}

6.3 Theoretical propellant specific impulse

1000/14.7, optimum area ratio; equilibrium composition — I°_{sps}

6.4 Measured delivered propellant specific impulse.

The following must be designated; chamber pressure, exit pressure, area expansion ratio, nozzle divergence half angle, interval, and propellant weight assumption. — I_{spd}

6.5 Standard propellant specific impulse at sea level standard conditions of 1000 psia average chamber pressure, optimum area expansion ratio, to 14.7 psia, 15° nozzle divergence half angle. — I_{sps}

6.6 Motor specific impulse

Impulse (define time limits) divided by weight of loaded motor. — I_{sm}

7. GEOMETRY

7.1 Area of (initial) propellant burning surfaces (in^2) — A_b

7.2 Area at nozzle exit plane (in^2) — A_e

7.3 Grain port area (in^2) — A_p

7.4 Nozzle throat area (in^2) — A_t

7.5 Web thickness of propellant (in) — w

7.6 Nozzle divergency half angle (deg) — α

7.7 Outside diameter of case (in)

The outside diameter of the case is defined as the diameter of the pressure chamber. — D_c

8. TEMPERATURE (°F)

8.1 Temperature

General parameter representation — T

8.2 Chamber temperature

Temperature of combustion products in the chamber generally considered to be the isobaric flame temperature — T_c

8.3 Exhaust gas static temperature

At the exit plane — T_e

8.4 Motor firing temperature — T_o

8.5 Static gas temperature at nozzle throat — T_t

9. COEFFICIENTS, DIMENSIONLESS UNITS, ETC.

9.1 Constant in the burning rate equation: $r=?p^n$ (in/sec) — a

9.2 Characteristic exhaust velocity (ft/sec) — c*

9.3 Mass discharge coefficient — C_D

9.4 Thrust coefficient — C_F

9.5 Theoretical thrust coefficient — C_F^*

9.6 Port to throat ratio $J = \frac{A_t}{A_p}$. — 1/J

The minimum port to throat ratio is defined as the minimum acceptable ratio between the initial port area of the grain to the initial nozzle throat area.

9.7 Ratio of specific heats (Cp/Cv) — γ

9.8 Burning surface to throat area ratio (initial) — K_n

9.9 Nozzle area expansion ratio $\varepsilon = \frac{A_e}{A_t}$ — ε

9.10 Propellant mass fraction $\lambda = \frac{W_p}{W_p + W_i} = \frac{W_p}{W_m}$ — λ

9.11 Temperature sensitivity of pressure at a particular value K_n. (%/°F) — $(\pi_p)_k$

9.12 Propellant density — ρ

9.13 Maximum expected operating pressure (MEOP) — MEOP

MEOP is defined as that chamber pressure which may be expected when utilizing a 3 sigma variation in propellant burn rate, at maximum motor operating temperature.

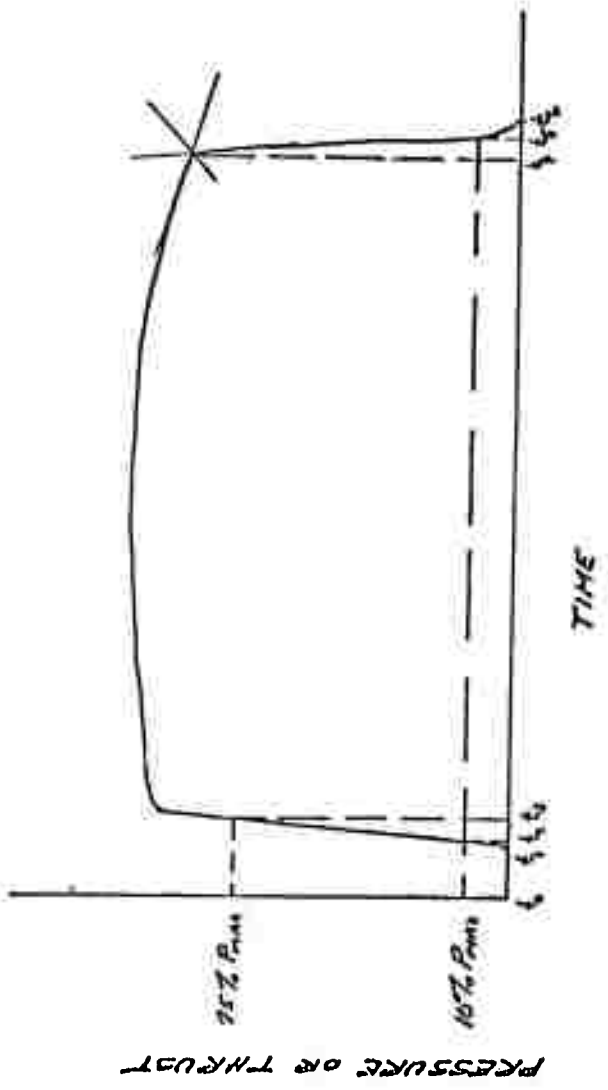
TIME
PRESSURE OR THRUST

10. NOZZLE SUBMERGENCE

A ratio of the submerged nozzle length to the total nozzle length where the submerged nozzle length is measured from the forward extreme point on the nozzle to the geometric extension of the closure intersection with the longitudinal centerline.

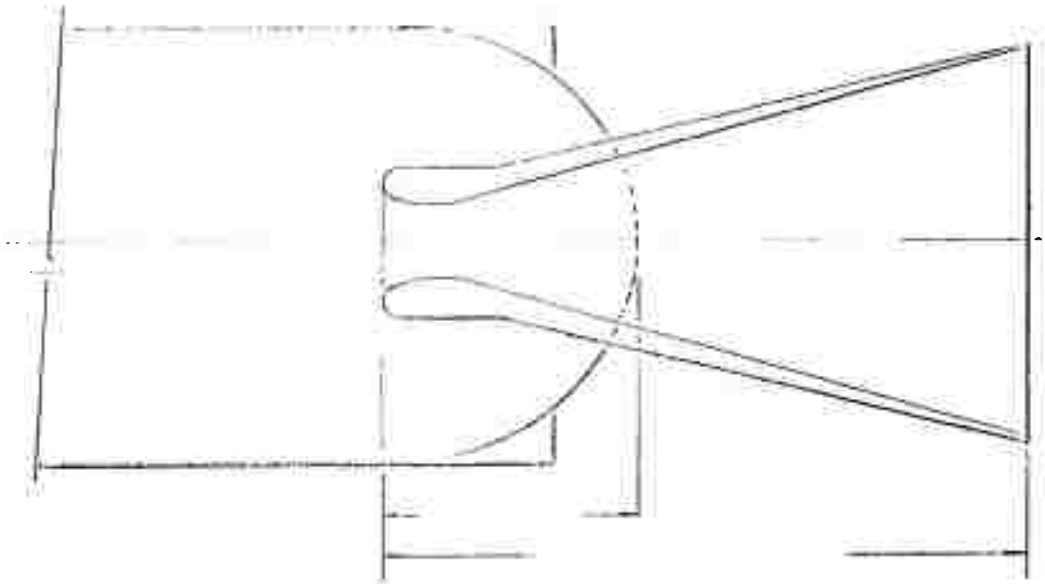

Appendix III

SUPPLEMENTARY TEST-FIRING DATA

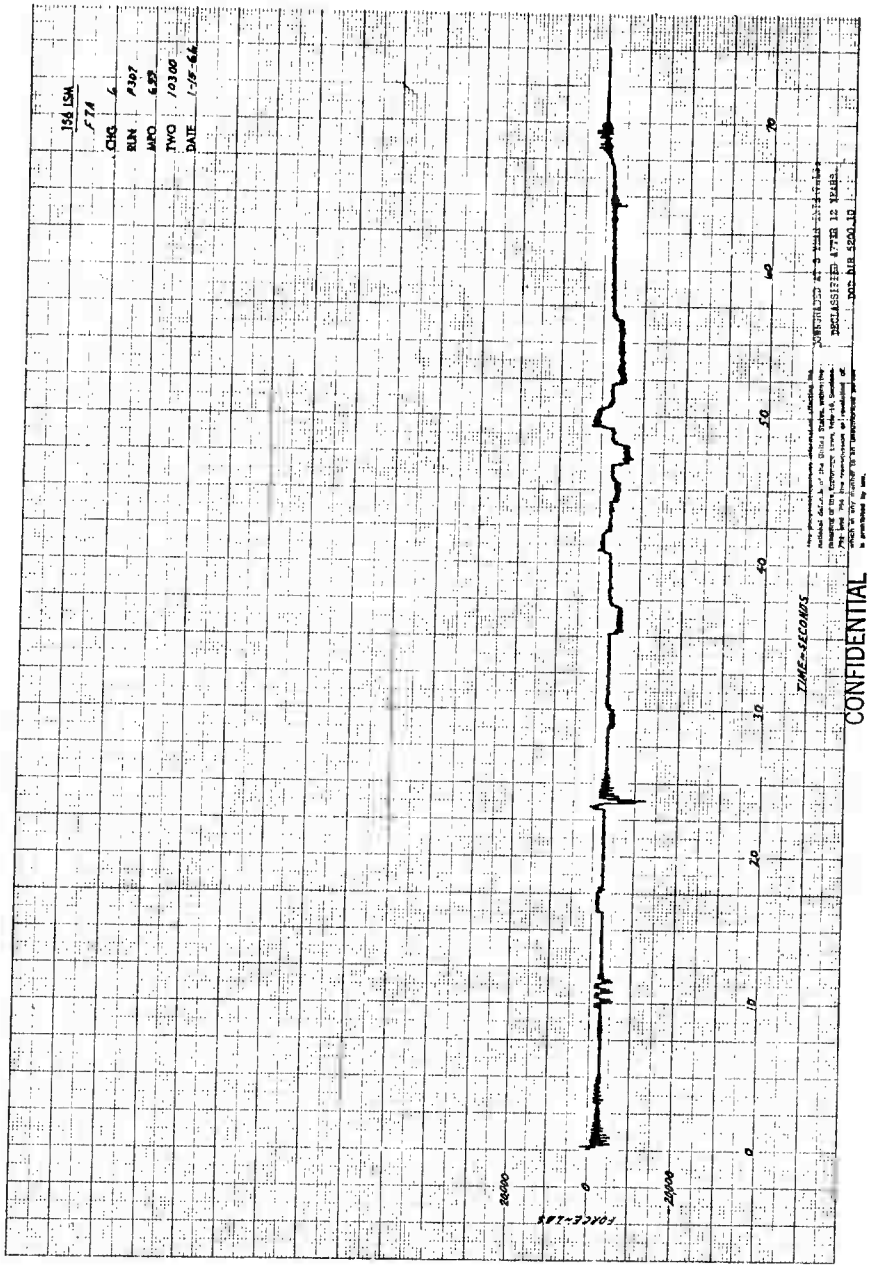

Figure 49 Side Thrust versus Time, Load Cell No. 7, Motor 156-6

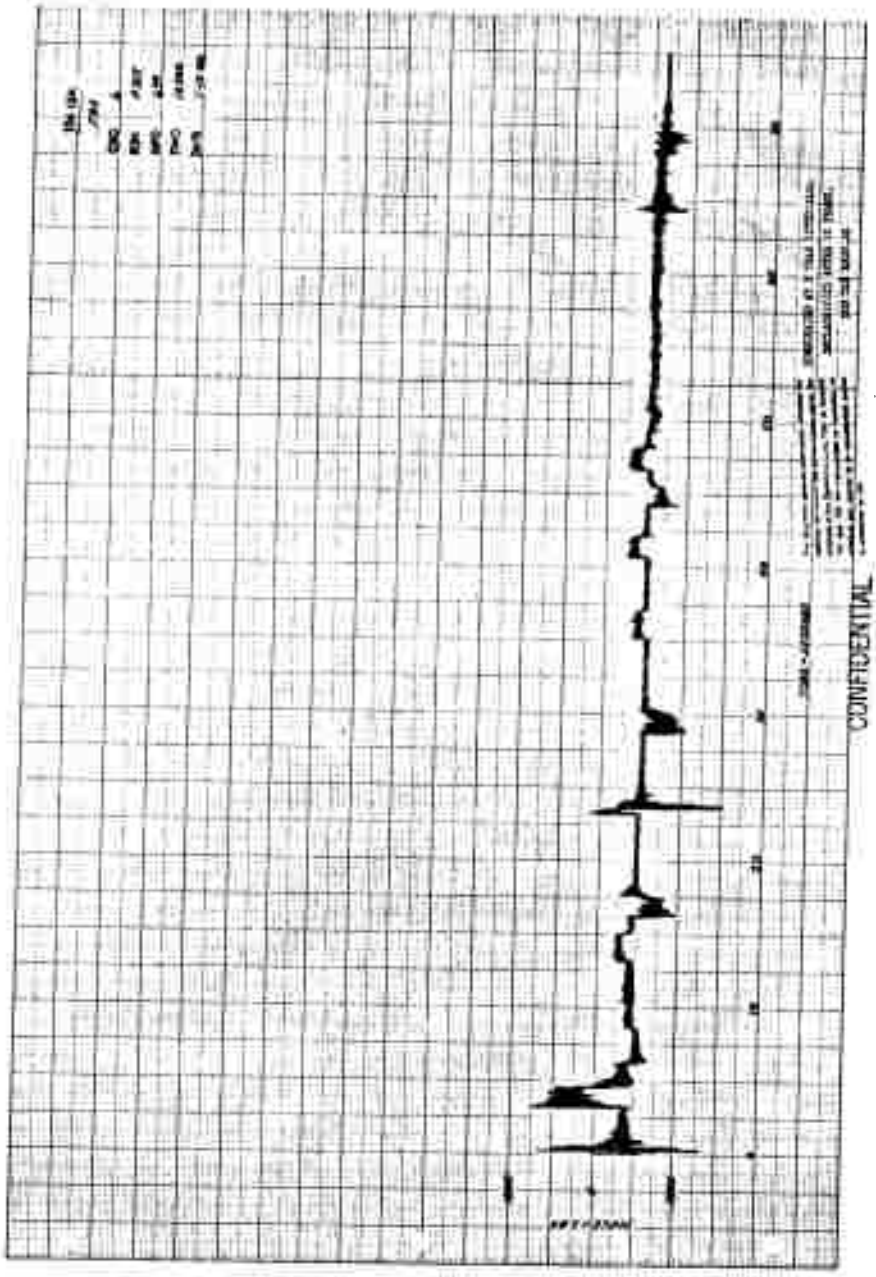

Figure 50 Side Thrust versus Time, Load Cell No. 8, Motor 156-6

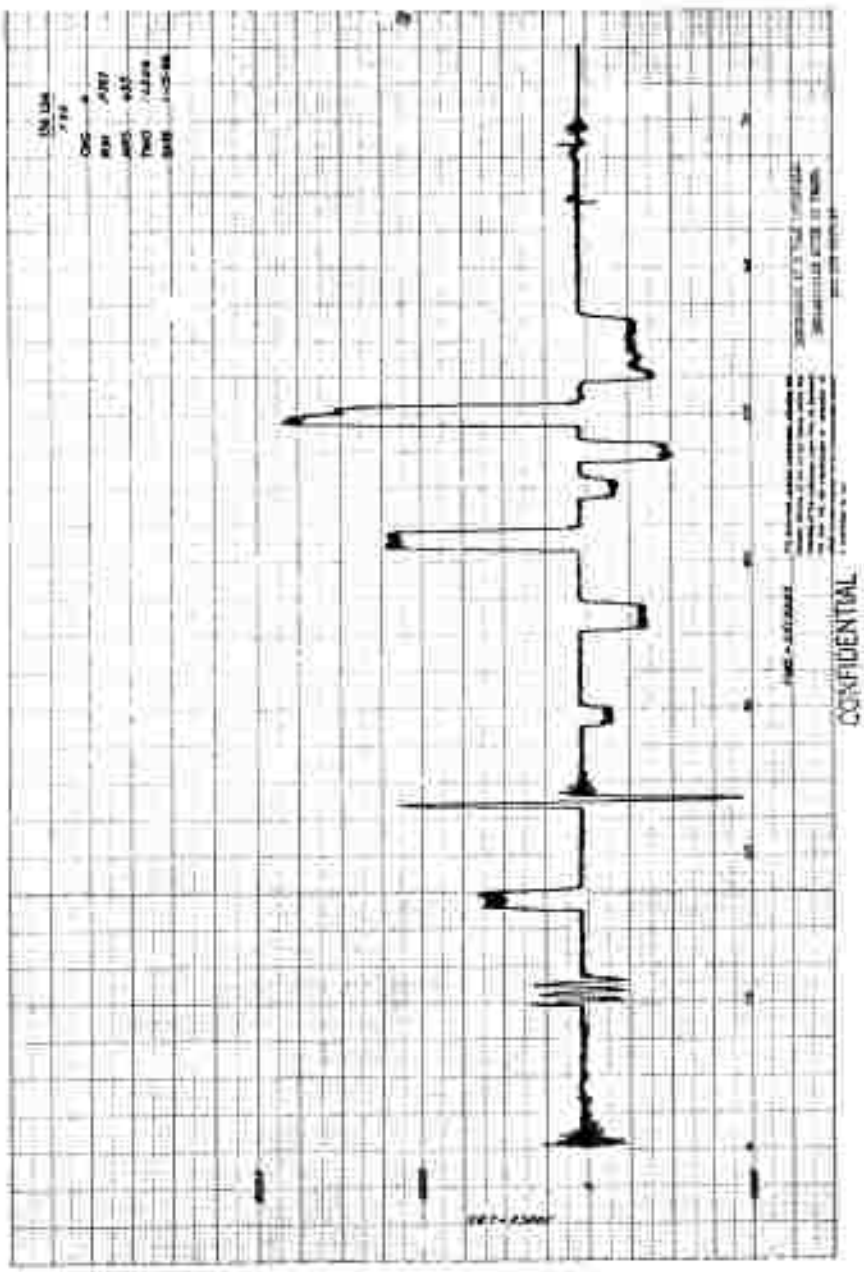

Figure 51 Side Thrust versus Time, Load Cell No. 9, Motor 156-6

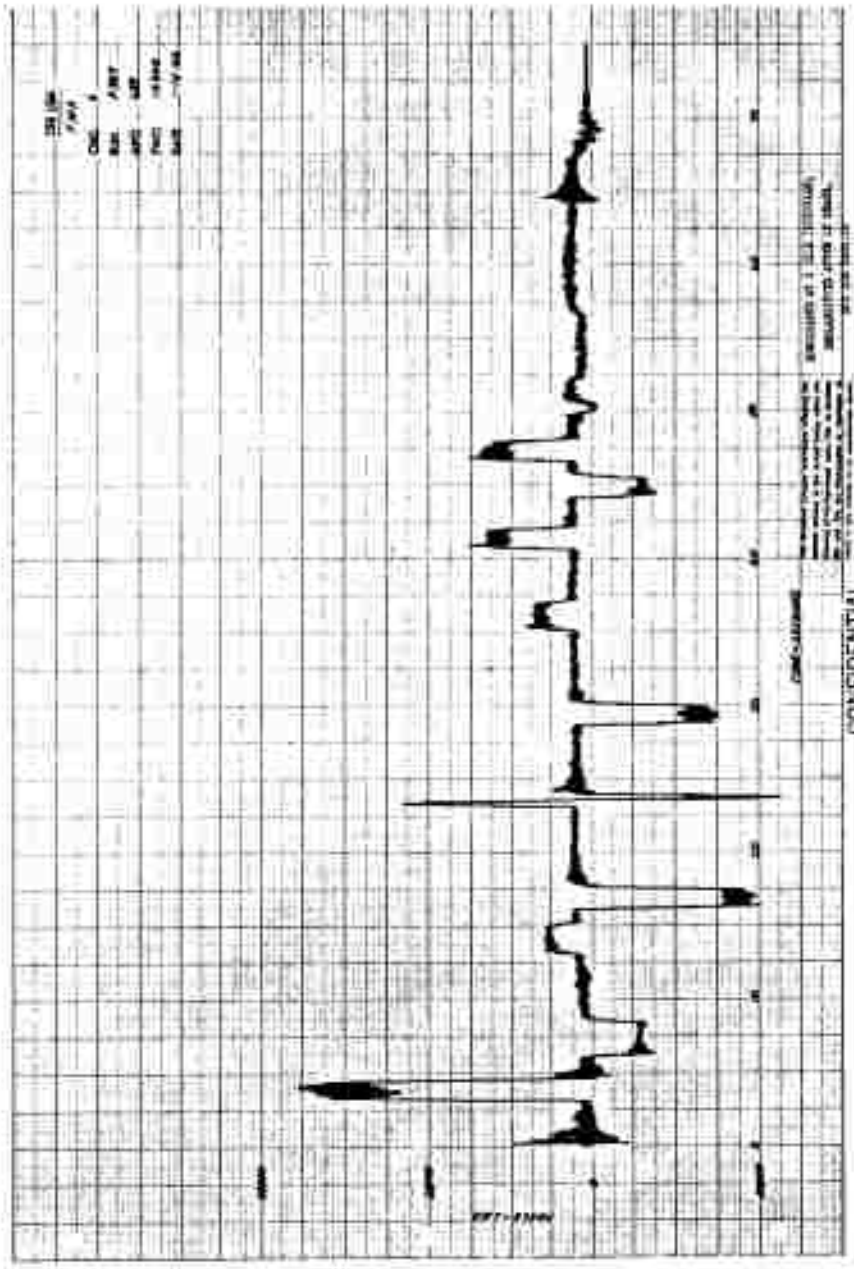

Figure 52 Side Thrust versus Time, Load Cell No. 10, Motor 156-6

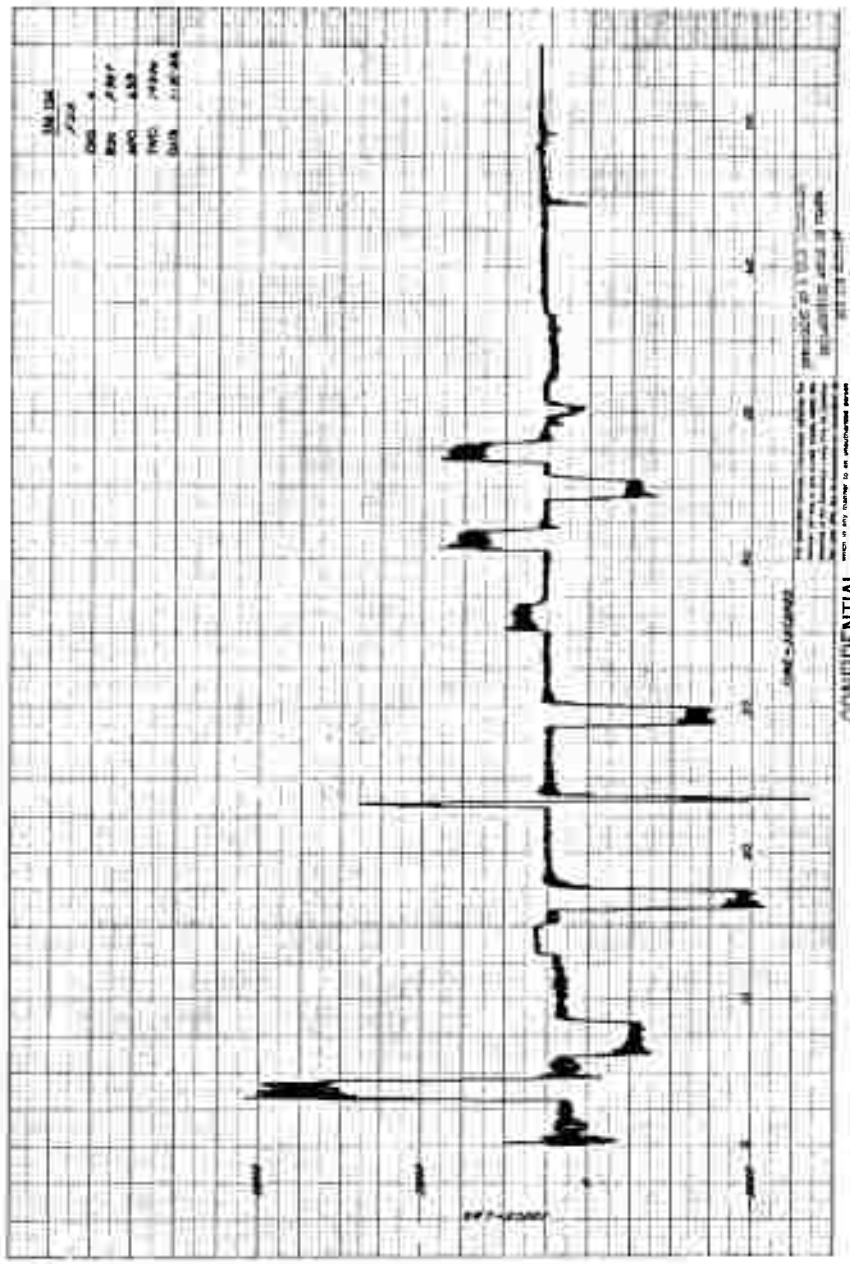

Figure 53 Side Thrust versus Time, Load Cell No 11, Motor 156-6

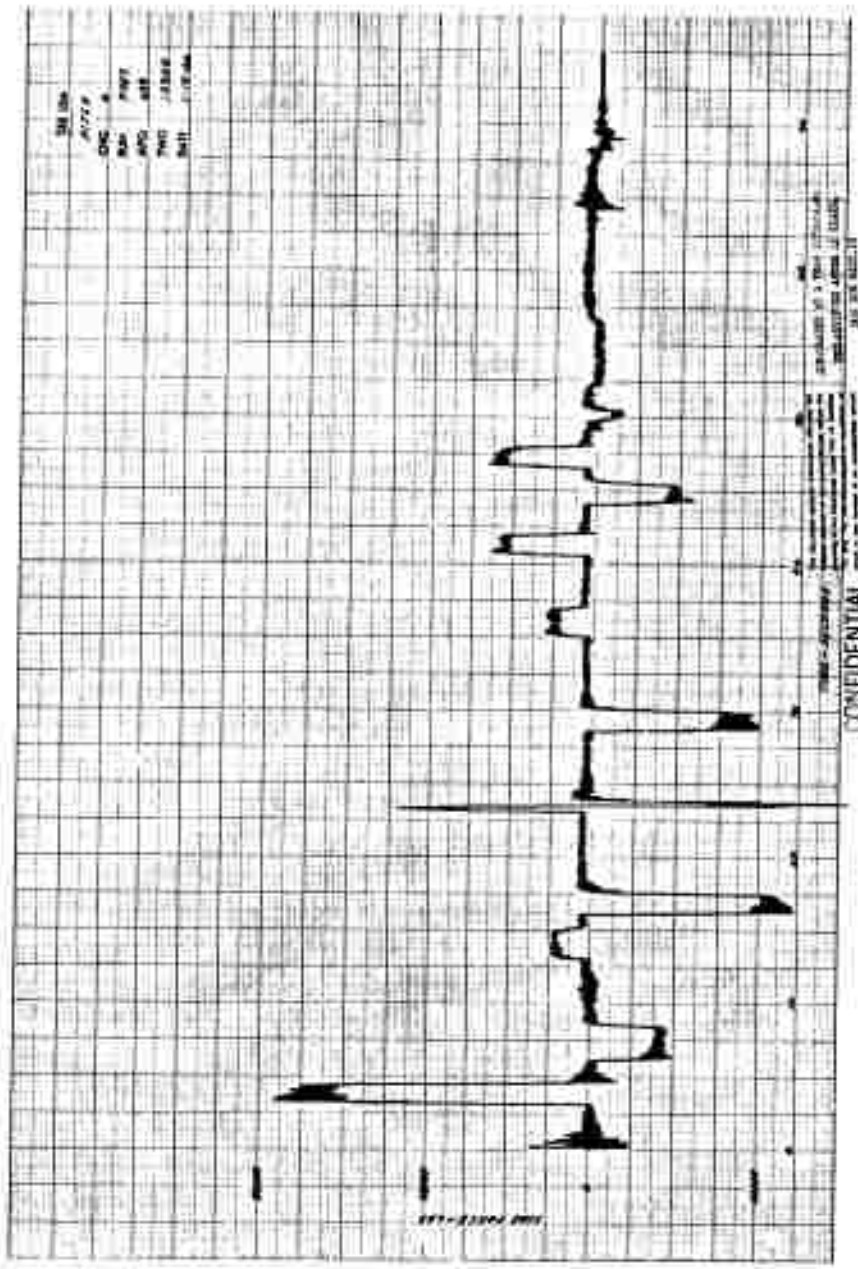

Figure 54 Pitch Thrust versus Time, Motor 156-6

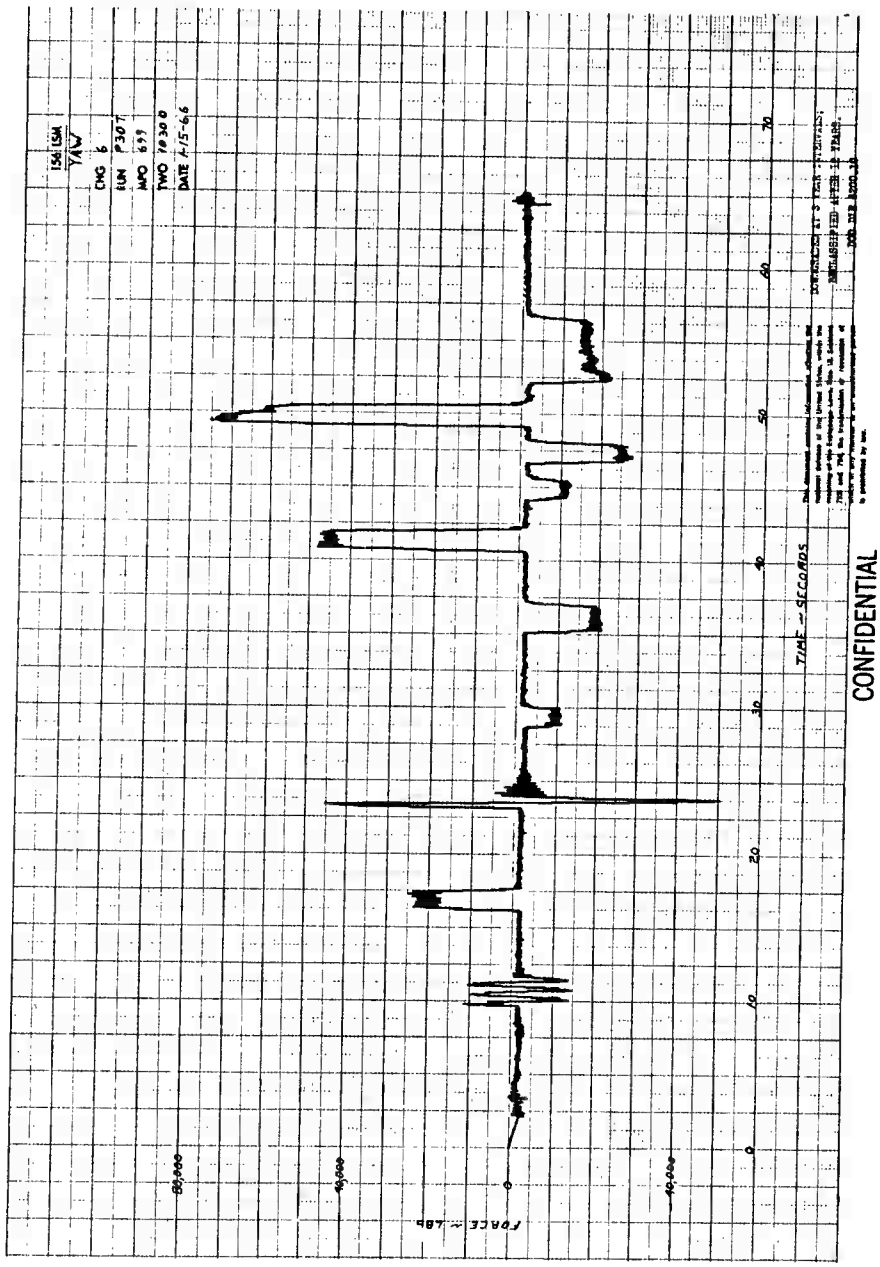

Figure 55 Yaw Thrust versus Time, Motor 156-6

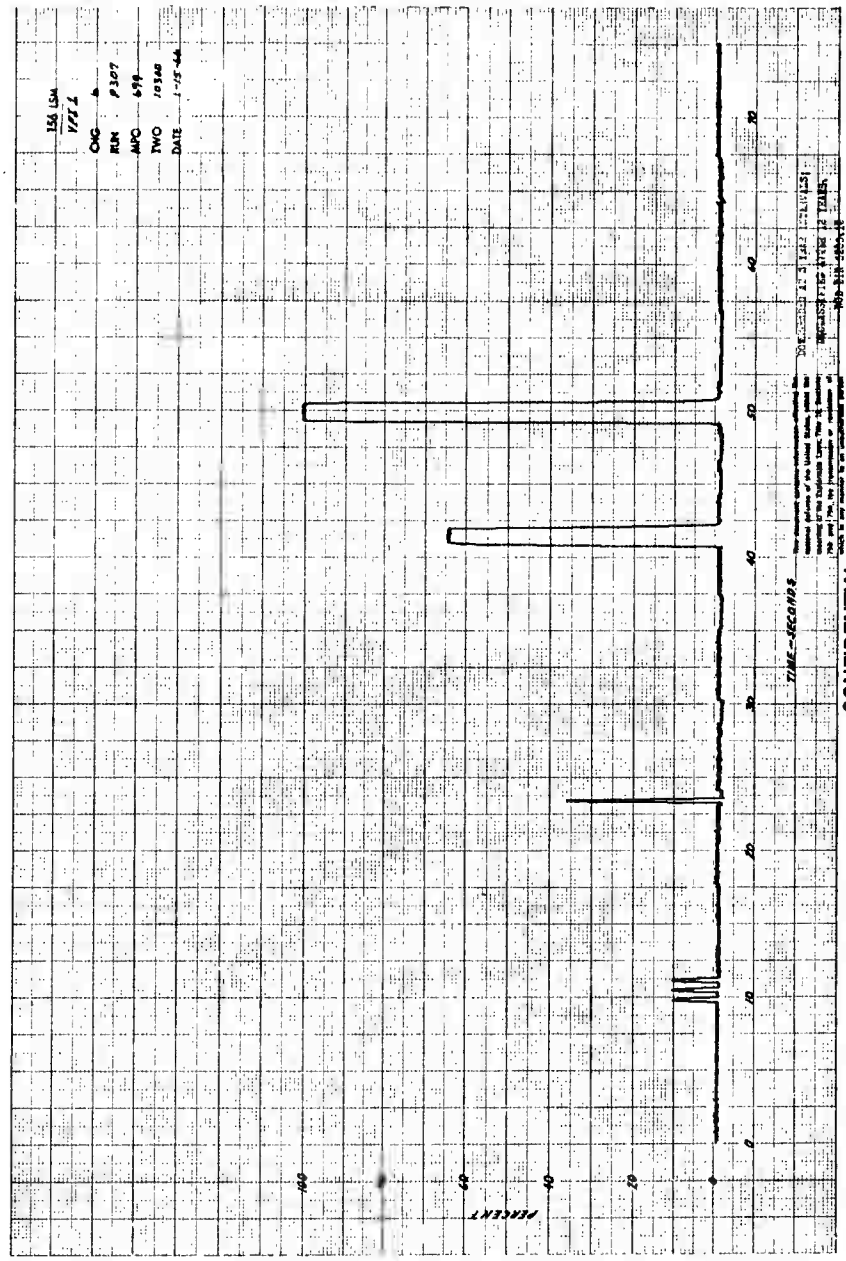

Figure 56 Injector Valve Pintle Position (Feedback) versus Time, Injector Valve No. 1, Motor 156-6

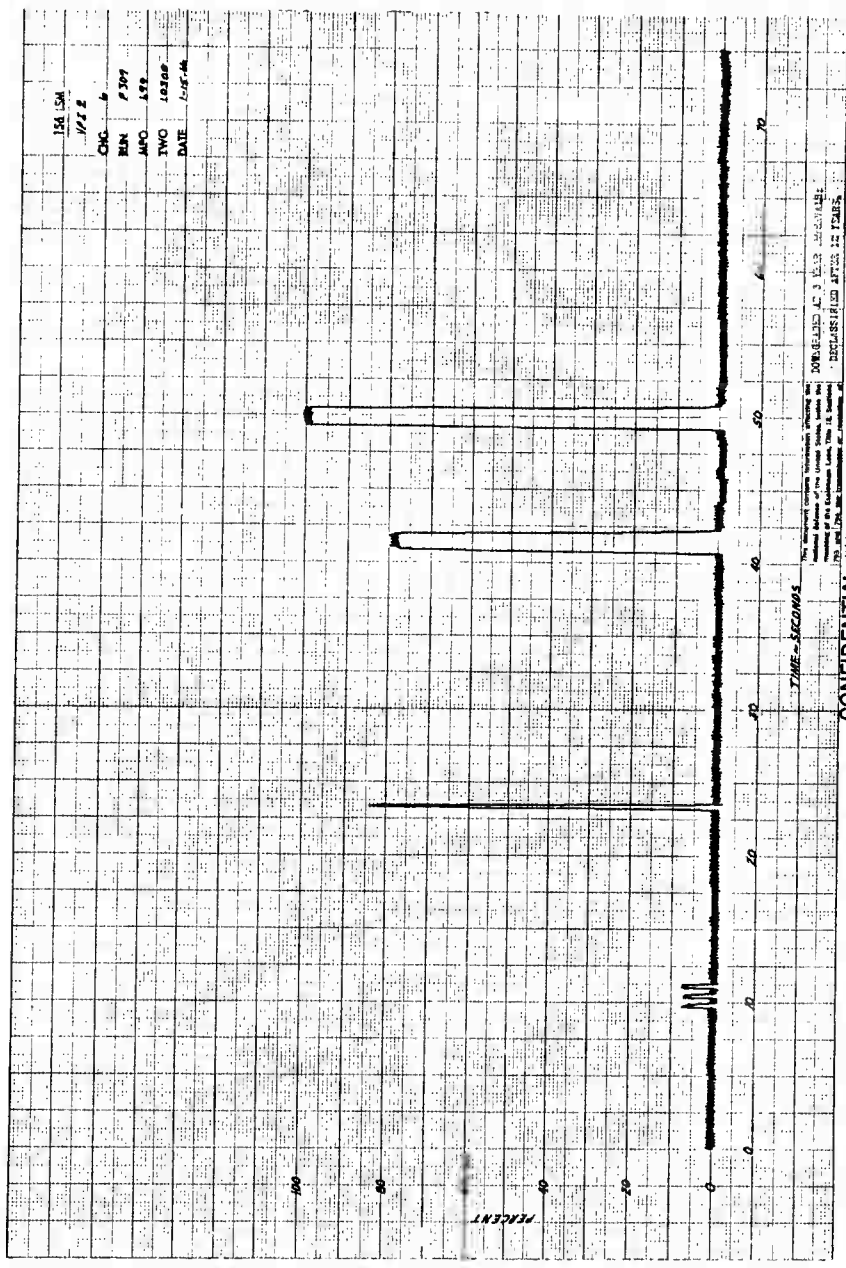

Figure 57 Injector Valve Pintle Position (Feedback) versus Time, Injector Valve No. 2, Motor 156-6

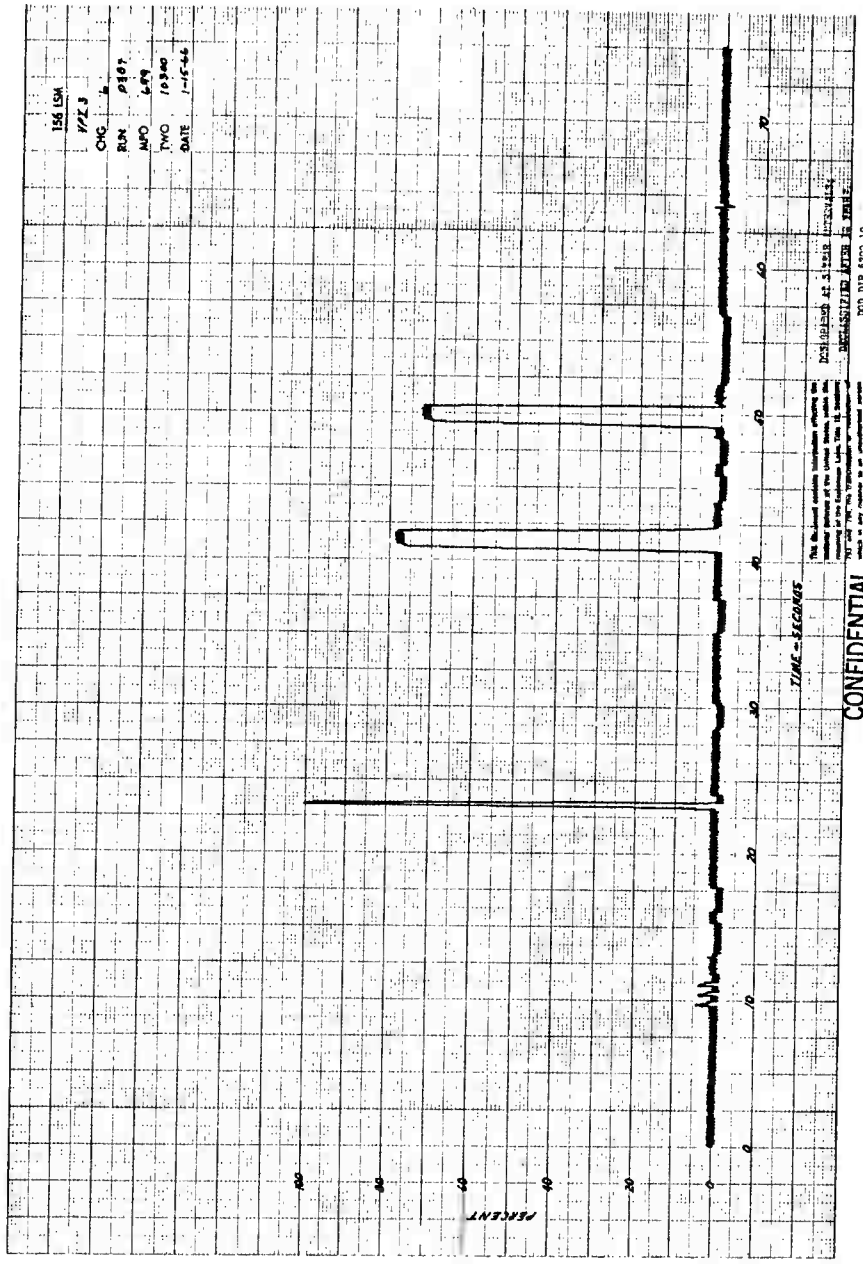

Figure 58 Injector Valve Pintle Position (Feedback) versus Time, Injector Valve No. 3, Motor 156-6

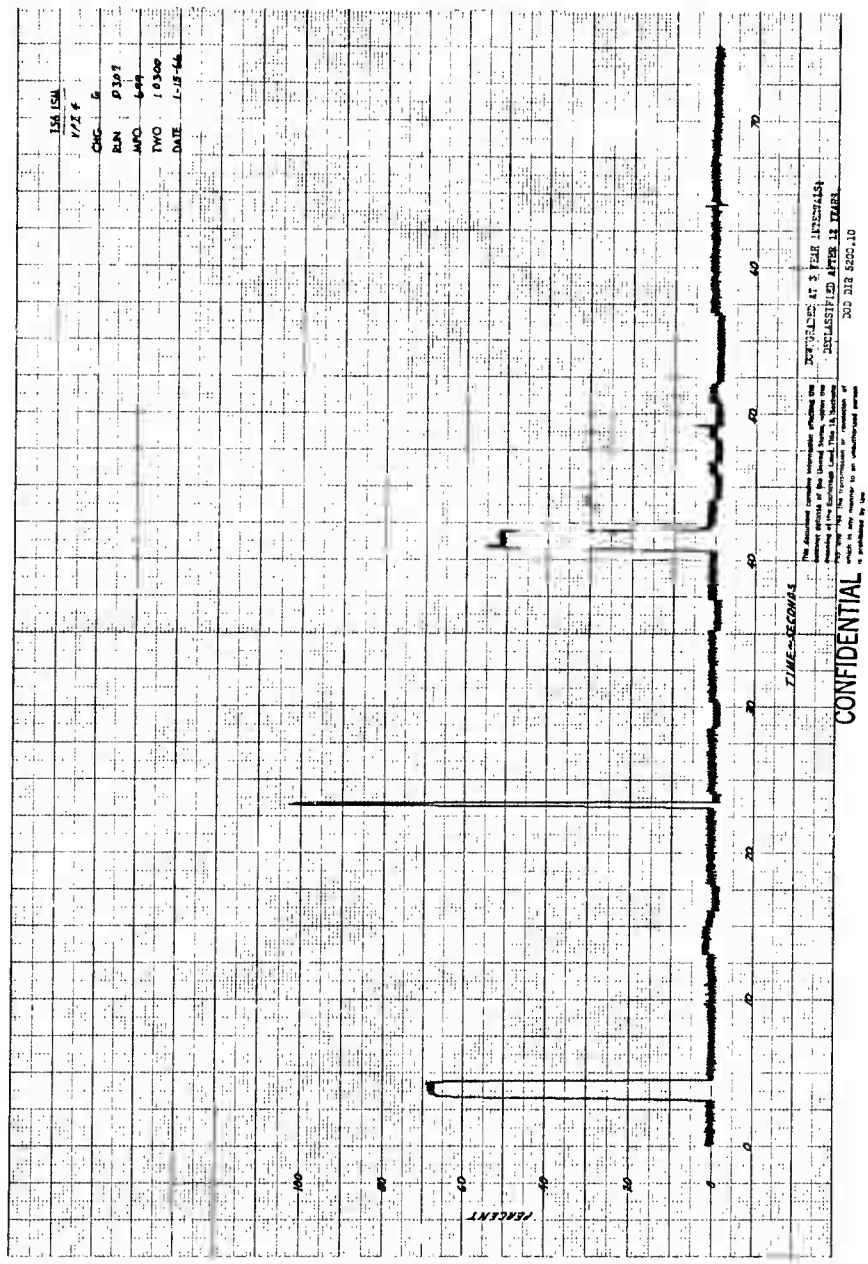

Figure 59 Injector Valve Pintle Position (Feedback) versus Time, Injector Valve No. 4, Motor 156-6

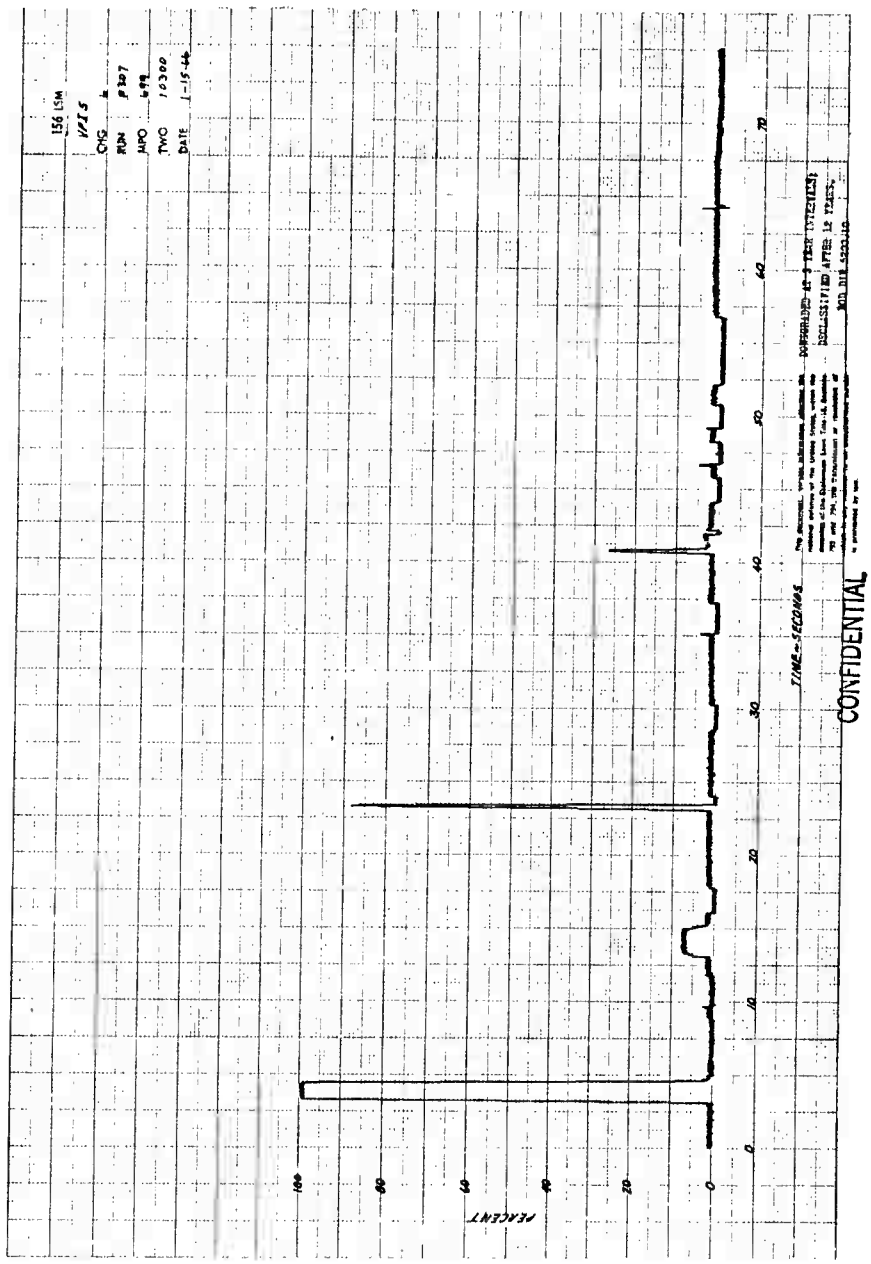

Figure 60 Injector Valve Pintle Position (Feedback) versus Time, Injector Valve No. 5, Motor 156-6

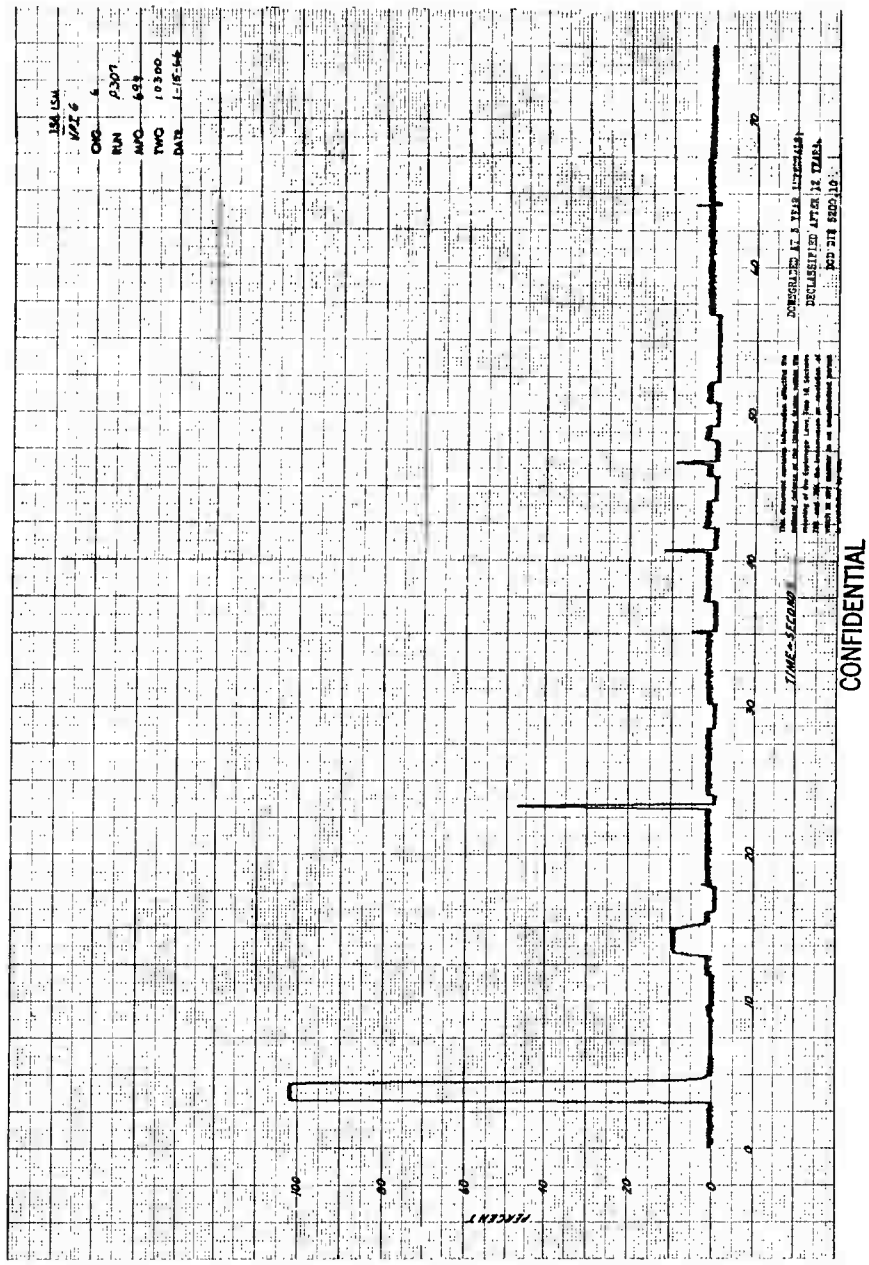

Figure 61 Injector Valve Pintle Position (Feedback) versus Time, Injector Valve No. 6, Motor 156-6

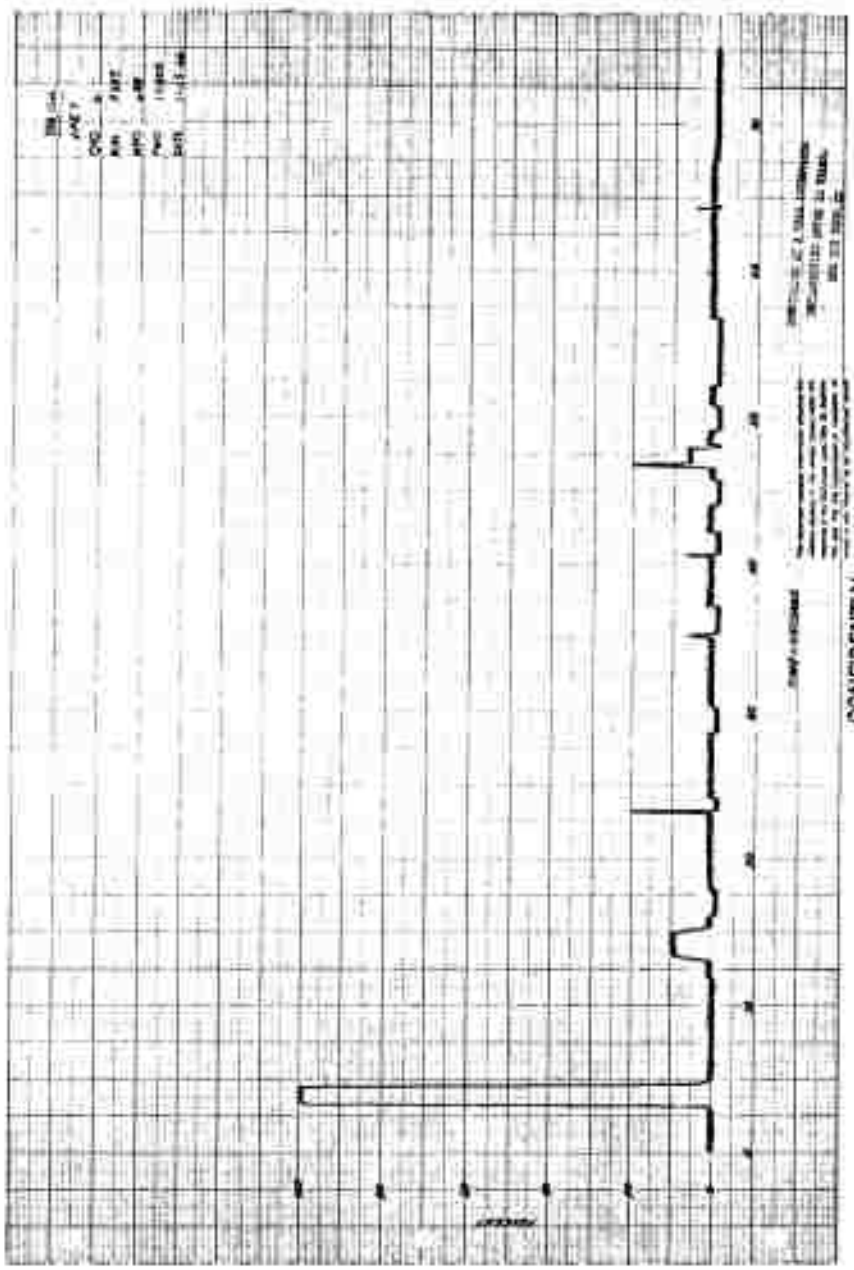

Figure 62 Injector Valve Pintle Position (Feedback) versus Time, Injector Valve No. 7, Motor 156-6

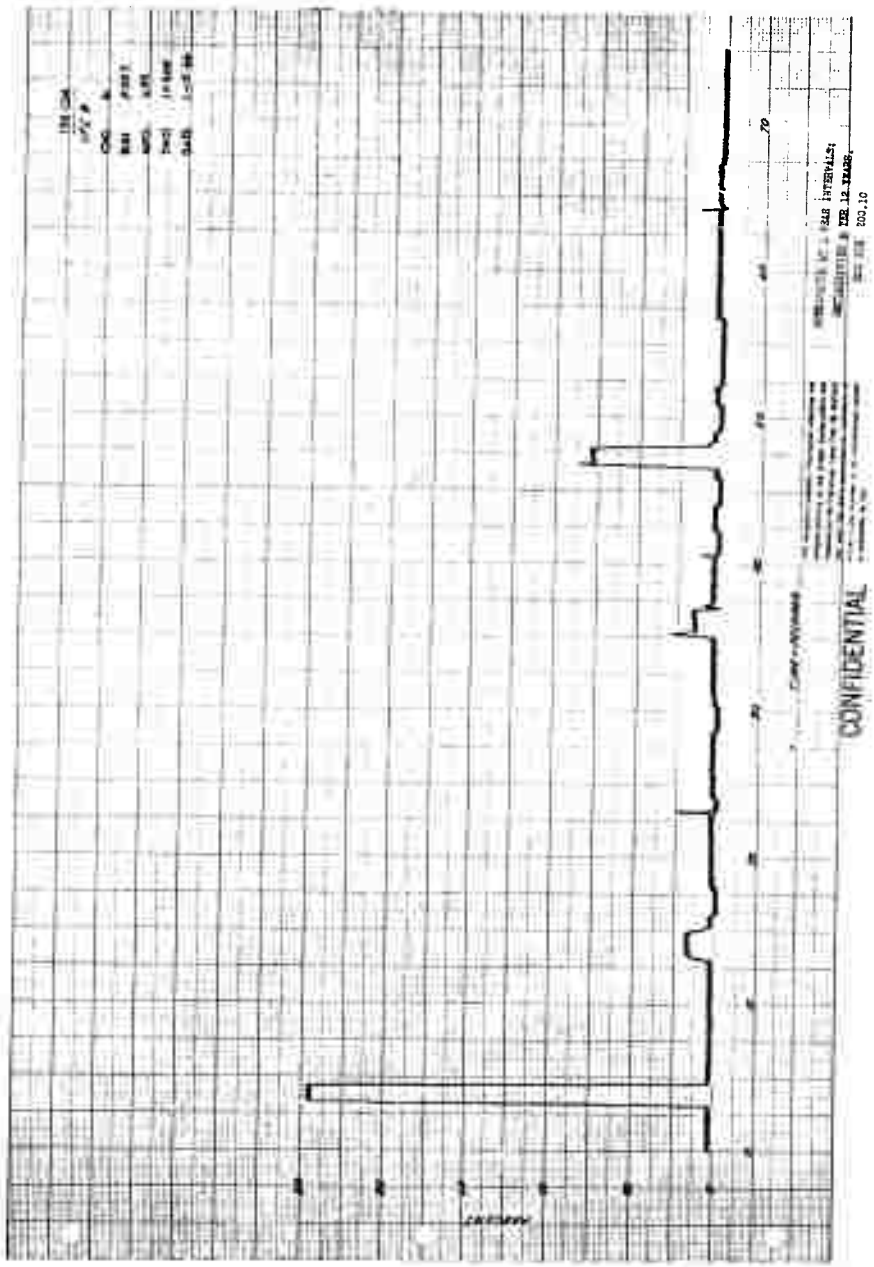

Figure 63 Injector Valve Pintle Position (Feedback) versus Time, Injector Valve No. 8, Motor 156-6

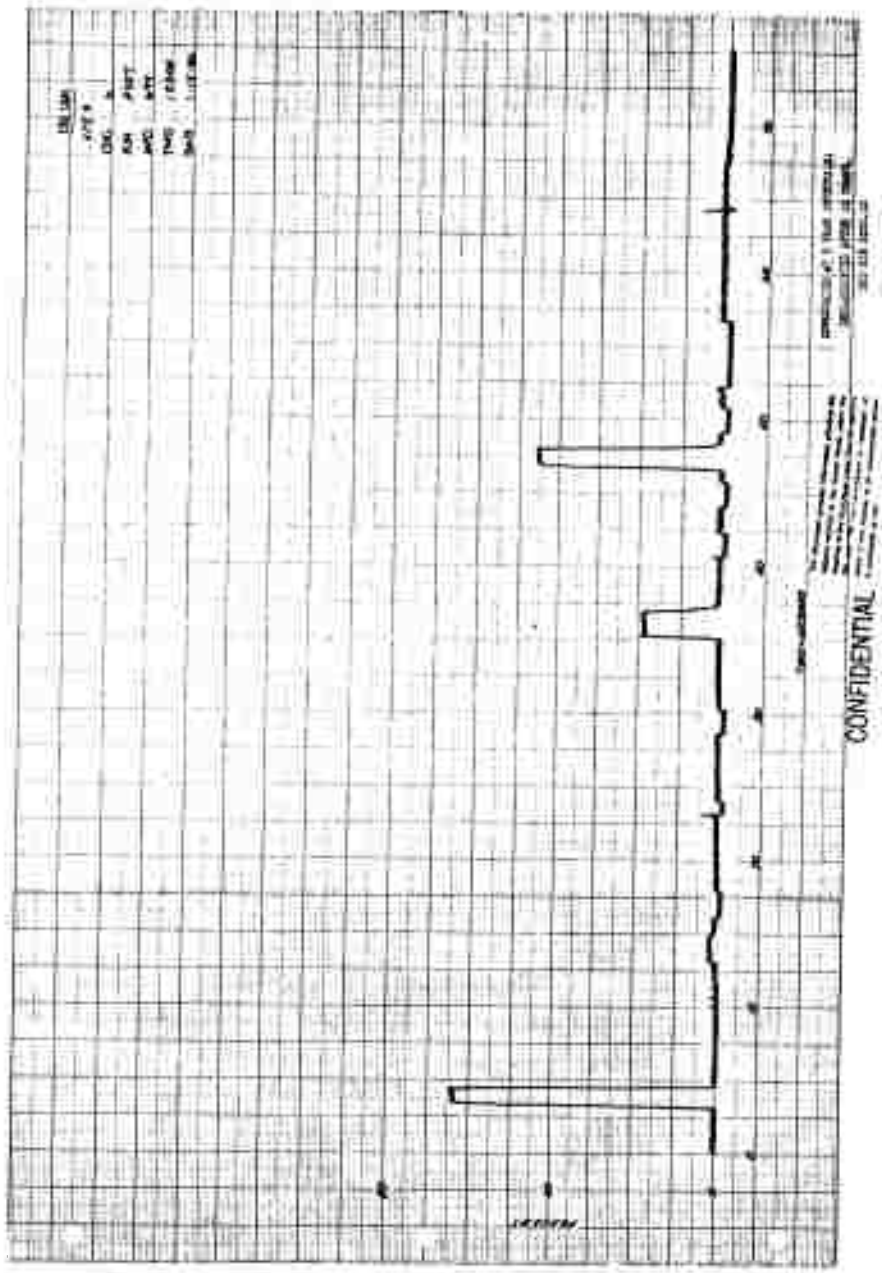

Figure 64 Injector Valve Pintle Position (Feedback) versus Time, Injector Valve No. 9, Motor 156-6

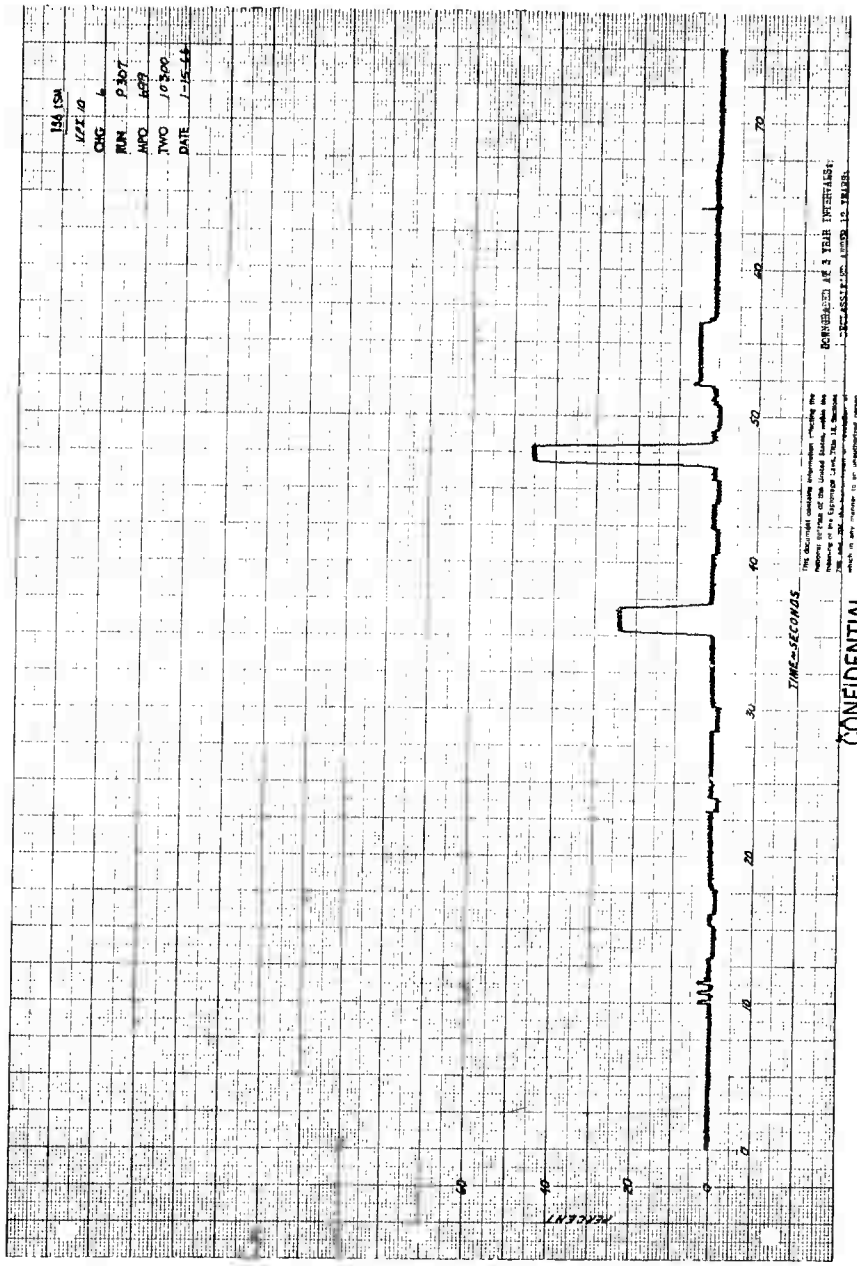

Figure 65 Injector Valve Pintle Position (Feedback) versus Time, Injector Valve No. 10, Motor 156-6

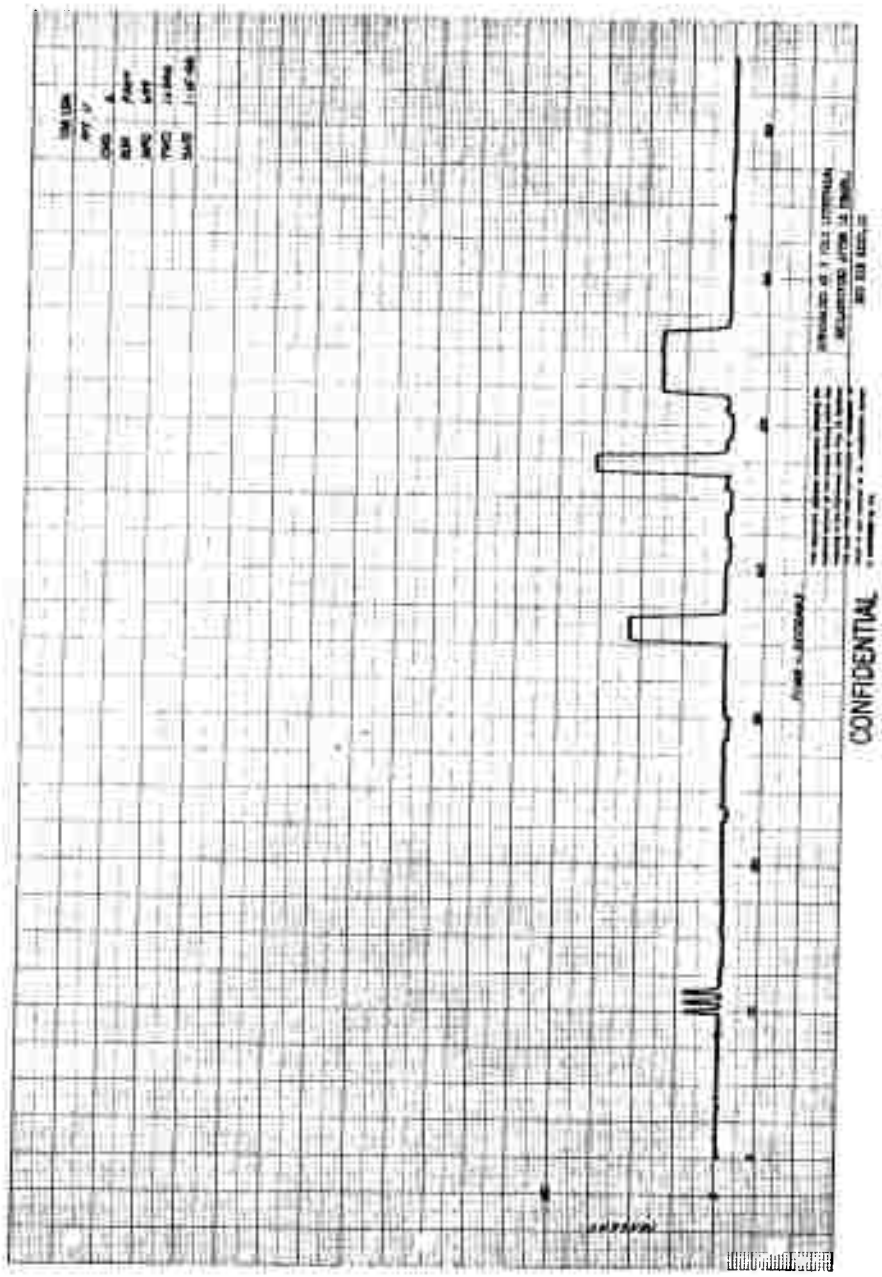

Figure 66 Injector Valve Pintle Position (Feedback) versus Time, Injector Valve No. 11, Motor 156-6

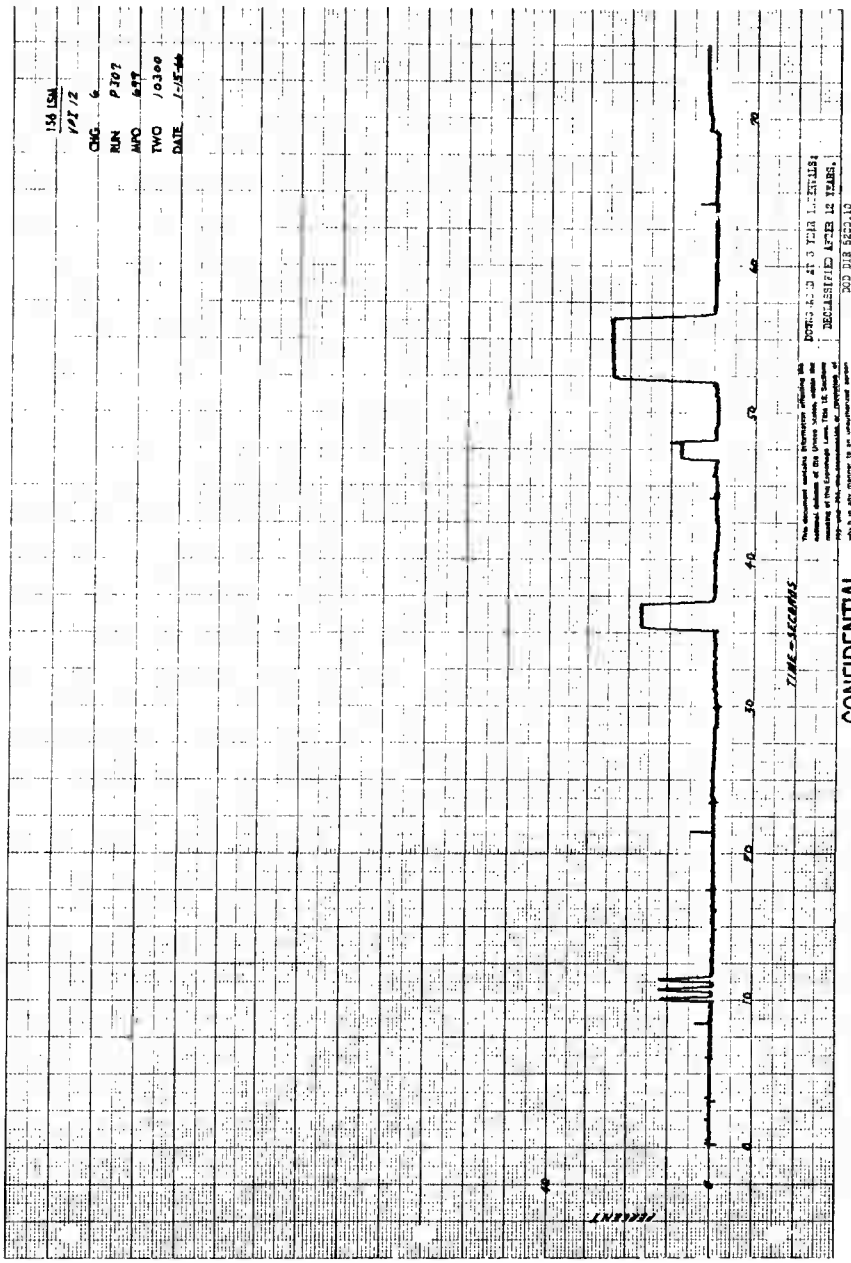

Figure 67 Injector Valve Pintle Position (Feedback) versus Time, Injector Valve No. 12, Motor 156-6

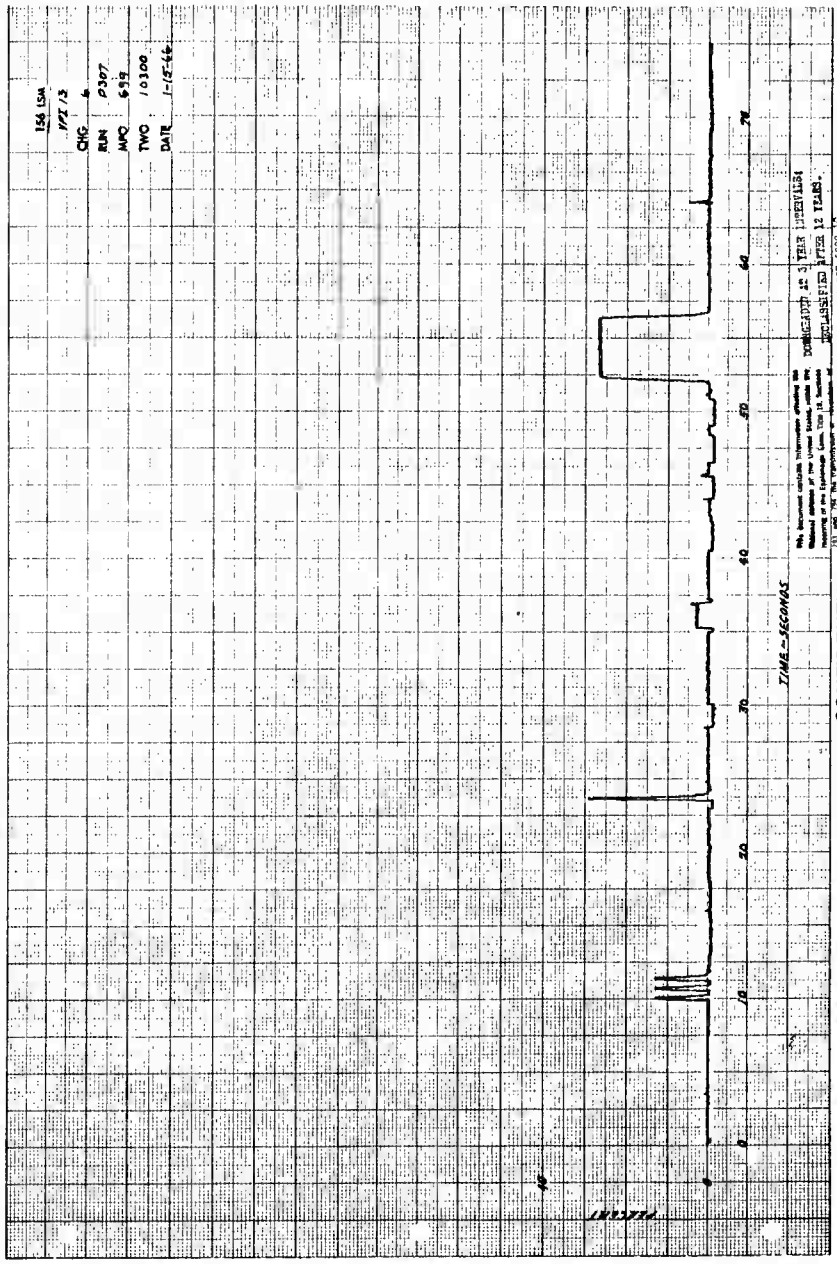

Figure 68 Injector Valve Pintle Position (Feedback) versus Time, Injector Valve No. 13, Motor 156-6

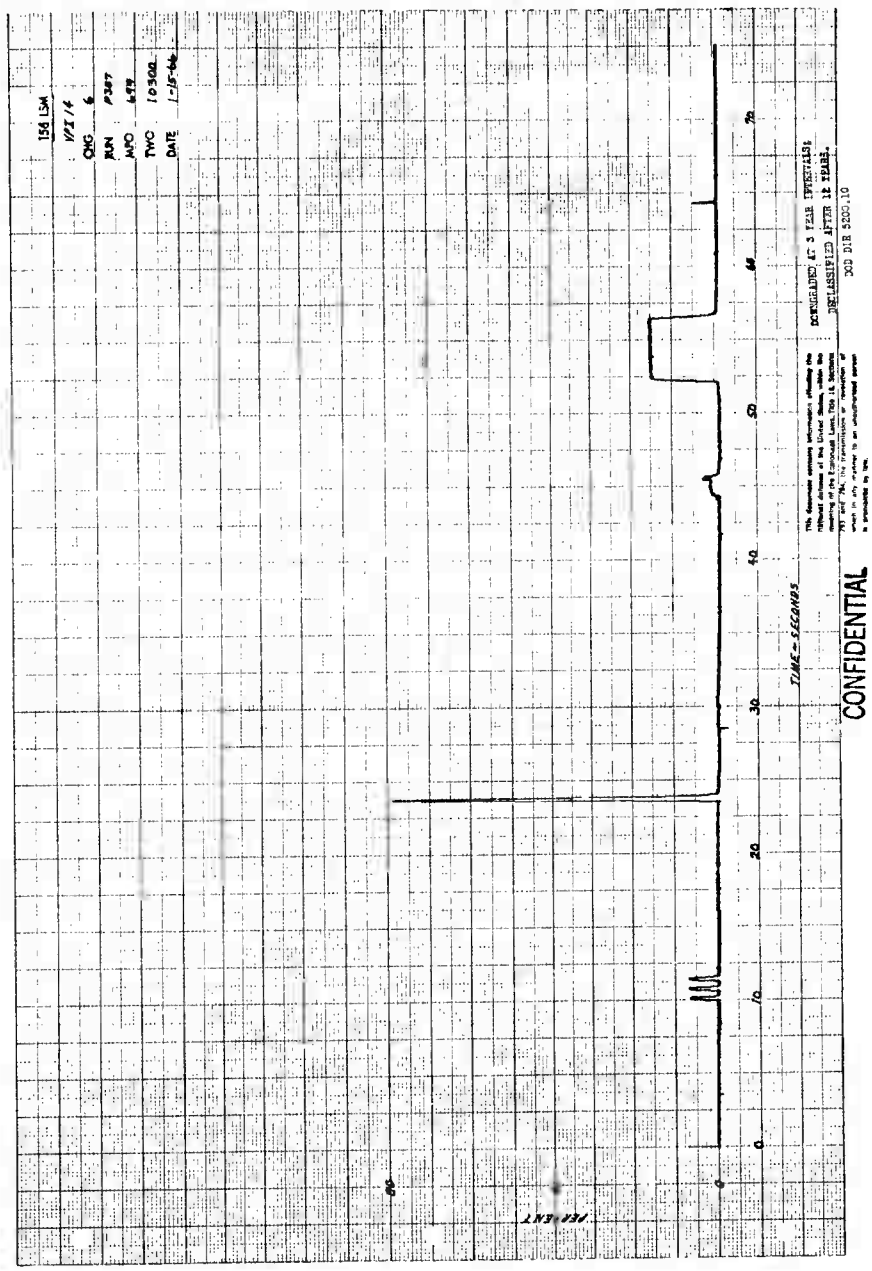

Figure 69 Injector Valve Pintle Position (Feedback) versus Time, Injector Valve No. 14, Motor 156-6

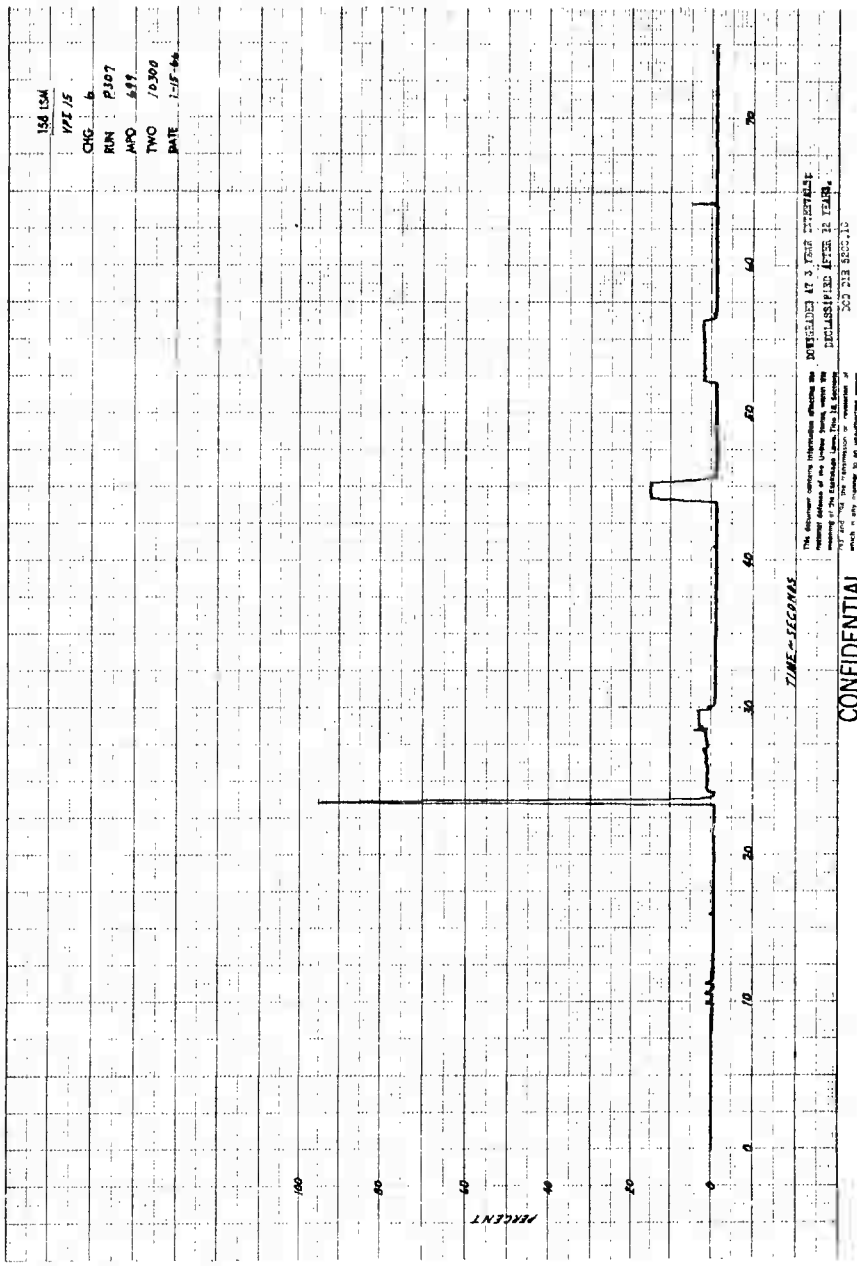

Figure 70 Injector Valve Pintle Position (Feedback) versus Time, Injector Valve No. 15, Motor 156-6

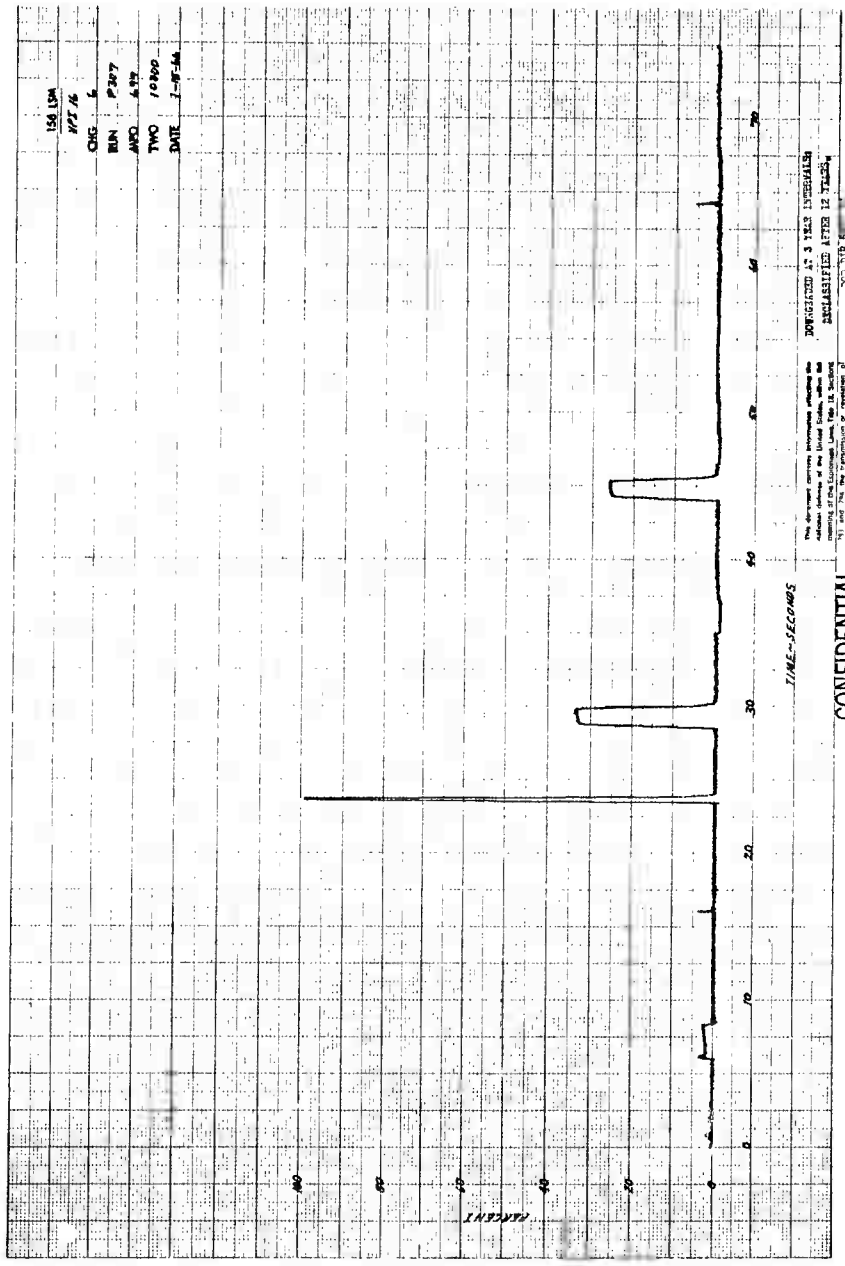

Figure 71 Injector Valve Pintle Position (Feedback) versus Time, Injector Valve No. 16, Motor 156-6

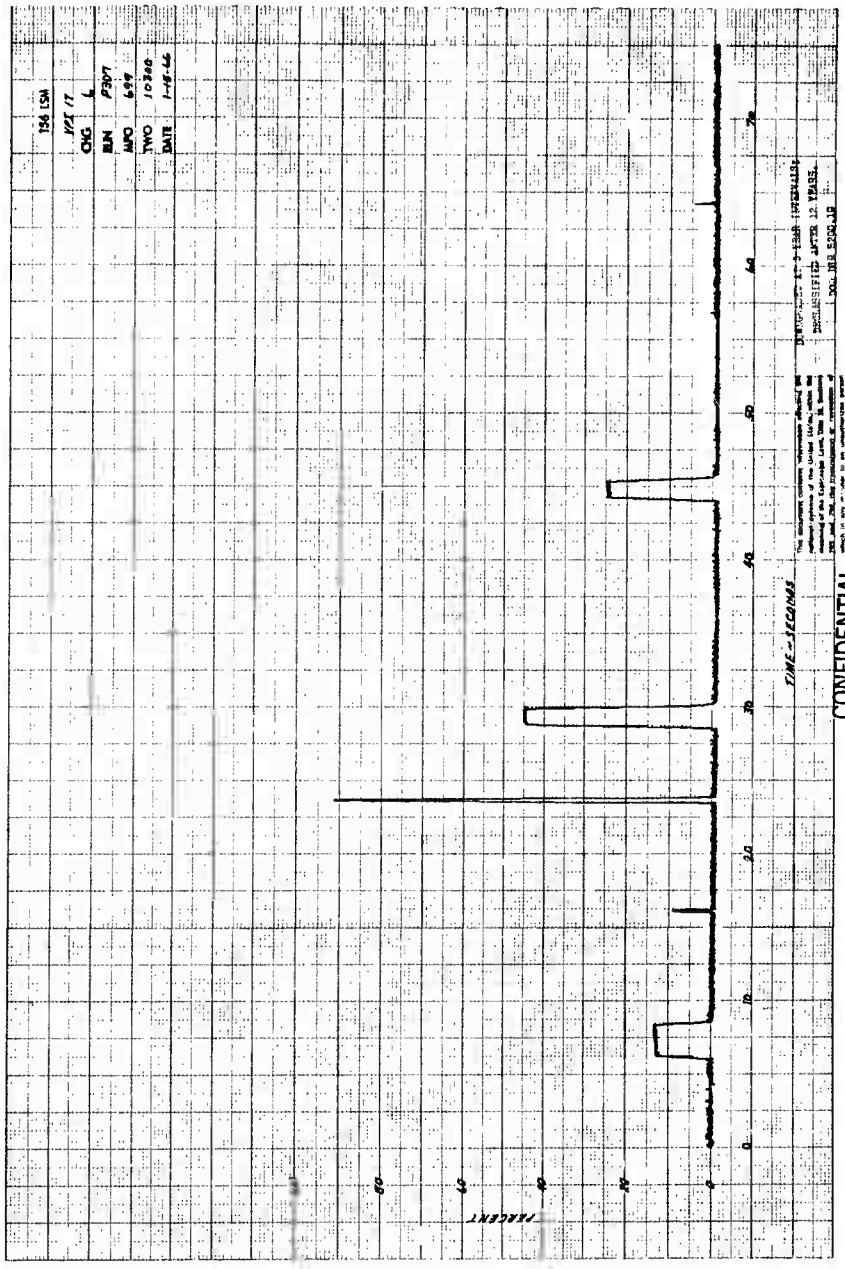

Figure 72 Injector Valve Pintle Position (Feedback) versus Time, Injector Valve No. 17, Motor 156-6

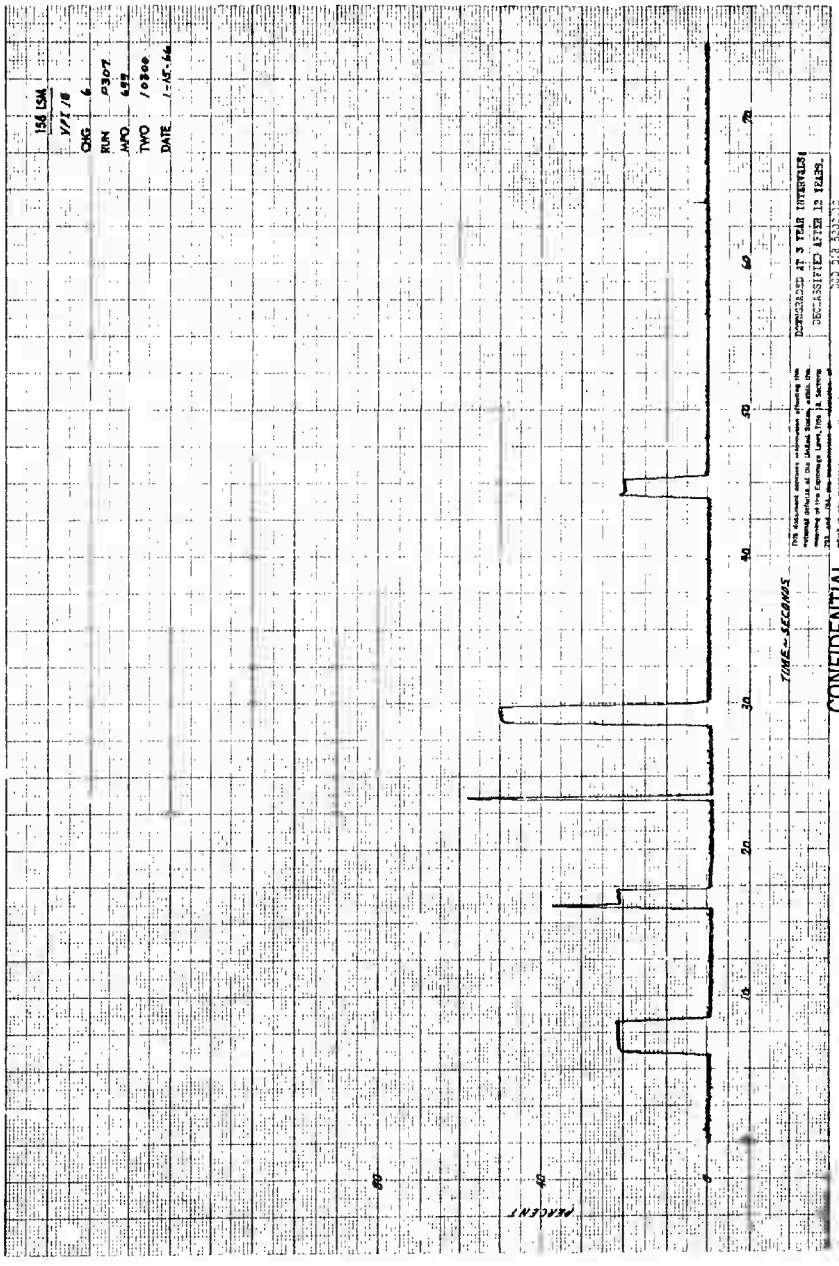

Figure 7. Injector Valve Pintle Position (Feedback) versus Time. Injector Valve No. 18, Motor 156 6

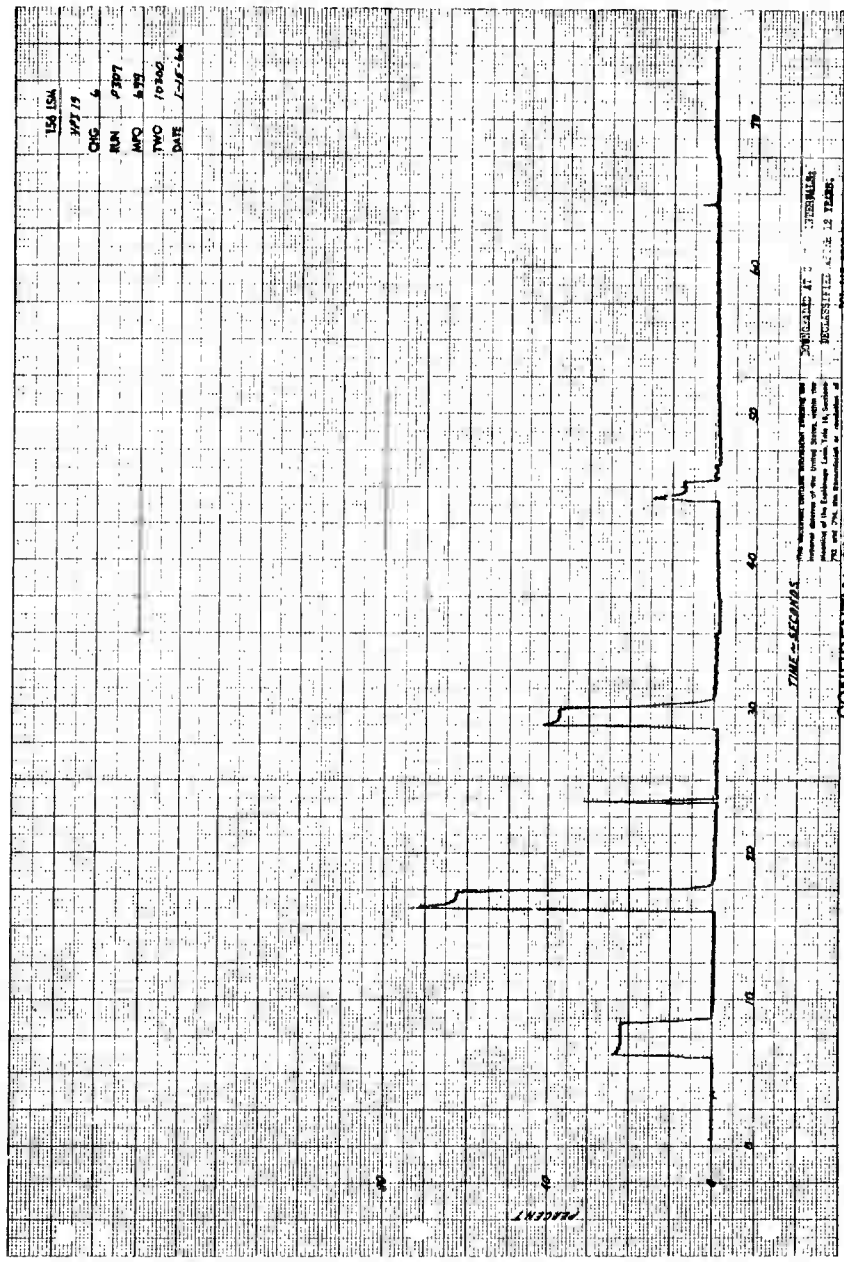

Figure 74 Injector Valve Pintle Position (Feedback) versus Time, Injector Valve No. 19, Motor 156-6

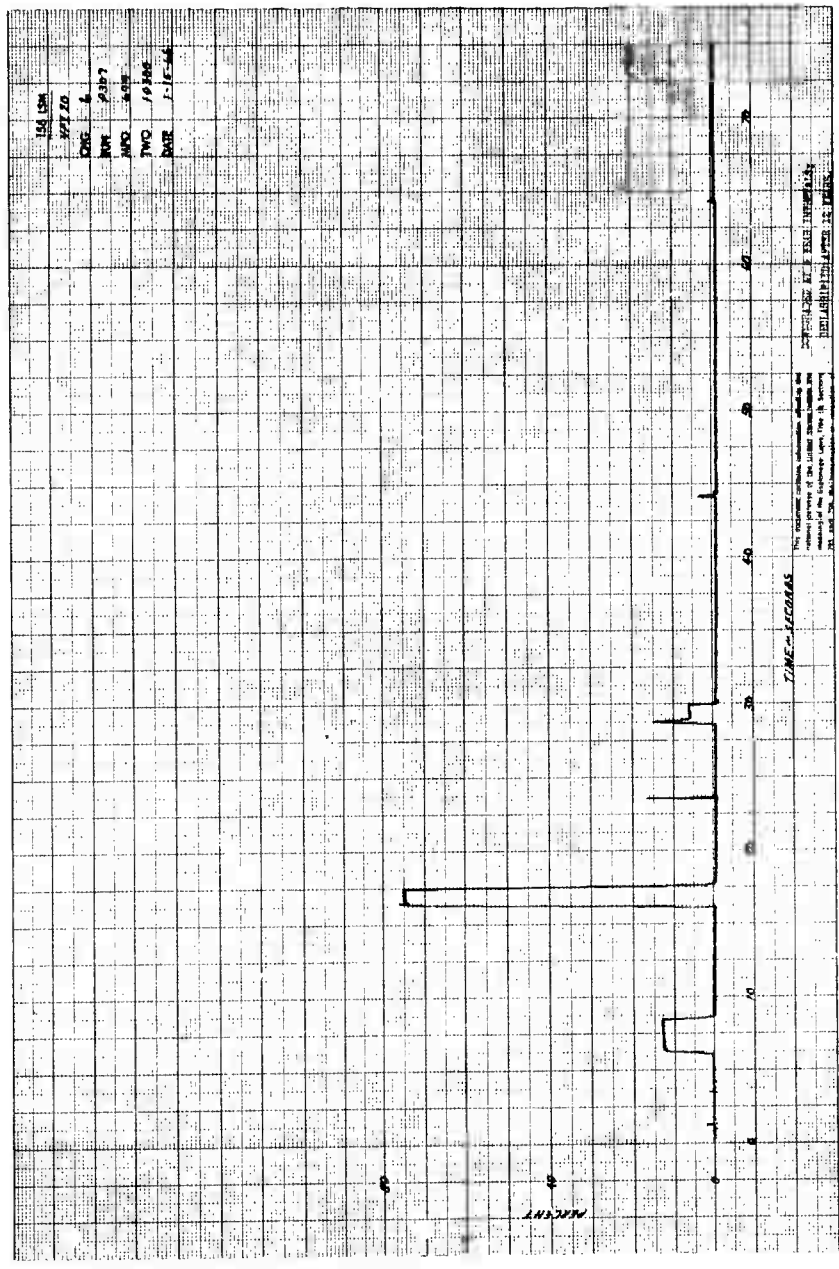

Figure 75 Injector Valve Pintle Position (Feedback) versus Time Injector Valve No. 20
Motor 15b 6

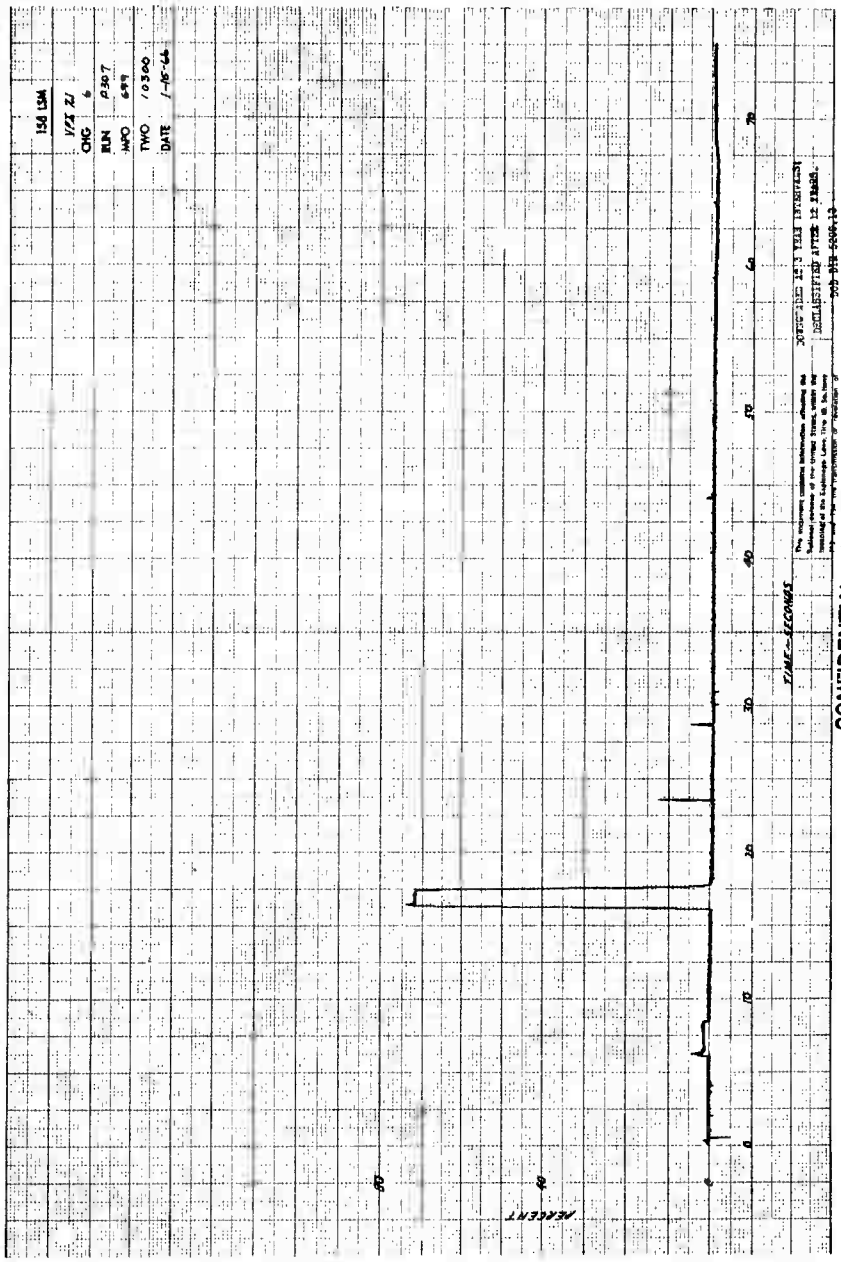

Figure 76. Injector Valve Pintle Position (Feedback) versus Time, Injector Valve No. 21, Motor 156-6

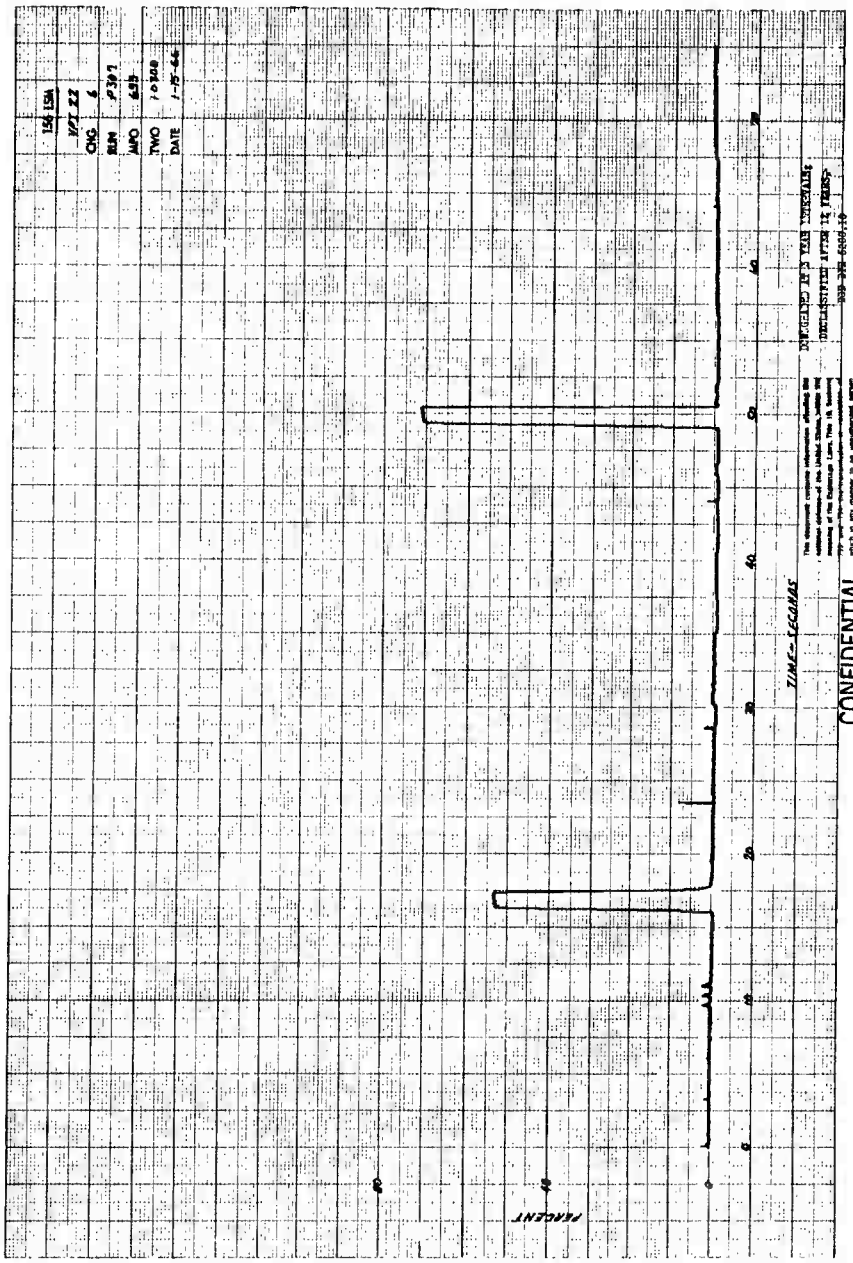

Figure 77 Injector Valve Pintle Position (Feedback) versus Time, Injector Valve No. 22, Motor 156-6

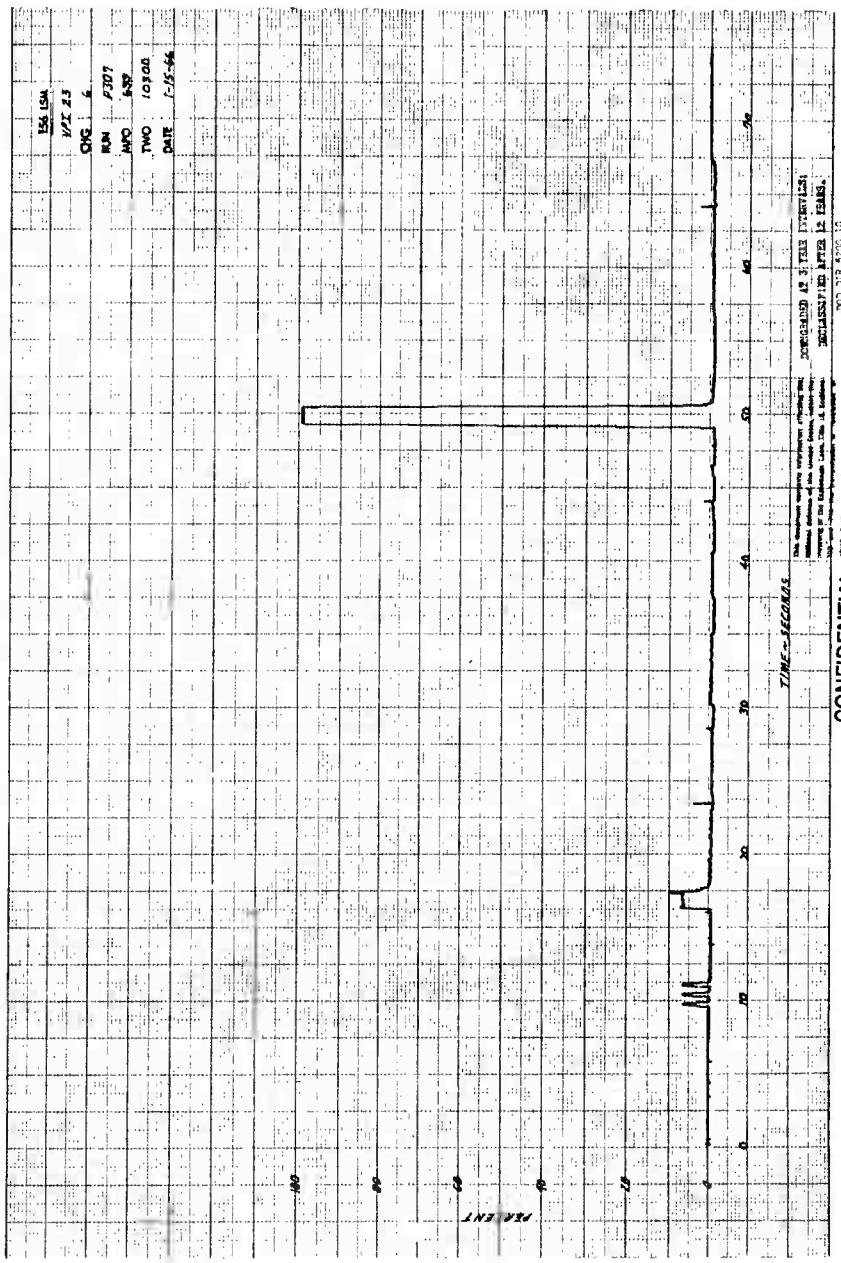

Figure 78 Injector Valve Pintle Position (Feedback) versus Time, Injector Valve No. 23, Motor 156-6

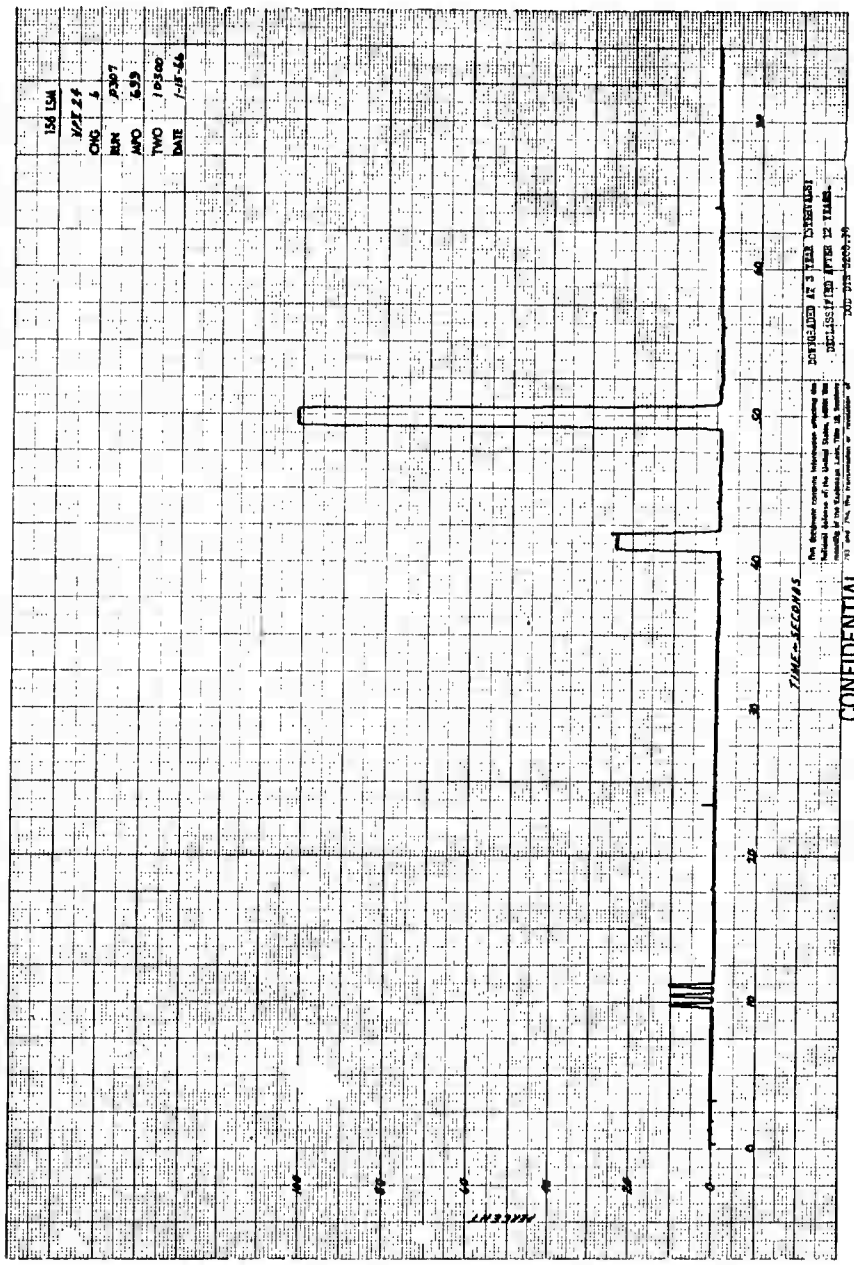

Figure 79 Injector Valve Pintle Position (Feedback) versus Time, Injector Valve No. 24, Motor 156-6

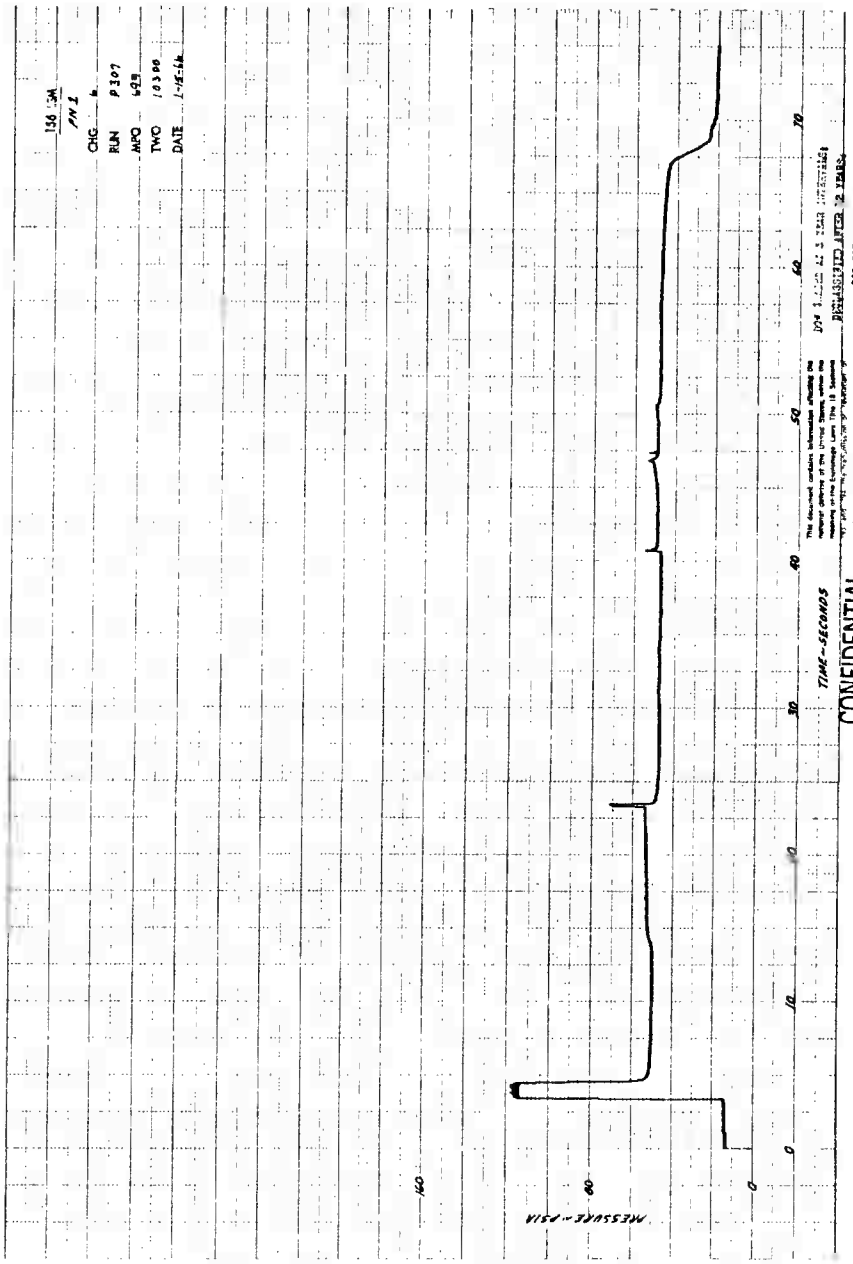

Figure 80 Nozzle Pressure versus Time, Location No. 1, Motor 156-6

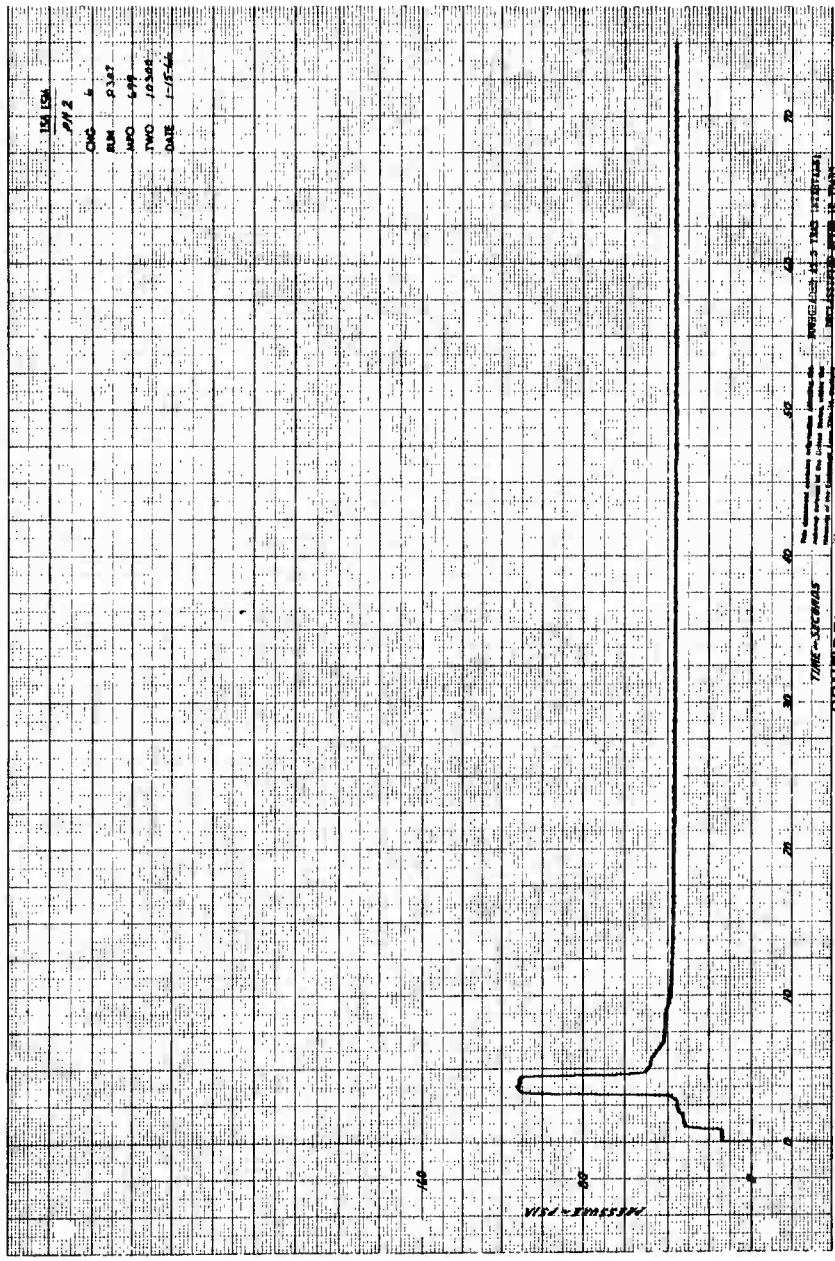

Figure 81 Nozzle Pressure versus Time, Location No. 2, Motor 156-6

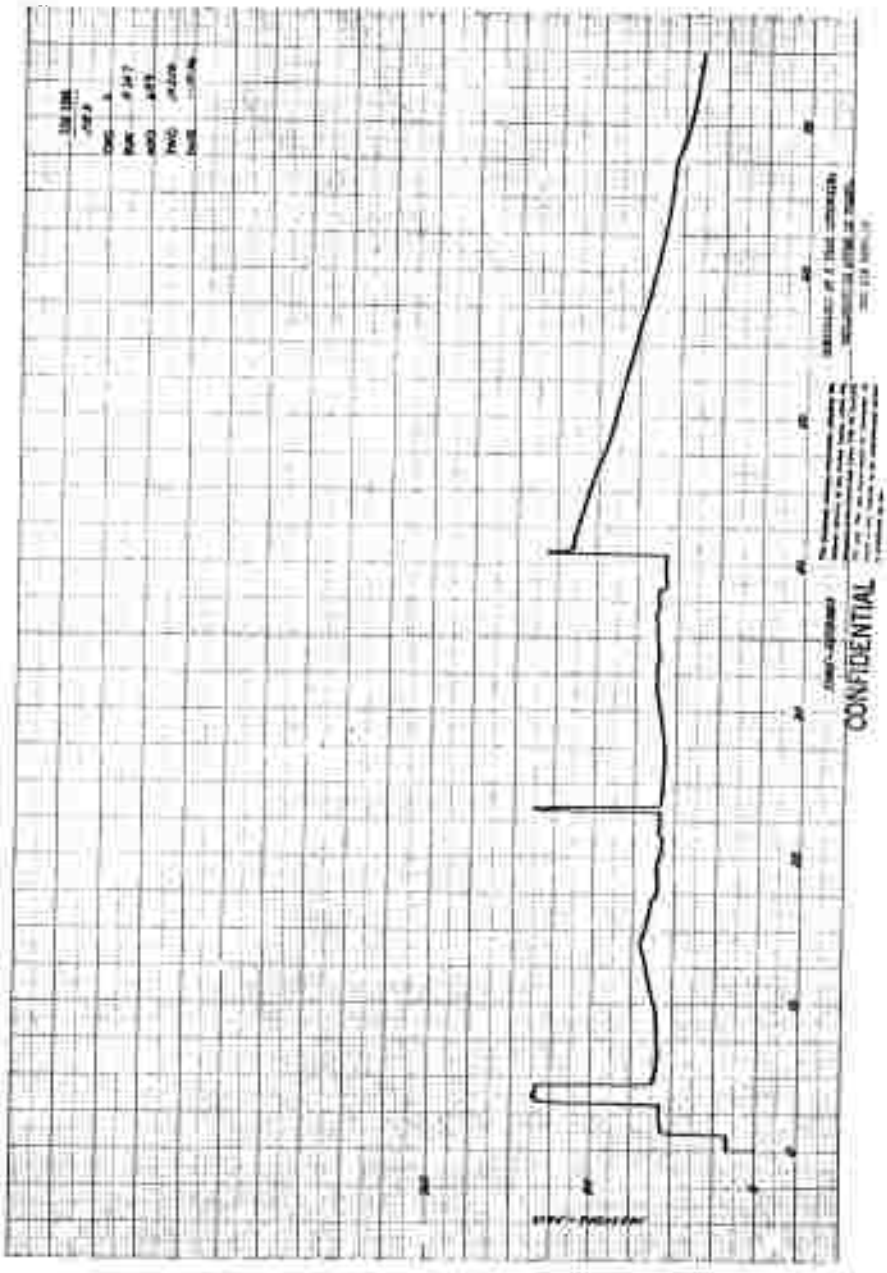

Figure 82 Nozzle Pressure versus Time, Location No. 3, Motor 156-6

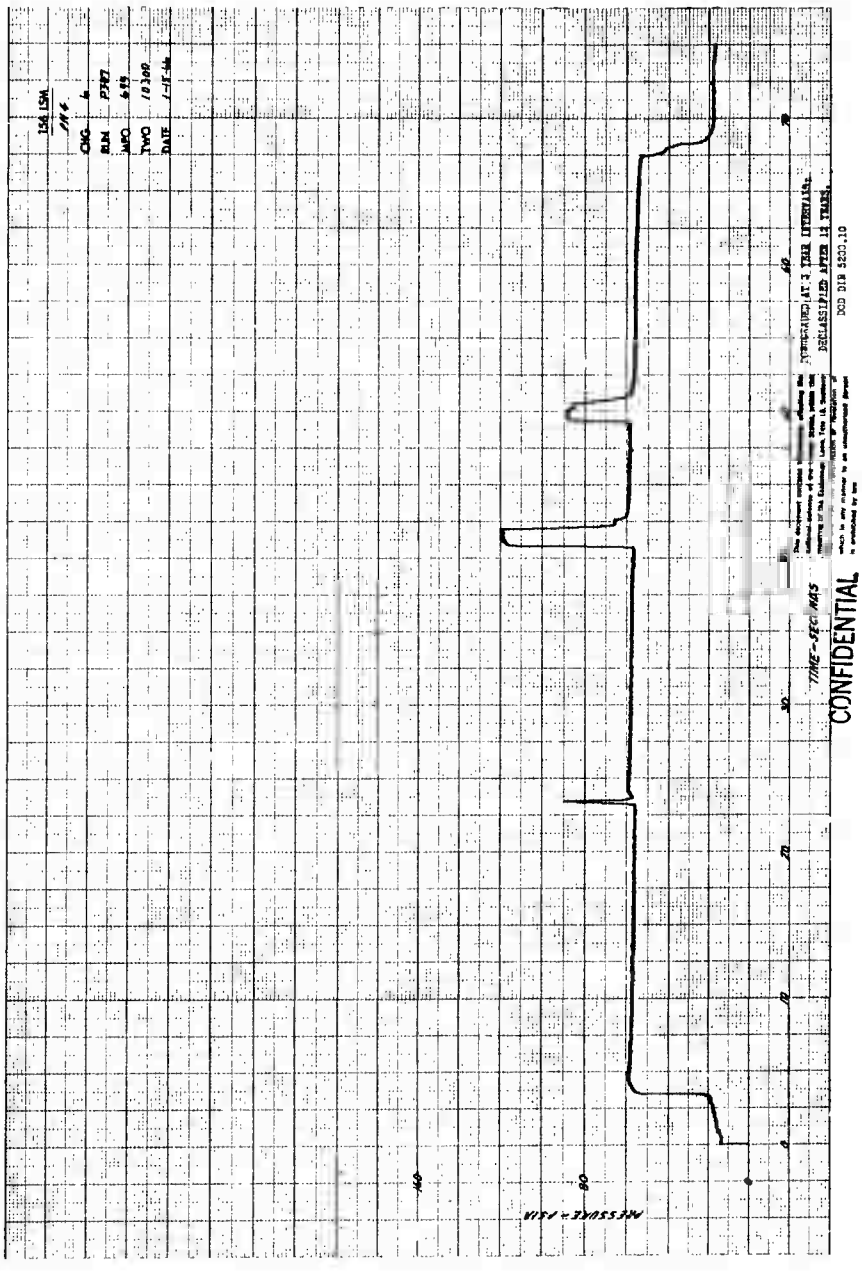

Figure 83 Nozzle Pressure versus Time, Location No. 4, Motor 156-6

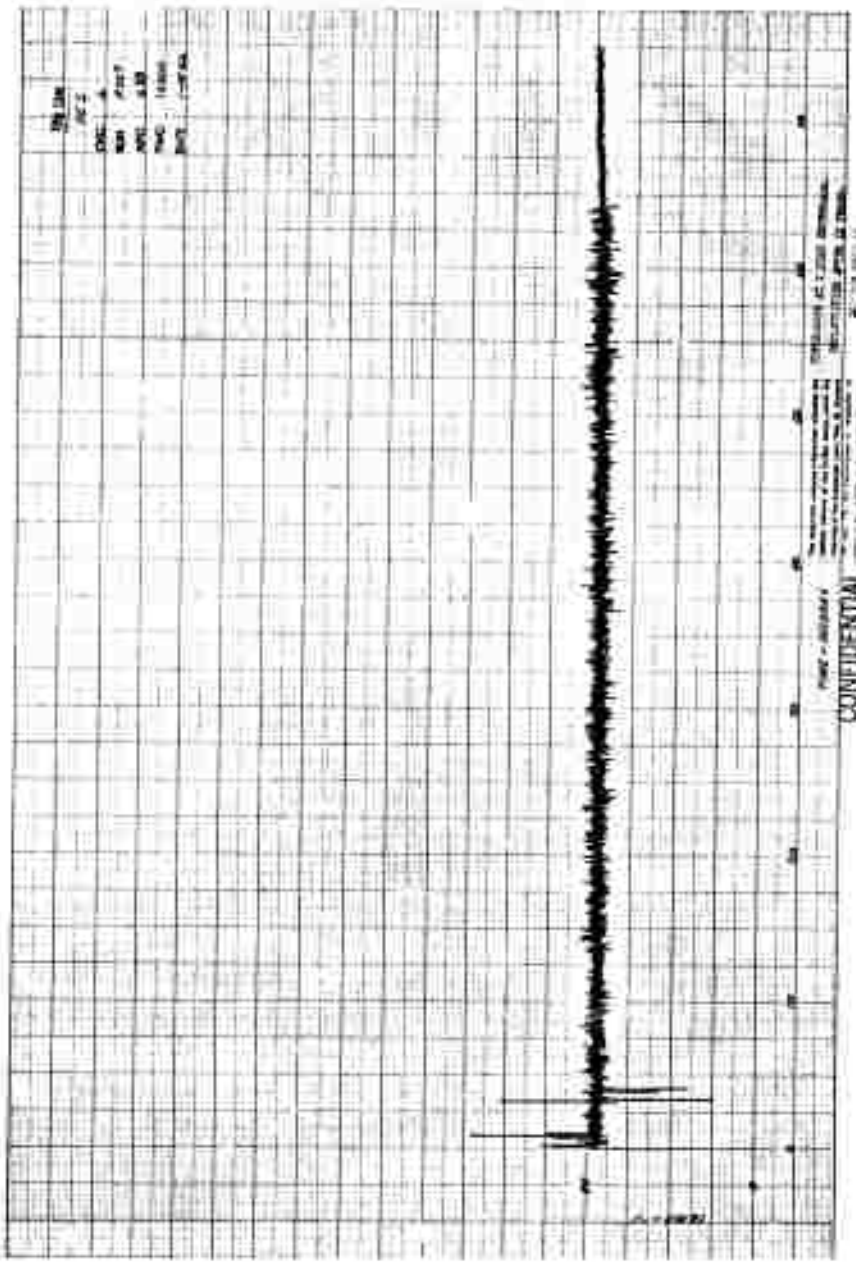

Figure 84 Motor Case Temperature versus Time, Location No. 1, Motor 156-6

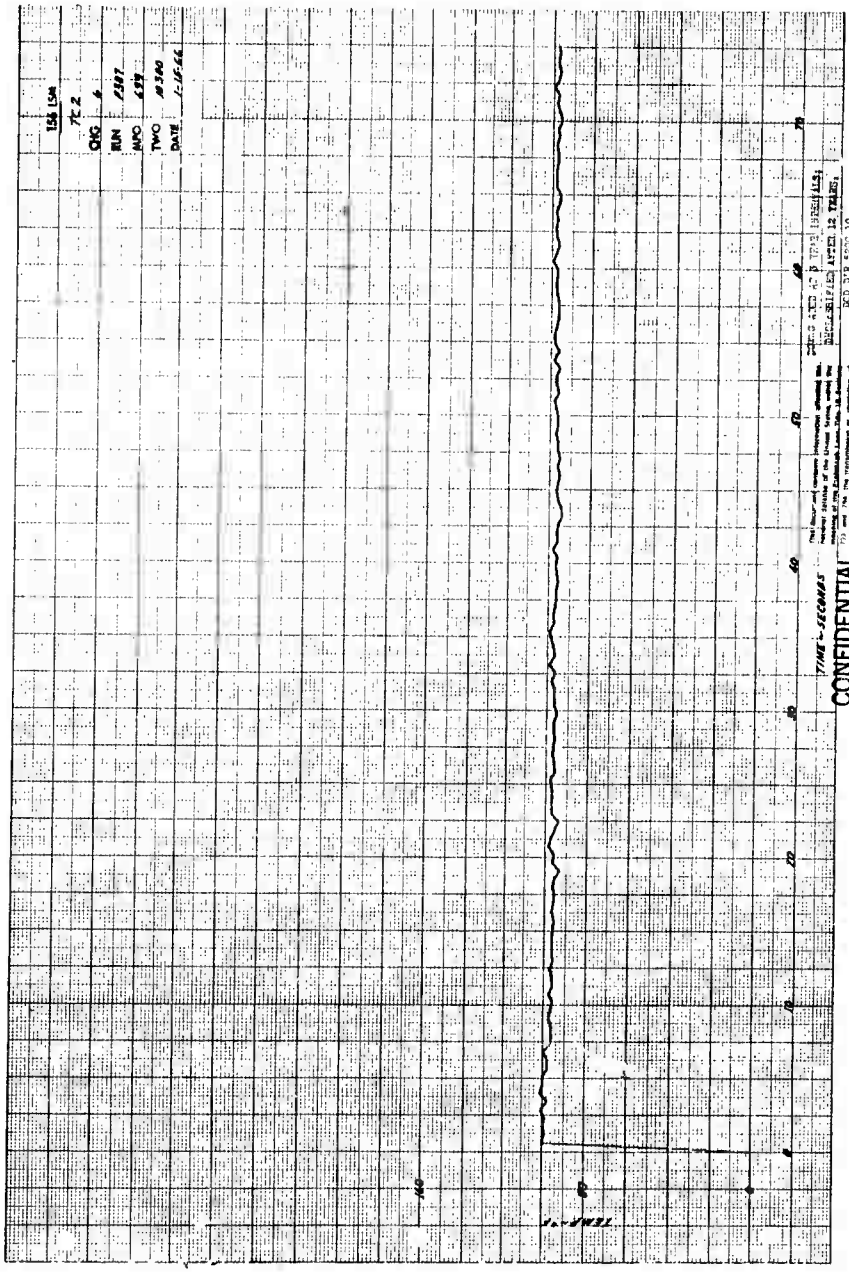

Figure 85 Motor Case Temperature versus Time, Location No. 2, Motor 156-6

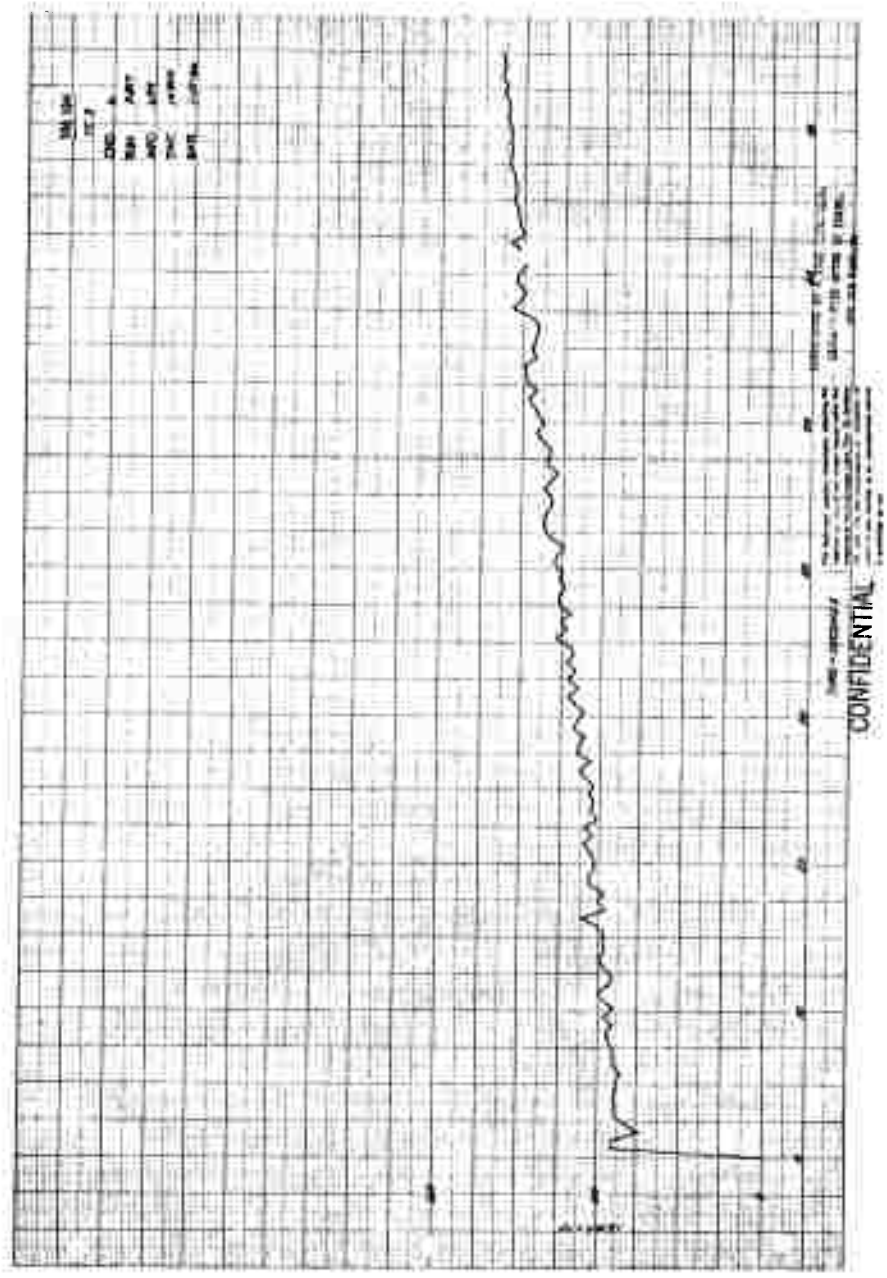

Figure 86 Motor Case Temperature versus Time, Location No. 3, Motor 156-6

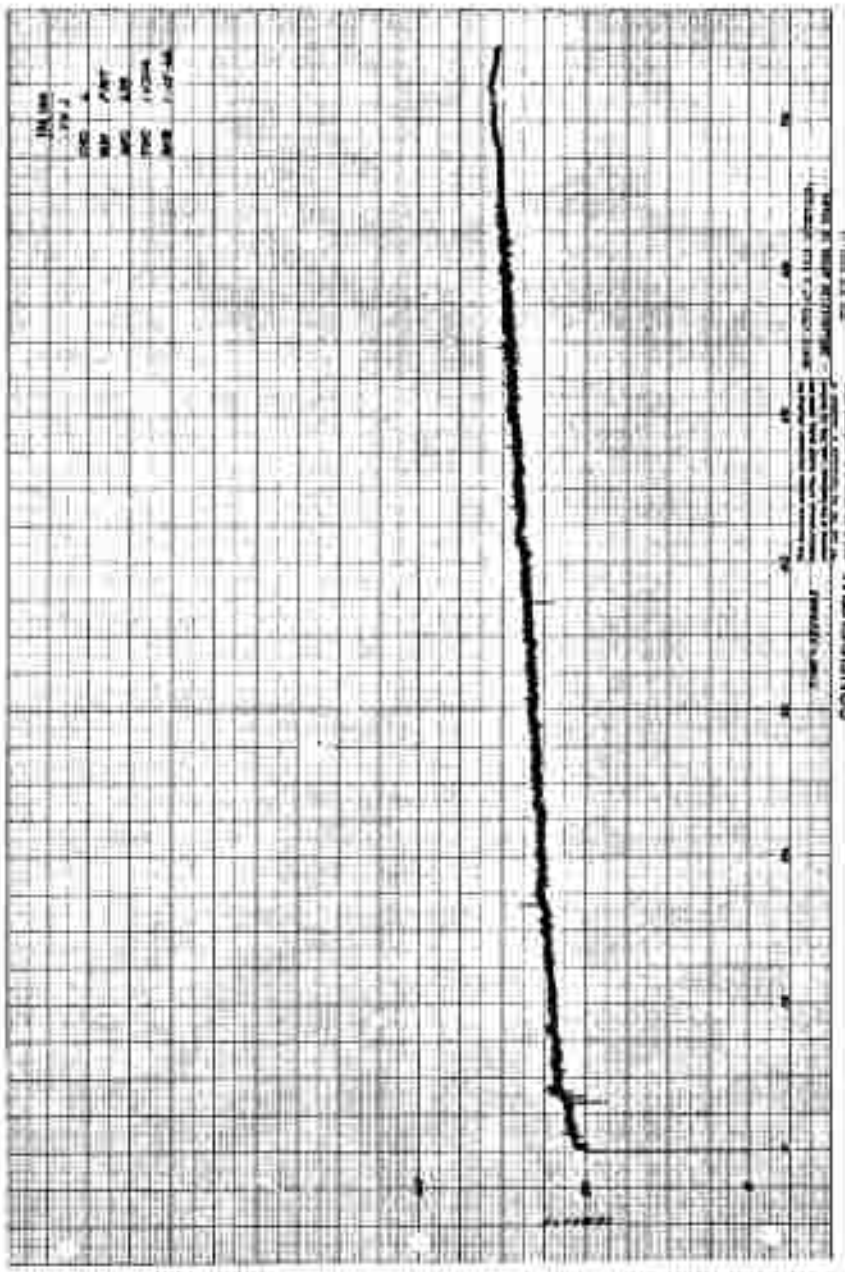

Figure 87 Nozzle Temperature versus Time, Location No. 1, Motor 156-6

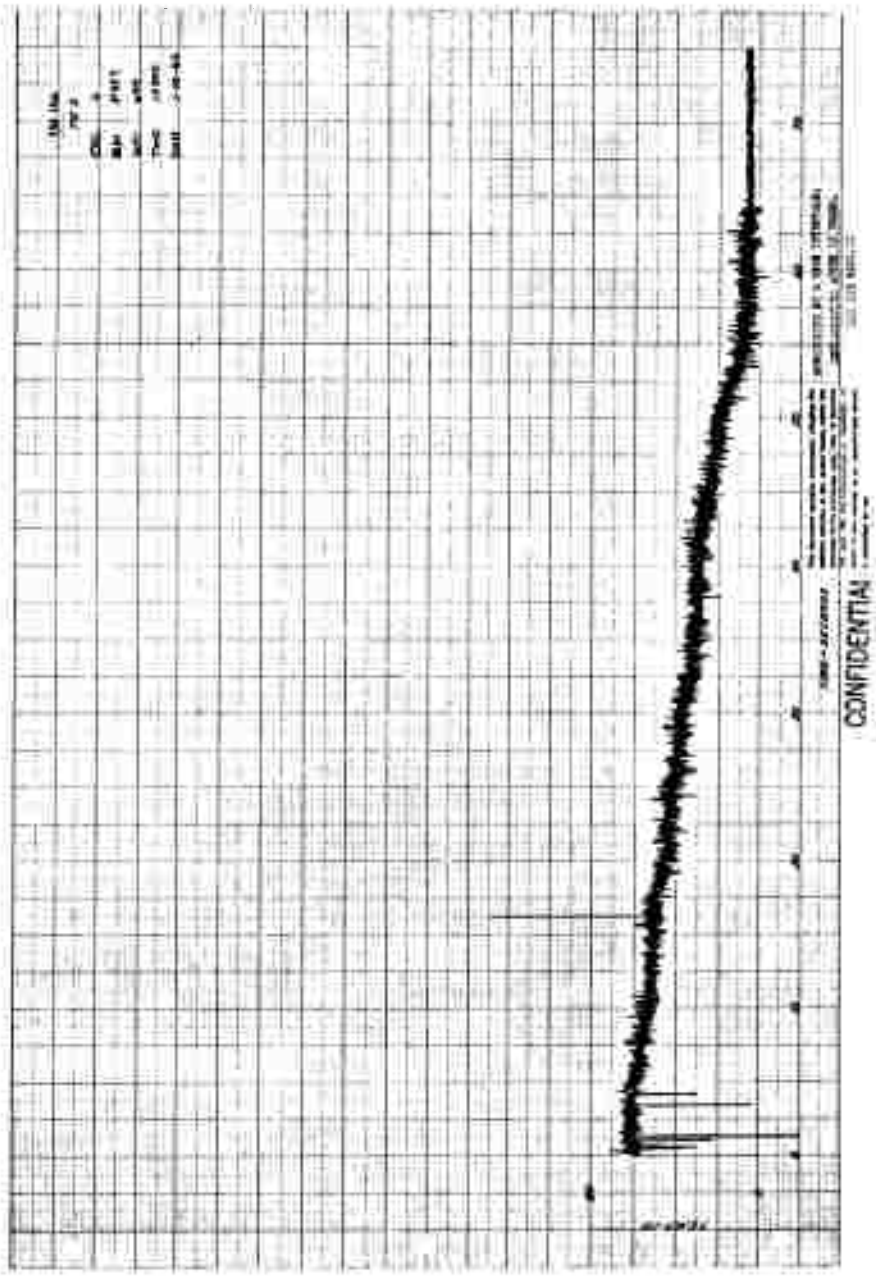

Figure 88 Nozzle Temperature versus Time, Location No. 2, Motor 156-6

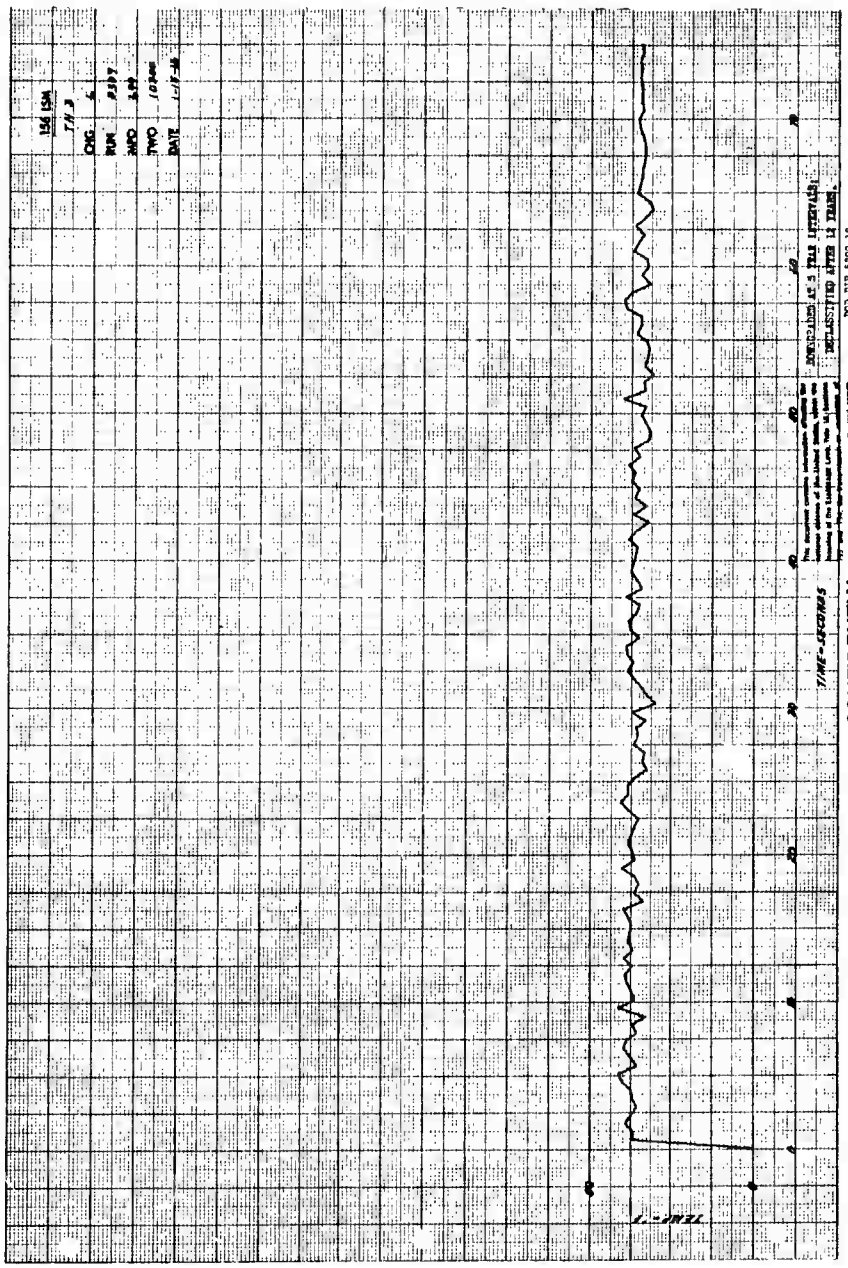

Figure 89 Nozzle Temperature versus Time, Location No. 3, Motor 156-6

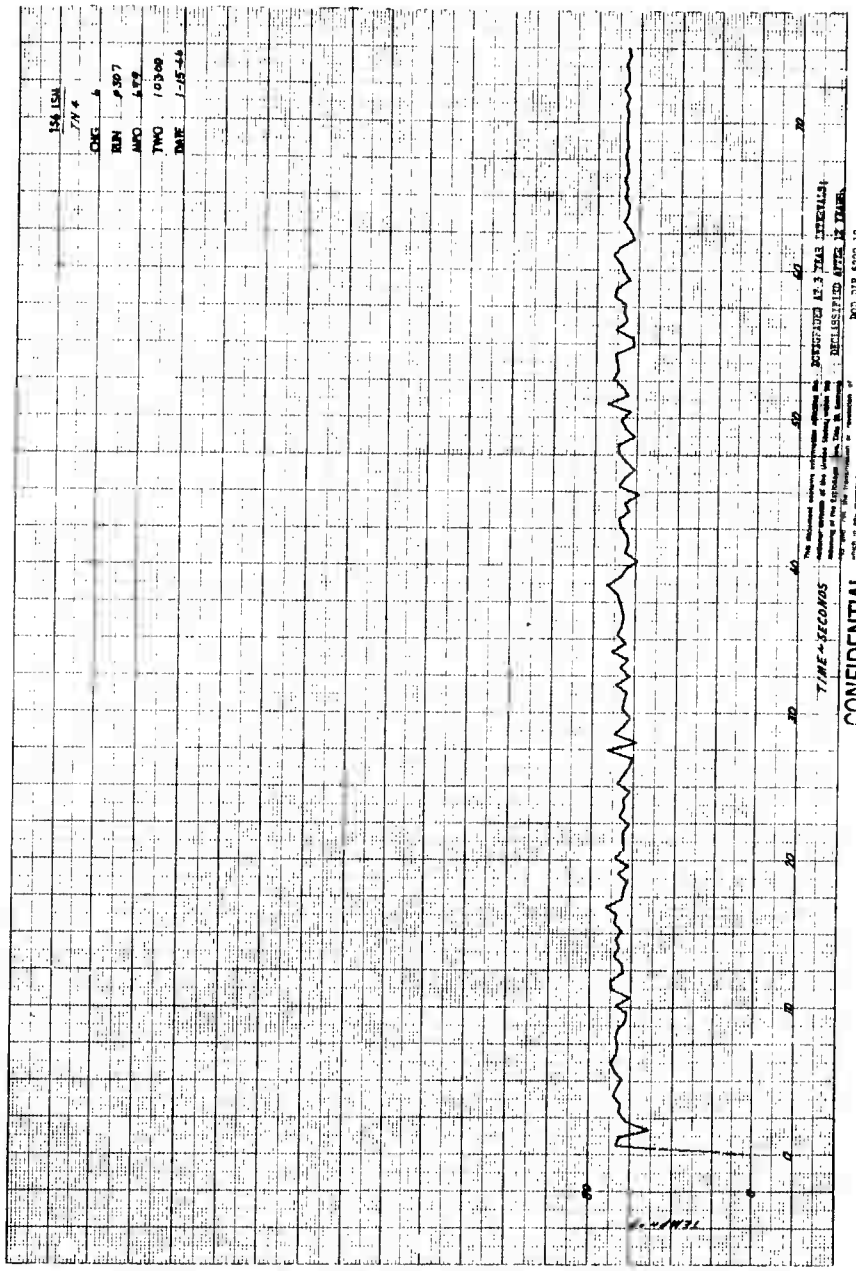

Figure 90 Nozzle Temperature versus Time, Location No. 4, Motor 156-6

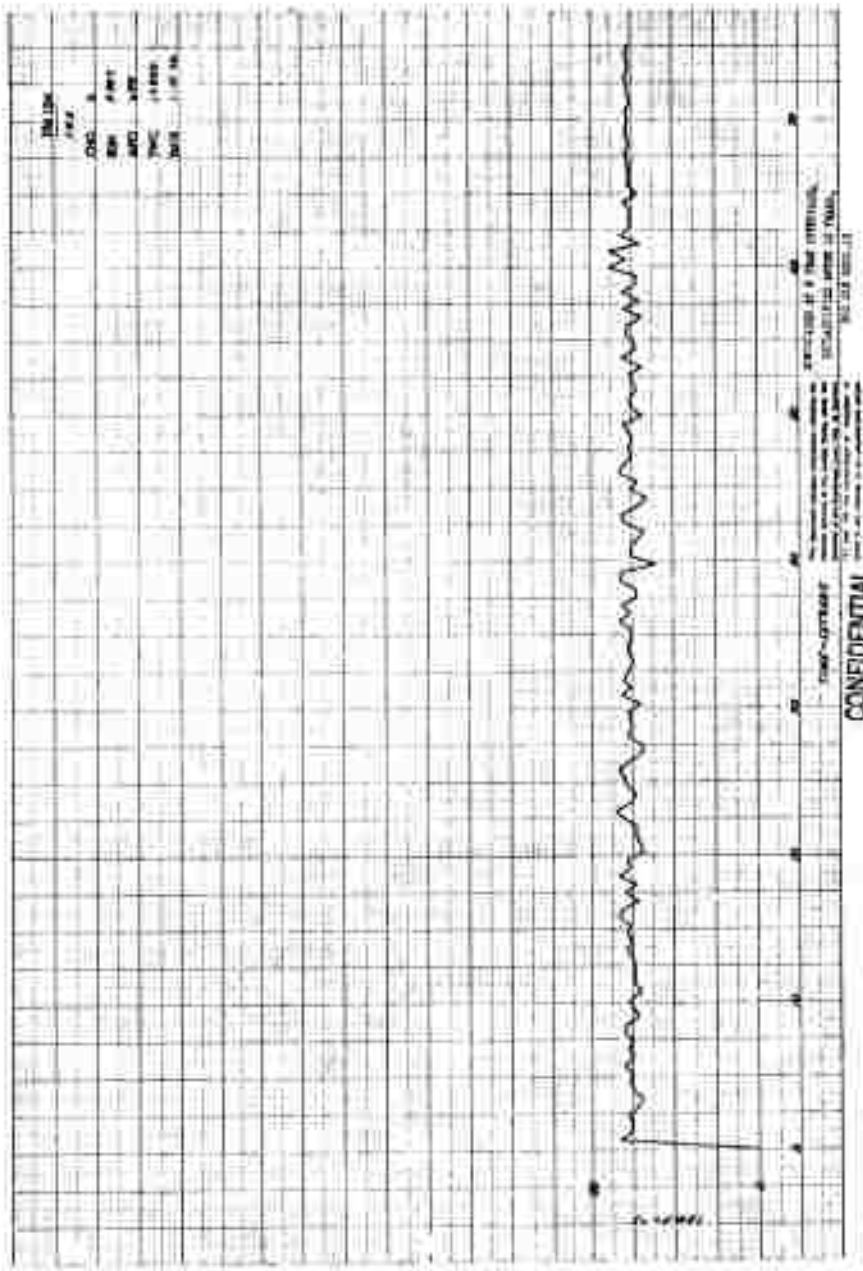

Figure 91 Nozzle Temperature versus Time, Location No. 5, Motor 156-6

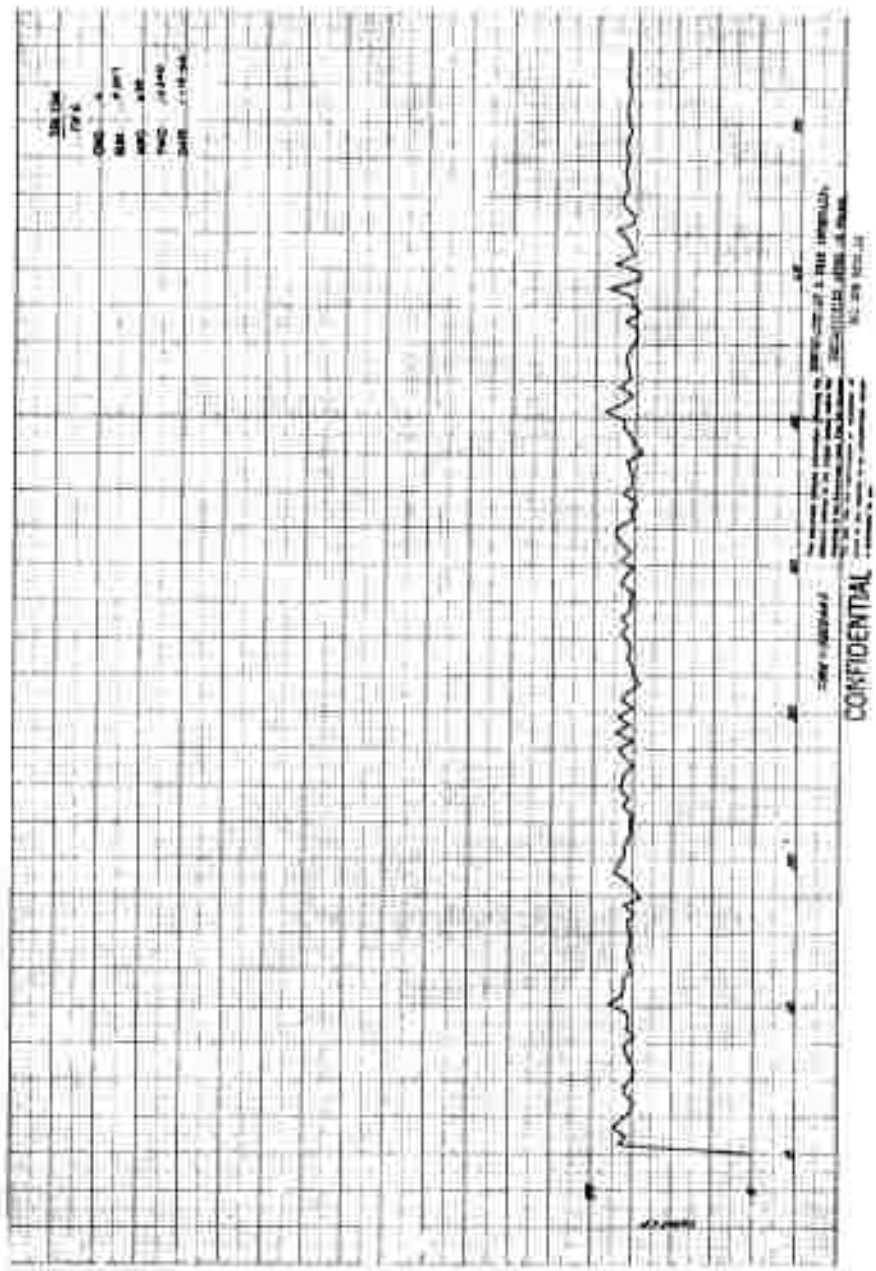

Figure 92 Nozzle Temperature versus Time, Location No. 6, Motor 156-6

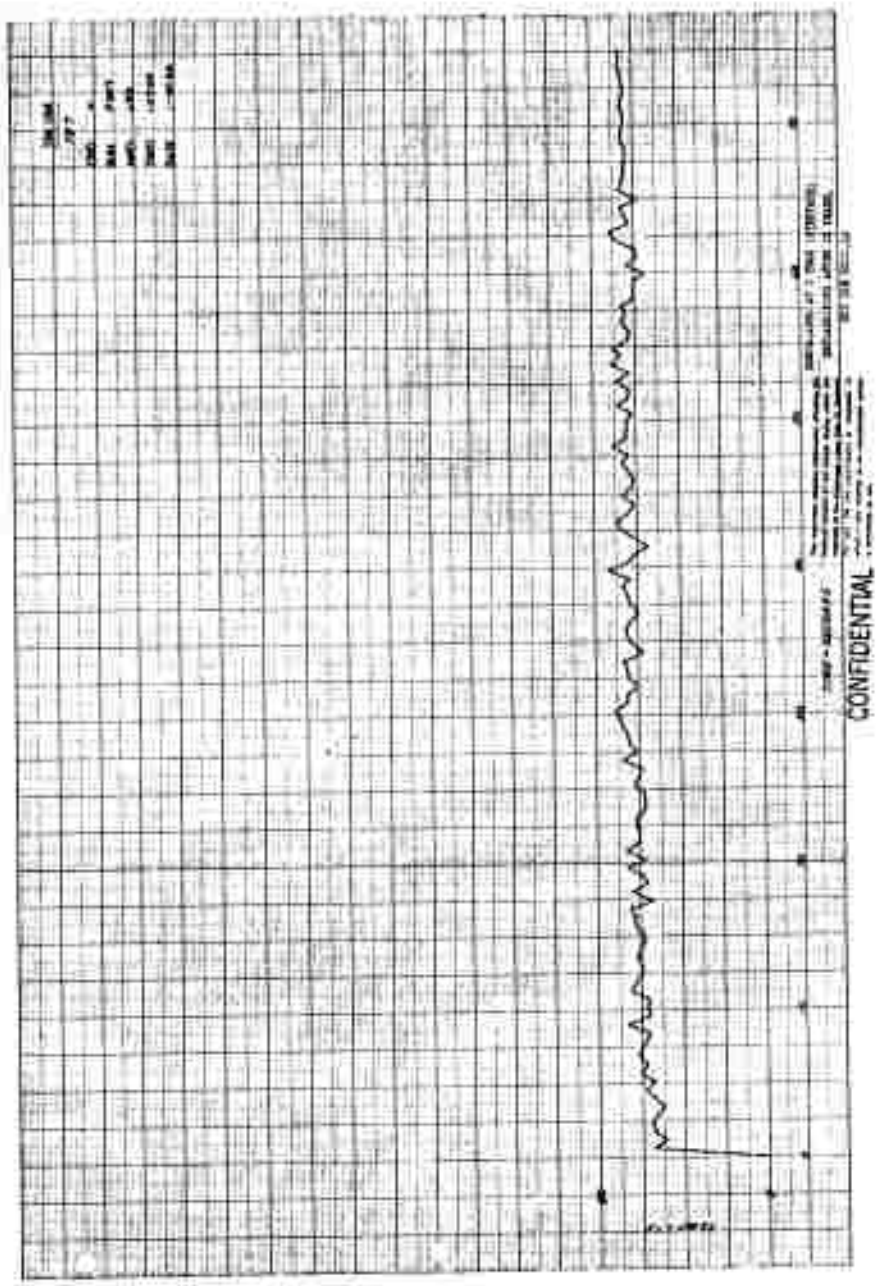

Figure 43 Nozzle Temperature versus Time, Location No. 7, Motor 156-6

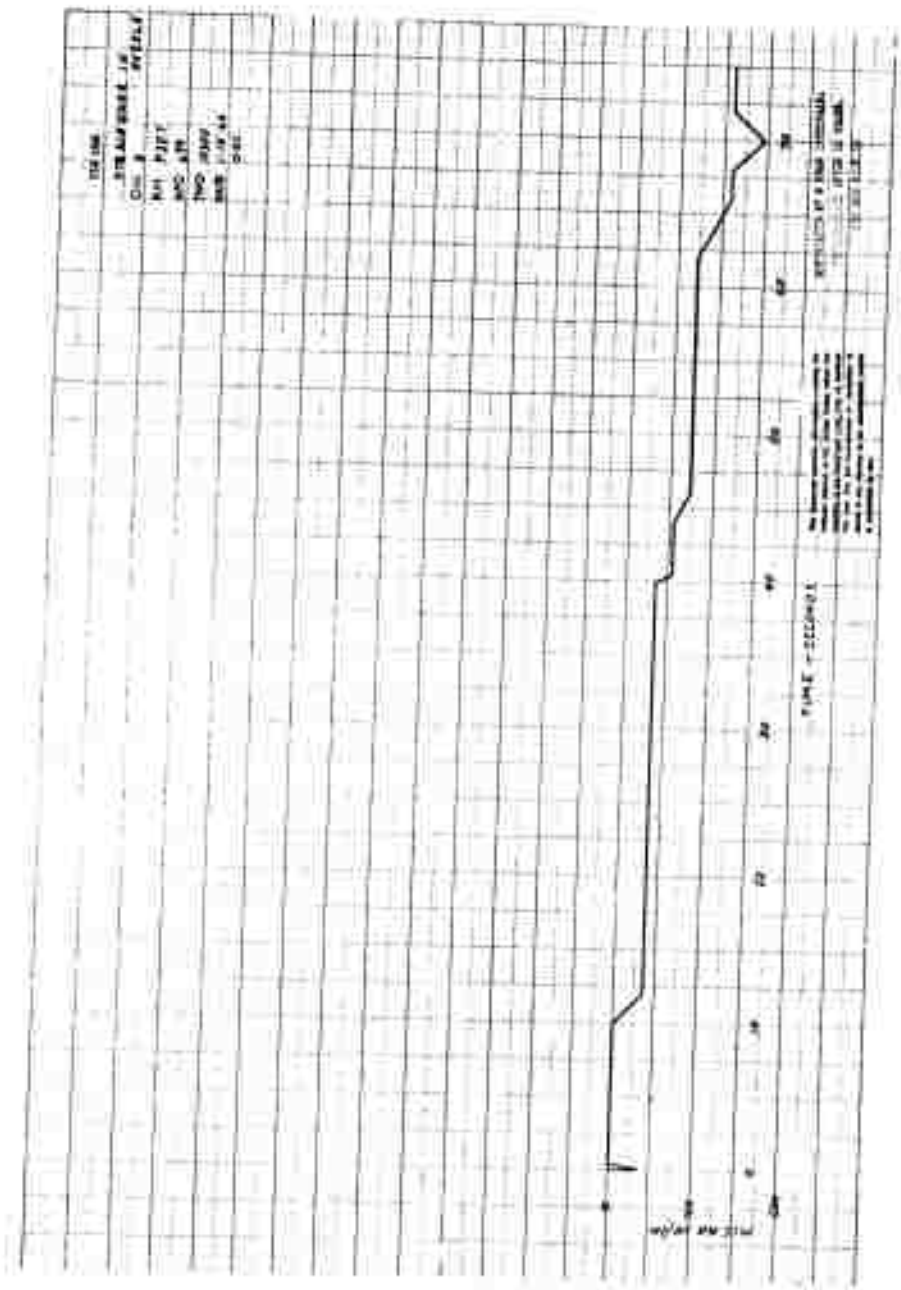

Figure 94 Nozzle Strain versus Time, Gage 1H, Motor 156-6

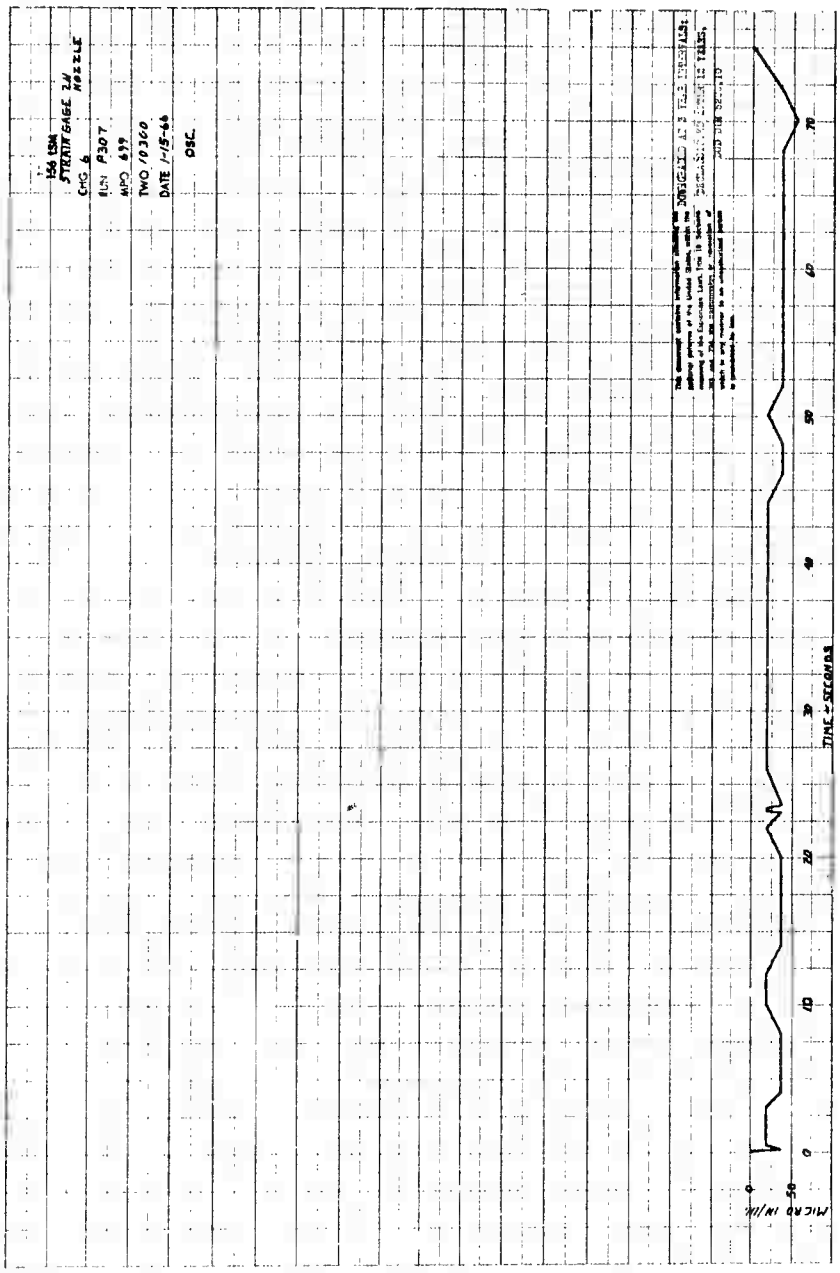

Figure 95 Nozzle Strain versus Time, Gage 2H, Motor 156-6

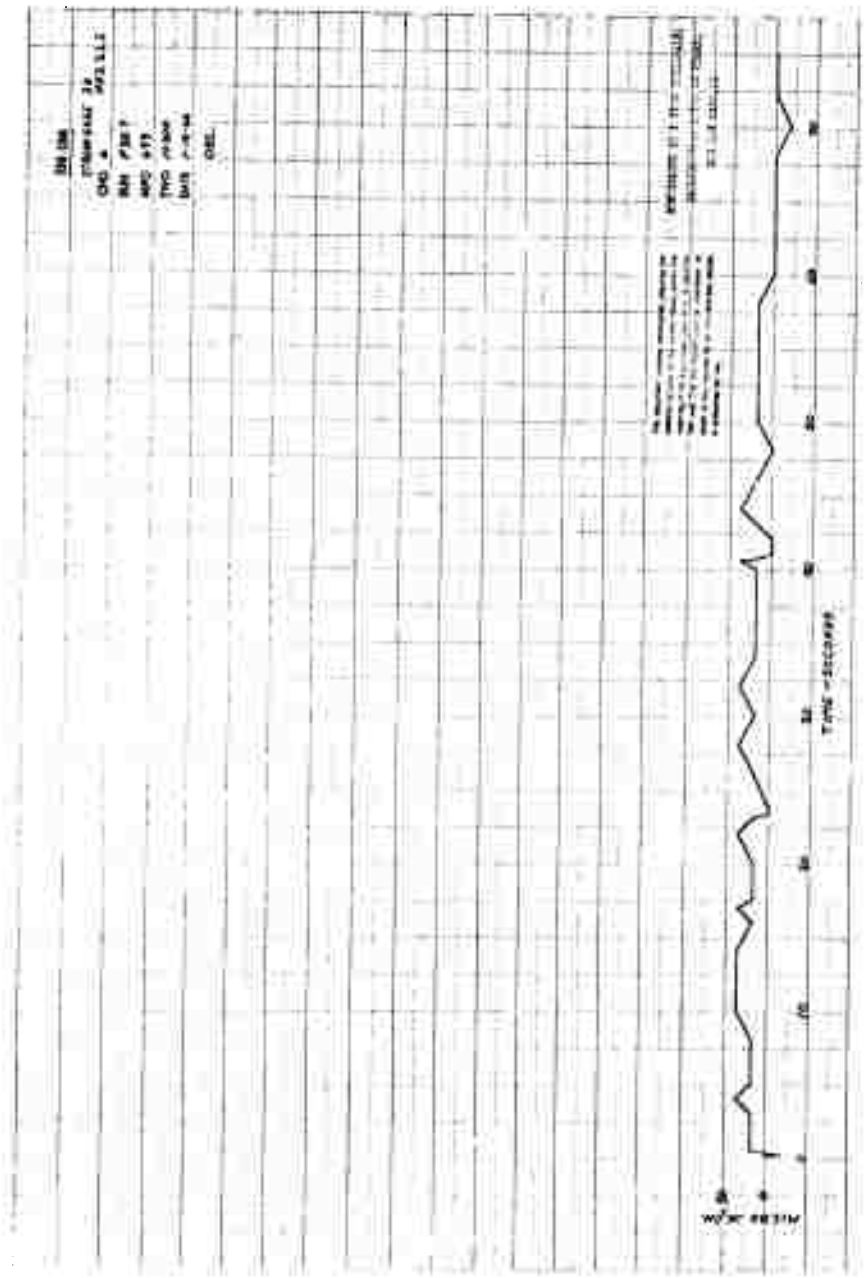

Figure 96 Nozzle Strain versus Time, Gage 3H, Motor 156-6

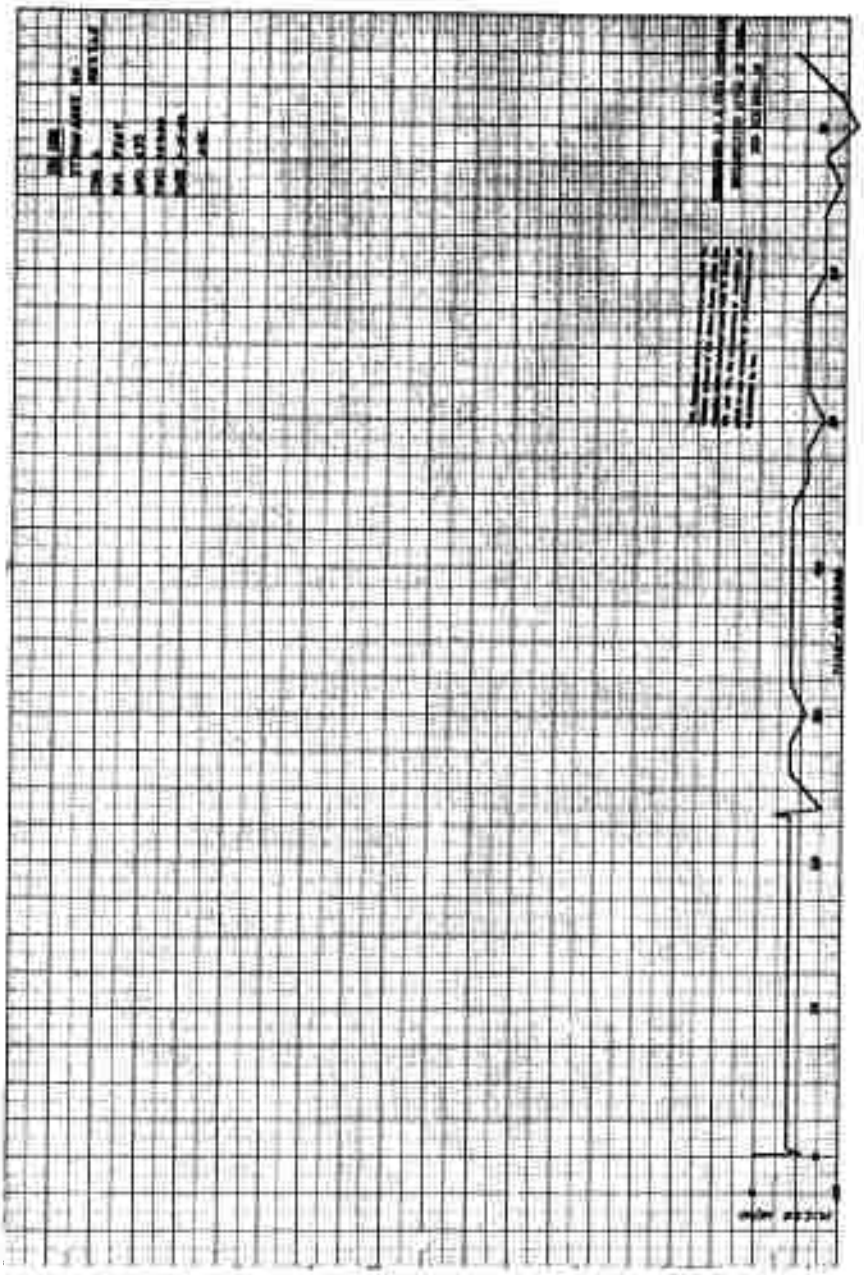

Figure 97 Nozzle Strain versus Time, Gage 4H, Motor 156-6

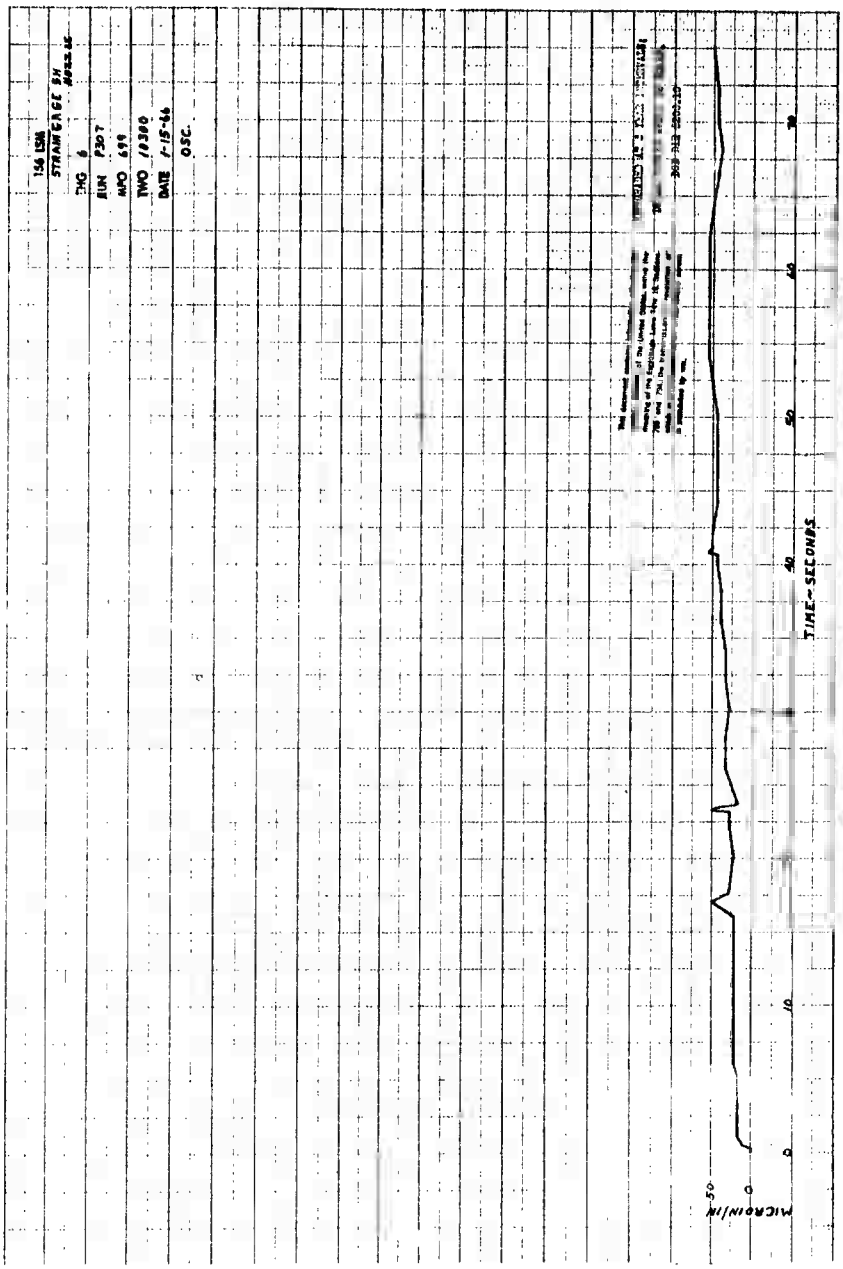

Figure 98 Nozzle Strain versus Time, Gage 5H, Motor 156-6

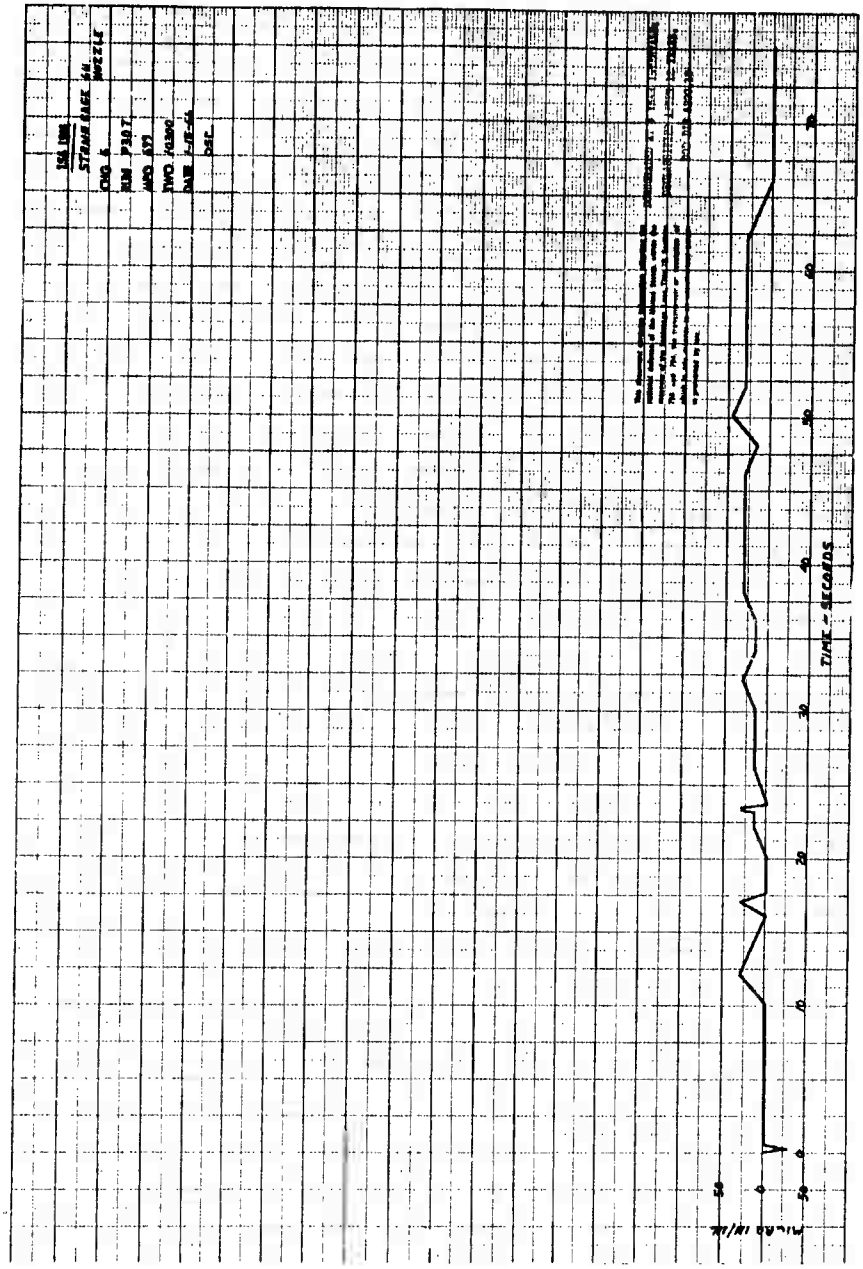

Figure 99 Nozzle Strain versus Time, Gage 6H, Motor 156-6

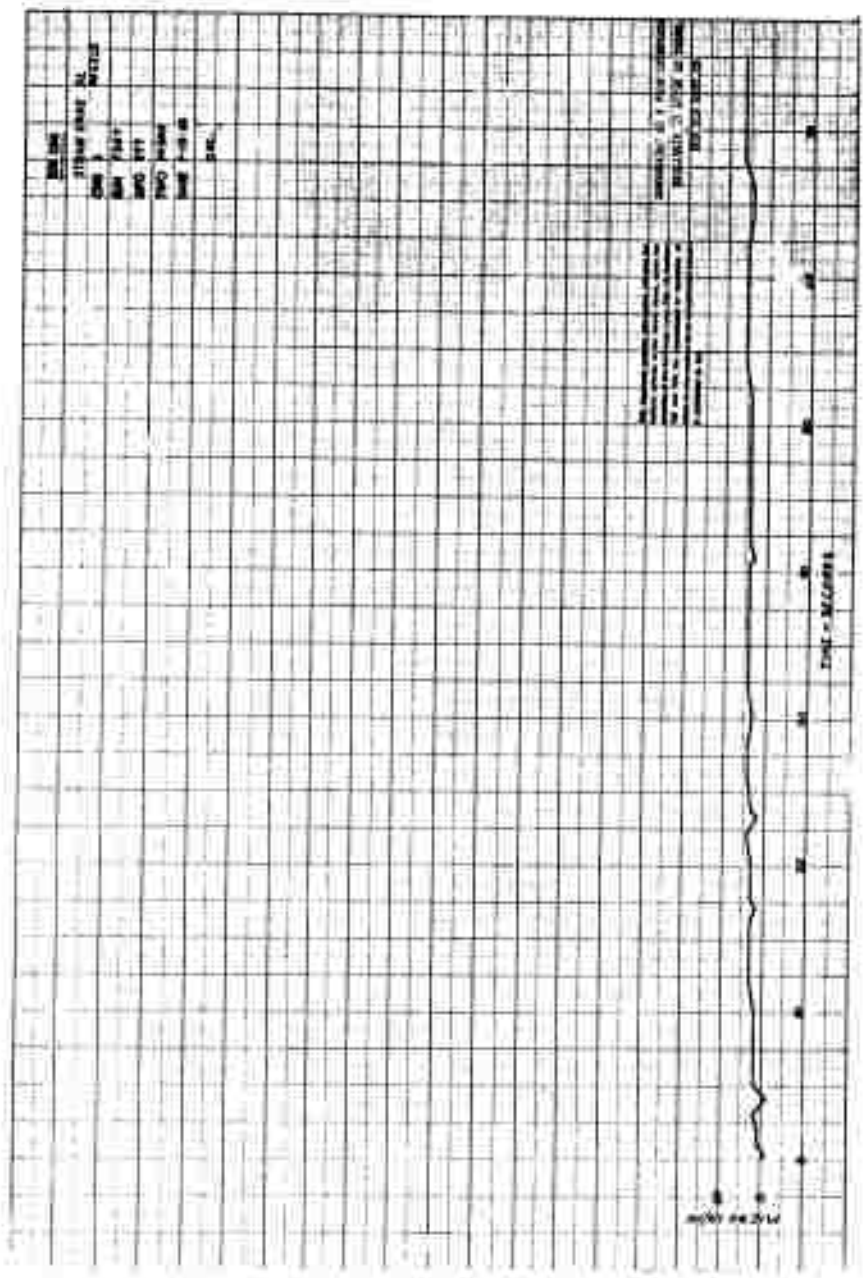

Figure 100 Nozzle Strain versus Time, Gage 5L, Motor 156-6

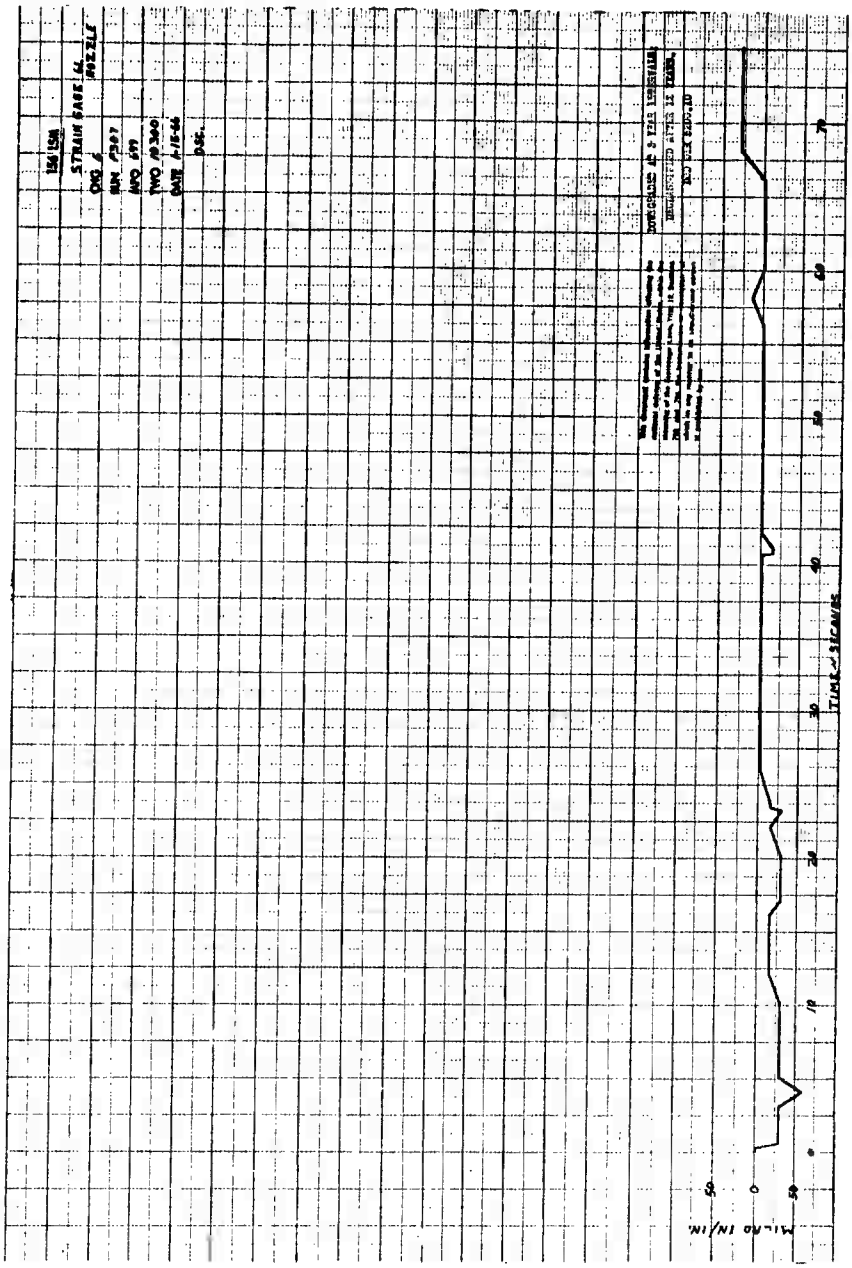

Figure 101 Nozzle Strain versus Time, Gage 6L, Motor 156-6

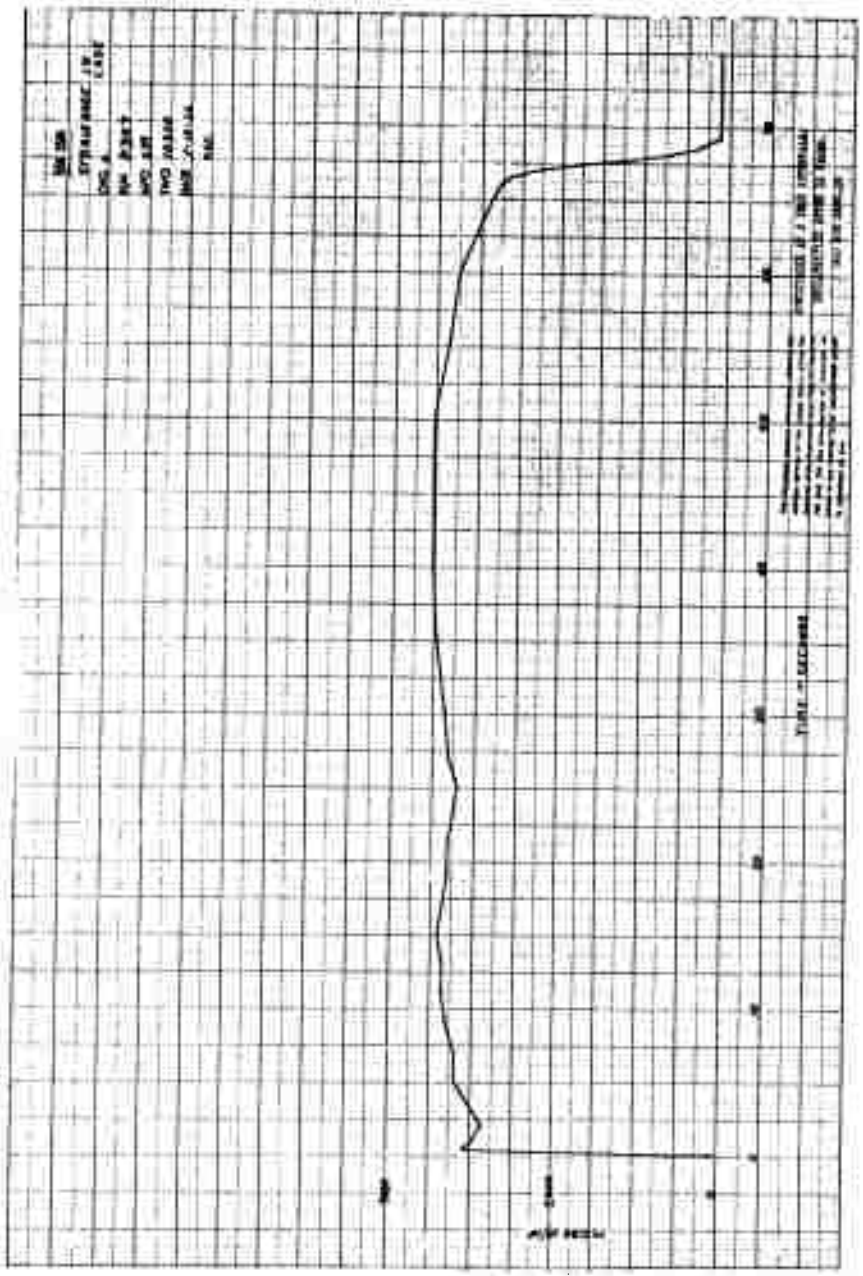

Figure 102 Case Strain versus Time, Gage 1H, Motor 156-6

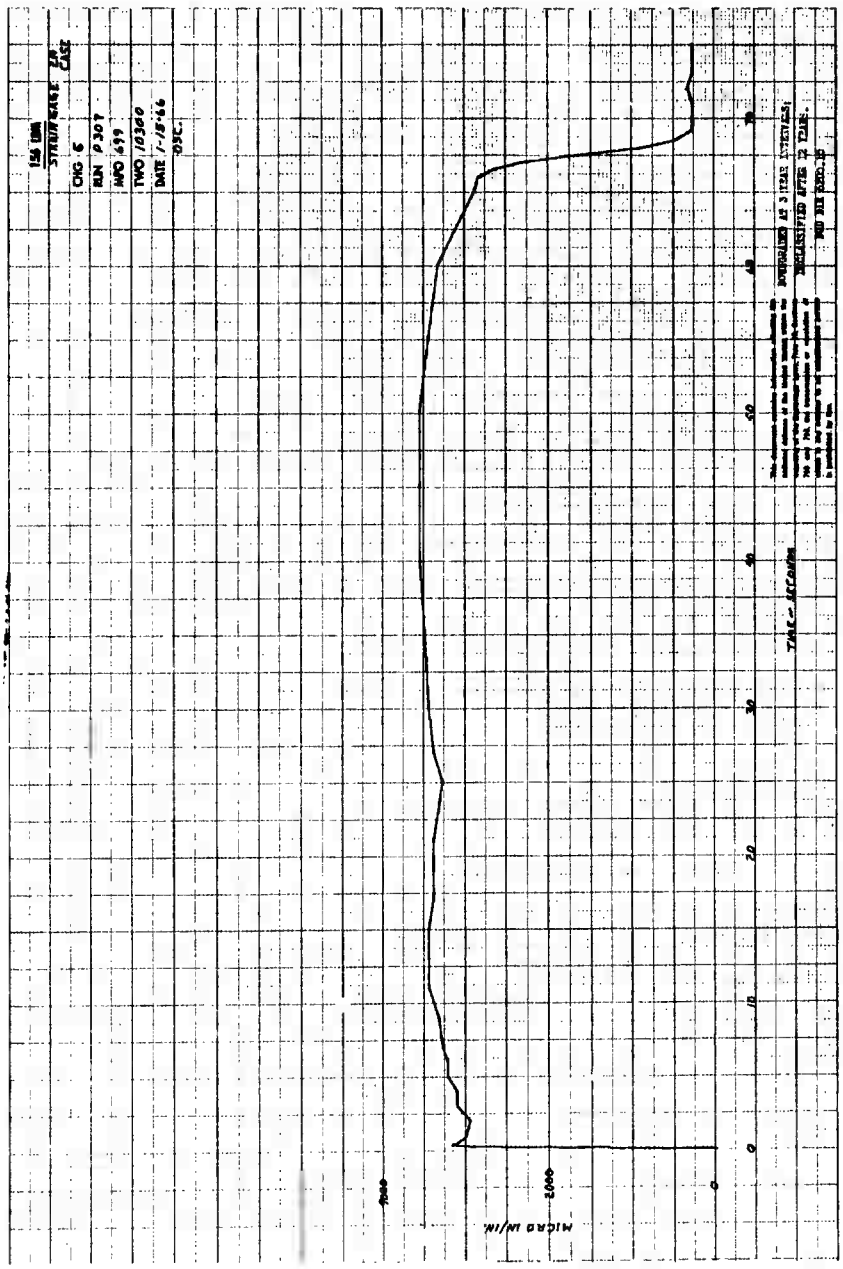

Figure 103 Case Strain versus Time, Gage 2H, Motor 156-6

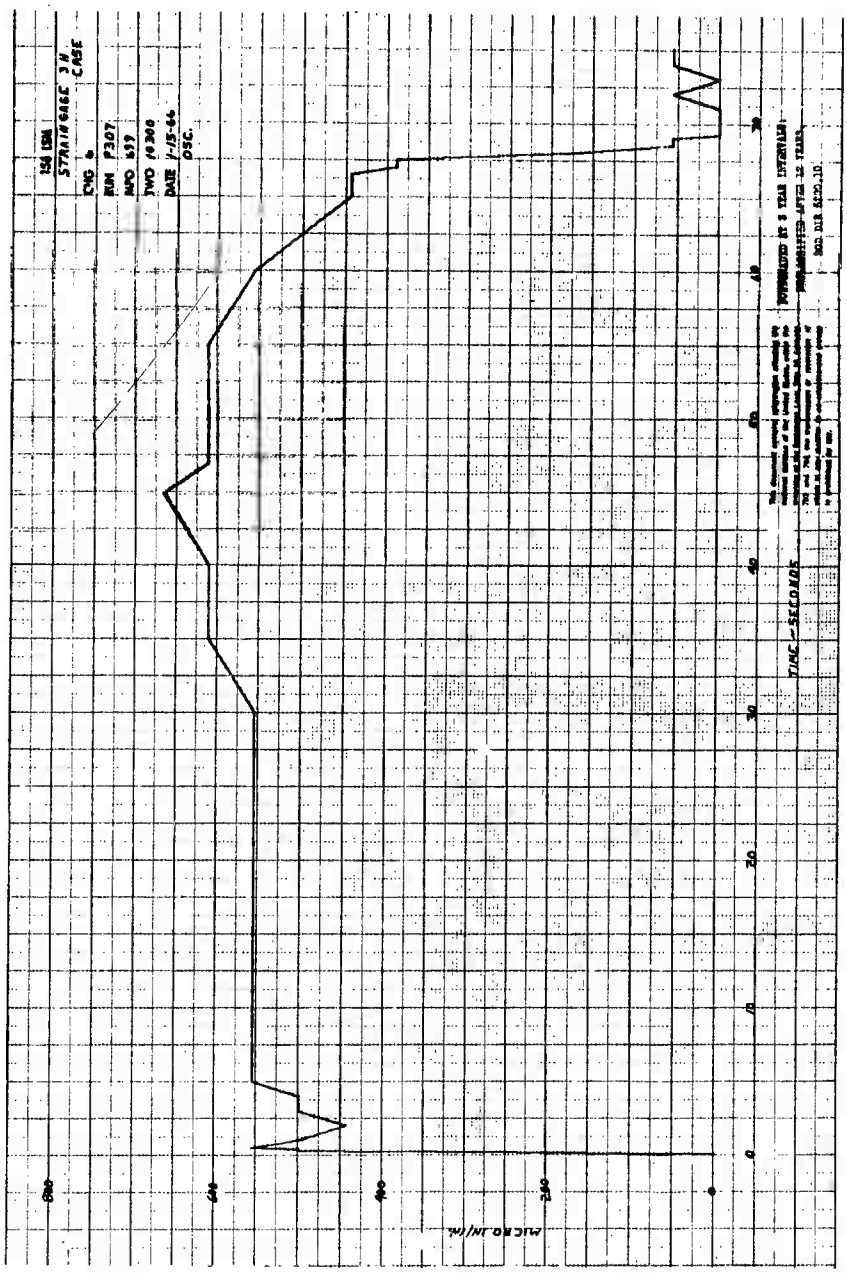

Figure 104 Case Strain versus Time, Gage 3H, Motor 156-6

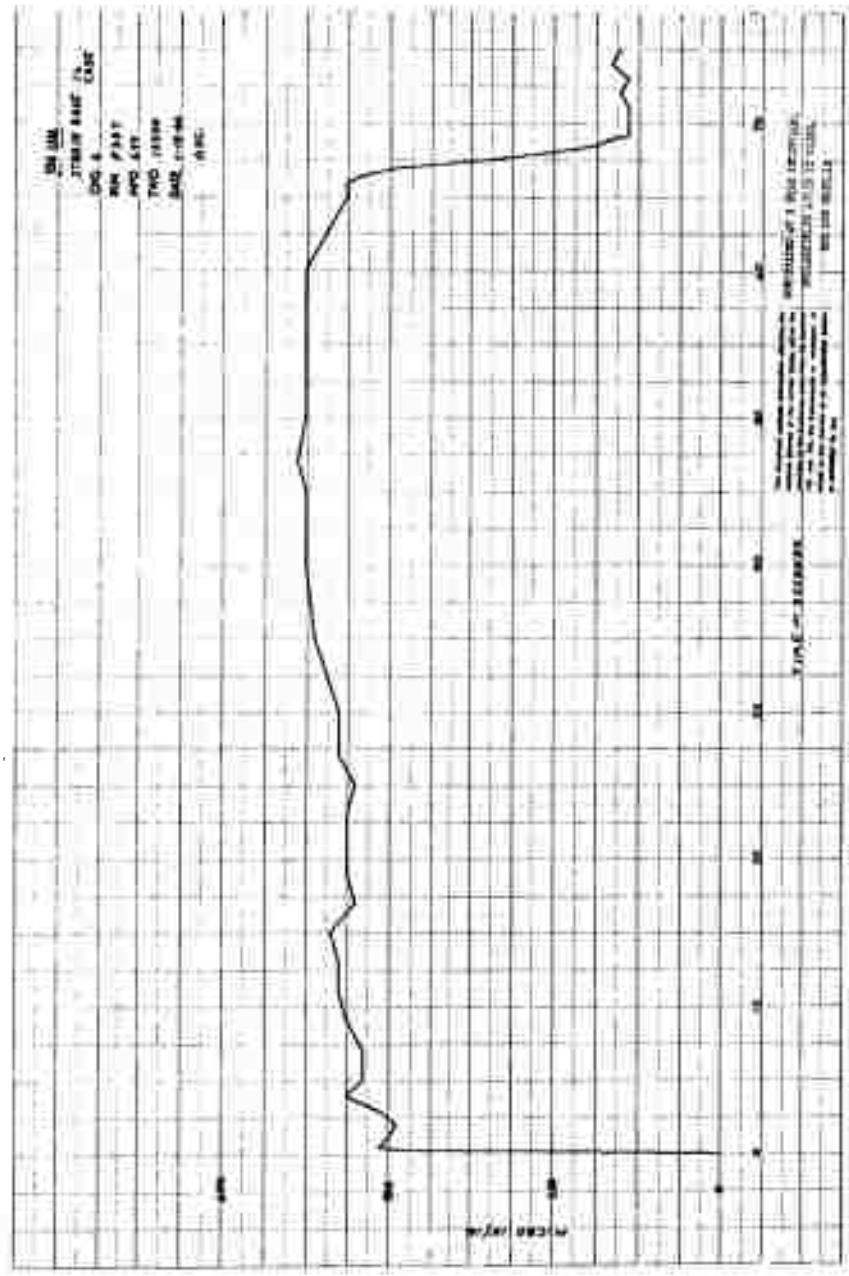

Figure 105 Case Strain versus Time, Gage 1L, Motor 156-6

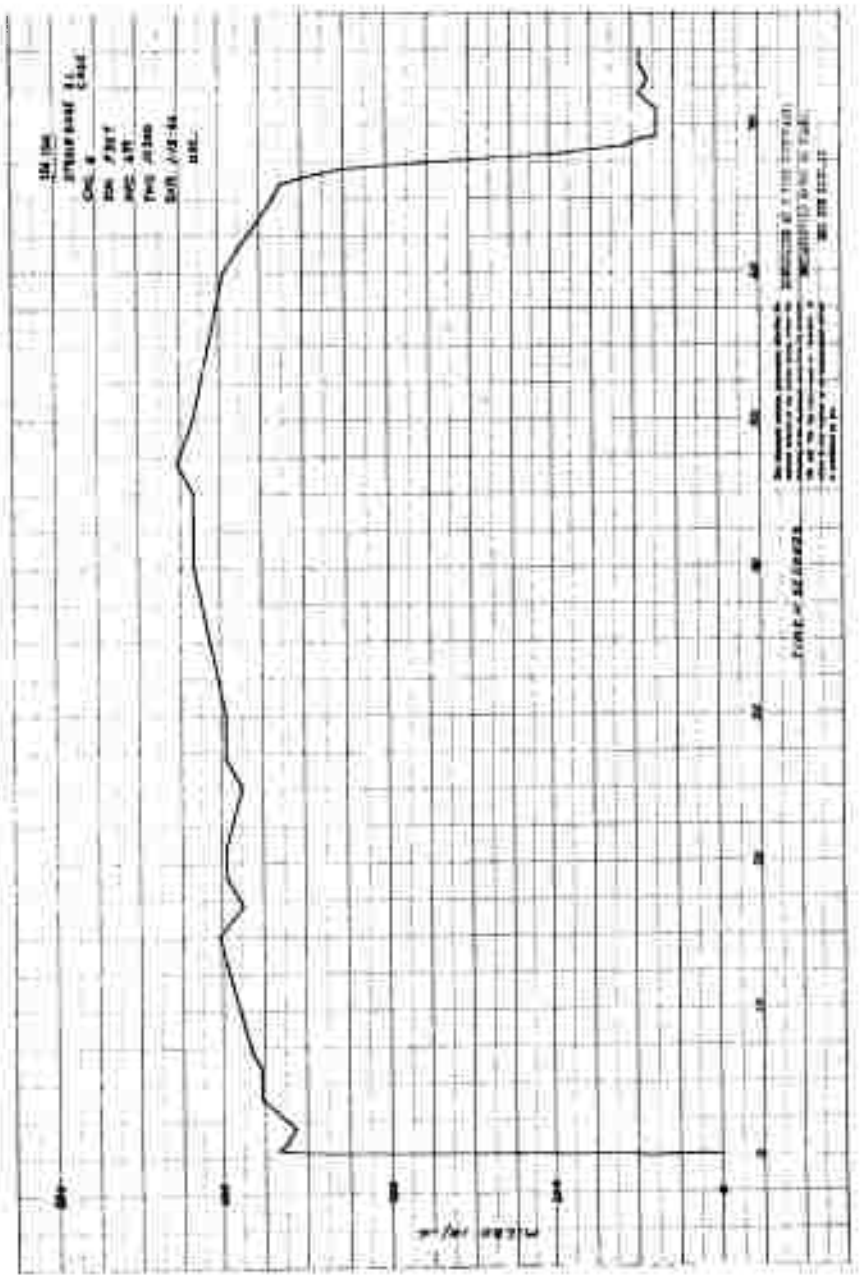

Figure 106 Case Strain versus Time, Gage 2L, Motor 156-6

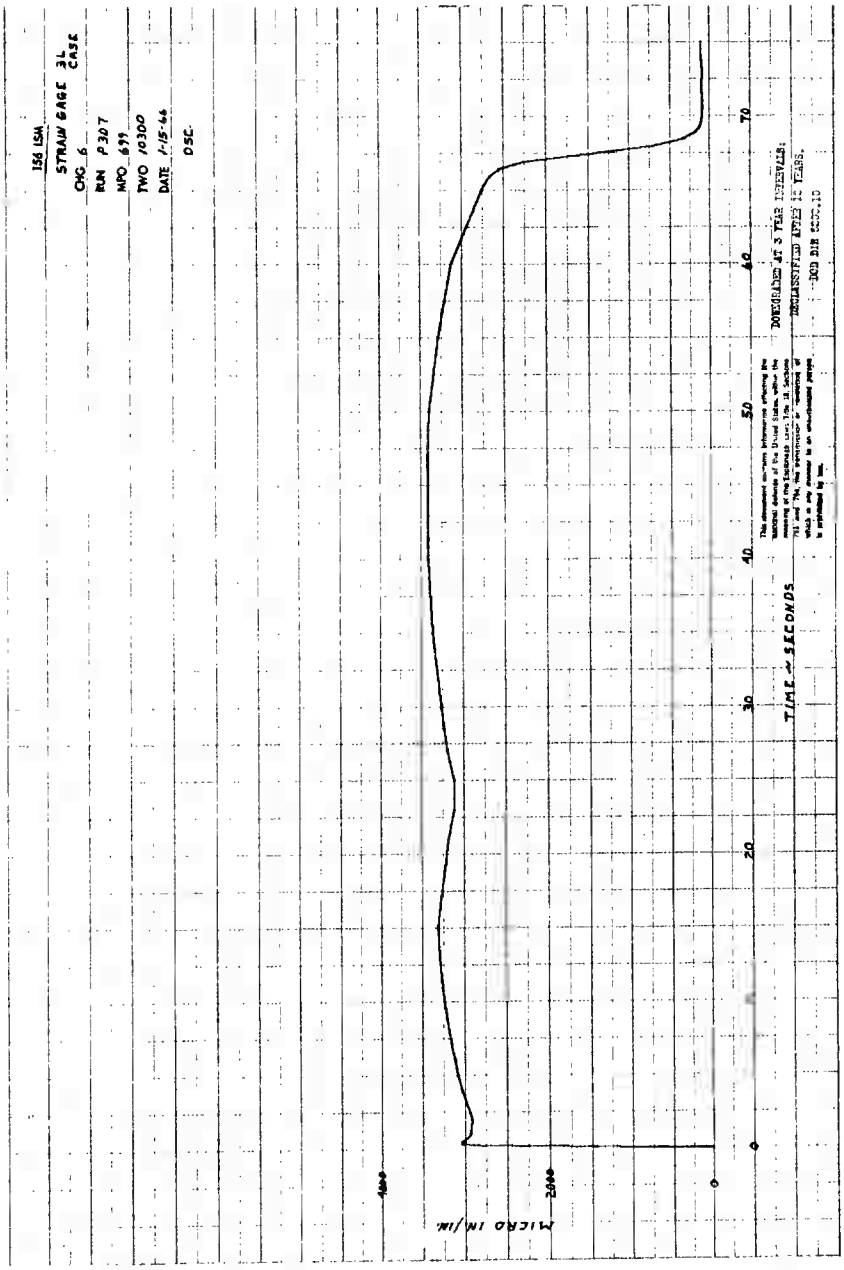

Figure 107 Case Strain versus Time, Gage 3L, Motor 156-6

CONFIDENTIAL

Security Classification

DOCUMENT CONTROL DATA - R&D

(Security classification of title, body of abstract and indexing annotation must be entered when the overall report is classified)

1 ORIGINATING ACTIVITY (Corporate author)
Lockheed Propulsion Company
P.O. Box 111, Redlands, California

2a REPORT SECURITY CLASSIFICATION
CONFIDENTIAL

2b GROUP
Group 4

3 REPORT TITLE
156-Inch Diameter Motor Liquid Injection TVC Program (U)

4 DESCRIPTIVE NOTES (Type of report and inclusive dates)
Final Report: Vol. I, Books 1 and 2; Vol. II; Vol. III. Covers 1 Apr '65 to 31 Mar '66

5 AUTHOR(S) (Last name, first name, initial)

6 REPORT DATE	7a TOTAL NO OF PAGES	7b. NO. OF REFS
July 1966	1193	15

8a CONTRACT OR GRANT NO.	9a ORIGINATOR'S REPORT NUMBER(S)
AF 04(695)-772	LPC Report No. 699-F
b PROJECT NO	
c	9b. OTHER REPORT NO(S) (Any other numbers that may be assigned this report)
d	Technical Report No. AFRPL-TR-66-109

10 AVAILABILITY/LIMITATION NOTICES
"In addition to security requirements which must be met, this document is subject to special export controls, and each transmittal to foreign governments or foreign nationals may be made only with prior approval of AFRPL (RPPR/STINFO), Edwards, California 93523."

11 SUPPLEMENTARY NOTES	12 SPONSORING MILITARY ACTIVITY
	Space Systems Division Air Force Systems Command United States Air Force

13 ABSTRACT

The design, manufacture, and successful static testing of two motors designated 156-5 and 156-6 are described. Under Contract No. AF 04(695)-772, Lockheed Propulsion Company statically test-fired these motors, each having a flightweight submerged ablative nozzle and a flight-prototype, nozzle-mounted N_2O_4 secondary injection TVC system ~~on 14 December 1965 and 15 January 1966, respectively~~. The single center-segment Motor 156-5, containing 687,000 pounds of high-energy LPC-580 PBAN propellant, generated an average thrust of 2,280,000 pounds over a burn time of 55 seconds. Monolithic Motor 156-6, containing 273,000 pounds of LPC-580 propellant, delivered an average thrust of 964,000 pounds for a burn time of 65 seconds.

The submerged ablative nozzles utilized a wide variety of silica, carbon, and graphite-reinforced phenolic plastics designed to qualify these materials for future large motor applications. Severe erosion and gouging was experienced in the helical lay-up carbon-phenolic throat rings of Motor 156-6; erosion in all other areas of both nozzles was as predicted. The throat ablation rate was 8.9 and 9.9 mil/sec in Motors 156-5 and 156-6, respectively.

The N_2O_4 secondary injection TVC design was an on-board system mounted within the 156-inch diameter motor envelope. The positive expulsion, dual-bladder fluid control system was designed to permit long-term storage of N_2O_4 in a flight readiness condition, and an omniaxis signal resolver provided vectorial summation of pitch-yaw signal inputs. The TVC system of both motors functioned throughout the full duration, although the pressure control system of Motor 156-6 functioned only on by-pass pressure regulation values, resulting in lowered injection pressure. Maximum TVC deflection angles were 3.5 degrees and 4.4 degrees for Motors 156-5 and 156-6, respectively.

These systems, in addition to the maraging steel case fabrication and propellant processing operations, are described in detail.

DD FORM 1 JAN 64 1473

CONFIDENTIAL

Security Classification

CONFIDENTIAL

Security Classification

14 KEY WORDS	LINK A		LINK B		LINK C	
	ROLE	WT	ROLE	WT	ROLE	WT
156-inch Diameter Motor						
Secondary Injection Thrust Vector Control						
Submerged Nozzles						
Solid Propellant						

INSTRUCTIONS

1. ORIGINATING ACTIVITY: Enter the name and address of the contractor, subcontractor, grantee, Department of Defense activity or other organization *(corporate author)* issuing the report.

2*a*. REPORT SECURITY CLASSIFICATION: Enter the overall security classification of the report. Indicate whether "Restricted Data" is included. Marking is to be in accordance with appropriate security regulations.

2*b*. GROUP: Automatic downgrading is specified in DoD Directive 5200.10 and Armed Forces Industrial Manual. Enter the group number. Also, when applicable, show that optional markings have been used for Group 3 and Group 4 as authorized.

3. REPORT TITLE: Enter the complete report title in all capital letters. Titles in all cases should be unclassified. If a meaningful title cannot be selected without classification, show title classification in all capitals in parenthesis immediately following the title.

4. DESCRIPTIVE NOTES: If appropriate, enter the type of report, e.g., interim, progress, summary, annual, or final. Give the inclusive dates when a specific reporting period is covered.

5. AUTHOR(S): Enter the name(s) of author(s) as shown on or in the report. Enter last name, first name, middle initial. If military, show rank and branch of service. The name of the principal author is an absolute minimum requirement.

6. REPORT DATE: Enter the date of the report as day, month, year; or month, year. If more than one date appears on the report, use date of publication.

7*a*. TOTAL NUMBER OF PAGES: The total page count should follow normal pagination procedures, i.e., enter the number of pages containing information.

7*b*. NUMBER OF REFERENCES: Enter the total number of references cited in the report.

8*a*. CONTRACT OR GRANT NUMBER: If appropriate, enter the applicable number of the contract or grant under which the report was written.

8*b*, &*c*, & 8*d*. PROJECT NUMBER: Enter the appropriate military department identification, such as project number, subproject number, system numbers, task number, etc.

9*a*. ORIGINATOR'S REPORT NUMBER(S): Enter the official report number by which the document will be identified and controlled by the originating activity. This number must be unique to this report.

9*b*. OTHER REPORT NUMBER(S): If the report has been assigned any other report numbers *(either by the originator or by the sponsor)*, also enter this number(s).

10. AVAILABILITY/LIMITATION NOTICES: Enter any limitations on further dissemination of the report, other than those imposed by security classification, using standard statements such as:

(1) "Qualified requesters may obtain copies of this report from DDC."

(2) "Foreign announcement and dissemination of this report by DDC is not authorized."

(3) "U. S. Government agencies may obtain copies of this report directly from DDC. Other qualified DDC users shall request through

_____."

(4) "U. S. military agencies may obtain copies of this report directly from DDC. Other qualified users shall request through

_____."

(5) "All distribution of this report is controlled. Qualified DDC users shall request through

_____."

If the report has been furnished to the Office of Technical Services, Department of Commerce, for sale to the public, indicate this fact and enter the price, if known.

11. SUPPLEMENTARY NOTES: Use for additional explanatory notes.

12. SPONSORING MILITARY ACTIVITY: Enter the name of the departmental project office or laboratory sponsoring *(paying for)* the research and development. Include address.

13. ABSTRACT: Enter an abstract giving a brief and factual summary of the document indicative of the report, even though it may also appear elsewhere in the body of the technical report. If additional space is required, a continuation sheet shall be attached.

It is highly desirable that the abstract of classified reports be unclassified. Each paragraph of the abstract shall end with an indication of the military security classification of the information in the paragraph, represented as *(TS)*, *(S)*, *(C)*, or *(U)*.

There is no limitation on the length of the abstract. However, the suggested length is from 150 to 225 words.

14. KEY WORDS: Key words are technically meaningful terms or short phrases that characterize a report and may be used as index entries for cataloging the report. Key words must be selected so that no security classification is required. Identifiers, such as equipment model designation, trade name, military project code name, geographic location, may be used as key words but will be followed by an indication of technical context. The assignment of links, rules, and weights is optional.

CONFIDENTIAL

Security Classification